Thermo-hydrodynamics of Closed Loop Pulsating Heat Pipes

Von der Fakultät Maschinenbau der Universität Stuttgart
zur Erlangung der Würde eines Doktoringenieurs (Dr.-Ing.)
genehmigte Abhandlung

Vorgelegt von

Sameer Khandekar

aus Jabalpur (MP), Indien

Hauptberichter:	Prof. Dr.-Ing. habil. M. Groll
Mitberichter:	Prof. Dr.-Ing. habil. H. Müller-Steinhagen

Tag der mündlichen Prüfung: 19. Juli 2004

Institut für Kernenergetik und Energiesysteme der Universität Stuttgart
2004

Acknowledgements

The secular and objective spirit of scientific philosophy has been the greatest attraction for me and I thank God almighty to have directed me on this path of scientific research. I am glad to have got the opportunity to explore a tiny bit of Him.

This journey would have been impossible had I not received the guidance of Dr. Groll, my 'Doktorvater'. He has been much more to me than all the meanings and interpretations this word can embody. His personality has left an unprecedented impression on me and I am not audacious enough to thank him by words; I'll do it through my actions in the years to come! I also thank Dr. H. Müller-Steinhagen for accepting to be the thesis co-examiner.

Another indispensable teammate was indeed my wife, Pradnya. An elixir of life, she has been a perfect 'Yin' for the 'Yang' inside me. I have a full life to thank her and I plan to utilize every bit of it! Pravah, my son, also supported our pursuits through his extraordinary qualities. Through him, we are reminded for our duties as natural beings as well as obligations towards continuing the tradition of a sound social infrastructure. Lovingly doing these duties is my way of thanking him.

Back in India, my parents and family members have played their special role in the most exemplary manner. The best way to express gratitude will be to follow the way of life which they have taught.

All the friends, at the institute and outside, made the journey extremely enriching and I heartily thank all of them for everything which they have done for me. People requiring special mention are of course, Marcus - who provided invaluable support in the initial days of my stay, and Patrick - who incidentally is the 'greatest' (Note: This latter personality is indescribable in words and only the Matrix knows how to deal with him - probably!). As 'executive manager' of our group, 'Rudi-Rainer GmbH' was also very supportive for which I am grateful. Thanks are also due to all the students who helped me during my research work.

Indeed, this thanksgiving task will be incomplete if I fail to mention my gratitude towards Prof. G. Lohnert, the director of IKE, who gave constant encouragement and support. I would also like to thank the institute/university administrators, research collaborators/financiers and technical/secretarial staff for their active support throughout my doctoral program.

Life in Germany has taught me gamut of new things and I thank all those persons who made this experience possible for me. The society, as a whole, has meticulously played its role in carving my personality over the years and has brought me to a stage in life where I can begin carving younger brains independently. The baton has been given in my hands now. What more can I expect?

Danke Schön and Dhanyavad!

Table of contents

CHAPTER 4 RESULTS AND DISCUSSION

CHAPTER 5 MATHEMATICAL MODELING

CHAPTER 6 SUMMARY AND CONCLUSIONS

Abstract

Thermal management of electronics is a contemporary issue which is increasingly gaining importance in line with the advances in packaging technology. Immediate and consistent multi-disciplinary research is needed to cater to the prevailing trends of net power and flux levels of upcoming microelectronics products. Material science, packaging concepts, fabrication technology and novel cooling strategies are some of the key areas requiring synchronal research for successful thermal management. Focusing on the latter area, this thesis attempts to describe the complex thermo-hydrodynamics of Closed Loop Pulsating Heat Pipes (CLPHPs) which are new entrants in the family of closed passive two-phase heat transfer systems. These apparently simple looking devices are extremely intriguing for theoretical and experimental investigations alike. It is rare to find a combination of such events and mechanisms, like bubble nucleation/collapse and agglomeration, bubble pumping action, pressure/temperature perturbations, flow regime changes, dynamic instabilities, metastable non-equilibrium conditions, flooding/bridging etc., all together contributing towards the thermal performance of a device. The thermal performance objective function is multi-dimensional and embodies major multi-disciplinary two-phase flow physics.

To achieve the goal, five different experimental set-ups have been envisioned, fabricated and tested. The set-ups are designed for flow visualization (including videography and infra-red thermography) coupled with standard thermometry. Six major parameters have emerged as the primary influence parameters which affect the system dynamics. These include:

- Internal diameter of the CLPHP tube,
- Volumetric filling ratio of the working fluid,
- Input heat flux,
- Total number of turns,
- Operational orientation and,
- Thermo-physical properties of the working fluid.

The thesis provides detailed discussion on the various design parameters. Apart from the multitude of geometrical, physical and operational variables, the performance is also strongly linked with the flow patterns existing inside the device. Subtle aspects of this two-phase flow dynamics and their interactions with the heat transfer characteristics have been highlighted leading to the formulation of primary design rules.

Mathematical modeling of the device operation has also been successfully accomplished by applying two approaches which are quite diverse in nature, viz. (a) Semi-empirical modeling with non-dimensional groups, and (b) Modeling by artificial neural networks. The handicaps and problems of conventional modeling by ‘first principles’, e.g Navier-Stokes equation, are also scrutinized.

At the end of this study program, although some nuances of the device operation still remain unexplored, it is believed that major advancement in the understanding of the thermo-hydrodynamics of CLPHPs has been accomplished. With the progress achieved so far, the prospects for this exemplary and unprecedented technology seems quite promising.

Kurzfassung

Das Thermalmanagement von Elektronikbauteilen ist ein Thema, welches aufgrund der Fortschritte in der Mikrosystemtechnik zunehmend an Bedeutung gewinnt. Multidisziplinäre Forschung ist notwendig, um dem vorherrschenden Trend zu immer höheren Leistungen und Wärmestromdichten in künftigen Mikroelektronikbauteilen Rechnung zu tragen. Materialforschung, neuartige modulare Konzepte, Herstellungs-technologien und Strategien in der Kühlung sind einige der Schlüsselbereiche, in denen Forschungsbedarf für ein erfolgreiches Thermalmanagement besteht. Im Mittelpunkt dieser Doktorarbeit steht der letztgenannte Bereich, die Beschreibung der komplexen Thermo-hydrodynamik von geschlossenen pulsierenden Wärmerohren (CLPHPs). Sie sind neu zur Familie der geschlossenen passiven 2-Phasen-Wärmeübertragungssysteme hinzugekommen. Diese auf den ersten Blick sehr einfach ausschauenden Bauteile sind sowohl für theoretische als auch für experimentelle Untersuchungen außerordentlich faszinierend. Es ist selten eine solche Kombination verschiedenster Mechanismen zu finden, wie Wachstum/Kollabieren und Agglomerieren von Blasen, Druck- und Temperaturstörungen, Änderungen im Strömungsmuster, dynamische Instabilitäten, metastabile Nichtgleichgewichtszustände, Flooding/Bridging, usw., die alle die thermische Leistungsfähigkeit des Bauteils beeinflussen. Die Zielfunktion der thermischen Leistungsfähigkeit ist mehrdimensional und beinhaltet komplexe Phänomene der 2-Phasen-Thermofluiddynamik.

Um dieses Ziel zu erreichen, wurden fünf unterschiedliche Experimente geplant, aufgebaut und getestet. Die experimentellen Aufbauten erlauben eine Visualisierung der Strömungsvorgänge (inklusive Videoaufzeichnungen und Infrarotthermographie) verbunden mit üblicher Temperaturmessung. Sechs Parameter wurden als Haupteinflussgrößen auf die Systemdynamik erkannt. Diese sind:

- der Innendurchmesser der CLPHP
- der volumetrische Füllgrad des Arbeitsfluids
- die eingebrachte Wärmestromdichte
- die Anzahl der Windungen
- die Ausrichtung der CLPHP im Betrieb sowie
- die thermophysikalischen Eigenschaften des Arbeitsfluids

Diese Doktorarbeit beinhaltet eine ausführliche Diskussion der zahlreichen Auslegungsparameter. Abgesehen von der Vielzahl von geometrischen, physikalischen und Betriebsvariablen hängt die thermische Leistungsfähigkeit auch stark von den Strömungs-mustern innerhalb der CLPHP ab. Aspekte dieser 2-Phasenströmungsdynamik und ihrer Interaktion mit der Wärmeübergangscharakteristik wurden herausgearbeitet und in grundsätzlichen Auslegungsrichtlinien formuliert.

Die mathematische Modellierung der Betriebszustände der CLPHP ist mit zwei unterschiedlichen Ansätzen erfolgreich bewerkstelligt worden. Zum einen mit einer halbempirischen Modellierung mit dimensionslosen Kennziffern und zum anderen mit künstlichen neuronalen Netzen. Die Nachteile und Probleme konventioneller Modellierungs-methoden, die auf grundlegenden Gleichungen (z.B. Navier-Stokes) aufbauen, sind ebenfalls eingehend untersucht worden.

Wenngleich einige Teilaspekte des Betriebsverhaltens der CLPHP weiterhin nicht vollständig geklärt sind, so ist doch als Ergebnis dieser Forschungsarbeit ein großer Fortschritt im Verständnis der Thermohydrodynamik von CLPHP erzielt worden. Mit den bisher erzielten Ergebnissen erscheinen die Aussichten für diese einzigartige Technologie sehr vielversprechend.

Nomenclature

A_c	: area of cross section (m^2)
c_p	: specific heat at constant pressure (J/kg·K)
D	: characteristic duct dimension, diameter (m)
F	: enhancement factor
$\vec{F}$	: force (N)
f	: friction factor
G	: mass flux ($kg/m^2 \cdot s$)
g	: acceleration due to gravity (m/s^2)
h	: heat transfer coefficient ($W/m^2 \cdot K$)
h_{fg}	: latent heat of vaporization (J/kg)
k	: thermal conductivity (W/m·K)
L	: length (m)
$\dot{m}$	: mass flow rate (kg/s)
N	: number of turns
P	: pressure (N/m^2)
$\hat{P}$	: perimeter (m)
Q	: heat energy (J)
$\dot{Q}$	: heat throughput rate (W)
$\dot{q}$	: heat flux (W/m^2)
R_{th}	: thermal resistance (K/W)
R	: radius (m)
S	: suppression factor
T	: temperature (°C or K)
V	: volume (m^3)
x, x^*	: two-phase mass quality

Greek Symbols

α	: liquid-solid contact angle (deg/rad)
β	: inclination angle from horizontal axis (deg/rad)
σ	: surface tension (N/m)
ρ	: density (kg/m^3)
μ	: dynamic viscosity ($N \cdot s/m^2$)
τ	: shear stress (N/m^2)

υ, υ^* : characteristic velocity (m/s)

$\Gamma_{vap}\big|_{eq}$: mass rate of vapor generation per unit volume (kg/s·m^3)

Ω_{eq} : equilibrium frequency of phase change (1/s)

ξ_h : heated perimeter (m)

Non-dimensional numbers

Bo : Bond number = $D \cdot \left(g(\rho_{liq} - \rho_{vap})/\sigma\right)^{0.5}$

Eö : Eötvös number = $(Bo)^2$

Fr : Froude number = $\dfrac{\rho \cdot \upsilon_\infty^2}{D \cdot g \cdot (\rho_{liq} - \rho_{vap})}$

Ja : Jakob number = $\dfrac{h_{fg}}{c_p \cdot \Delta T}$

Ka : Karman number = $f \cdot Re^2 = \dfrac{\rho \cdot (\Delta P) \cdot D^3}{\mu^2 \cdot L_{eff}}$

$N_{pc}\big|_{eq}$ or Q* : Equilibrium phase change number = $\left(\dfrac{4 \cdot \dot{q} \cdot L}{D_{hyd} \cdot h_{fg} \cdot (G/\rho_{liq,\,in})}\right)\left(\dfrac{\rho_{liq} - \rho_{vap}}{\rho_{liq} \cdot \rho_{vap}}\right)$

Pr : Prandtl number = $\dfrac{c_p \cdot \mu}{k}$

Ps : Poiseuille number = $\dfrac{(u_\infty \cdot \mu_{liq})/D}{D \cdot g \cdot (\rho_{liq} - \rho_{vap})}$

Re : Reynolds number = $\dfrac{\rho \cdot \upsilon^* \cdot D}{\mu}$

Y : Property number = $\dfrac{g \cdot \mu^4}{\rho \cdot \sigma^3} = \dfrac{Ps^4 \cdot Eö^3}{Fr^2}$

Su or N_{sub} : Subcooling number $\dfrac{c_{P,liq} \cdot (T_{sat} - T_{in})}{h_{fg}}\left(\dfrac{\rho_{liq} - \rho_{vap}}{\rho_{vap}}\right)$

Subscripts

a	: adiabatic section
CB	: convective boiling
c	: condenser section
cap	: capillary
e	: evaporator section
eff	: effective
exp	: experiment
ext	: external
crit	: critical
hyd	: hydraulic
i	: inner, inlet
int	: internal
liq	: liquid
max	: maximum
NB	: nucleate boiling
o	: outer, outlet
pre	: predicted
sat	: saturation
tot	: total
vap	: vapor
∞	: terminal

Abbreviations

ANN	: Artificial Neural Network
CLPHP	: Closed Loop Pulsating Heat Pipe
CHF	: Critical Heat Flux
FFT	: Fast Fourier Transformation
FR	: Filling Ratio of the working fluid (V_{liq}/V_{tot}) at room temperature
ID	: Inside Diameter (m)
IGBT	: Insulated Gate Bipolar Transistor
MCM	: Multi Chip Modules
PHP	: Pulsating Heat Pipe
OD	: Outside Diameter (m)

List of figures

Chapter 1

Chapter 2

Chapter 3

Chapter 4

Chapter 5

List of tables

CHAPTER 1

INTRODUCTION

1.1 Background information

1.1.1 Thermal management of electronics

Miniaturization is in vogue and this euphoria has especially gripped the electronics and allied industry. The insatiable urge for 'going nano' does come with associated inter-disciplinary technological problems. Although this 'increase power-decrease size' scenario has been prevalent for many decades, in recent years, thermal management has become the major feasibility bottleneck for microelectronics.

Each conceived new design coming up in the market is with higher power dissipation levels. In addition, total dissipated power is not the only problem; heat density (power per unit area) is complimentary to it. Market expectations towards higher functionality at reduced package sizes have led to denser electronics and increased clock frequencies which pose a simultaneous challenge to thermal management of increased power levels coupled with high heat fluxes.

As shown in Figure 1-1, Moore's law states that the semiconductor transistor density, and hence the performance, doubles roughly every 18 months [Moore, 1965, 1975]. History has supported the conclusions of Moore's law ever since its inception in 1970. These trends of

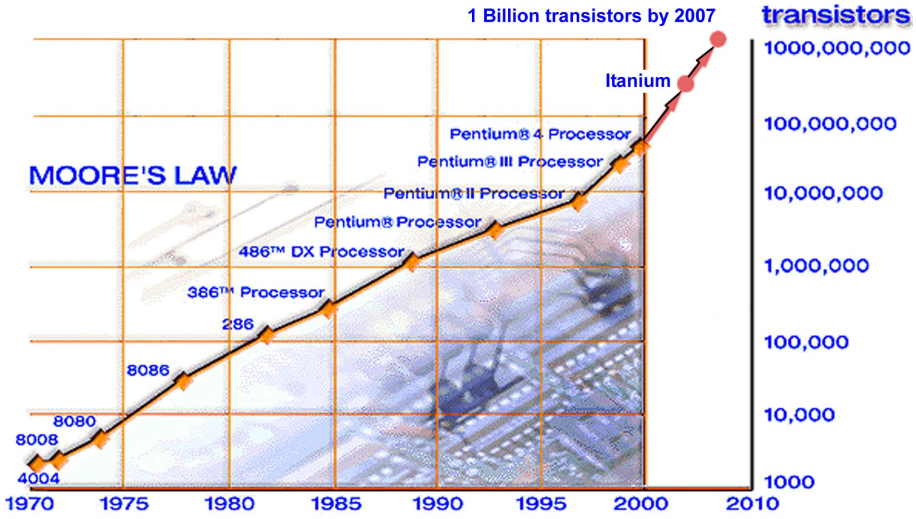

Figure 1-1: Moore's law for transistor count in electronics industry

device advancement are directly correlated with the power dissipation as shown on Figure 1-2 [Chu et al., 1999] and Figure 1-3 [Azar, 2000]. The introduction of CMOS technology as an alternative to bipolar devices has further amplified the problem. An unprecedented exponential growth of power densities has occurred from 0.5 W/cm² in the eighties to more than 15 W/cm² by the turn of the last century [Chu et al., 1999]. There is nothing in the timeline projections to suggest that device or system level power dissipation is on the decline nor is it likely to reach a plateau in the next decade. All future predictions and indicators point towards die level heat fluxes of 40 to 60 W/cm² as the norm rather than exception. While the power consumption per typical gate has come down to the range of 15 µW/Gate/MHz, the number of gates per device has dramatically increased with the 'system on chip' concept bringing the net dissipated power to over 100 W per module.

Mass access to consumer electronics, personal computers, internet facilities and telecommunications has further boosted the 'need for speed'. Consequently, power-dissipation management has become a major challenge in the electronics industry. Unfortunately, strategic development of thermal solutions did not match the speed of silicon technology transformation for quite some time. 'Thermal management', which simply boiled down to adding more heat sinks in the past, is now maturing. A dramatic change in the package design philosophy has resulted in the incorporation of thermal design checks much before the development of a prototype. To address the future issues and projections, technological advancement is likely to be the only savior. This includes development of new materials, novel cooling strategies and a paradigm shift in the cooling technology concepts and modes of implementation e.g. development of metal matrix composite materials, silicon nano-technology and MEMS, mini/micro heat pipes, loop heat pipes, microscale boiling/ condensation etc.

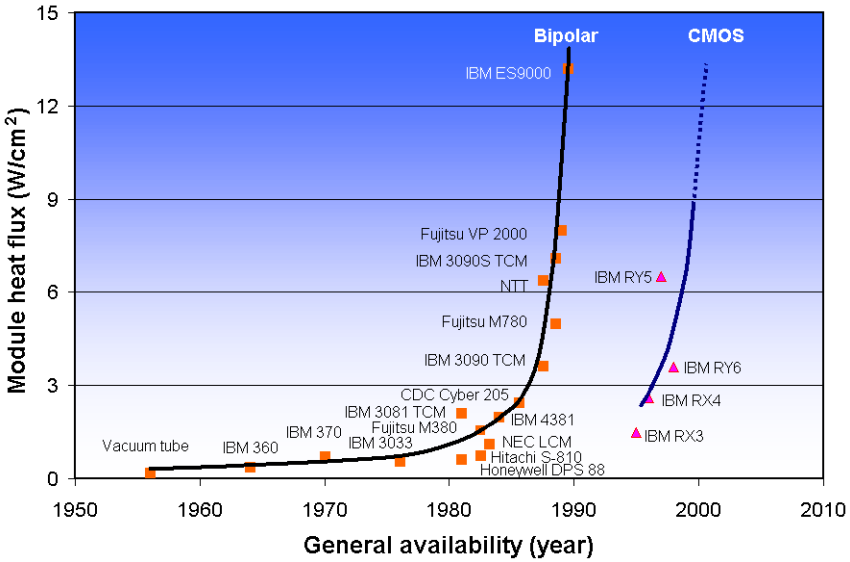

Figure 1-2: Timeline of module heat fluxes in microprocessors

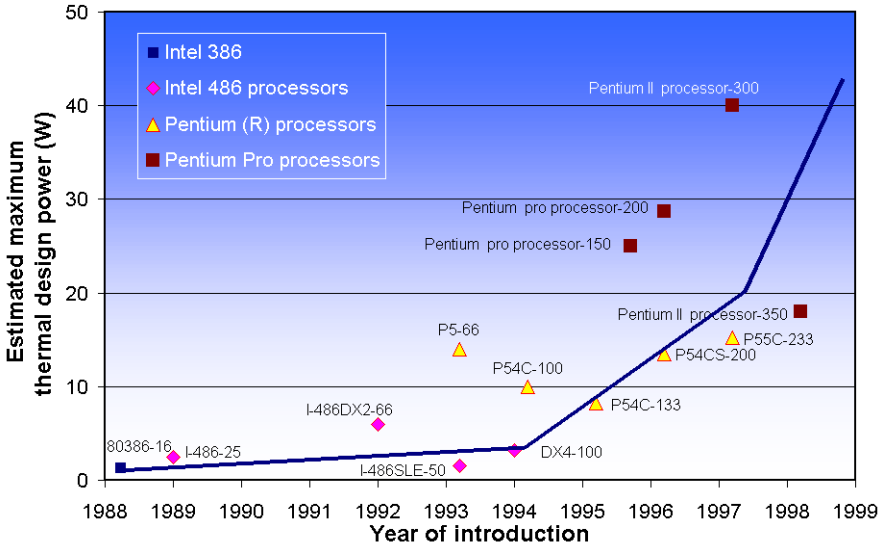

Figure 1-3: Trends for maximum thermal power dissipation for microprocessors

1.1.2 Motivation for present research

In the wake of the ongoing trends, the demands from the contemporary thermal solutions of electronic equipment are as follows:

- Thermal resistance from chip to heat sink < 1 K/W
- High heat transport capability (5 W to 250 W)
- Heat flux spreading (1 W/cm^2 to 40 W/cm^2)
- Mechanical & thermal compatibility
- Long term reliability
- Miniaturization
- Low cost

The primary goal of any cooling system is to enhance the package or module performance and the reliability, which incidentally are strong functions of temperature. The temperature plays a role in the following:

- Device functionality: since many electrical parameters are temperature dependent,
- Device safety: as all exposed parts etc. must abide by the international standards of operating temperature and,
- Device failure: since most mechanisms of physical failure are dependent on absolute temperature, temperature differences or spatial/temporal gradients, common examples being electro-migration, corrosion and solder fatigue, to name a few. This aspect is the most critical since quality and reliability issues are inherently linked to the junction temperature or gradients.

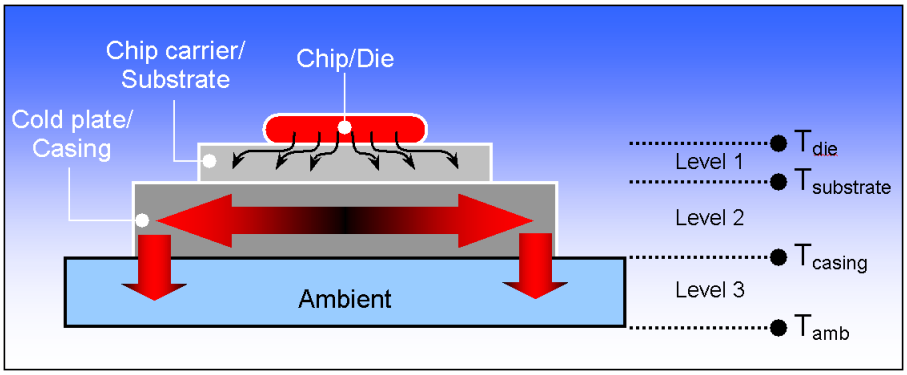

Figure 1-4: Thermal management levels of a typical package

Further, modern electronics cooling problems can be broadly divided primarily into three levels (refer Figure 1-4) [Nakayama, 1988]:

- **First level cooling** is concerned with heat dissipation from a chip to a directly connected chip carrier. The carrier is either the chip package (plastic, ceramic, etc.) in case of single chip packages, or a substrate in case of multi chip modules.
- **Second level** involves the thermal path from a chip carrier to a casing/cold plate.
- Finally, **third level cooling** is the heat rejection from casing/cold plate to the ambient.

With these boundary conditions in mind, novel cooling strategies are continuously being developed. Considerable research in new material development and characterization has drastically improved the performance of the first level cooling. Historically, the second and third level cooling were primarily based on natural convection or forced convection air-cooling techniques. Continued stringent demands led to the development of phase change techniques such as pool boiling, jet impingement cooling and more recently mini/micro channel flow boiling concepts. In parallel, heat pipes in various configurations and designs, have played a decisive role in many second/third level cooling applications. Introduction of micro heat pipes has led to the development of many hybrid-cooling concepts combining different levels of cooling [Bar-Cohen, 1994].

Meandering tube Pulsating Heat Pipes (PHPs) is another novel concept proposed by Akachi [1990, 1993] and shown in Figure 1-5, which seems to meet all the present day cooling requirements. Typically suited for second/third level management, PHPs have already found some applications in micro and power electronics applications owing to the unique operational characteristics coupled with relatively low costs. Although grouped as a subclass of the overall family of heat pipes, the complexity of thermo-hydrodynamic coupling is distinctly unique. A completely different research outlook is needed due to its singular thermofluidic behavior. The subtle nuances of this conceptually simple device are quite intriguing for theoretical and experimental studies alike.

This research work aims to understand the fundamental thermo-hydrodynamic operational characteristics of closed loop pulsating heat pipes. Attention is focussed

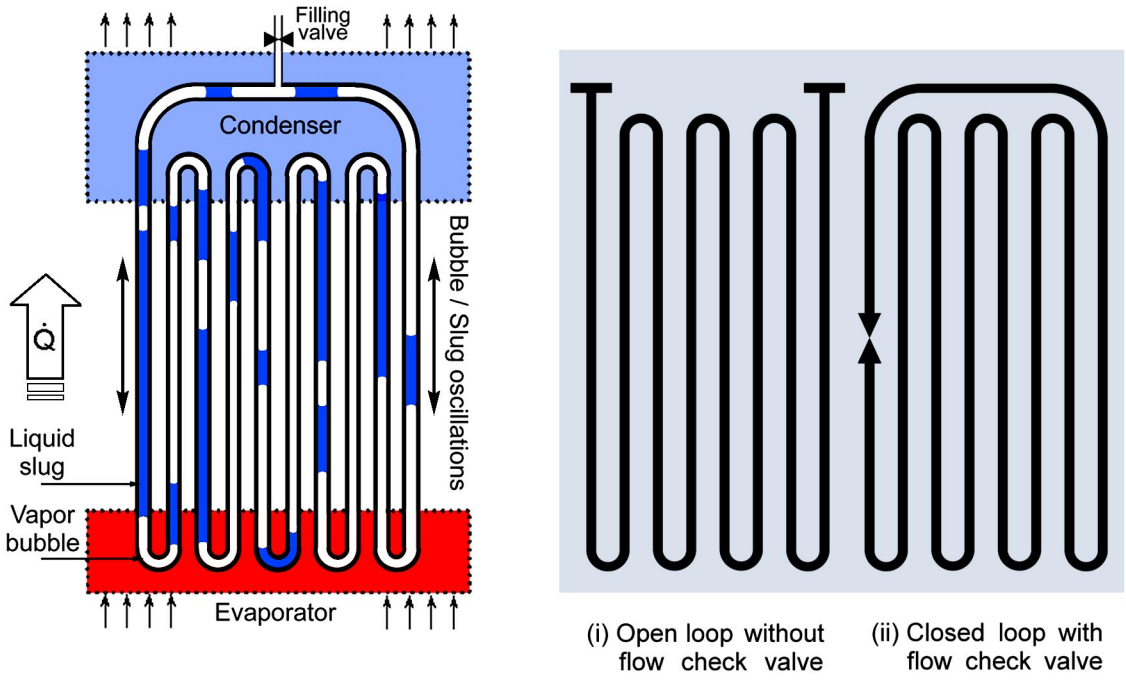

Figure 1-5: Schematic of a typical pulsating heat pipe with design variations

particularly on Closed Loop Pulsating Heat Pipes (CLPHPs) without directional flow control check valve, the details of which will be presented in subsequent chapters. The thermofluidic behavior is studied with the aid of a series of visualization experiments (high speed videography and infra-red thermography), heat transfer measurements and mathematical modeling. Before commencement of this research, the available literature on PHPs was rather sparse. The fundamental understanding of the operating principles was also vague in spite of the fact that some prototypes were already in the market. Comprehensive theory of operation and reliable database or tools for the design of CLPHPs according to a given microelectronics-cooling requirement was an unrealized task. Although such a comprehensive design scheme is still not complete, it is strongly believed that this work will bridge the gap in our understanding of CLPHPs and provide a concrete foundation for future research direction.

Before proceeding further, a review of contemporary cooling strategies is presented so that the concept of CLPHPs can be better appreciated in the context of prevailing trends.

1.1.3 Electronics thermal management strategies: A review

Electronics thermal management techniques have undergone a drastic evolutionary change over the last fifty years. Figure 1-6 chronicles the role of cooling and circuit technology in the past several decades [Azar, 2000]. The age of vacuum tubes witnessed large power dissipation levels but a low technology solution was enough as there were no spatial constraints. Mounting the systems in large rooms was the usual way out. Dramatic developments in material science and the introduction of transistors drastically changed the

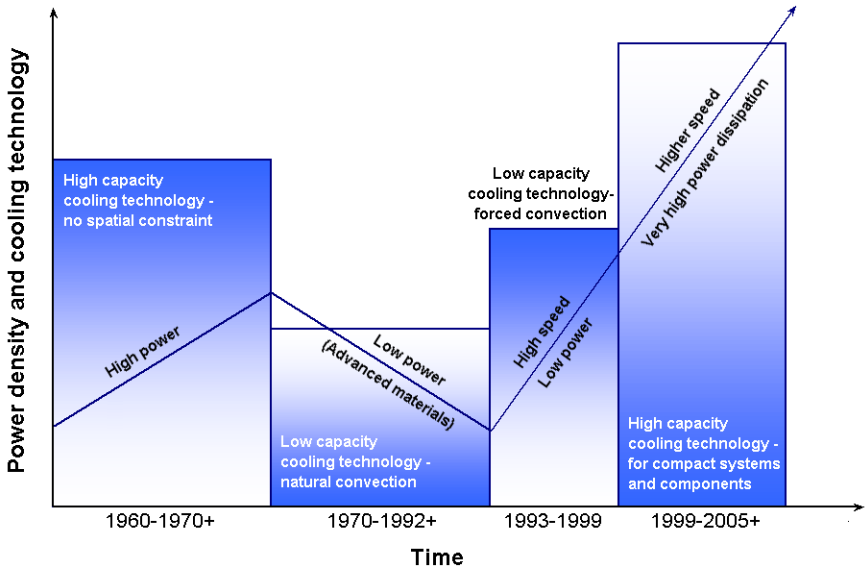

Figure 1-6: Trends for thermal management strategies

scene. Typical system dimensions were reduced but with a simultaneous decrease of power levels too. Again, low capacity cooling technology, primarily with natural convection, provided the solution except for some special applications where forced air-cooling was necessary. For a comparatively long time this low capacity cooling technology, a combination of natural and forced air convection dominated the solution strategy. In the last decade, this scenario is again being challenged as outlined before. As a result, several new techniques have emerged. Table 1-1 below summarizes the electronic thermal management strategies [Kakac, 1994; Lin et al., 2002]:

Table 1-1: Summary of electronic cooling methods

Single-phase Technology	Two-phase Technology	Special Technology
Natural convection (air or liquid) Forced convection (air or liquid)	Pool boiling Falling film Liquid jet impingement/ Spray/mist cooling Flow boiling	Thermoelectric devices Heat pipes, various designs **Pulsating heat pipes**

A further distinction may be made between indirect cooling, in which the heat-dissipating electronic components are physically separated from the coolant, and direct cooling, for which the components come in direct contact with the coolant.

Natural convection: employing air is the classical and most convenient technique for thermal management. Alternatively, dielectric fluids, having better thermal properties than air, may be used to enhance the performance. The principal heat transfer mechanism involves thermally induced buoyancy driven flow and hence no pump etc. is required. Thus,

cooling is achieved in a noise and vibration free environment. However, relative to forced convection, natural convection is characterized by much larger thermal resistances. Possible heat fluxes for a prescribed temperature are also quite low. Even if a typical chip were immersed in a dielectric liquid, maximum allowable heat flux for a temperature limit of 85°C would only be about 1 W/cm² under natural convective conditions. To exceed this limit in a passive cooling system, some form of heat transfer enhancement, e.g. plate or pin fins, must be implemented. Typical heat transfer coefficients for natural convection with air range from 5-12 W/m²K, while about 200-500 W/m²K is achievable with fluoro-chemical dielectric liquids (refer Figure 1-7) [Cengel, 1998]. Typically, this option is attractive due to its simplicity, low cost and reliability [Kakac, 1994].

Forced convection: cooling techniques can enhance the heat transfer coefficient by a factor ranging from 5-12 as compared to cooling by natural circulation depending on the configuration [Moffat, 1988]. An additional fan/pump, with related circuitry, is required which affects the cost, reliability, acoustic levels, ease of operation etc. For long, air has been the preferred fluid for cooling electronic packages ranging from PCBs to multi-chip modules. Although low cost, easy availability, reliability and simplicity are advantageous, relative to liquids, the thermophysical properties of air render it less attractive. Its comparatively low Prandtl number diminishes its efficacy for convective transport. In addition, the thermal capacitance is low because of low density and specific heat. Comparatively, liquids have superior thermal properties and are hence better suited for forced convection techniques. However, liquid cooling comes with its own risks and potential problems, such as leakage, corrosion, extra weight, condensation etc. While water may be employed for indirect cooling, use of dielectric fluids is mandatory for direct cooling options.

Pool boiling: with dielectric fluids is the simplest example of phase change electronic cooling techniques. The essence of two-phase cooling is the fact that high heat transfer rates

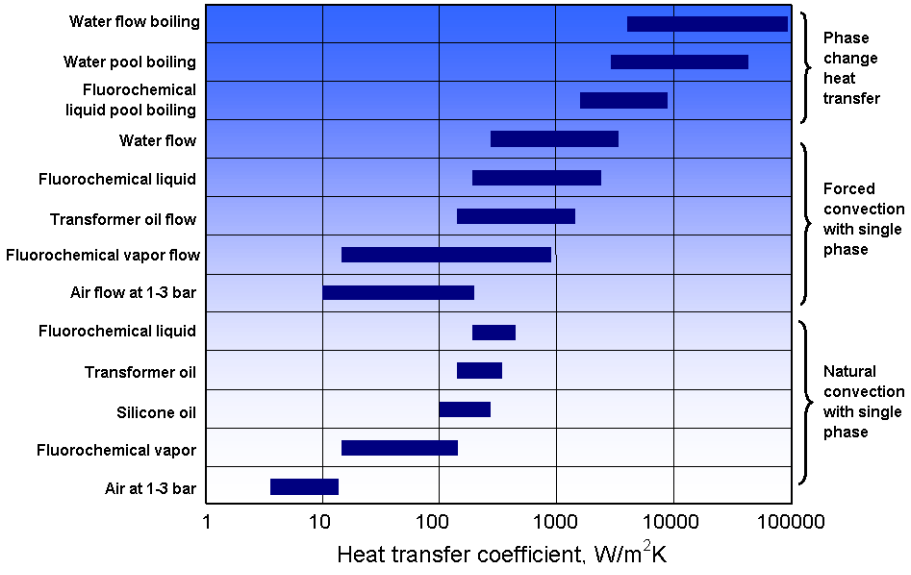

Figure 1-7: Achievable range of heat transfer coefficients by various cooling technologies

can be achieved with relatively very low wall superheat. The heat transfer coefficient is about 10-50 times higher than that for a single phase forced convection with the same working fluid [Chu, 1999]. Pool boiling technique is limited in application due to space constraints. The critical heat flux imposes a higher limit to the cooling capacity.

Falling film cooling is achieved by gravity driven flow of coolant passing over a vertical/inclined hot surface or chip assembly. Boiling is induced to enhance performance. Although this technique has demonstrated higher CHF than pool boiling, due to various constraints, it is not very popular. Some major limitations include space and support system requirements, lack of versatility and uncontrolled cooling [Grimley et al., 1988].

Liquid jet impingement involves jets of liquid coolant passing over the heated surface providing an extremely effective means of dissipating large heat fluxes at low operating temperatures. The design may involve solely single-phase jets or alternatively surface boiling may be induced achieving very high heat fluxes of the order of 70 W/cm^2. The impinging jet forms a very thin hydrodynamic and thermal boundary layer and heat transfer coefficients of the order of 10^4 W/m^2K have been obtained for single-phase jets [Incropera, 1999]. The performance is affected by jet geometry, flow Reynolds number, presence of confinement walls and distance between the jet and the dissipating heated chips [Vader et al., 1995; Chrysler et al., 1995]. However, the need of a re-circulation loop, control of jet velocity, possibility of surface erosion and nozzle obstruction are some of the major disadvantages. Another variation of jet impingement to achieve a more uniform temperature distribution and to avoid surface erosion is to use spray/mist cooling. A much slower stream of coolant is applied and continuous formation and evaporation of a thin liquid film is achieved.

Thermoelectric devices are based on the Peltier effect which explains the development of a temperature gradient across two joined dissimilar materials when a DC current is applied across them. Although the thermoelectric phenomenon is known since over 150 years, the practical applications were limited by the availability of suitable materials. Later, development of typical semiconductor materials like Bi_2Te_3 (Bismuth-Telluride) made it possible to attain temperatures below the ambient. Thermoelectric coolers have the advantage of being compact, quiet, free of moving parts and easy to control. Major disadvantages include low flux handling capacity coupled with low coefficient of performance, material costs and additional consumption of power. These factors have generally limited thermoelectrics to specialized niche applications characterized by low heat flux applications [Simons, 2000; Riffat and Ma, 2003].

Flow Boiling in microchannels involves a liquid coolant being pumped through an array of microchannels which can be attached to hot surfaces. Boiling occurs in the microchannels and high CHFs, of the order of 100 W/cm^2 or even more, can be achieved [Bowers and Mudawar, 1994]. A closed loop containing an evaporator with microchannels, a micropump and a condenser, usually employing water, can be very compact and relatively inexpensive [Lin et al., 2002]. This technology forms part of the emerging trends and major emphasis is given to research and development in this area of boiling heat transfer.

1.2 Conventional Heat Pipes

Heat pipes, due to their unique physical features, operational characteristics and applications, deserve a special mention in the field of microelectronics thermal management (Figure 1-8). Historical development of heat pipes dates back to 1942 when the first patent for a heat pipe employing a capillary wick for pumping liquid against gravity was applied by Gaugler [1942]. In the words of Grover [1963, 1964], who along with his co-workers reinvented the 'heat pipe' in 1963, a heat pipe is a "«... synergistic engineering structure which is equivalent to a material having a thermal conductivity greatly exceeding that of any known metal...»". In other words, a heat pipe is a passive two-phase heat transfer device capable of transferring large quantities of heat with a minimal temperature drop.

In the light of the present work, the basic understanding of the conventional heat pipe concept is of primary importance. It will be demonstrated in subsequent chapters how a CLPHP is not a 'true heat pipe' in the generally accepted sense. The association of the words 'heat pipe' with the present study is, in fact, a misnomer; incidentally, this is one of the results of the present study. A more appropriate name for the range of devices under study could be 'interconnected closed loop array of mini bubble pumps'. These and related aspects will be highlighted later in subsequent chapters.

1.2.1 Operating mechanism

In general, typical heat pipes utilize the continuous evaporation/condensation of a suitable working fluid for two-phase heat transport utilizing latent heat of vaporization in a closed system. As shown in Figure 1-8, a heat pipe consists of three sections: (1) evaporator,

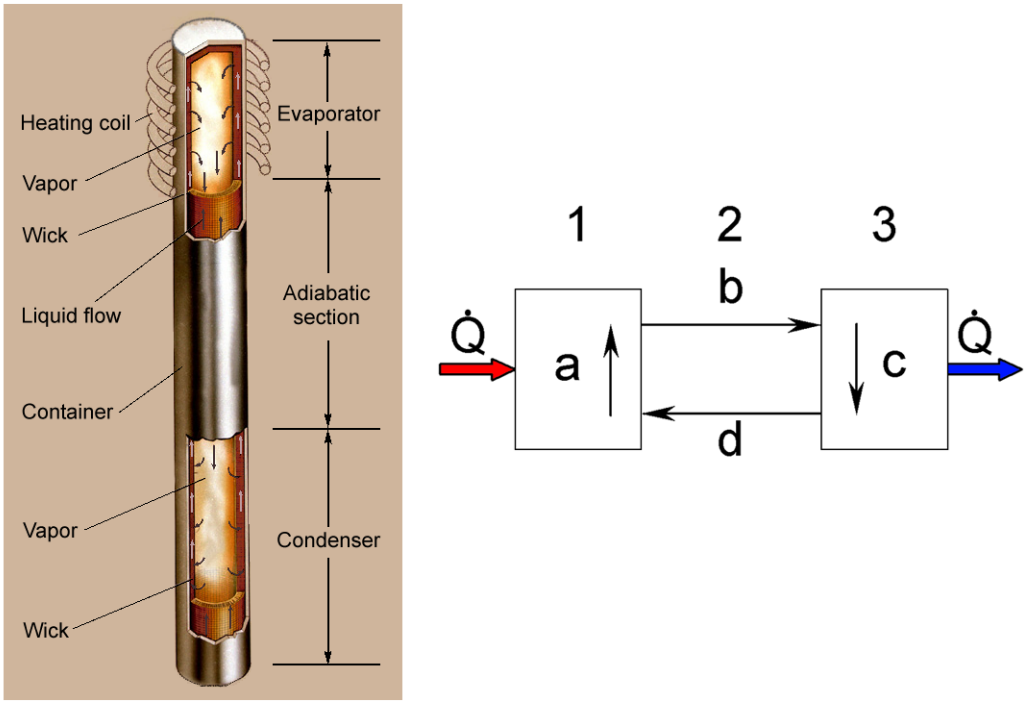

Figure 1-8: A conventional heat pipe and its transport processes [Reid et al., 1990]

(2) adiabatic section and (3) condenser. Heat (Q) is added to the evaporator section (1) and thereby the working fluid, which is in equilibrium with its own vapor, is vaporized (a). Driven by the small pressure difference between the hot evaporator section and the cold condenser section, the vapor flows (b) to the condenser section (3) and is condensed there (c). During the phase changes, the fluid takes up or releases, respectively, latent heat of vaporization/condensation. The liquid returns through the capillary structure from the condenser to the evaporator driven by capillary forces (d). By virtue of capillary pumping action, the heat pipe can be operated in a micro gravity field (as in satellites) or against gravity (on the ground with the evaporator above the condenser).

The components of a conventional heat pipe, as shown in Figure 1-8 are:

- a container, usually made of metal; glass and ceramics can also be employed,
- a small amount of working fluid, depending on the temperature range (4K to 2200K) and,
- a wick structure, made of sintered metal powders, screens or grooves; woven fiberglass or metals; metal and carbon fibers can also be employed.

The conventional heat pipe dimensions range from a few centimeters in length and millimeters in diameter up to lengths of more than 10 meters and diameters of the order of many centimeters. Since a wick structure is used to transport the fluid from the condenser to the evaporator and the most significant performance limitation is the capillary limit, for high performance applications, complex wick designs have been developed. Other limitations include the viscous, the sonic, the entrainment and the boiling limit.

Some of the limitations can be avoided or the operating range of the device can be widened by using design variations such as Capillary Pumped Loops (CPLs) or Loop Heat Pipes (LHPs). Like a conventional heat pipe, a LHP utilizes capillary action to circulate the working fluid in a closed loop by the action of the input heat. Hence, a LHP also contains no mechanical moving parts nor any electrical power for operation. But in contrast to a heat pipe, the wick structure of a LHP is confined only to the evaporator section as shown in Figure 1-9 a. The LHP design thus allows vapor and liquid to flow in separate smooth wall pipes, greatly reducing the dissipative losses. For these and other reasons, LHPs are thermally a better option than conventional heat pipes and have demonstrated reliability and robustness in both ground and micro gravity applications. Currently, miniaturization of LHPs is at the forefront of an extensive research and development to provide cooling solutions to the high heat load/ flux problems of advanced electronics packaging. If the heat pipe is operated in the gravity field with the evaporator below the condenser, the external body force field can be utilized to drive the condensate back to the evaporator and therefore no capillary structure may be necessary. Such devices are called closed two-phase thermosyphons as shown in Figure 1-9 b.

A large spectrum of literature on the topic is available in text books [Chi, 1976; Ivanovskii, 1982; Dunn and Reay, 1982; Peterson, 1994; Faghri, 1995] and in the proceedings of International Heat Transfer Conferences and Symposia.

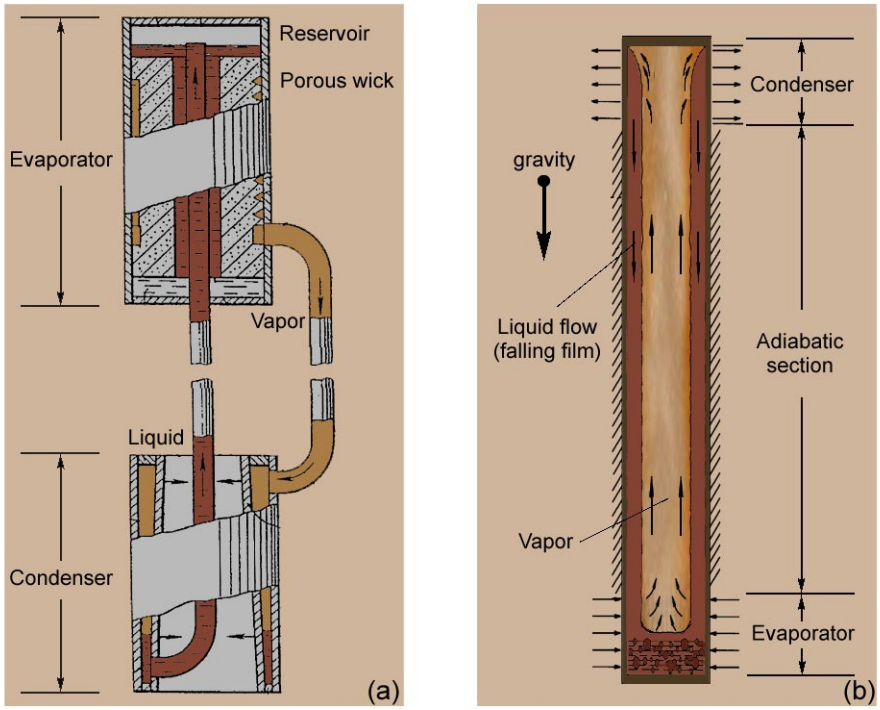

Figure 1-9: Schematic of (a) a loop heat pipe [Maidanik et al., 1985] (b) gravity assisted thermosyphon [Faghri, 1995]

1.2.2 Micro Heat Pipes

Stringent cooling requirements posed by the electronics industry concerning miniaturization and higher heat fluxes led to the conceptual introduction of a micro heat pipe by Cotter [1984]. Micro heat pipes are very small, wickless heat pipes having internal geometries containing sharp angled corner regions responsible for generating the required capillary pressure and which serve as liquid arteries (Figure 1-10). There are two supplementary definitions of a micro heat pipe. According to the original definition of Cotter [1984], the hydraulic radius of a micro heat pipe is of the order of (greater than or equal to) the capillary radius of the vapor-liquid interface. The additional definition of Chen et al. [1992] reflects not only the geometry, but also the physical behavior and defines a heat pipe as 'micro' if the Bond number, $Bo \leq 2$. Typical cross sectional dimensions of micro heat pipes range from some 10 to some 100 μm with heat transport capabilities of some 1/100 to some 1/10 W [Itoh and Polášek, 1990]. It is emphasized that a sizable volume of the so-called 'micro' heat pipes reported in the literature does not represent the true 'micro' heat pipes as defined above. There exist various hybrid and transitional heat pipe designs in the 'meso' or 'mini' range which are frequently misnamed. Examples are the copper-water conventional heat pipes with typical outside diameters of 2.5 to 4 mm, which are routinely employed, for example, in cooling the CPUs in laptop computers. A performance comparison of such 'mini' heat pipes with CLPHPs having similar tube geometry will be done later in the study.

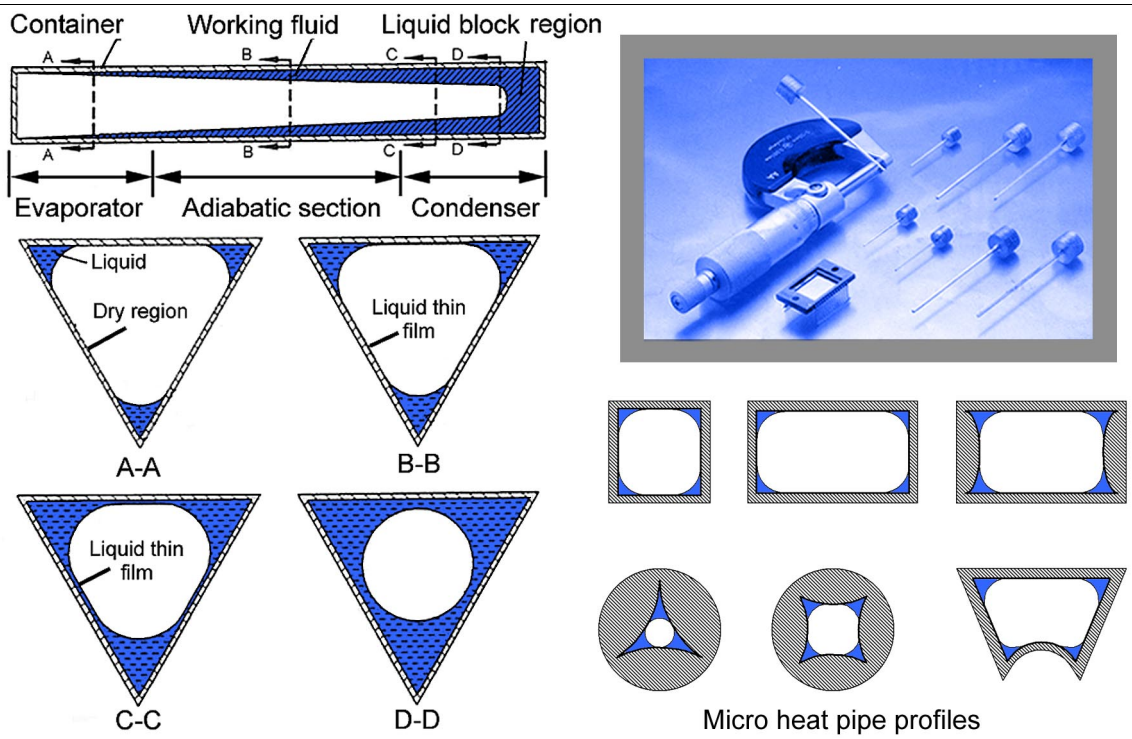

Figure 1-10: Micro heat pipes [Groll and Khandekar, 2002]

1.3 Pulsating Heat Pipes

All the family of structures similar in phenomenological and thermofluidynamic operation to the structure as depicted in Figure 1-5 will be henceforth referred to as Pulsating Heat Pipes (PHP). These structures are characterized by the following basic features:

(a) The structure is made of a meandering tube of capillary dimensions with many turns, filled partially with a suitable working fluid. This tube may be either:

- Open Loop: tube ends are not connected to each other.
- Closed Loop: tube ends are connected to each other in an endless loop.

(b) There is no internal wick structure as in conventional heat pipes.

(c) At least one heat-receiving (evaporator/heater) zone is present.

(d) At least one heat-dissipating (condenser/cooler) zone is present.

(e) There can be an optional adiabatic section between evaporator and condenser zone.

The device is first evacuated and then filled partially with a working fluid, which distributes itself naturally in the form of liquid-vapor plugs and bubbles inside the capillary tube. There is no external control over the initial plug/bubble distribution inside the tube. One end of this tube bundle receives heat transferring it to the other end by a pulsating action of the liquid-vapor system. A PHP is essentially a non-equilibrium heat transfer device driven by complex combination of various types of two-phase flow instabilities. The performance success primarily depends on the continuous maintenance or sustenance of these non-equilibrium conditions within the system. The liquid plugs and vapour bubbles are

transported because of the pressure pulsations caused inside the system. The construction of the device inherently ensures that no external mechanical power source is needed for the fluid transport. The driving pressure pulsations are fully thermally driven.

Although many of the arguments and discussions that follow in this chapter and thereafter throughout the text apply to both open and closed loop systems, attention is primarily focussed only on CLPHPs, the principal candidate of present scrutiny.

1.3.1 Operating mechanism

Consider a case when a CLPHP is kept completely isothermal, say at room temperature. In this case, the liquid and the vapour phases inside the device must exist in equilibrium at the saturation pressure corresponding to the fixed temperature. Referring to the pressure-enthalpy diagram, Figure 1-11, the thermodynamic state of all the liquid plugs, irrespective of their size and position, can be represented by point-A. Similarly point-B represents the thermodynamic state of all the vapour bubbles present in the PHP. Suppose the temperature of the entire CLPHP structure is now quasi-statically increased to a new constant value, then the system will again come to a new equilibrium temperature and corresponding saturation pressure, points A' and B' in Figure 1-11. In doing so, there will be some evaporation mass transfer from the liquid until equilibrium is reached again. A similar phenomenon will be observed if the system is quasi-statically cooled to new equilibrium conditions A" and B" (exaggerated representation for clarity).

An actual working CLPHP is not isothermal; there exists a temperature gradient between the evaporator and the condenser section. Temperature differences also exist amongst the 'U' bends within the evaporator and the condenser due to local non-uniform heat transfer rates that are always expected in real systems. The net effect of all these temperature gradients within the system is to cause non-equilibrium pressure conditions that, as stated earlier, are

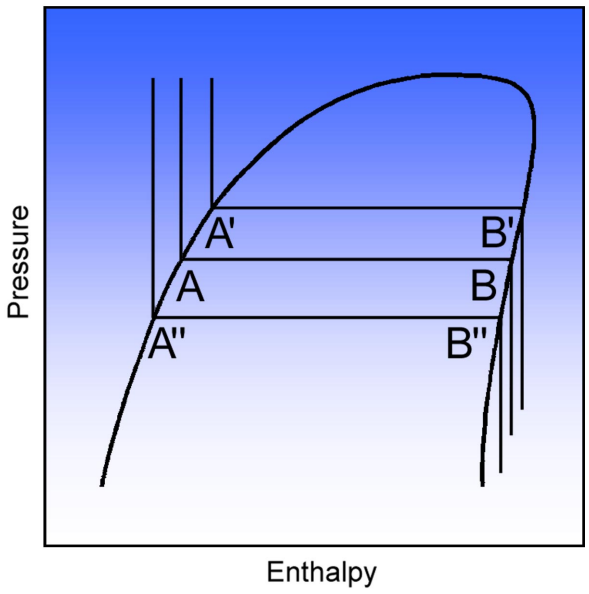

Figure 1-11: Typical pressure-enthalpy diagram of a pure working fluid

the primary driving force for the thermofluidic transport. This leads to thermally driven two-phase flow instabilities. The heating process in the evaporator continuously tries to push the point-A upwards on the liquid saturation line of the pressure-enthalpy diagram. Simultaneously the point-B is forced to move downwards on the vapour line. In this way, a sustained non-equilibrium state exists between the driving thermal potentials and the natural causality that tries to equalize the pressure in the system. Further, inherent perturbations are always present in real systems. These perturbations are due to:

- Pressure fluctuations within the evaporator and condenser tube sections due to local non uniform heating and cooling,
- Unsymmetrical liquid-vapour distributions causing uneven void fraction in the tubes, and
- Presence of an approximately triangular or saw-tooth alternating component of pressure drop superimposed on the average pressure gradient in a capillary slug flow due to the presence of vapour bubbles [Wallis, 1969]

Thus, a self-sustained thermally driven oscillating flow is obtained in a CLPHP.

1.3.2 Other salient operational features

Before attempting a detailed explanation of CLPHP characteristics, it is worthwhile to consider the fundamental processes that occur in the device operation. Figure 1-12 suggests the various forces including heat and mass transfer processes acting on a typical liquid-plug vapor-bubble system as formed in the CLPHP. It is emphasized that scrutinizing the same control volume on a micro scale will, in general, manifest much more complicated molecular

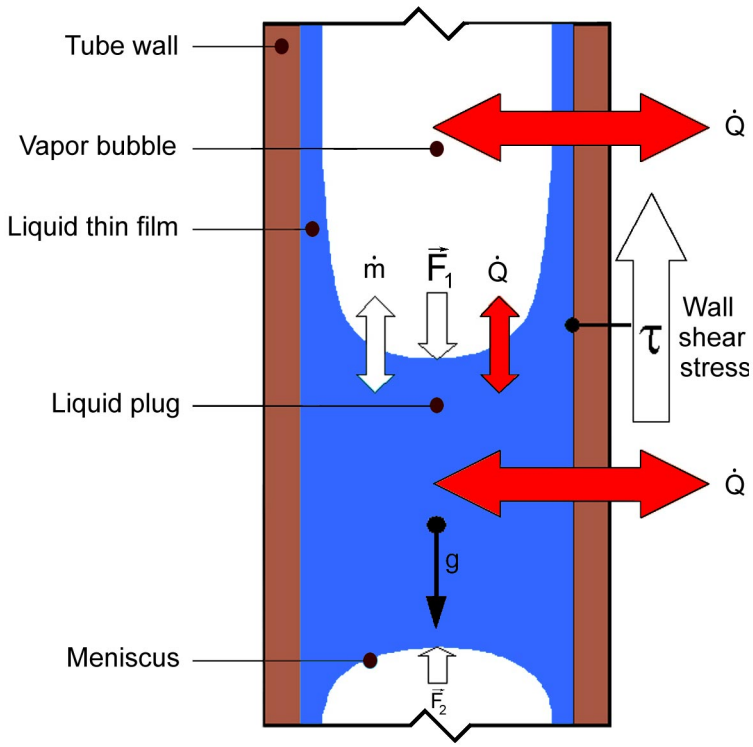

Figure 1-12: Forces acting on a typical slug-bubble system

forces and heat and mass transfer processes than what has been depicted in Figure 1-12. Such a system will be too complicated and impractical for analysis. Therefore, only the primary processes have been summarized below:

- The flow pattern in the CLPHP tubes may be broadly categorized as capillary slug flow. This type of flow is characterized by [Suo and Griffith, 1964; Fukano and Kariyasaki, 1993]: (a) the flow pattern is axisymmetric and, (b) the velocity of large vapour bubbles relative to the liquid plug is somewhat faster.
- Due to the capillary dimensions of the CLPHP tube, liquid plugs having menisci on the plug edges are formed due to surface tension forces. A liquid thin film may also exist surrounding the vapour bubble. The angle of contact of the menisci, the liquid thin film stability and its thickness depend on the fluid-solid combination and the selected operating parameters. These interfacial effects seem also to be important as demonstrated by experimental studies of this research.
- Although surface tension forces predominate, the liquid plugs and vapour bubbles move against the gravity vector, in its direction or at an angle to it depending on the global orientation of the PHP and the location of the plugs and bubbles in the up-header or down-header tubes. The extent of the effect of gravity on PHP operation is highlighted later through the experimental results.
- The liquid plugs and vapor bubbles are subjected to pressure forces from the adjoining plugs/bubbles, e.g. in the configuration shown in Figure 1-12, the forces $\vec{F}_1$ and $\vec{F}_2$, acting on the depicted liquid plug, are caused due to the capillary pressures created by the menisci curvatures of the adjacent vapor bubbles.
- The liquid plugs and vapour bubbles experience internal viscous dissipation as well as wall shear stress as they move in the CLPHP tube. The relative magnitude of these forces will decide the predominant force to be considered.
- The liquid plugs and vapour bubbles may receive heat, reject heat or move without any external heat transfer depending on their location in the evaporator, condenser or the bridging adiabatic section, respectively.
- In the evaporator, the liquid plug receives heat which is simultaneously followed by evaporation mass transfer to the adjoining vapour bubbles or breaking up of the liquid plug itself with creation of new bubbles in between as a result of nucleate boiling in the slug flow regime. The saturation pressure and temperature thus increase locally.
- Probability of events frequently places vapour bubbles in direct contact with the internal tube surface of the evaporator. In this case, saturated vapour bubbles receive heat via the liquid thin film surrounding them, which is simultaneously followed up by evaporation mass transfer from the film as well as the adjoining liquid plugs. Depending on the respective 'celerity' of heat and mass transfer, coupled to the fact that the complete system is isochoric which leads to 'constant-volume heat addition', the instantaneous local saturation pressure and temperature increase. This aspect will be further clarified in the coming chapters.

- The above processes, as described for the evaporator, are repeated in a reverse direction in the condenser.
- In the adiabatic section, while passing from the evaporator to the condenser, the train of vapor bubbles and liquid plugs is subjected to a series of complex heat and mass transfer processes. Essentially non-equilibrium conditions exist whereby the high pressure, high temperature saturated liquid plugs/vapor bubbles are brought down to low pressure, low temperature saturated conditions existing in the condenser. If ideal adiabatic conditions are maintained, with no axial conduction of heat through the tube wall and through the fluid itself, then an inherently irreversible isenthalpic process can accomplish this task. Internal enthalpy balancing in the form of latent heat takes place by evaporation mass transfer from the liquid plugs to the vapour bubbles whereby saturation conditions are always imposed on the system during the bulk transit in the adiabatic section. In real systems, this transit is certainly much more complex with non-equilibrium metastable conditions existing throughout.

It is to be noted that there occurs no 'classical steady state' in CLPHP operation as far as the internal hydrodynamics is concerned. Instead, pressure waves and pulsations are generated in each of the individual tubes, which interact with each other possibly generating secondary and ternary reflections with perturbations. The self-exited thermally driven oscillations seem to be dependent on a plethora of variables. An attempt has been made in this study to recognize, evaluate and assess the relative importance of the major influence parameters.

1.4 Closure

The semi-conductor technology is changing the face of the world in an unprecedented manner. Thermal management of electronics is the elixir to transform dreams and imaginations of the designers into reality. In this light, the chapter introduced the motivation and need for research in the development of novel cooling strategies for modern day electronics. Pulsating heat pipes have emerged as extremely suitable candidates for this very cause; research impetus on this contemporary topic of research cannot be overemphasized. With this brief introduction, attention will now be focussed on the review of available literature on the subject. A state of the art on both experimental studies and mathematical analysis of pulsating heat pipes will be presented in the next chapter.

CHAPTER 2

LITERATURE REVIEW

2.1 Historical perspective

'Drinking or Dunking Duck', the popular toy which has amused generations of children may be the 'Neanderthal', symbolizing a vital link in the evolutionary chain of modern pulsating heat pipes. The details of the toy are shown in Figure 2-1. While most of the children playing with the toy (and their parents!) are unaware of the technical nuances of its operation, the kernel of two-phase physics and associated thermo-mechanical interactions are inherent in the design. The bird's body is usually made up of a glass tube with a bulb on one end (the bird's head), a tube extending into another glass bulb at the lower end making up the tail/buttocks. The whole device, an isochoric system, is partially filled with a volatile working fluid (generally Methylene Chloride, boiling point ≈ 40°C). When the bird is upright, the vapor in the head does not connect with that in the tail section (refer Figure 2-1). The evaporative mass transfer of water from the wet beak/mouth end (aided by the oscillating

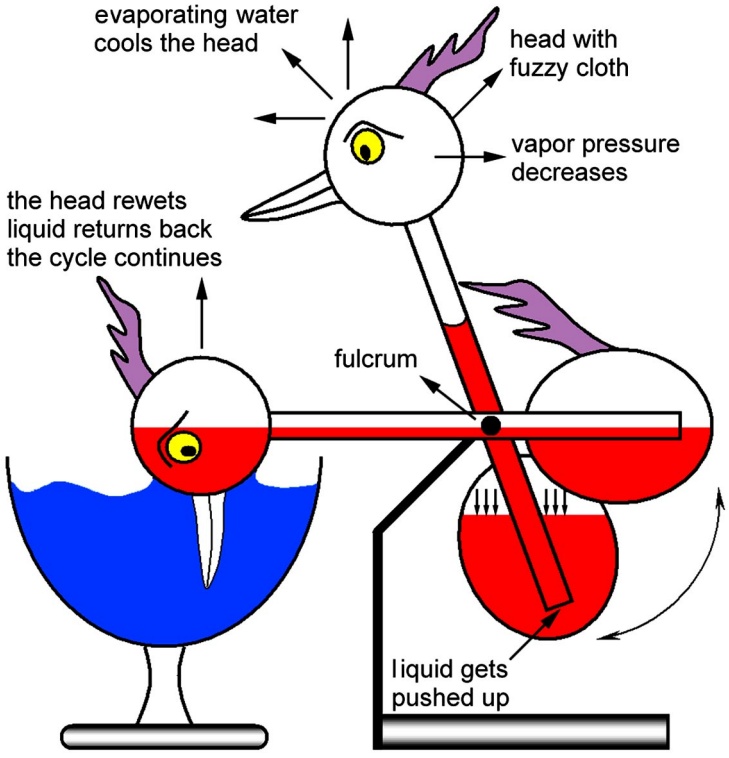

Figure 2-1: Schematic of a 'Dunking Bird'

motion), generates a low vapor pressure inside. The working fluid thus gets pushed up in the neck disturbing the mechanical dynamic equilibrium vis-à-vis the position of the fulcrum. A time comes when the mouth end weighs more than the tail end because of liquid accumulation and the duck starts 'drinking' water again (to rewet the fuzzy cloth attached at the beak!). In this horizontal position, the two vapor pockets are connected so that the liquid in the body can flow freely. All the liquid is pulled back by gravity again to the tail bulb. As an upward vapor pressure difference builds up again due to evaporation of water from the mouth end, the liquid will rise up and the cycle thus continues. This toy is a classic example of a closed passive two-phase system in which the primary objective is to generate 'sustained mechanical oscillations' through heat transfer. It is to be noted that the total mass inventory of liquid and vapor phases remains constant throughout the operation.

While it is difficult to trace the origin of the 'drinking duck', a more formal presentation of an analogous concept is contained in a patent filed in the former USSR [Smyrnov and Savchenkov, 1975]. The conceptual details, as shown in Figure 2-2, consist of an evaporator and a condenser bulb, connected by a tube. At the beginning of the operation the evaporator end and the connecting tube are completely filled with the working fluid while the condenser end is partially filled, the rest being a passive, non-participating gas, as shown. Heating at the evaporator end expands the working fluid and pushes it into the condenser. Further heating generates vapor in the evaporator bulb and pushes the liquid further in the condenser, thereby compressing the trapped passive gas. Simultaneously, the vapor also starts being condensed at the inner surface of connecting tube thereby reducing the pressure locally. In addition, the passive gas is compressed substantially by this stage. Depending on the instantaneous pressure (mal)-distribution in various subsections, the potential energy stored in the passive gas will, at some stage, push the liquid back to the evaporator. The cycle is thus repeated by sustained thermo-mechanical non-equilibrium generated by the closed passive two-phase system trapped in special isochoric geometry.

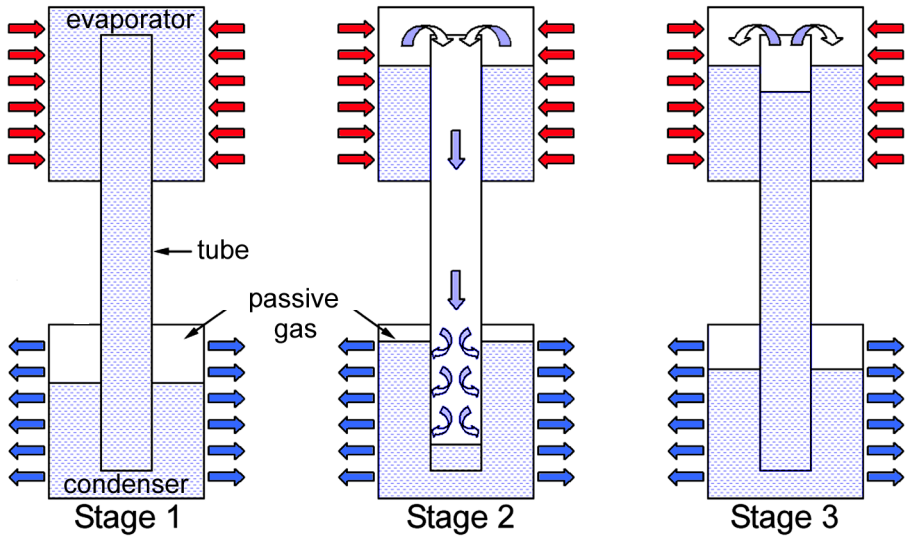

Figure 2-2: Details of the patent by Smyrnov and Savchenkov [1975]

With this brief introduction to the historical links, we venture into reviewing the contemporary literature pertaining to the modern form of pulsating heat pipes.

2.2 Literature review on pulsating heat pipes

While our area of interest lies in the two-phase regime, it is worthwhile to mention briefly about relevant studies in pulsating/oscillating single phase flows. Experimental and numerical analyses of such flows require more stringent time and spatial resolutions, and therefore there exist fewer investigations of oscillatory flow heat/ mass transfer. In general, oscillatory flows can be grouped into two-categories: pulsating (modulated) and reciprocating (fully reversing) flows. Pulsating flows are always unidirectional and can be decomposed into steady and unsteady components. For reciprocating flows, the flow direction cyclically changes. Hence these flows convect zero net mass flow. Fundamental and applied studies on pulsating and reciprocating single phase flows have been performed among others by Siegel and Pearlmutter [1962], Kurzweg and Zhao [1984], Zhao and Cheng [1995] and more recently by Sert and Beskok [2003].

2.2.1 Experimental studies

Although the fundamental aspect of a 'Pulsating Heat Pipe' is contained in the patent by Smyrnov and Savchenkov [1975], the exploitation of the concept from an engineering point of view was done by Hisateru Akachi. Thus, the first examples of the family of modern PHPs appeared in 1990 [Akachi, 1990] as shown in Figure 2-3. In this patent, twenty-four different preferred embodiments of what is referred to as *Loop Type Heat Pipe* were described. All the proposed structures were characterized by the presence of at least one non-return flow check valve integrated in the tubes for imposing a preferred flow direction. The typical tube inner diameters employed were 2.0 mm or more, always ensuring that the inner diameter is below

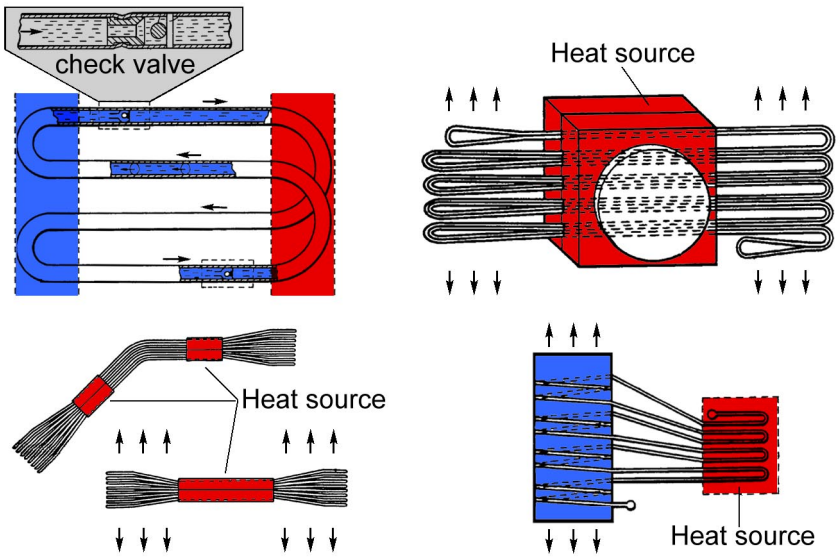

Figure 2-3: Loop type heat pipe and its different design variations [Akachi, 1990]

a maximum permissible value, D_{crit} (refer Section 4.1.2). These loop-type heat pipes were claimed to overcome some of the shortcomings of the conventional heat pipes. Typical representative values of thermal resistance ranged from 0.082 to 0.233 K/W for water and 0.077 to 0.189 K/W for R-11, in the power range of 920 to 310 W, R-11 filled heat pipes operating better in all cases. It was also claimed that working fluids, which are unsuitable for conventional heat pipes, might be used in the loop-type heat pipes with comparable or even better performance. It was also highlighted that fluids having a large saturation pressure gradient coupled with a low dynamic viscosity were to be preferred as working fluids.

Long-term reliability issues of the flow check valves and their inability to deliver the desired results, if further miniaturization of the pipe cross section is done, lead to the development of loop type heat pipes without check valves [Akachi, 1993, 1996]. These structures, as shown in Figure 2-4, represent the true *Pulsating Heat Pipes* as referred to in this text. Open loop and closed loop structures, having internal tube diameters of the order of 1.0 mm, were proposed. Structures were fabricated with metallic tubes (ID 0.7 mm, OD 1.0 mm) and filled with R-142b. Experimental results for a power range of 5 to 90 W in top and bottom heating mode obtained an average thermal resistance from 0.64 to 1.16 K/W.

After these introductory patents, results of various experimental investigations on PHPs have appeared in the literature. A major source of information are the proceedings of the International Heat Pipe Conferences and International Heat Pipe Symposiums. The intriguing operational characteristics have led many researchers to undertake visualization and flow characterization. Qualitative results with emphasis on phenomenological understanding are presently more abundant than quantitative data. Various geometrical configurations of the PHP have also been proposed.

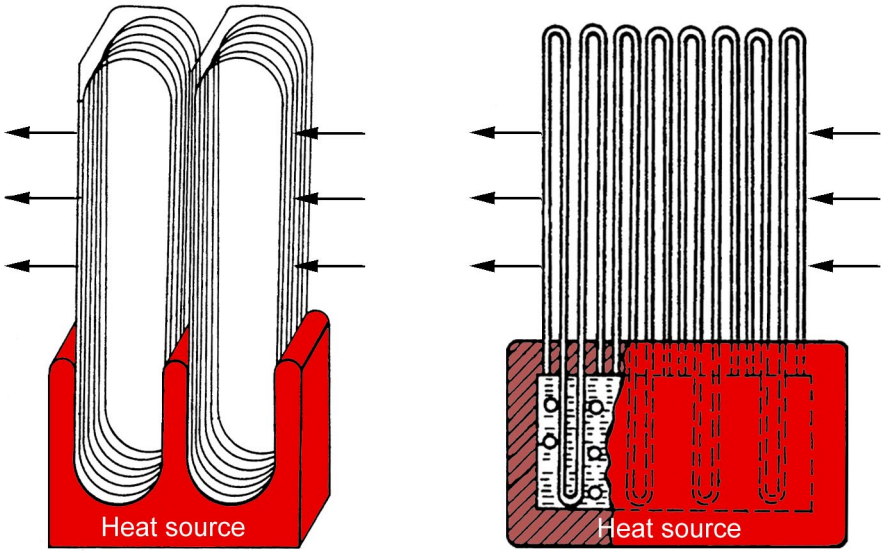

Figure 2-4: Pulsating heat pipes as described by Akachi [1993, 1996]

Maezawa et al. [1995] studied an open loop PHP consisting of 20 turns of copper tube (ID 1.0 mm) of total length 24 meters. R-142b was used as the working fluid. Heat was supplied with flat electrical heaters sandwiched around the evaporator section and a water jacket was used in the condenser section. Filling ratio and inclination were varied and the typical results with the set-up are shown in Figure 2-5. Temperature fluctuations at the adiabatic wall section were also recorded.

Kawara et al. [1996] have undertaken a visualization study of an open loop PHP employing proton radiography for motion visualization (refer Figure 2-6) . A 20.0 mm proton beam was passed through the test section and converted to visible light by a fluorescent screen. The PHP was formed of rectangular grooves of 0.6 x 0.7 mm^2 in a 190 x 50 x 1.3 mm^3 base plate.

TS-Heatronics Ltd., Japan [Akachi et al. 1996; Akachi and Miyazaki, 1997; Akachi and Polášek, 1997] have developed a range of PHPs termed as 'HEATLANE' and 'KENZAN' fins (Figure 2-7 a, b) with material combinations such as stainless steel-liquid N2, copper with water, methanol, R-113 and R-142b and aluminum-R-142. Typical thermal resistance of about 0.3 K/W at an air cooling velocity of 3 m/s was obtained for KENZAN fins (outside dimensions 60.0 x 60.0 x 65.0 mm^3) fabricated from copper tubes (ID 0.7 mm, OD 1.0 mm) filled with R142b, having 152 turns and soldered to a copper base plate. Similar fin structures, as depicted in Figure 2-7 b, have been employed for MCM and IGBT cooling.

Maezawa et al. [1997] have tested another set of open loop PHPs with R-142b and water as the working fluid with a filling ratio of 50%. The heat pipes, both having 40 turns with a total length of 52.5 meters were made of copper tube of ID 2.0 mm and 1.0 mm respectively. Effect of diameter and working fluid was observed as shown in Figure 2-8. It can be seen that the performance for the bottom heat mode was better than the horizontal operation mode. In addition, poor performance for top heat mode was observed.

Hosoda et al. [1999] fabricated a CLPHP consisting of 10 turns with a glass tube having OD 4.0 mm and ID 2.4 mm. Water was used as the working fluid with a small amount of black ink added for visualization. The evaporator and condenser sections were enclosed in an acrylic box and supplied with hot water (varied from 55°C to 70°C) and cold water (30°C fixed). The adiabatic section was also enclosed and evacuated. Figure 2-9 shows the effect of heat throughput and filling ratio vs. temperature difference between the evaporator and condenser. The accuracy of measurements was not very high and so the data should be looked at as providing only quantitative trends.

During the course of the present research work also, studies on PHPs have been reported in the literature. Tong et al. [2001] have undertaken a visualization study using a charge coupled device (CCD) on a CLPHP having tubes of ID 1.8 mm and made of pyrex glass. It consisted of 10 turns and the distance from the evaporator to the condenser was 400.0 mm. The filing ratio was always 60%. The findings showed that uneven plug/bubble distribution and non-concurrent boiling at the evaporator contributed to the driving and restoring forces for fluid circulation/oscillations. In general, capillary slug flow was observed throughout the operation but bubbles smaller than the tube diameter were also observed. This study highlights the existence of a minimum critical heat flux to initiate sustained oscillations.

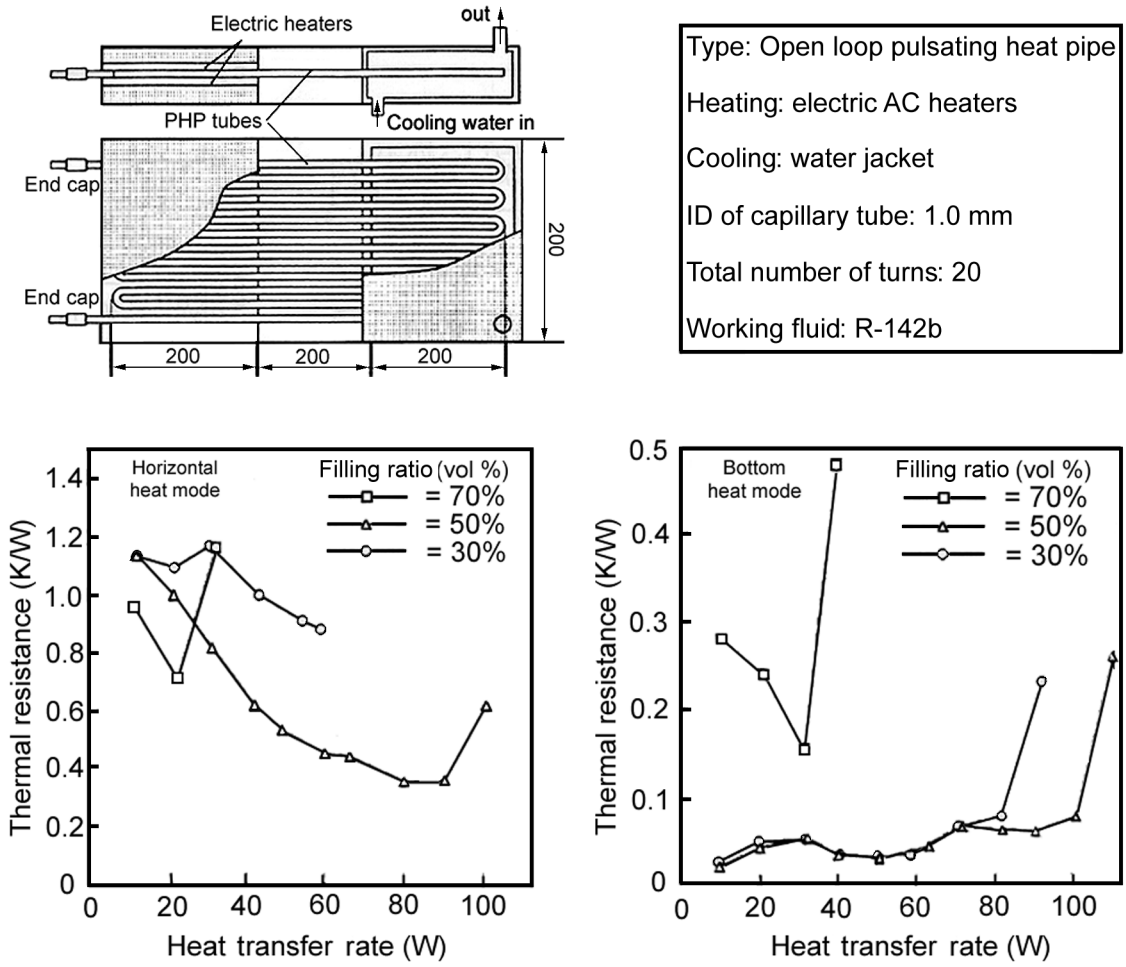

Figure 2-5: Experimental setup and typical results of Maezawa et al. [1995]

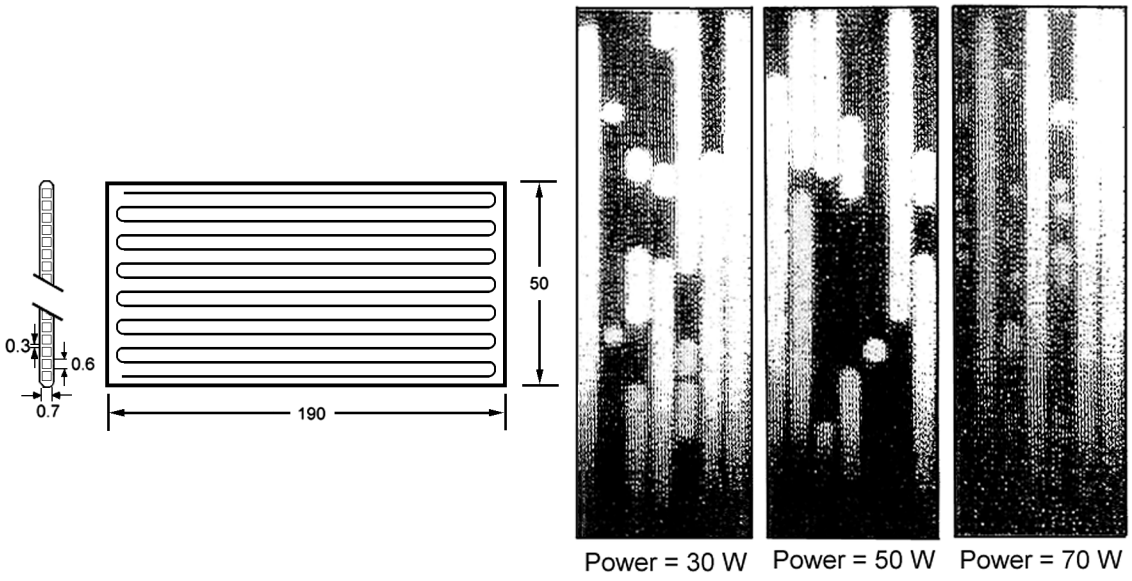

Figure 2-6: Experimental setup and radiographs of PHP by Kawara et al. [1996]

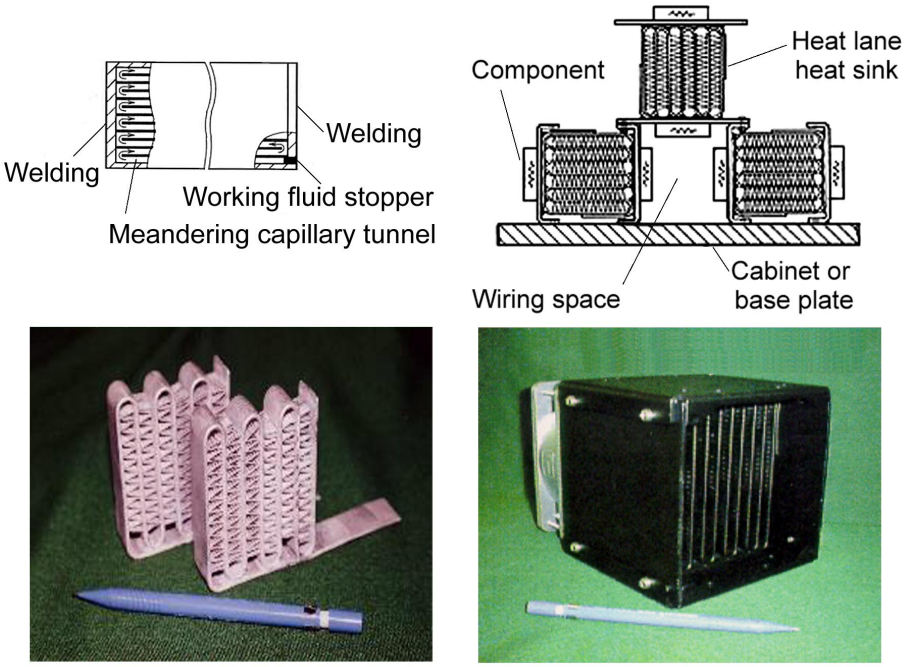

Figure 2-7: (a) Heat Lane heat pipes by Akachi et al. [1996]

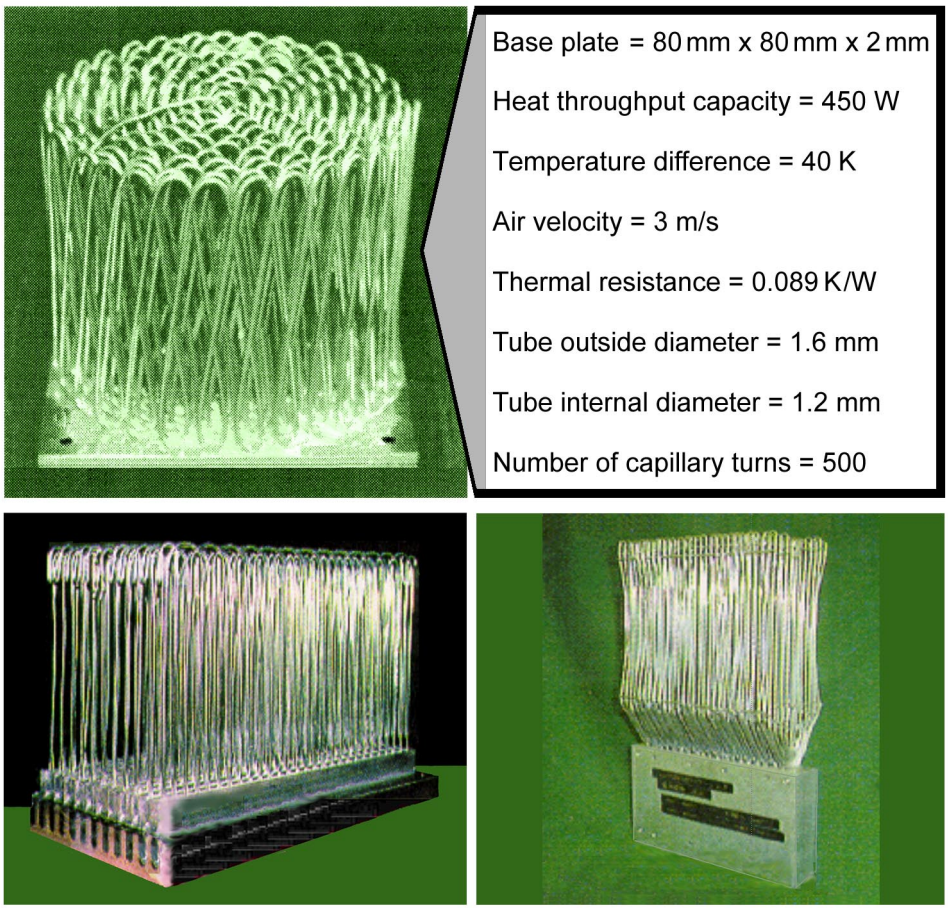

Figure 2-7: (b) Typical examples of Kenzan fins by Akachi et al. [1996]

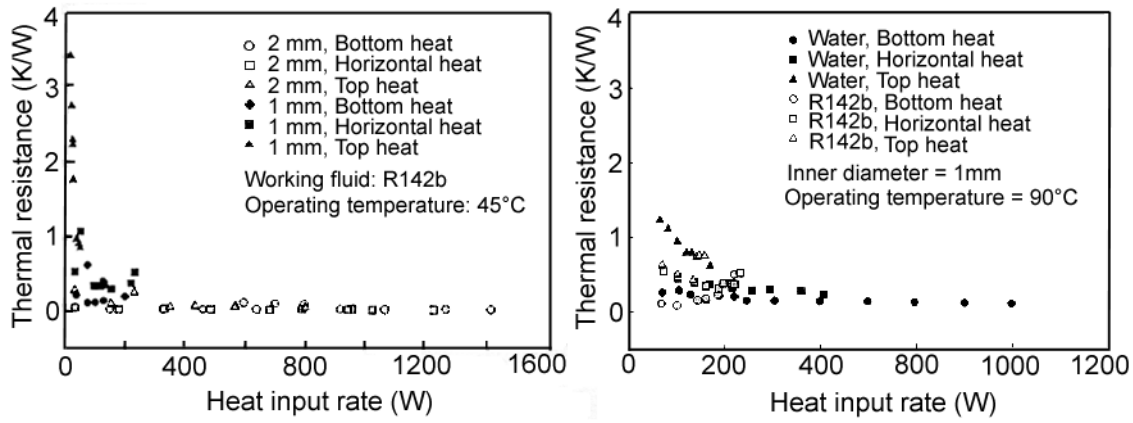

Figure 2-8: (a) Effect of tube diameter, (b) Effect of working fluid [Maezawa et al., 1997]

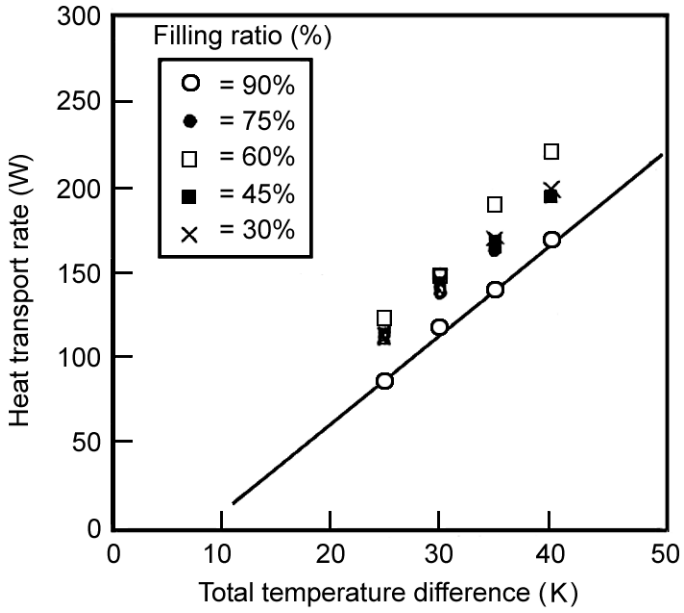

Figure 2-9: Performance characteristics as measured by Hosoda et al. [1999]

Qu and Ma [2002] have also undertaken detailed experimental study on a CLPHP having eight turns and made of copper and glass tube (ID 1.8 mm, OD 2.0 mm) alternatively placed to form a semi-visualization set-up. The effect of input power and angle of inclination on the flow pattern and thermal performance is reported. Capillary oscillating slug flow as well as net-circulation is reported depending on the applied power. Preliminary qualitative results also show that the presence of non-condensable gases affects the thermal performance. Incidentally, many of their observations compliment the findings of the present research.

In another contemporary study, Charoensawan [2003] has also reported results of copper CLPHPs with three working fluids (water, ethanol and R-123) and two internal diameters (2.0 mm and 1.0 mm). In all the experiments, the filling ratio was maintained at 50%. In these experiments, instead of controlling the input heat power, the evaporator and condenser

were always maintained at fixed temperatures by supplying water at 80°C and 20°C respectively. The net quasi steady state heat transfer under these conditions was recorded. In parallel, visualization in glass tube set-ups was also undertaken. The effect of internal diameter, inclination angle (from vertical heater down position to horizontal operation) and number of turns was determined. Figures 2-10 a, b summarize the thermal performance for the entire experimental matrix, with respect to the inclination angle. For a given case, the performance was scaled by the maximum performance achieved for that case during operation in the full range of inclination angles. It can be clearly seen that the performance dependence with orientation is affected by the number of turns. For D_i = 2.0 mm devices, the effect could be clearly separated into two cases by using a certain critical value of number of

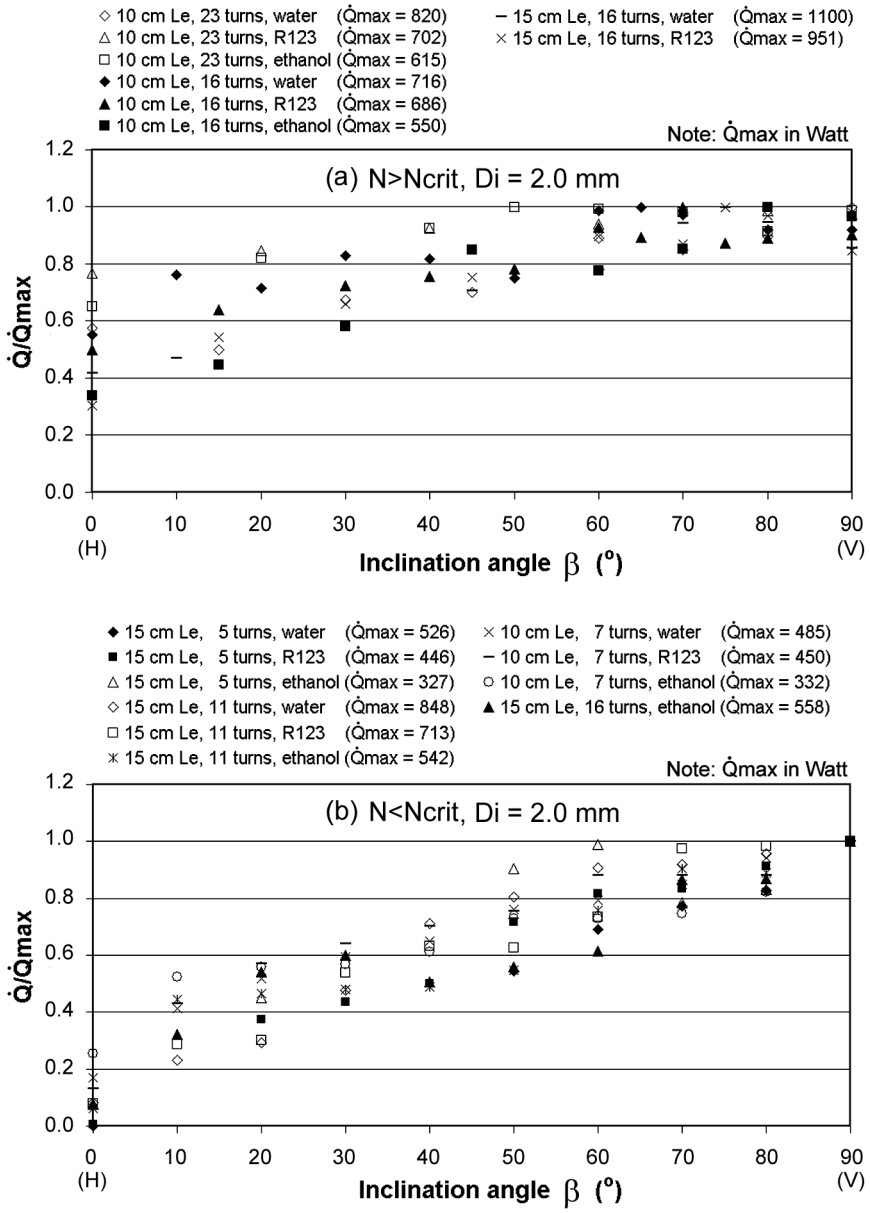

Figure 2-10 : (a) Experimental results by Charoensawan [2003], D_i = 2 mm

turns (N_{crit}). In this case, the critical number of turns was approximately 16 (with the exception of L_e = 15 cm, 16 turns and ethanol as working fluid). In case of D_i = 1.0 mm devices too, similar trends are seen as depicted in Figure 2-10 b. For this case, the critical value of number of turns tends to be higher than for 2.0 mm tubes. In addition, for 1.0 mm tubes, measurable heat transfer was not possible with water filled devices in the entire range of operating orientation. When N was more than a certain N_{crit}, the CLPHP could satisfactorily operate in the horizontal as well as vertical orientation. For $N < N_{crit}$, the highest thermal performance normally occurred at vertical bottom heating mode decreasing continuously as the device was turned towards horizontal. However, when the number of turns was higher than the critical value, although the performance improved with increasing the inclination angle from horizontal orientation, it remained nearly constant from about 60° up to vertical position. In the visualization study the existence of various flow patterns vis-à-vis inclination angle and the geometry of the device were observed.

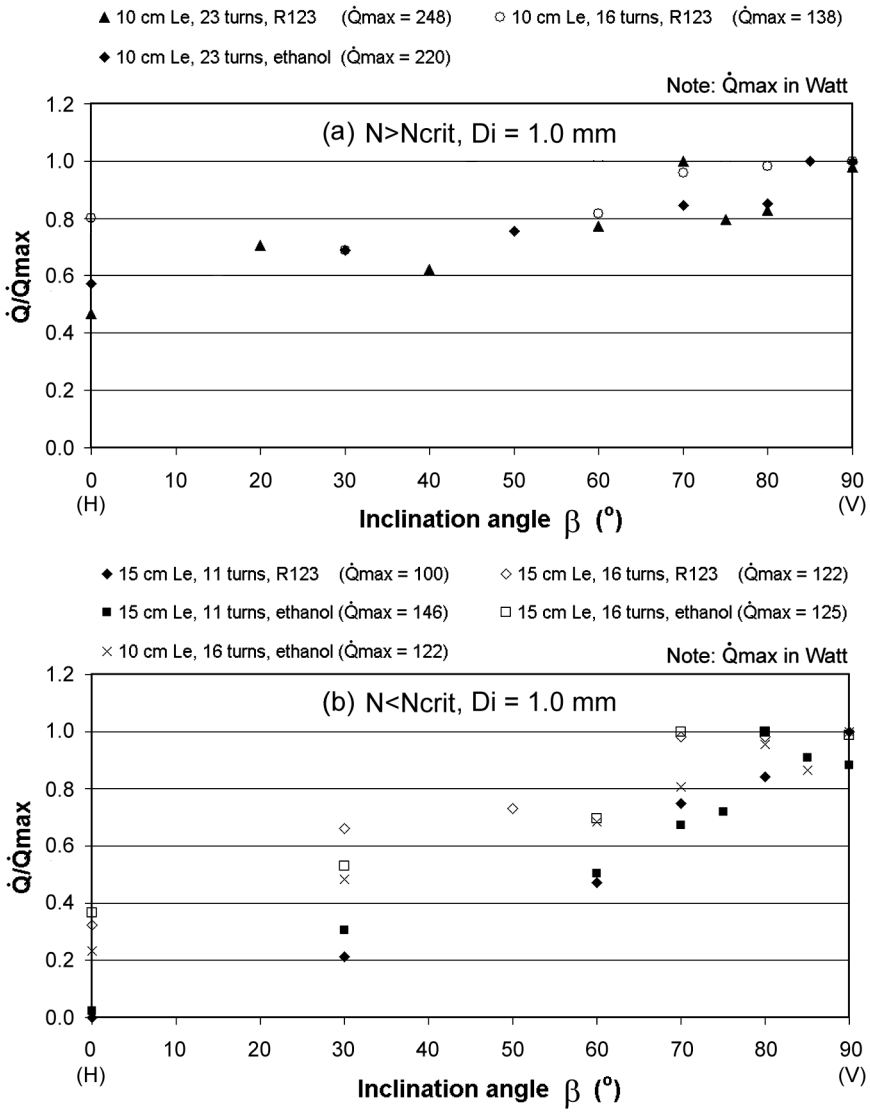

Figure 2-10 : (b) Experimental results by Charoensawan [2003], D_i = 1 mm

2.2.2 Mathematical modeling

Mathematical modeling and theoretical analysis of PHPs has been attempted in the recent past with many simplified approaches. The models which appeared so far in the literature may be categorized as per the simplification scheme adopted. These may be summarized as:

(a) comparing PHP action to equivalent single spring-mass-damper system [Zuo and North, 2000],

(b) kinematic analysis by a multiple spring-mass-damper system [Wong et al., 1999],

(c) applying fundamental equations of mass, momentum and energy conservation to specified PHP control volume [Swanepoel et al., 2000; Shafii et al., 2001; Zhang and Faghri, 2002] and,

(d) mathematical analysis highlighting the existence of chaos under some operating conditions [Maezawa et al., 1996, 2000].

Zuo and North [2000] have tried to model the pulsating action of a PHP by comparing the action to a single spring-mass-damper system represented by a second order homogeneous differential equation with time dependent spring constant. As can be seen from the proposed equation and its solution in Figure 2-11, even if the viscous damping is force is made equal to zero, the nature of the equation suggests that the spring stiffness coefficient is increasing with time for the entire range of the filling ratios. Thus, the amplitude of oscillations has to decrease which contradicts the results that are presented. Further, while second order differential equations represent oscillating systems, a non-homogeneous system of equations with a driving force term is required to sustain the oscillations in the presence of viscous damping. There is also no inherent back up system in the model, which accounts for the replenishment of the evaporating fluid. This oversimplified model has very limited applicability especially when compared to the experimental evidences of the flow patterns

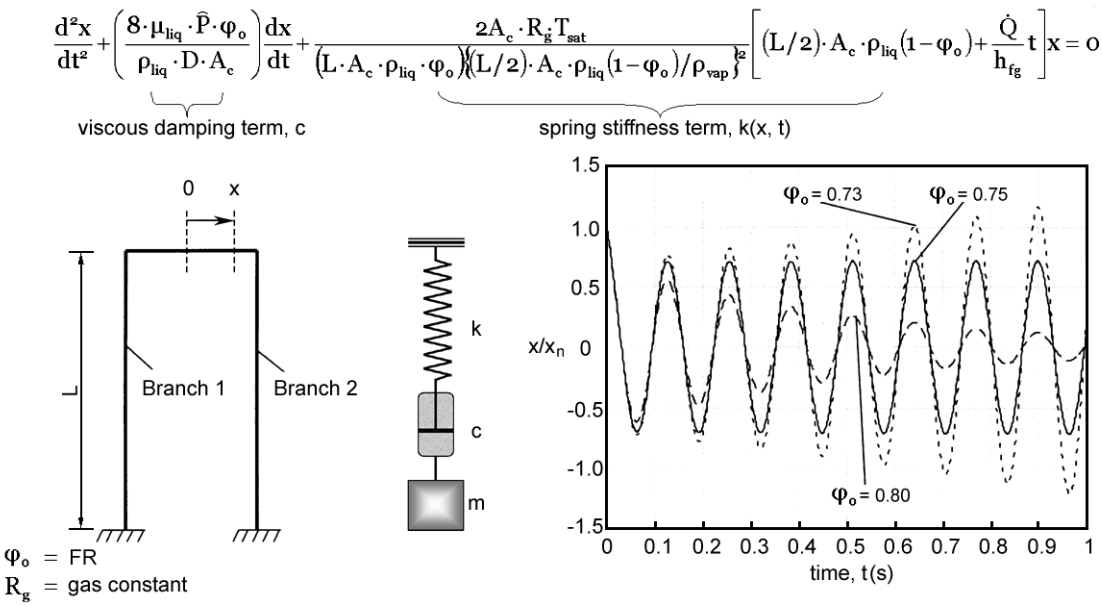

Figure 2-11: Model with single spring-mass system approach by Zuo and North [2000]

and visualization studies [Suo and Griffith, 1964; Duminy, 1998; Hosoda et al., 1999; Lee et al., 1999]. After the initial introduction of this model, no exhaustive results using the model have yet been presented.

The modeling approach presented by Wong et al. [1999] is without any heat transfer considerations and only predicts the kinematics of the liquid plug-vapor bubble system through a Lagrangian approach. In this case, an open loop PHP is modeled as shown in Figure 2-12. The effect of imposed pressure pulses of the system is studied and results of parametric analysis with respect to plug lengths and filling ratios of the PHP are presented. While this approach can give important insights into the device operation, the oversimplifications cannot be ignored. It has been experimentally demonstrated that pressure waves and pulses in and out of phase are simultaneously present in a PHP with complex heat transfer implications. The model has no practical engineering applicability, i.e. it does not allow designing a PHP or predicting its performance.

Swanepoel et al. [2000] have applied the fundamental governing equations to a simplified PHP consisting of a single liquid plug with vapor bubbles on both its sides (refer Figure 2-13). The control volume consisted of the vapor bubbles, the liquid thin film surrounding the bubbles, the tube and the liquid plug. They also built an experimental setup for model validation. It was found that the model did not give exact results of the movement of the plug but only predicted the general tendencies of the plug movement. No indication has been given so that the model can be extended to a multiple plug-bubble system.

Shafii et al. [2001] and Zhang and Faghri [2002] have also attempted to model open and closed loop PHPs with detailed numerical models based on a combination of explicit and implicit schemes. These models have a complex structure with a multitude of assumptions and empirical correlations governing evaporation, condensation and plug/bubble dynamics. While some useful conclusions may be drawn which support the experimental evidence, there is a significant difference in the physical structure of the models as compared to the observations of the experimental studies. The models provide no insight into the complex two-phase dynamics, bubble agglomeration, multiple flow-patterns and chaotic oscillations that are present under the actual operating conditions (as will be discussed later). Therefore, there is no practical engineering applicability of this modeling scheme.

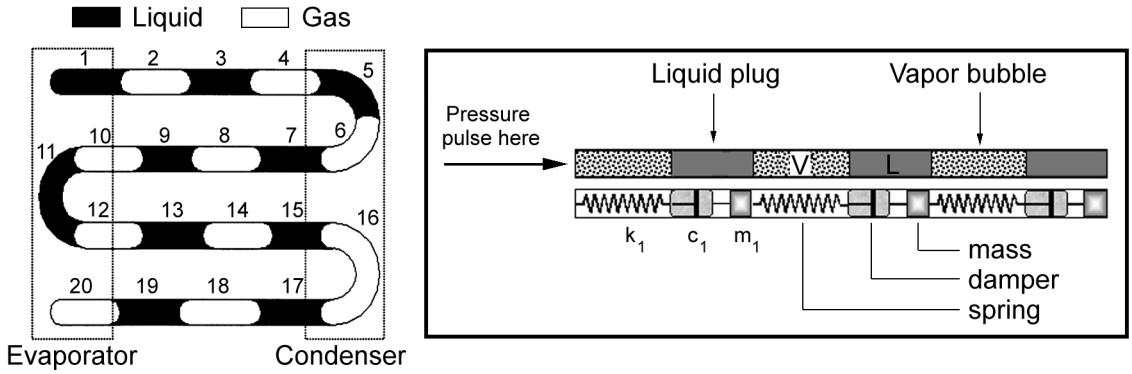

Figure 2-12: Modeling by multiple spring-mass system approach by Wong et al. [1999]

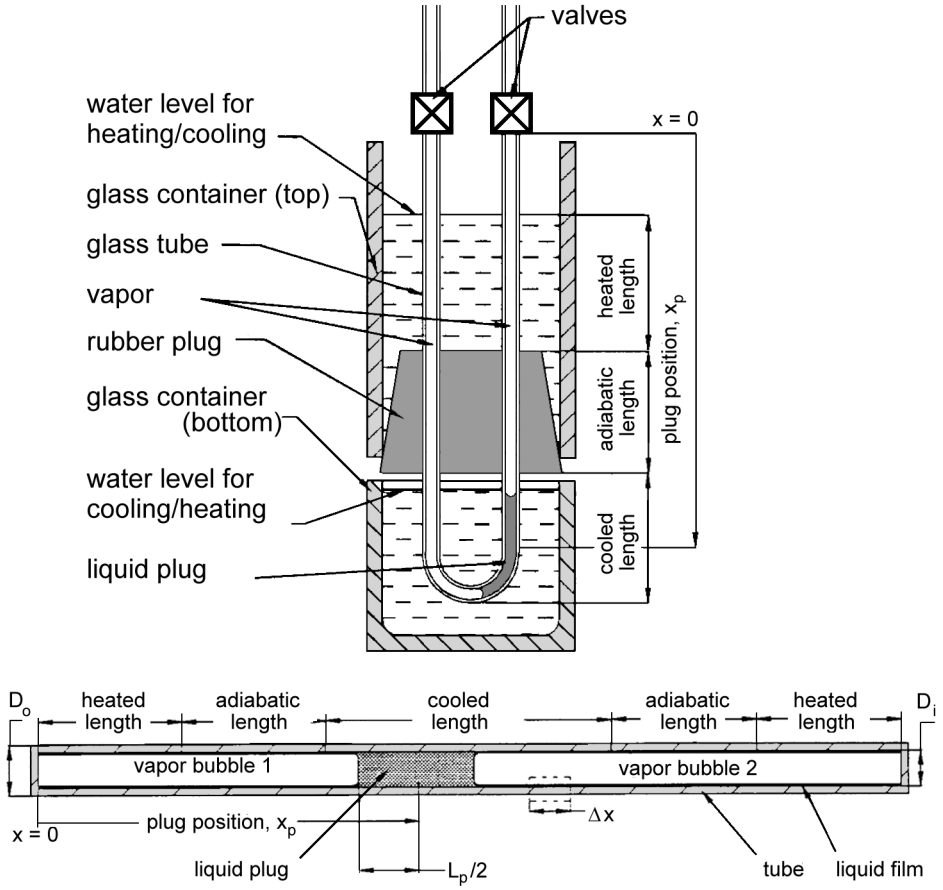

Figure 2-13: Schematic of the mathematical model presented by Swanepoel et al. [2000]

There have been studies that propose the existence of chaos under some operating conditions in PHPs [Maezawa et al., 1996, 2000]. The time-temperature series at a specified location on the wall of PHP tube (adiabatic section) was analyzed by power spectrum calculated through FFT. Two-dimensional mapping of the strange attractor and subsequent calculation of the Lyapunov exponent have been done. Simultaneously, a theoretical study on a single PHP loop was also undertaken. It was concluded that the flow is governed by chaotic dynamics over a wide range of input heat power. While these studies have certainly added another dimension to the already complex PHP behavior, the results should be judged cautiously. Firstly, there should be more investigations of similar nature for further confirmation of the existence of chaotic phenomena. Secondly, it must be emphasized that there exist considerable differences in temperature patterns between the actual working fluid and what is generally measured at the tube wall [Hosoda et al., 1999]. Therefore, (i) the tube wall temperature does not truly represent the actual fluid temperature fluctuations and may be misleading if mathematical chaos tools are used to analyze and draw conclusions thereof, and (ii) the temperature measuring frequency is critical in analyzing non-equilibrium PHP behavior, as misleading information may be generated if it is less than the characteristic time of actual internal fluctuations.

2.3 Closure

The state of the art strongly suggests that an insight into the complex thermo-hydrodynamic phenomena governing the operation of CLPHPs is only in sophomore stages. Authoritative quantitative data base explicitly connecting the thermal performance with individual influence parameters is extremely limited. With the available database, very preliminary conclusions regarding CLPHP design procedures may be made. At present, major research direction is focussed on understanding the underlying physics governing the operating mechanisms of the device. The present research work aims to considerably bridge the gap in the fundamental understanding of the device operation, thereby providing vital design rules.

Concerning mathematical modeling, extreme simplification has been adopted in all the modeling approaches developed thus far. The results have only limited validity and contribution in the understanding of the device, not to mention in their performance prediction and optimization. It is concluded that this continues to pose a challenge. In the present work, mathematical modeling is tackled from an engineering point of view, with the aim of formulating techniques that have direct practical engineering design application. The description of these approaches along with their effectiveness and limitations will be taken up in Chapter 5. The next chapter provides a detailed description of all the experimental set-ups conceived, fabricated and tested during the course of this research program.

CHAPTER 3

DESCRIPTION OF EXPERIMENTS

3.1 Introduction

As outlined in the previous chapter, the overall understanding of the CLPHP operation was still in the burgeoning stages at the commencement of the present research work. A similar or even worse scenario existed in mathematical modeling of CLPHPs. Indeed, it was a futile exercise to start any modeling activity unless there was a reasonable understanding of the device operation. The extremely limited success (euphemism for 'failure') of the then existing models was an obvious proof that their developmental foundations either overlooked or oversimplified the strategic and inherent aspects of operational physics of the device. Thus, there was a need of focused experiments to determine the specific operational characteristics of the CLPHPs.

The problem at hand involved strong and complex two-phase thermo-hydrodynamic interactions of the working fluid having decisive implications on the net heat transfer. Therefore, a series of experiments was envisaged to understand the operational phenomena under the influence of various imposed thermo-mechanical boundary conditions. Details of all the conducted experiments during the course of this research were certainly not planned from the very beginning; rather, the unanswered questions from one experiment led to the development and evolution of the next experimental set-up.

The following section first briefly describes the common peripheral devices used in all the experiments. This includes the data logging system, infrared thermocamera and the high-speed video camera. Thereafter, brief description and procedure of the individual experimental set-ups follow. Also highlighted here are the specific thermo-hydrodynamic aspects of CLPHP operation on which a particular experiment focussed. The serial order of description of experiments approximately follows the timeline of their actual development.

3.2 Common peripheral devices

All the experiments were performed with the help of some peripheral support equipment. A short description of these support systems is given below.

3.2.1 Data logging system

In all the experiments, an 'Ahlborn-Almemo®' programmable universal data logging system was employed; type 2290-8 (up to maximum 5 channels) and type 5590-1 (up to maximum 50 channels) were used as per the need. Sensor programming was done by AMR

Data-Control DC-41-100 (v-4.1) software. The data reporting frequency was always 1 Hz, with a resolution of 0.1°C for temperature and 0.1 m/s for air velocity measurements.

For all temperature measurements, ungrounded, sheath protected NiCr-Ni (Chromel-Alumel, Type-K) thermocouples of 0.5/1.5 mm OD by Thermacoax® were used (prescribed accuracy ±2.5°C without calibration as per DIN-IEC 584). The voltage-temperature curve for these sensors was virtually linear in the applicable temperature range and the mean sensitivity was 41 mV/°C with a time constant of 70 ms. These thermocouples were factory calibrated and programmed with claimed net accuracy of ±0.5°C after calibration.

A hot wire probe, Type EE-60 with a linear output signal of 0-10 V (thermoanemometer, range 0.1 m/s to 20 m/s, maximum error < ±0.3 m/s for air conditions 10°C to 36°C, RH 45%, 1.013 x 10^5 Pa) was used to measure the coolant air velocity whenever required.

3.2.2 Infrared camera

For obtaining complete thermographs and temperature field distribution of CLPHPs, wherever applicable and required, an infrared thermo-camera Varioscan-2011-Compact was used (supplied by Jenoptik®). This camera was fitted with a MCT detector (Mercury-Cadmium-Telluride) having a spectral sensitivity of 8-12 μm, which was cooled by liquid nitrogen. The temperature measurement range was from -40°C to 1200°C with a thermal resolution of ±0.03°C (30°C black body radiator) and geometrical resolution on 1.5 mrad. The object could be placed from 0.2 m to infinity from the lens. The lens was having a measurement area of 30°(H) x 20°(V). The A/D conversion rate was 16 bit and video signal could be seen on a 100 mm TFT display or through separate RGB cable to PAL/TV systems. Individual images could be stored on a PCMCIA card in a bit map format and could be analyzed by supporting software. The thermocamera was always calibrated with standard emitting surface, the reported data being compared to the actual reading of thermocouple placed on the reference surface.

3.2.3 High speed video camera

For obtaining slow motion pictures of the working fluid oscillations/bubble dynamics, high-speed camera, the Kodak® Ektapro HS-Motion Analyzer model-4540 was used. The camera had a sensor with a resolution of 256 x 256 pixels. Frame recording rates of up to 4500 Hz were possible with full frames. A higher speed of up to 40500 Hz was possible at reduced resolution. A 64 MB DRAM (1024 full frames) stored the digital information that could be directly replayed through PAL/NTSC compatible interface.

3.2.4 Cooling water cryostat

For supplying coolant in water-cooled experiments, a Haake-Fisons® cryostat, model DC-5-K-20 with total coolant volume of 3.0 l, maximum possible flow rate 12.5 l/min and maximum pump pressure of 300 mbar was used. The heating capacity was 2.0 kW and the cooling capacity (at 20°C) 300 W, respectively. The operating temperature range was -28°C to 100°C. The microprocessor based PID temperature controller had an accuracy of ±0.02°C.

3.2.5 Power supply

For AC power, a standard power supply transformer connected to the building mains was used (0-220 V, 50 Hz). For DC power, laboratory power supply units, model PS 240-03, manufactured by Conrad® Electronics, were used. Voltage and current were measured by digital multi-meters with accuracy of 0.5% and 1.2%, respectively, of the full scale reading with a resolution of 0.01 V and 0.01 A.

3.3 Experiment-I (Glass tube visualization set-up)

This experiment was the starting point of the present research. Literature survey revealed that there were many lingering unanswered questions concerning CLPHP operation. A need of a proper visualization set-up was strongly felt in which the nuances of two-phase capillary slug flow could be easily captured. This experiment proved valuable for evaluating bubble patterns, phenomenological trends for thermo-fluidic behavior vis-à-vis input heat load,

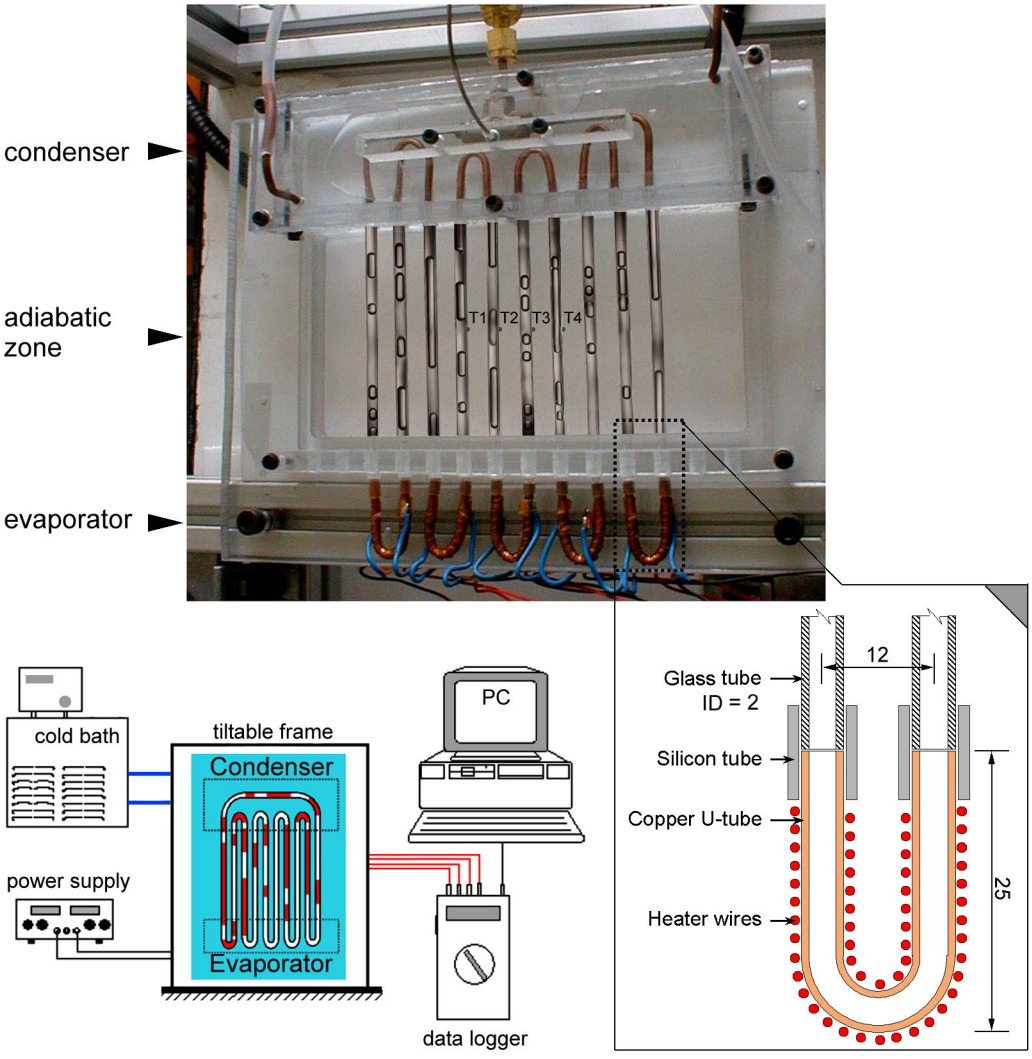

Figure 3-1: Photograph and schematic details of Experiment-I (dimensions in mm)

effect of inclination angle, effect of working fluids, pressure drop due to capillarity etc. In addition, important conclusions could be drawn by comparing the CLPHP dynamics with a single-phase thermosyphon mode of operation. Some preliminary CLPHP design rules could also be formulated based on the results of this experiment.

3.3.1 Set-up description and experimental procedure

The set-up consisted of the CLPHP, the controllable water-cooling cryostat, the DC power source, the data logger and a PC. The CLPHP was made of five copper looped U-turns each in the evaporator and condenser zones coupled with ten glass tubes (ID 2 mm, OD 3.6 mm, length 100 mm and inter-tube axial distance 12 mm) forming the adiabatic section. These glass tubes were interconnected by the copper U-turn tubes (ID 2.0 mm, OD 3.0 mm) with the help of flexible silicon tubes as detailed in Figure 3-1. Nichrome resistance wires, wrapped around the copper U-turns on one side formed the heater section. The U-turns of the other side were routed through a cooling box, supplied by water, always maintained at 20°C. The mass flow rate of the coolant always ensured that near isothermal conditions prevailed in the condenser. The adiabatic section was covered from all sides by transparent PE foil (for proper visualization) at a distance of about 10 mm from the glass tubes so that convective losses were minimized. The height of the copper U-turns in the heater and cooler zones was 25.0 mm and 20.0 mm respectively as shown in Figure 3-1.

Four thermocouples (Type-K, 0.5 mm at locations T1, T2, T3 and T4) were used to measure the adiabatic tube temperatures; two thermocouples each were placed in the condenser section and on the evaporator U-tubes to measure the average temperatures respectively. The CLPHP was mounted on a tiltable frame. A (dis-) charging valve was attached to the outer-most two tubes with a T-part forming the closed loop as shown. The evacuation/filling was done via this valve, which could be fitted to either the vacuum pump or the fluid inventory metering arrangement, as desirable.

The filling could either be done by first evacuating the set-up (vacuum < 10^{-4} mbar) and then administering the desired quantity of working fluid through a calibrated pipette and the metering valve. In another procedure, the device could be first filled with 100% working fluid with a syringe by opening up one of the silicon connecting tubes. Later, desired quantity of fluid could be sucked out. The working fluids were always distilled, deionized and degassed. All experiments with this set-up were done with a volumetric fluid filling ratio of 50%. For aiding flow visualization, in some experimental runs, the working fluid was also seeded with a 500-mesh glass powder. The seeding ascertained the flow direction of the working fluid.

In this experiment, absolute heating power of not more than 15 W could be employed because of the presence of flexible silicon tube connectors that ruptured due to overheating/internal overpressure. At this heat power, the flux levels achieved were of the order of 1 W/cm^2 based on the inner diameter of the tube. Even with these design limitations, important insights into the thermo-hydrodynamics of the device could be explored.

3.4 Experiment-II (Copper CLPHP-Low pressure operation)

With the obvious limitations of Experiment-I concerning maximum deliverable heat flux, it was natural to develop a system with improved performance levels. Additionally, it was important to generate quantitative data. This was only possible with metallic structures. Thus, Experiment-II was planned with geometrical specifications inline with Experiment-I. This would also make it possible for a direct comparison with phenomenological observations of Experiment-I.

3.4.1 Set-up description and experimental procedure

The set-up details are schematically shown in Figure 3-2. The evaporator part of the CLPHP was made up of an aluminum block (125 x 30 x 5 mm^3) heated by two electrical surface mounted and series connected resistance heaters of 5 Ω resistance each. Thermal grease was applied to decrease thermal contact resistances. Maximum heat power achievable for safe operation was about 70 W with corresponding flux of 3.5 W/cm^2 (based on tube ID).

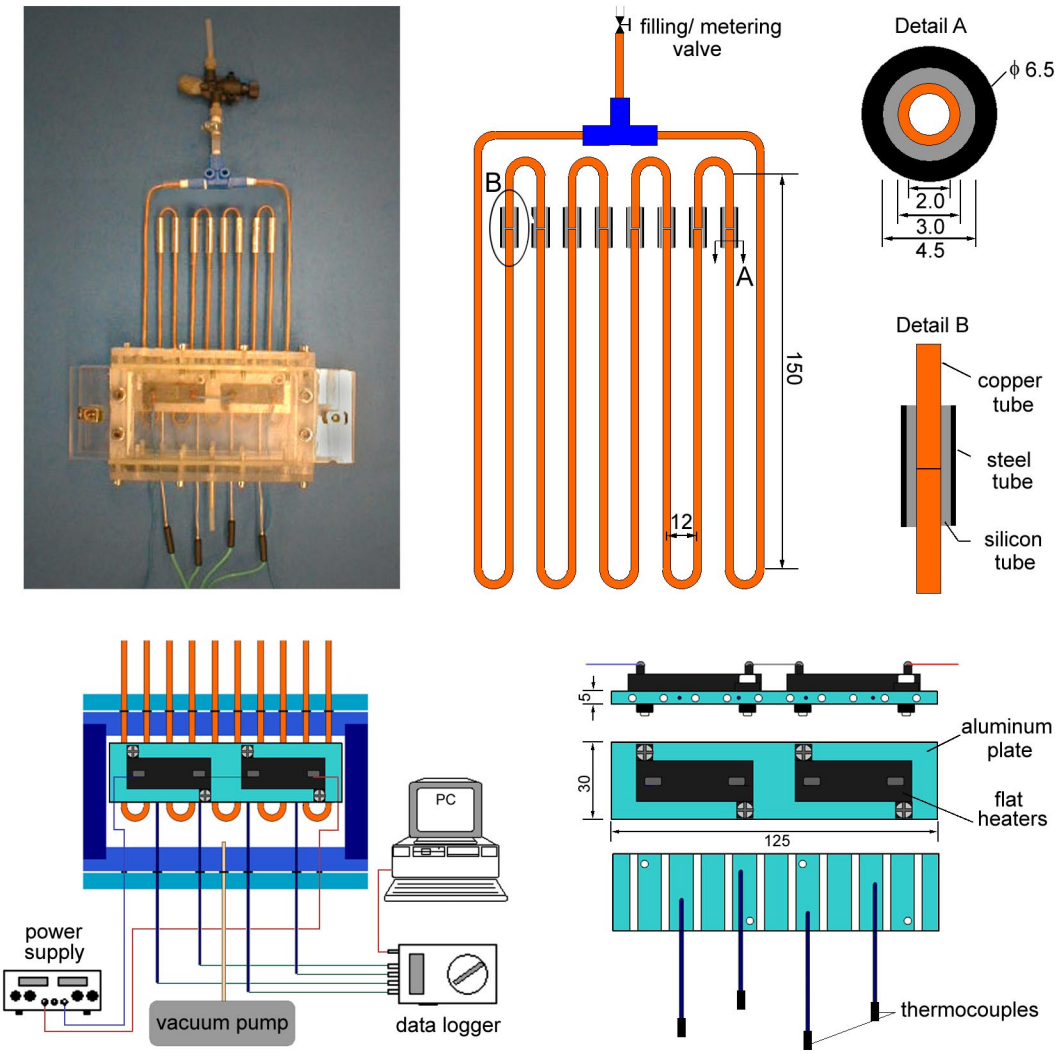

Figure 3-2: Photograph and schematic details of Experiment-II (dimensions in mm)

Copper tubes of ID 2.0 mm and OD 3.0 mm were bent in a U-shape. Two of the bends located at two extreme ends were kept longer on one side in order to complete the closed loop circuit through the T-connector. Four small U-turns were also made from the same copper pipe forming the junctions with the main tubes as shown. Before connecting the copper U-tubes together, they were inserted in suitably sized and located holes in the aluminum evaporator block. A mechanical interference fit ensured an excellent thermal contact.

The final connection between these copper U-turns was made with flexible silicon tubes, present only in the colder condenser section. An additional small steel tube was also fixed as a sleeve on the silicon tube connecting the copper bends to resist the likely deformation of the silicon tubes in case of over-pressure. Thus, overheating/overpressure leak problems of Experiment-I were avoided. The T-connector was fitted with a filling/-metering valve. The final assembly was tested under vacuum; 10^{-4} mbar pressure could be easily maintained.

Air-cooling was applied by blowing air directly on the bare copper tubes by a standard axial flow fan (AC 230 V, size 120 x 120 x 38 mm^3, capacity 190 m^3/hr) and connecting wind tunnel arrangement at average air velocity of 5 m/s (ambient air temperature at 25°C ±1°C).

For achieving good insulation, the evaporator assembly was fully enclosed in an acrylic glass enclosure in which low pressure (< 10^{-3} mbar) was maintained continuously by running a vacuum pump during the experiment. A re-radiating foil shield was placed around the evaporator to prevent radiation losses. The CLPHP copper tubes passed out of the acrylic box through ten holes with O-ring seals ensuring leak tightness. The entire set-up along with the CLPHP, wind tunnel and blower could be turned to a desired inclination angle.

Six thermocouples (1.5 mm) were used in the set-up. Two thermocouples were located in the wind tunnel path measuring the condensing air temperature (average T_c). The other four thermocouples were located in the drilled passages in the aluminum evaporator block. These four thermocouples passed through the evaporator enclosure with O-rings ensuring vacuum tightness. The thermocouples were inline with the copper CLPHP tubes but were located at different positions inside the aluminum plate to give an average representative value of the aluminum block temperature (average T_e). All these thermo-couples were connected to a PC via the data logger. The DC power supply provided the necessary power input.

For filling the working fluid into the CLPHP, one of the connector flexible silicon tubes in the condenser was removed and the working fluid was filled using a syringe injector. The silicon tube was put back onto the copper tube again always ensuring that there was no air bubble left in the tube. In this way the CLPHP volume was filled with 100% working fluid. This filling ratio was then reduced to the desired value by sucking through the metering valve, which was fitted to a vacuum pump. Since the weight of the CLPHP in the dry state and in the 100% filled state was previously measured, the exact filling ratio could be calculated.

At fixed filling ratio, input heat power was varied until the average evaporator temperature reached 100°C (in case of water and ethanol) or 60°C (in case of R-123). Since the saturation pressure of R-123 at 100°C (about 7.8 bars) was too high for safe operation of the copper CLPHP due to the presence of flexible silicon tubing, all experiments with R-123 were carried

out till a maximum T_e = 60°C. It is clear from the thermophysical properties compiled in the Appendix-II that even at this low operating temperature (i.e. T_e = 60°C), R-123 has a much better pressure-rise response than ethanol and water. The thermal resistance of the CLPHP, in all cases, was evaluated based on the steady state average evaporator temperature and the corresponding condenser air temperature. Since the evaporator was completely insulated (under vacuum), the thermal power was directly calculated from the source electrical power. After reaching a steady state in vertical orientation, the set-up was turned to a new orientation and allowed to stabilize again. Suitable corrections were applied after accounting for the losses.

3.5 Experiment-III (Two-phase loop device)

One of the aims of the present research work was to study the effect of number of turns of a pulsating heat pipe on its performance. Therefore, one primary building block i.e. a capillary two-phase loop (with single turn) was fabricated. The loop was constructed with the primary aim of phenomenological visual observations and preliminary quantitative

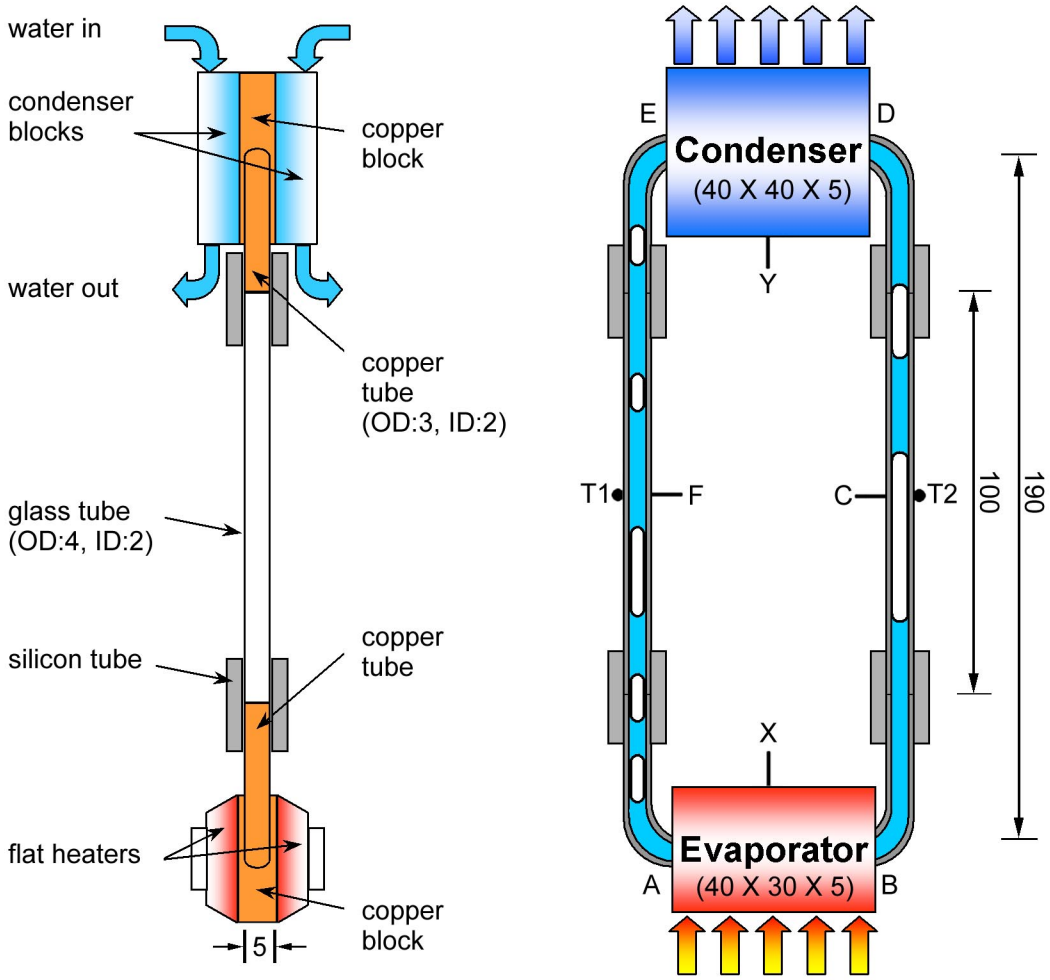

Figure 3-3: Schematic details of Experiment-III (dimensions in mm)

measurements. The assumption whether one loop truly represents all the thermo-fluidic characteristics of the real CLPHP was to be scrutinized. The limitations of this analogy and conclusions drawn thereof were investigated. The fundamental thermo-hydraulic operational characteristics of the loop could be investigated with this set-up, which provided vital information for multi-turn CLPHP performance characteristics.

3.5.1 Set-up description and experimental procedure

The geometrical details of the set-up are shown in Figure 3-3. The evaporator section was made up of a copper block of size 40 x 30 x 5 mm^3. Two small copper tubes (ID 2.0 mm, OD 3.0 mm) were brazed on its two sides and connected to each other by an internal through hole (ID 2.0 mm). Two surface mounted DC heaters attached to the copper block provided the input power. The condenser section was similar in construction with a copper block size of 40 x 40 x 5 mm^3. The loop was completed by two glass tubes (ID 2.0 mm, OD 4.0 mm) of length 100 mm each forming the adiabatic section. These tubes were connected to the respective open ends of the copper tubes by short flexible silicon tubes. A filling valve assembly was attached to the condenser section. Armaflex® foam insulation was used wherever necessary. A maximum heat input of about 80 W could be achieved for safe operation with corresponding flux levels of 30 W/cm^2.

Cooling water always maintained at 20°C flowed through two additional copper cold blocks tightly clamped via thermal grease to the condenser section. The mass flux ensured near isothermal conditions in the cold blocks. The loop was first evacuated to 10^{-4} mbar and then filled partially with the working fluid, i.e. ethanol. Temperature measurements were done with thermocouples of 1.5 mm diameter coupled to the data logger. Two thermocouples each were placed in drilled passages in the evaporator and condenser copper blocks recording the average temperatures (T_e and T_c). Two thermocouples (T1 and T2) were attached centrally on the wall of the glass tubes in the adiabatic section. It is important to note that the temperature recorded by these two thermocouples, i.e. T1 and T2 did not truly represent the exact temperature fluctuations inside the working fluid. Further, the data recording frequency by the data logger was limited to 1 Hz. Nevertheless, the essence of the phenomenological condition of the fluid was certainly captured by these measurements coupled with visualization and important conclusions could therefore be drawn which are reported in the next chapter.

3.6 Experiment-IV (Multiturn high performance CLPHP)

This set-up was the final in the series of CLPHPs fabricated during the course of this research. The need for this set-up was strongly felt based on the results of the previous experimental results. In fact, practically all the burgeoned hypotheses and remaining unanswered questions could be convincingly clarified by the results of this experiment. It helped to bring the domain of the present research program to a logical closure.

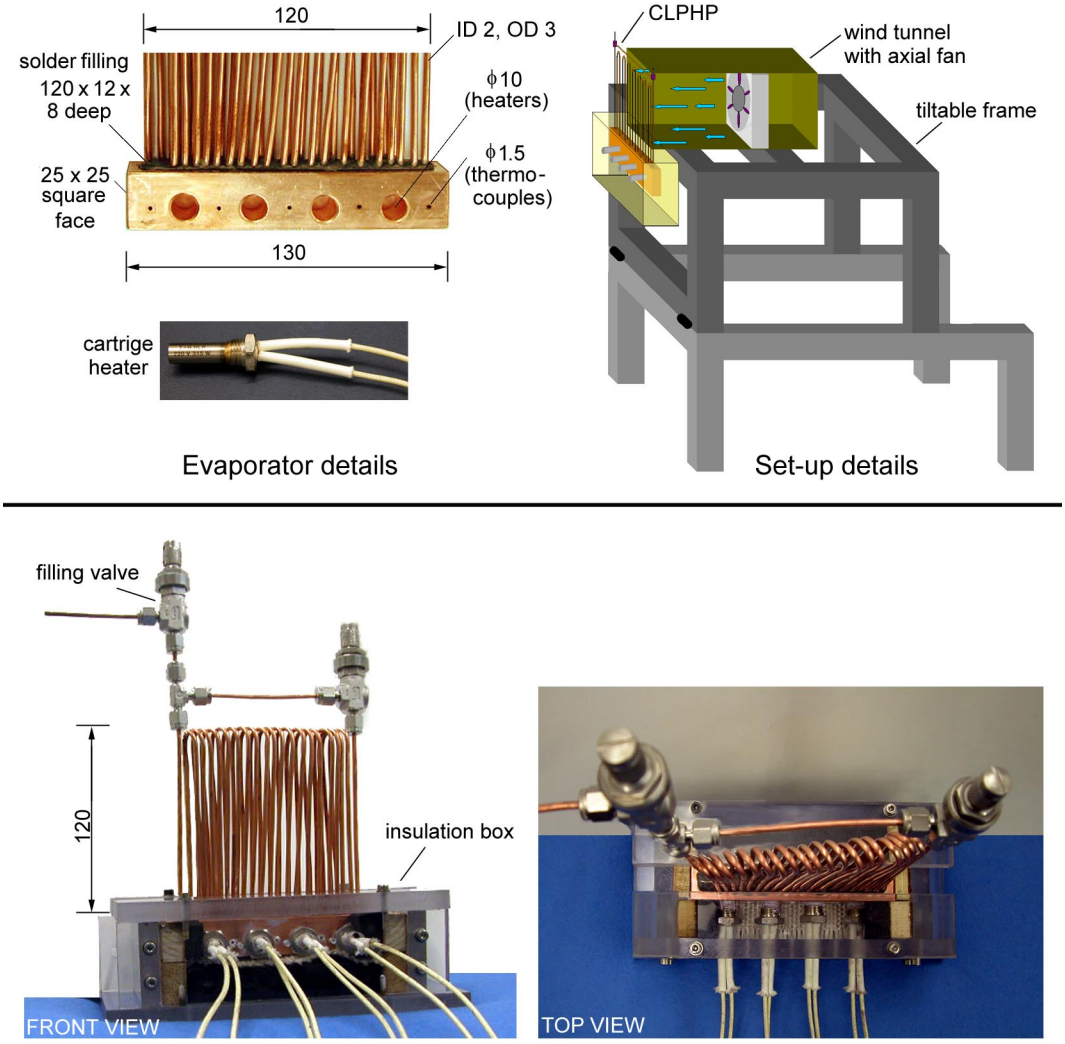

Figure 3-4: Photograph and schematic details of Experiment-IV (dimensions in mm)

3.6.1 Set-up description and experimental procedure

The details of the set-up are shown in Figure 3-4. The set-up consisted of a copper block of size 130 x 25 x 25 mm^3 forming the evaporator. Four holes were laterally drilled into this copper block to accommodate four circular cartridge AC heaters (ø 10.0 x 25 mm) by mechanical fit. Additionally, five holes were also laterally drilled half way through to locate the thermocouples measuring the average evaporator block temperature. To accommodate the U-turns of the CLPHP, a preformed cavity (size 120 x 12 x 8 mm^3) was machined into the copper block. After vertically locating the CLPHP U-turns into this cavity, tin based solder alloy was poured and allowed to solidify. The evaporator block was secured into a Makrolon® box providing insulation. The safe maximum heat flux (limited by the set-up elements) based on the U-turn tube section area welded in the evaporator block was about 12 W/cm^2.

The CLPHP was formed from copper tube (ID 2.0 mm, OD 3.0 mm), with 20 turns on each side, having a staggered pitch of 10 mm between the tubes. The total length of the tube used was about 5.4 m with a filling volume of 17.0 cc. Leaving apart the welded length of the

U-turns embedded into the evaporator block, the entire CLPHP was cooled by forced air cooling (axial fan, Sunon-DP200A-2123XBT, AC 230 V, size 120 x 120 x 38 mm^3, 180 m^3/hr) as shown in Figure 3-4. The average air velocity was 3.5 m/s with ambient air temperature of 27°C ±1.5°C. Air temperature and velocity were recorded with sensors suitably placed in the wind tunnel. The entire set-up was mounted on a revolving frame so that experiments could be performed at all orientations. Metered quantities of the working fluids (i.e. ethanol and water) could be dosed by calibrated pipette and filling valve arrangement.

The effect of number of turns (as compared to the previous experiments), input heat flux, filling ratio, inclination angle (including anti-gravity operation) and working fluid on the thermal performance could be obtained with this set-up. The general experimental procedure remained the same as for the previous experiment.

3.7 Experiment-V (Mini heat pipe performance testing)

If a CLPHP having a specified geometry and 'N' number of turns is replaced with 'N' individual conventional mini heat pipes of comparable geometry, then, under similar imposed external boundary conditions, which system will perform better? In addition, it is also of interest to compare the CLPHP based system with equivalent solid copper fins in terms of weight and thermal performance. To answer such questions, performance mapping of conventional mini heat pipes of ID/OD 4.0/3.0 mm, 3.0/2.5 mm, 2.5/2.0 mm was done. A direct comparison also gives an insight into the respective roles of latent and sensible heat in the overall heat transfer in CLPHPs.

3.7.1 Set-up description and experimental procedure

All the tested mini heat pipes were made of copper with water as the working fluid. The wick structure was copper screen mesh, except that of heat pipe with ID 3.0 mm, in which case the wick was sintered copper powder. Specific details of the respective meshes, e.g. pore size distribution, effective permeability etc., were not explicitly known since the heat pipes were supplied by external agencies. These heat pipes were standard products for electronics cooling applications (e.g. in laptops etc.) and believed to be optimally operating.

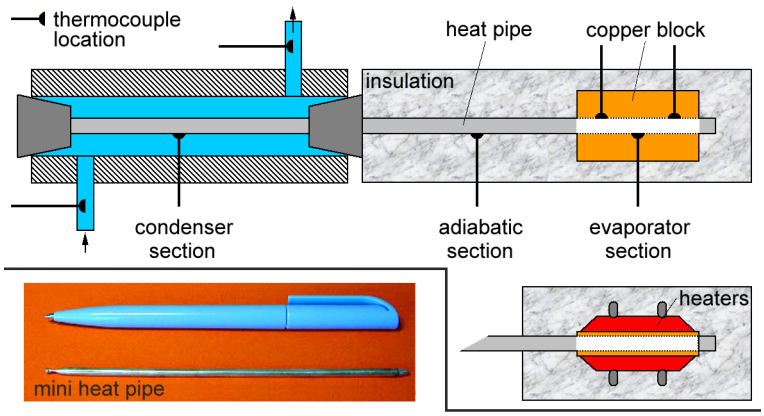

Figure 3-5: Photograph and schematic details of Experiment-V

The generic design of the experimental set-ups for performance testing is as shown in Figure 3-5. The heat pipes were mechanically inserted into suitably sized copper blocks with application of thermal paste. Two surface mountable ceramic heaters were attached to the copper block to form the evaporator section. The water-cooled condenser section was made by drilling a cavity in poly-acrylic Makrolon® material. Heat pipes were firmly located in this section by natural rubber stoppers. The entire set-up was well insulated. In all set-ups, three thermocouples were placed in the evaporator section, one in the adiabatic section and three in the condenser section as shown in Figure 3-5. The entire set-up could be tilted at the desired angle. The performance testing was done as per prescribed standard testing procedure [Faghri, 1995].

3.8 Closure

This chapter described the experimental set-ups used to explore, extract and assimilate the operational physics of CLPHPs. The results of these experiments along with the conclusions drawn thereof with supporting discussions, including conjectural evaluation, will be presented in the next chapter. Thereafter, mathematical modeling of CLPHP systems will be dealt with in Chapter 5.

CHAPTER 4

RESULTS AND DISCUSSION

4.1 Fundamental perspectives

4.1.1 Cooling philosophy of pulsating heat pipes

Before proceeding to appreciate the subtleties of thermo-hydrodynamics of CLPHPs, it is worthwhile to get an overall perspective on the principal ideas behind some contemporary heat transfer technologies, as applicable to electronics cooling. This will ascertain the relative position of CLPHPs in the hierarchy of modern day heat transfer solutions. This exercise is deemed necessary to benchmark the performance limits and to help later in system analysis.

Figure 4-1 shows a range of heat transfer/cooling strategies in comparison to CLPHPs. If a given heater block is to be cooled, thereby maintaining it at a fixed temperature by convective air-cooling (the external heat transfer coefficient is known and fixed), there are various techniques which may be adopted. The most primitive method is by making use of extended surfaces or fins, thereby employing conduction heat transfer. Here, the thermal conductivity of the fin material generally limits the performance. The effective thermal conductivity of the material may be greatly enhanced by replacing the solid metallic fins by heat pipes or thermosyphons, thus making use of closed passive two-phase systems based on pure latent heat transfer mechanism. While the heat pipes may be made to operate at any inclination angle, since the capillary wick is the 'pump', (albeit with varying performance), traditional gravity assisted thermosyphons only operate in 'heater down' position. As far as the external air-cooling is concerned, the replacement of solid fins by heat pipe fins changes the longitudinal fin temperature profile which the ambient (approaching) air experiences. In the ideal case of a super conductor, the entire fin will be at the heater base temperature, thereby maximizing the fin efficiency. Maximum heat transfer will thus be achieved as the 'effective thermal conductivity' of the fin structure approaches infinity.

Another strategy to favorably change the fin longitudinal temperature gradient is to remove some solid material from inside the fin and circulate a suitable fluid in its place thus making use of the sensible heat transfer of the fluid. Traditional single phase Nusselt analysis informs us that performance may be enhanced by increasing the flow Reynolds number and/or choosing a fluid with a high Prandtl number. Thus, in stringent demand conditions, quite naturally, forced pump liquid circulation overshadows natural buoyancy driven free convection solutions. In addition, provided the reliability and cost handicap of the pumping system is acceptable, forced circulation is not restricted by the system orientation.

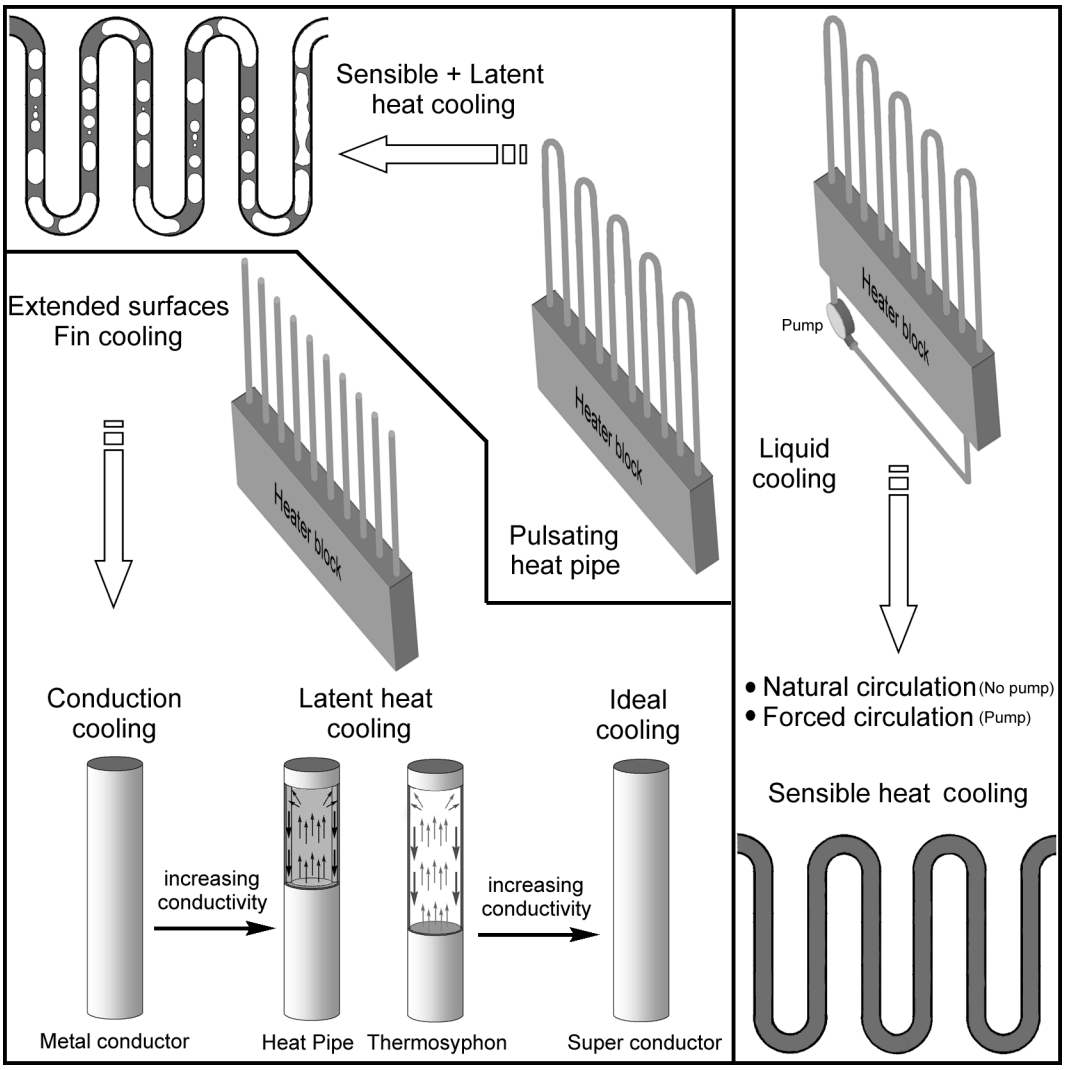

Figure 4-1: Comparison of various heat transfer technologies with CLPHPs

In between these two limits i.e. latent heat cooling and sensible heat cooling, lies the present area of interest. The inspiration for research is to find ways to eliminate the pump as in case of liquid cooling, to drastically reduce the manufacturing complexity involved in heat pipes and try to achieve a structure with thermal performance independent of the operating orientation. The CLPHP concept addresses these very issues. The liquid-vapor system formed in the simple closed tube is capable of generating self-sustained thermally driven oscillations. How much better these structures can be made with respect to solid metallic fins and how close they can go to the conventional heat pipe will depend on sound understanding of thermo-hydrodynamic behavior of these devices.

4.1.2 Diameter as the defining parameter

The expectations from a CLPHP system have been outlined in the previous section. To fulfill these expectations, system design must adhere to series of specifications and boundary

conditions in terms of geometry, operational modes and thermophysical properties of the working fluid. We begin the discussion by the most important geometrical dimension of the device, i.e. the internal tube diameter. This dimension essentially manifests the fundamental definition of PHPs. The following discussion explains this point.

In metallic fin cooling, the heat is 'pumped' by the atomic vibrations 'phonon conduction' and the 'electron conduction'. In conventional heat pipes, while the vapor phase is pumped by the small pressure difference existing between the evaporator and the condenser, the liquid phase is pumped back by the capillary action. In a gravity-assisted thermosyphon, the liquid returns by gravity assistance only. Single-phase natural circulation employs buoyancy driven 'pumping' while forced liquid cooling requires an external mechanical pump. As noted earlier, one CLPHP design criterion is passivity. This necessitates that some internal device element must act as a pump. This action is materialized by the generation of bubbles in the evaporator and the collapsing bubbles in the condenser. The heat input to the device itself provides part of the energy to run the system. Thus, the thermo-hydrodynamic objective function for CLPHP design is to ensure self-sustained thermally driven bubble pumping, ideally in any operating orientation of the device, which maximizes the heat transfer.

Before proceeding to discuss the actual design criteria of CLPHPs, it is worthwhile to take hints from the classical studies of cylindrical bubbles rising in isothermal static fluids (refer Figure 4-2). A bubble rises through the denser liquid because of its buoyancy. The velocity υ_∞ with which a single cylindrical bubble rises through stagnant liquid in a duct is governed by interaction between buoyancy and the other forces acting on the bubble because of its shape and motion. If the viscosity of the vapor in the bubble is neglected, the only forces besides buoyancy, which are important, are those from liquid inertia, liquid viscosity and surface tension. The balance between buoyancy and these three forces may be expressed in terms of three non-dimensional groups [Bretherton, 1960; Harmathy, 1960; Wallis, 1969]:

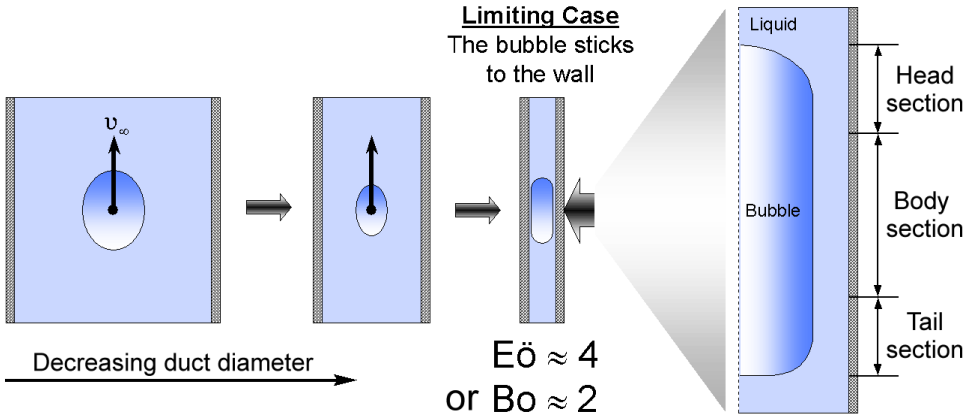

Figure 4-2: Critical conditions for zero terminal velocity of a cylindrical bubble rising through stagnant liquid contained in a channel

$$\text{Froude Number} = \text{Fr} = \frac{\rho_{liq} \cdot \upsilon_\infty^2}{D \cdot g \cdot (\rho_{liq} - \rho_{vap})} = \frac{\upsilon_\infty^2}{D \cdot g} \qquad \text{if } \rho_{liq} >> \rho_{vap} \qquad (4\text{-}1)$$

$$\text{Poiseuille Number} = \text{Ps} = \frac{(\upsilon_\infty \cdot \mu_{liq})/D}{D \cdot g \cdot (\rho_{liq} - \rho_{vap})} = \frac{(\upsilon_\infty \cdot \mu_{liq})/D}{D \cdot g \cdot \rho_{liq}} \quad \text{if } \rho_{liq} >> \rho_{vap} \quad (4\text{-}2)$$

$$\frac{1}{\text{Eötvös Number}} = \frac{1}{\text{Eö}} = \frac{(\sigma/D)}{D \cdot g \cdot (\rho_{liq} - \rho_{vap})} = \frac{(\sigma/D)}{D \cdot g \cdot \rho_{liq}} \quad \text{if } \rho_{liq} >> \rho_{vap} \qquad (4\text{-}3)$$

The Bond number is frequently used in place of Eötvös number and is defined as,

$$\text{Bo} = \sqrt{\text{Eö}} \qquad (4\text{-}4)$$

In the above equations, D is typically the characteristic dimension of the duct cross section. For circular ducts, D represents the internal diameter.

In situations where viscous forces and surface tension can be neglected, the rise velocity can be correlated only by Eq. 4-1 above. Similarly, when viscous force constitutes the only predominant factor, bubble rise velocity is obtained by the Poiseuille number. The last case, when surface tension dominates, is the case of present interest. Interestingly enough, the Eötvös number has no velocity term in it. So, how can this number be used to find the rise velocity under the dominance of surface tension?

Since the general solution is governed by three non-dimensional parameters as defined above, it can be represented as a two-dimensional plot of any two chosen dimensional groups with the remaining third independent group as a parameter. The three parameters may also be combined to generate new dimensionless quantities for convenience. For example, a convenient Property group, not containing either D or υ_∞ is frequently used,

$$\text{Property number} = \text{Y} = \frac{g \cdot \mu_{liq}^4}{\rho_{liq} \cdot \sigma^3} = \frac{\text{Ps}^4 \cdot \text{Eö}^3}{\text{Fr}^2} \qquad (4\text{-}5)$$

When the above problem was first attempted analytically for non-viscous systems, it was thought that Fr and Eö should tend to zero together [Bretherton, 1960]. In simpler terms this means that for a given fluid-bubble system, as the tube diameter is reduced, thereby making Eö approach zero, the bubble rise velocity should follow the trend and become zero when Eö = 0. Experimental observations have negated this hypothesis and showed that there is a critical value of Eö, below which no bubble rise takes place at all. Figure 4-3 shows experimental data for a wide range of fluids as reported by White and Beardmore [1962]. Main conclusions of present interest are:

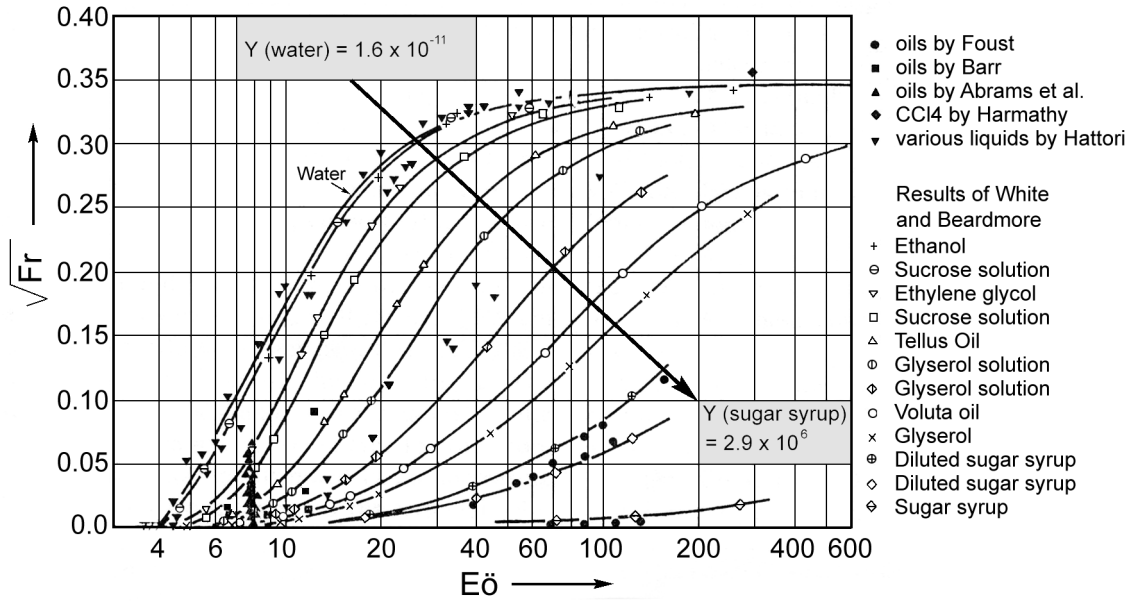

Figure 4-3: Parametric experimental results for rise velocity of a cylindrical bubble through various stagnant liquids contained in a channel [White and Beardmore, 1962]

- As Eö increases beyond a particular value (≈ 70 for many common fluids, e.g. water, ethanol etc.), the terminal velocity of bubbles approaches a constant value. The viscous forces and surface tension can be neglected and Eq. 4-1 takes the form $\sqrt{Fr} \approx 0.345$.
- Below Eö ≈ 70, the terminal velocity continuously decreases with decrease in Eö.
- Around Eö $\lesssim$ 4, the terminal velocity becomes zero. This is the surface tension dominated zone represented exclusively by Eq. 4-3.

This value of critical Eö, at which the terminal velocity becomes zero, is certainly not unique and varies somewhat under different experimental conditions, e.g. some sources quote $Eö_{crit} \lesssim 3.38$ [Bretherton, 1960]. It is reasonable to expect the liquid contact angle on the tube surface to have an effect on $Eö_{crit}$ if wetting of the surface is incomplete. This factor does not appear in any dimensional groups, as outlined above. Factors such as cleanliness or surface roughness may affect the experimental determination of $Eö_{crit}$ [White and Beardmore, 1962].

The foregoing discussion has important implications in defining a CLPHP. The rise velocity of cylindrical bubbles in liquid under adiabatic conditions becomes zero when surface tension predominates and this condition is given by,

$$Eö = (Bo)^2 = (Eö)_{crit} \approx \frac{D_{crit}^2 \cdot g \cdot (\rho_{liq} - \rho_{vap})}{\sigma} \approx 4 \qquad (4\text{-}6)$$

$$D_{crit} \approx 2 \cdot \sqrt{\frac{\sigma}{g \cdot (\rho_{liq} - \rho_{vap})}} \qquad (4\text{-}7)$$

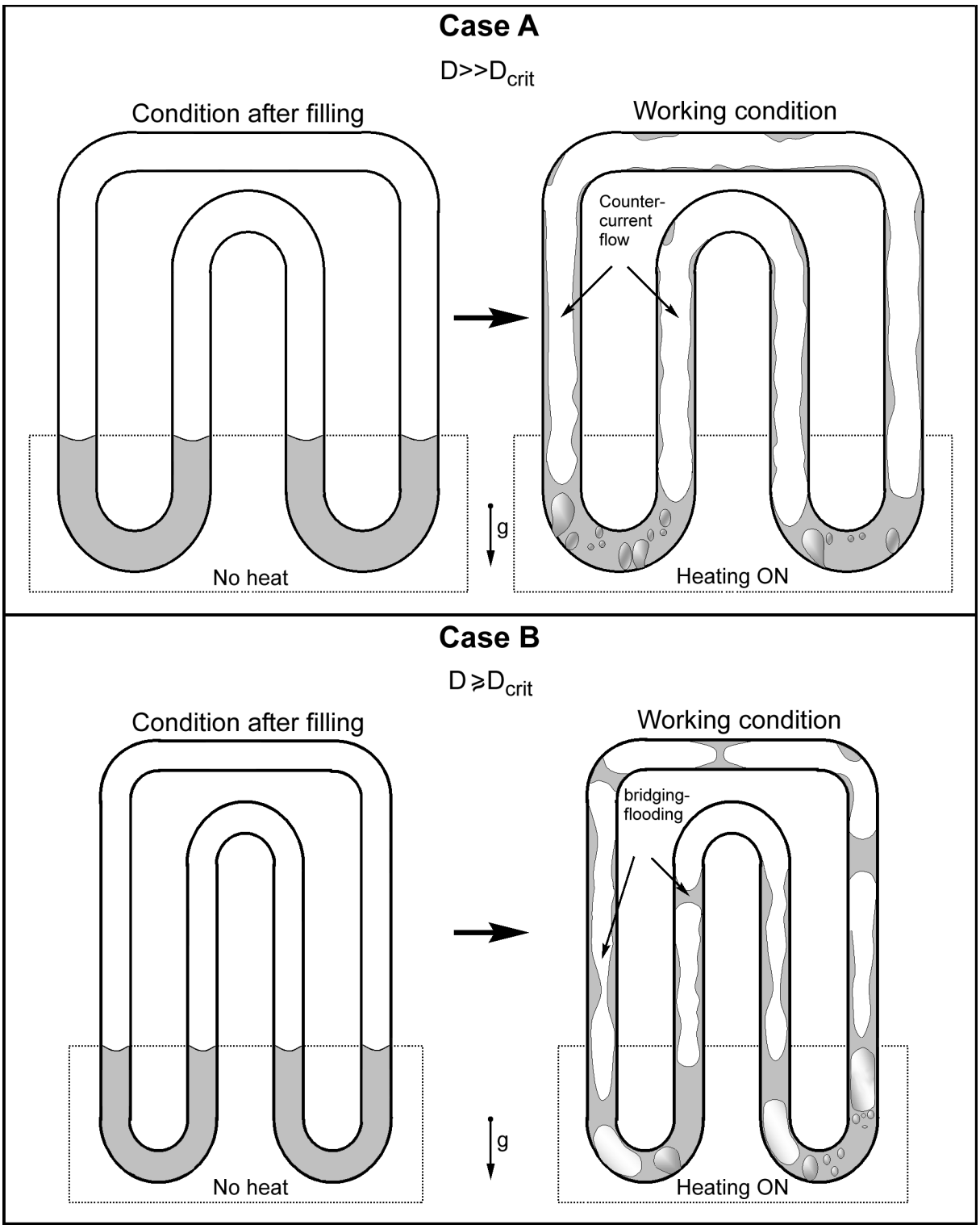

Figure 4-4: Effect of diameter on the fluid distribution inside circular tubes of CLPHPs under adiabatic and operating conditions

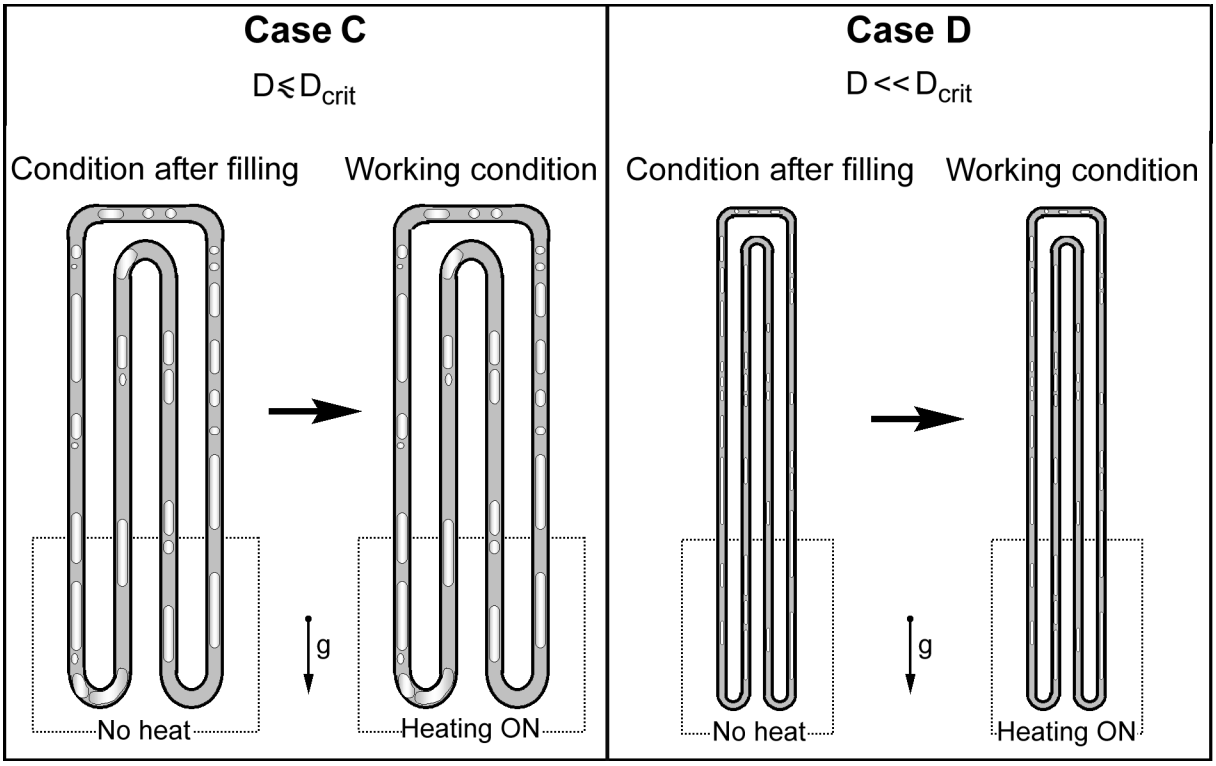

Figure 4-4: ...continued from the last page

Thus, for a given fluid contained in a vertical tube having a diameter smaller than the critical value defined by Eq. 4-7, if a cylindrical bubble is introduced in it, it will not rise up by buoyancy. This essentially means that distinct liquid plugs and vapor slugs can be formed without separation, stratification or self-agglomeration. Figure 4-4 depicts four scenarios, under adiabatic conditions, when $D >> D_{crit}$, $D \gtrsim D_{crit}$, $D \lesssim D_{crit}$, and $D << D_{crit}$. The likely events are schematically depicted when such systems are filled partially with a working fluid under adiabatic conditions. It is clear from Figure 4-4 that diameters below D_{crit} suggested by Eq. 4-7 will retain the distinct slug and plug characteristics after fluid filling.

Following this discussion on critical diameter in static, adiabatic conditions, focus is now turned to real conditions in which heat is applied to such systems (the cases as described in Figure 4-4) with the aim to make CLPHPs. Which of the cases A, B, C and D will truly function as a CLPHP? One of the requisite design criteria discussed earlier was that bubbles should act as liquid pumping elements. The success of bubble pumping action depends on the formation of distinct liquid-vapor plugs and slugs and so it is obvious that cases C, D will definitely function as a pulsating heat pipe. What about the cases A and B?

Another case to consider, which answers the above question, is a standard bubble pump shown in Figure 4-5. In such a system, the primary objective is to lift up or pump the liquid by application of heat, by its own bubbles. The pumping success is achieved by restricting the flow pattern to the slug flow regime (which lies between the bubbly and the annular flow). The transition from bubbly flow to slug flow is characterized by the churn-turbulent region.

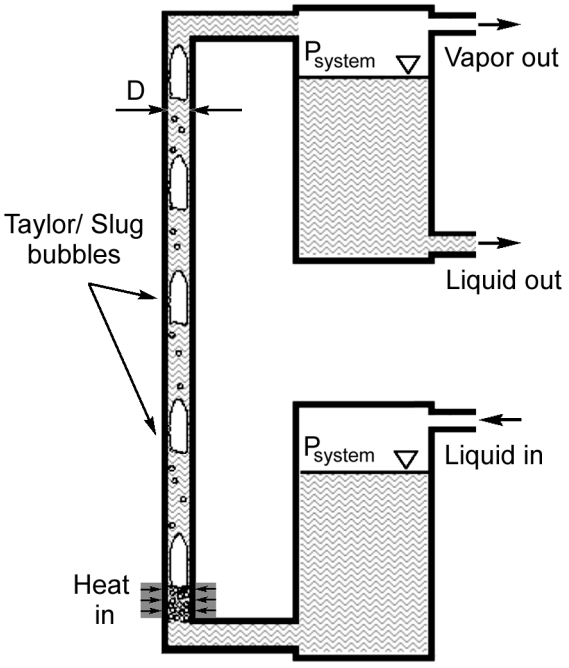

Figure 4-5: Schematic of a typical bubble pump

In this region, if agglomeration of smaller bubbles leads to the formation of stable Taylor-type bubbles, the flow transforms into the slug regime [Chisholm, 1983]. The larger bubbles, which nearly fill the tube diameter, are then able to transport liquid up the tube. Experiments on vertically oriented bubble pumps suggest that pumping is possible until [Delano, 1998],

$$D_{crit} \approx 19 \cdot \sqrt{\frac{\sigma}{g \cdot (\rho_{liq} - \rho_{vap})}} \qquad (4\text{-}8)$$

It is interesting to compare this criterion, which is under non-adiabatic, flow boiling conditions with that given by Eq. 4-7 for static, adiabatic conditions. Both are correct under the respective boundary conditions they represent. There is indeed a large variation of diameters possible for diabatic slug flow conditions that can transport trapped liquid masses.

We may therefore conclude that rather than a certain fixed D_{crit} for proper CLPHP operation, there is a finite transition zone as explained in Figure 4-6. If the outside diameter is fixed and the internal diameter is reduced, the thermo-hydrodynamic behavior changes from classical thermosyphon (liquid-vapor stratification) to a CLPHP in a gradual manner there being no distinct demarcation line. In the latter zone, the input heat produces bubble-pumping action. The dissipative internal pressure drops, which monotonously increase with decreasing diameter, retard the pumping bubbles. Thus, optimum liquid pumping is achieved at a certain diameter below which the pressure drops will overshadow the pump yield; the CLPHP will slowly tend towards a solid metal tube with further decrease in diameter. This leads us to the following two important conclusions regarding the CLPHP tube diameter:

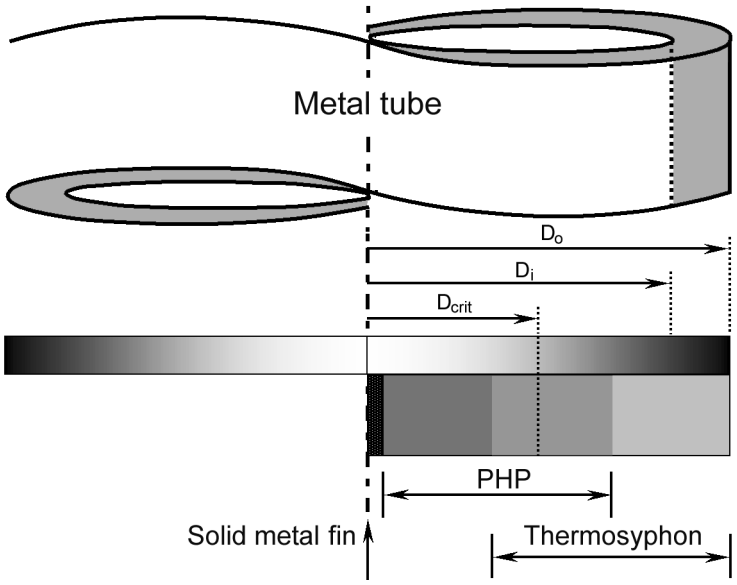

Figure 4-6: Overlapping zones of operating diameters for CLPHP and thermosyphon

- For a specified heat throughput and maximum allowable evaporator temperature and all other geometry remaining fixed, decreasing the diameter from an optimum value will decrease the performance. In addition, a smaller diameter tube amounts to less possible total liquid inventory in the system and thus less sensible heat transport.
- In general, maximum heat throughput until some sort of evaporator dryout will monotonously increase with increasing diameter. After a certain diameter range, the device will slowly loose its fundamental character and will no longer be a CLPHP. Instead, the structure will behave as an interconnected array of two-phase thermosyphons; there might still be some instability due to the interconnected tube geometry. Heat transfer will then be mainly governed by nucleate pool boiling characteristics. If the specified heat throughput can generate sufficient wall superheat creating favorable conditions for nucleate pool boiling then this interconnected array of thermosyphons may be thermally a better option, at least for a certain range of inclination angles. It is also important to note that the optimum diameter mentioned above is based on the premise that all other influence parameters (e.g. filling ratio) are optimally specified.

The following points may also be concluded for a true CLPHP in which bubble pumping results in net liquid transport (i.e. net heat transfer is a result of sensible and latent portions):

- CLPHPs may never be as good as an equivalent heat pipe or thermosyphon system (based on pure latent heat transfer). If the thermo-hydrodynamic characteristics of CLPHPs are well understood, the performance may be optimized towards an equivalent classical heat pipe fin system. At the least, the manufacturing complexities of heat pipes will be avoided.
- If the thermal performance of CLPHPs is below that of equivalent metal fin array systems (say, of copper), at the least there will be a weight advantage.
- If the performance is below that of equivalent single-phase forced convection options, at the least there will be a reliability advantage because of the absence of an external pump.

4.1.3 Two-phase flow instabilities

Instabilities in two-phase systems have been an area of research for a long time [Wallis and Heasley, 1961; Boure et al., 1973; Carey, 1992]. The phenomena of thermally induced two-phase flow instabilities are encountered in many industrial systems, nuclear reactor flow dynamics, steam generators, thermosyphon reboilers and other chemical process units. A generation of researchers has directed their efforts in understanding these instabilities with the primary motive of reducing their undesirable effects on system performance. CLPHPs present a strongly contrasting case; thermally induced two-phase flow instabilities are effectively harnessed for heat transfer augmentation.

It is clear from the foregoing discussion that the internal diameter is one of the fundamental defining parameters of a CLPHP. In addition, during the course of the present research, two more parameters emerged as demarcation parameters of these devices, i.e. the input heat flux and the filling ratio (FR, defined as the ratio of volume of the working fluid to total volume of the device at room temperature). It will be demonstrated later, as has been done in the previous section for the tube diameter, that CLPHPs loose their fundamental character if certain boundary conditions pertaining to input heat flux and filling ratio are not satisfied. This result is not surprising in the wake of the fact that these two parameters have also been explicitly responsible for affecting various types of two-phase flow instabilities (the effect of filling ratio in CLPHPs is analogous to the void fraction in open flow systems). Table 4-1 summarizes the basic types of two-phase flow instabilities usually encountered in wide ranging situations. The table is presented here with an intention to clarify some phenomena observed in case of CLPHPs, which are direct consequences of these flow instabilities.

Two-phase flow instabilities can be primarily classified into two groups: (a) Static instabilities, and (b) Dynamic instabilities. A flow is subject to a 'static' instability if, when the flow conditions change by a small step from the original steady-state ones, another steady-state is not possible in the vicinity of the original state. The cause of the phenomenon lies in the steady-state laws; hence, the threshold of instability can be predicted only by using steady-state laws. A static instability can lead either to a different steady-state condition or to a periodic behavior. On the other hand, a flow is subject to a 'dynamic' instability when the inertia and other feedback effects have an essential part in the process. The system behaves as a servomechanism and steady-state laws are not sufficient even for threshold prediction. An instability is 'compound' when several elementary mechanisms interact in the process and cannot be studied separately. It is said to be 'fundamental' (or pure) in the opposite sense.

In general, it has been established by various experimental observations and supporting analytical results that the following parameters/conditions affect the range of two-phase flow instabilities as outlined in Table 4-1 [Yadigaroglu and Bergles, 1972; Boure et al., 1973; Saha et al., 1976; Tong and Tang, 1997]:

- **Geometrical parameters:** single/multiple channels, length, size, flow restrictions,
- **Operating conditions:** pressure, velocity, inlet subcooling, power input and,
- **Boundary conditions:** axial heat flux distribution, pressure drop across channels.

Table 4-1: Classification of flow instabilities [adapted from Boure et al., 1973]

Class	Type	Mechanism	Characteristics
Static Instabilities			
Fundamental static instability	Flow excursion or Ledinegg instability	$\left.\frac{\partial \Delta P}{\partial G}\right\|_{\substack{\text{int} \\ \text{flow}}} \leq \left.\frac{\partial \Delta P}{\partial G}\right\|_{\substack{\text{ext} \\ \text{pump}}}$ flow characteristic curve has negative slope than pump characteristics at/near operating point	Flow undergoes sudden large amplitude excursion to a new, stable operating condition
	Boiling crisis	Ineffective removal of heat from the heated surface	Wall temperature excursion and flow oscillation
Fundamental relaxation instability	Flow pattern transition instability	Bubbly flow has less void but higher ΔP than annular flow	Cyclic flow pattern transitions and flow rate variations
Compound relaxation instability	Bumping, geysering and chugging	Periodic adjustments of metastable conditions, usually due to lack of nucleation sites	Periodic process of superheat and violent evaporation with possible expulsion and refilling
Dynamic instabilities			
Fundamental dynamic instability	Acoustic oscillations	Resonance of pressure waves	High frequencies (10-100 Hz) related to time required for pressure wave propagation in system
	Density wave oscillations	Delay and feedback effects in relationship between flow rate, density and ΔP	Low frequencies (1 Hz) related to transit time of a continuity wave
Compound dynamic instability	Thermal oscillations	Interaction of variable heat transfer coefficient with flow dynamics	Occurs in film boiling
	Parallel channel instability	Interaction among a number of parallel channels	Various modes of flow redistribution
Compound dynamic instability as secondary phenomena	Pressure drop oscillations	Flow excursion initiates dynamic interaction between channel and compressible volume	Very low frequency periodic process (0.1 Hz)

A preliminary conjectural conclusion, looking at the thermo-hydrodynamic coupling in the operational characteristics of CLPHPs, is the fact that 'complex' instabilities are inherently present in the system. The heat input is the 'cause' and the bubble pumping action is the primary 'effect', the secondary effect being (or ought to be) enhanced heat transfer. In the operational process, heating the multiple U-sections at one end and simultaneously cooling the other end produces sustained flow instabilities. This results, as an end effect, in pulsating two-phase fluid flow inside the tube sections causing heat transfer, as a combination of sensible and latent heat portions. The flow instabilities are a superposition of various underlying effects. Static instabilities occur because the bubble pumping characteristics get affected by the pressure drop characteristics of the tube sections (direct analogy with Ledinegg instability is not possible since 'pump' static characteristics are not explicitly known). This may also lead to relaxation type instabilities if the conditions are close to transition between slug and annular flows. In addition, fundamental and compound dynamic instabilities, especially the density wave oscillations and parallel channel instabilities, are inherent as a direct consequence of the link between vaporization/condensation processes and the two-phase flow behavior. Certain instabilities are also manifested through the metastable non-equilibrium conditions that are always expected in real systems.

All the parameters affecting general two-phase flow instabilities as outlined above must affect the thermal performance of CLPHPs. That this indeed is the case will be shown partly by the results of this research. It is important to remember that there are some parameters whose effect on CLPHPs may not be as explicitly stated as in the case of single-channel externally controlled flows. Since there is no separate pump in a CLPHP and the bubbles themselves are pumping liquid (and this action depends on the thermal boundary conditions), one of the major hurdles is the fact that the mass velocity of flow is governed by the input heat flux and is not known a priori. In addition, there is no direct control over the degree of fluid sub-cooling entering the respective evaporator U-turns. This is governed by various independent parameters including the tube diameter, length, condenser cooling conditions etc. Furthermore, inlet and exit restrictions are not present or not required to be present in case of CLPHPs. These facts clearly indicate that conventional (in-) stability analysis (e.g. method of small perturbations) seems unrealistic for CLPHPs. The results from such an instability analysis , as done in open micro/mini single and parallel channels, cannot be extrapolated for the case of CLPHPs.

4.2 Effect of filling ratio

In this section, we will go on to show the effect of the filling ratio on the thermo-hydrodynamics of CLPHPs. The summary of effects based on the experimental results is presented first, followed by the actual relevant results and supporting evidences.

4.2.1 Pulsating and non-pulsating mode of operation

A given CLPHP has two operational extremes with respect to the working fluid filling ratio, i.e. 0% filled or an empty device and 100% filled, equivalent to a single-phase thermosyphon. Thus, a dry CLPHP on the one hand and a fully filled CLPHP on the other serve as reference for the device operation. It is important to understand the fundamental characteristics of these operational modes to fully appreciate the CLPHP operation.

It is obvious that at a filling ratio of 0%, a CLPHP structure with only bare tubes having no working fluid inside, is a poor conduction mode heat transfer device obviously having a very high undesirable thermal resistance.

A 100% filled CLPHP is identical in operation to a single-phase natural thermosyphon. In this case, the liquid starts circulating inside the device due to a density difference associated with the temperature gradient. The buoyancy force must overcome the liquid phase viscous dissipation and the wall shear stresses to set the liquid into circulation, causing a net sensible heat transfer from the heater to the cooler. Since there exist no bubbles in the tube, the 'pulsating' effect is obviously nonexistent but substantial heat transfer can take place due to the circulating liquid in the tubes by thermally induced buoyancy. In this case, the local heat transfer coefficient in the tubes is only a function of fluid Grashof and Prandtl numbers.

A certain amount of heat transfer is achieved in the single-phase thermosyphon mode of CLPHP operation. If this heat transfer rate has to be augmented, a logical step is to introduce a two-phase flow regime rather than a single-phase system, as outlined in the previous section (refer Section 4.1). For example, a substantial performance augmentation is obviously achieved in case of a two-phase thermosyphon because the heat transfer is governed purely by latent heat mechanism. In between the operational extremes (0% and 100% filling ratio) although a CLPHP is a two-phase device, the obvious advantages as achieved in a two-phase thermosyphon, may not always be guaranteed, if the internal flow regime continues to be predominantly slug flow. Thus, the thermo-mechanical boundary conditions have to be chosen in such a way to maximize the advantage. Due to capillary dimensions of the CLPHP tubes, alternating liquid plugs and vapor bubbles are always present, in contrast to a two-phase thermosyphon where a clear liquid-vapor interface exists with no slugs, allowing an unhindered flow of vapor to the condenser. By partially filling the CLPHP, it is expected that:

- There will be a some latent heat advantage due to evaporation/condensation of bubbles,
- The temperature gradient between heater/cooler coupled with bubble growth and collapse will generate self-sustaining pressure perturbations, as explained earlier, causing liquid plug transport and thus sensible heat transfer.
- Unlike gravity thermosyphons, the device can function in any orientation.

The experimental results of the present study have also shown that in the partially filled pulsating mode of operation too, there exist three distinct sub-regions:

(a) Nearly 100% filling ratio: As soon as a very small amount of the working fluid is sucked out of the device (e.g. FR ≈ 95%), it results in the formation of few vapor bubbles in the tubes. As will be seen by the results that follow, there is a remarkable drop in performance with the introduction of these first few bubbles. In the single-phase mode (FR = 100%), the liquid could freely circulate in the tube resulting in substantial convective heat transfer. As soon as there is a single bubble (or few bubbles) in the device, this naturally circulating flow is hindered. Under the new working conditions, the driving force generated due to the density gradient has to overcome additional forces to induce a flow. These new retarding forces are due to: (i) the additional frictional resistance (or pressure drop) created due to the head and tail section of the bubble, (ii) the buoyancy force which acts on the bubble due to which it is difficult to bring the bubble in the downward direction against the gravity. In addition, since nearly 95% of the CLPHP is filled with an incompressible working fluid, the overall degree of freedom is very limited; the limited bubbles are not sufficient to generate the required perturbations. The buoyancy induced liquid circulation, which was present in the 100% filled CLPHP, is hindered due to additional flow resistance of the bubbles. Thus, the performance of the device is seriously hampered resulting in a thermal resistance that is much higher than for the 100% filled CLPHP.

(b) Nearly 0% filling ratio: In this mode, there is very little liquid to form enough distinct plugs and there is a tendency towards a dry-out (or partial multiple dry-outs) of the evaporator U-turns. The macro level operational characteristics are unstable and undesirable.

(c) CLPHP true working range: Between filling ratios of about 20% to 80%, the CLPHP operates as a true pulsating device. This working range will differ for different working fluids, operating parameters and construction. The more bubbles (lower filling ratios), the higher is the degree of freedom, but simultaneously there is less liquid mass for sensible heat transfer. Less bubbles (higher filling ratios) cause less perturbations and the bubble pumping action is reduced thereby lowering the performance. Thus, an optimum-filling ratio exists for a given thermal requirement.

With this summary on the effect of the filling ratio on the operational characteristics of CLPHPs, experimental evidences will now be presented.

4.2.2 Results of Experiment-I

In this experiment, two working fluids were employed, i.e. water and ethanol. Figure 4-7 a, b shows the time-temperature profile of adjacent tubes in the adiabatic section of the set-up for a heater power of 10 W and 100% filling ratio for both fluids, respectively. In vertical orientation (i.e. 90°, heater down) and at 45° inclination angle, the tubes in the adiabatic section were always alternately hot and cold, i.e. T1 and T3 were higher than T2 and T4. Moreover, just after switching on the heating (step increase), the CLPHP achieved a rapid

steady state following the short initial transient. Thereafter, the inter-tube temperature difference of adiabatic section tubes, the alternating hot and cold phenomenon, was continually maintained. This inter-tube temperature difference clearly suggests that there was a thermally driven directed fluid flow in the CLPHP tubes. This directional flow was also independently confirmed by seeding the flow with glass tracer particles. The system thus behaved as a naturally driven single-phase thermosyphon. The direction that the flow took was arbitrary for a given experimental run but once the direction was fixed it did not change for the entire period of experiment. As the inclination angle was changed from vertical to 45°, the adiabatic temperature difference increased (T1 increased and T2 dropped). Similarly, the net thermal resistance slightly increased. This happened because of a reduction of flow velocity due to reducing gravitational head. Later, when the orientation was changed to horizontal, the temperatures of all the adiabatic section tubes tended to equalize and the

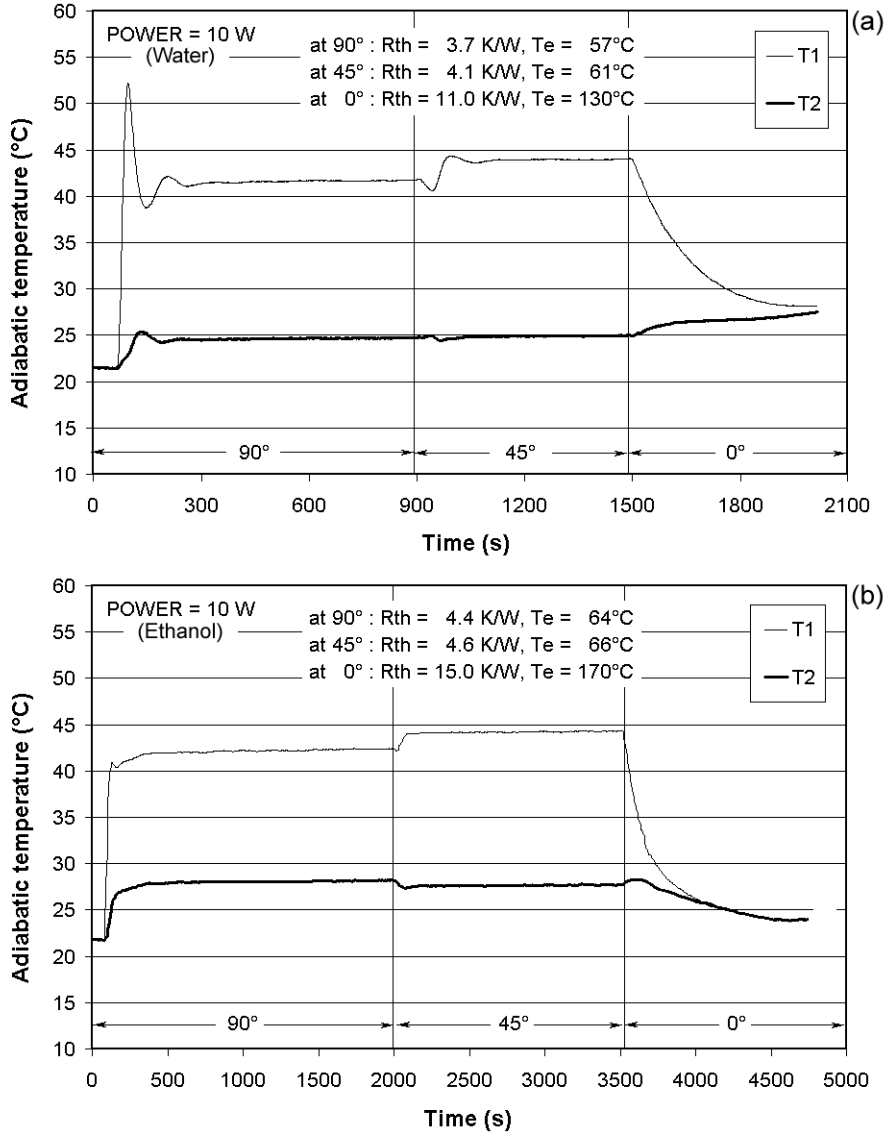

Figure 4-7: Temperatures of adjacent tubes in the adiabatic section of CLPHP (Experiment-I) with filling ratio = 100% and working fluids (a) water (b) ethanol

thermal resistance drastically increased to very high undesirable values. Bulk fluid circulation stopped in the absence of buoyancy and heat transfer took place purely by axial conduction.

On the same experimental set-up, tests were conducted with filling ratios of 90%, 50%, 30% and 0% for both fluids, respectively. Figure 4-8 a, b shows the thermal performance of tested CLPHP with respect to the filling ratio in vertical heater down position. Figures 4-9 and 4-10 depict the time history of adjacent tube adiabatic temperatures with a filling ratio of 50% and a power input of 10 W in vertical orientation for both the fluids. The magnified view of a time slot is included for clarity.

Referring to Figure 4-8 a, b, for FR = 50%, although the thermal resistance decreased with increasing the input power, in no case it was found to be better than in the single-phase thermosyphon mode of operation. For FR = 30% the combination of bubble dynamics and latent heat advantage coupled with the sensible heat transport through the liquid plugs was sufficient to get the pulsating mode advantage. This occurred at lower input power for

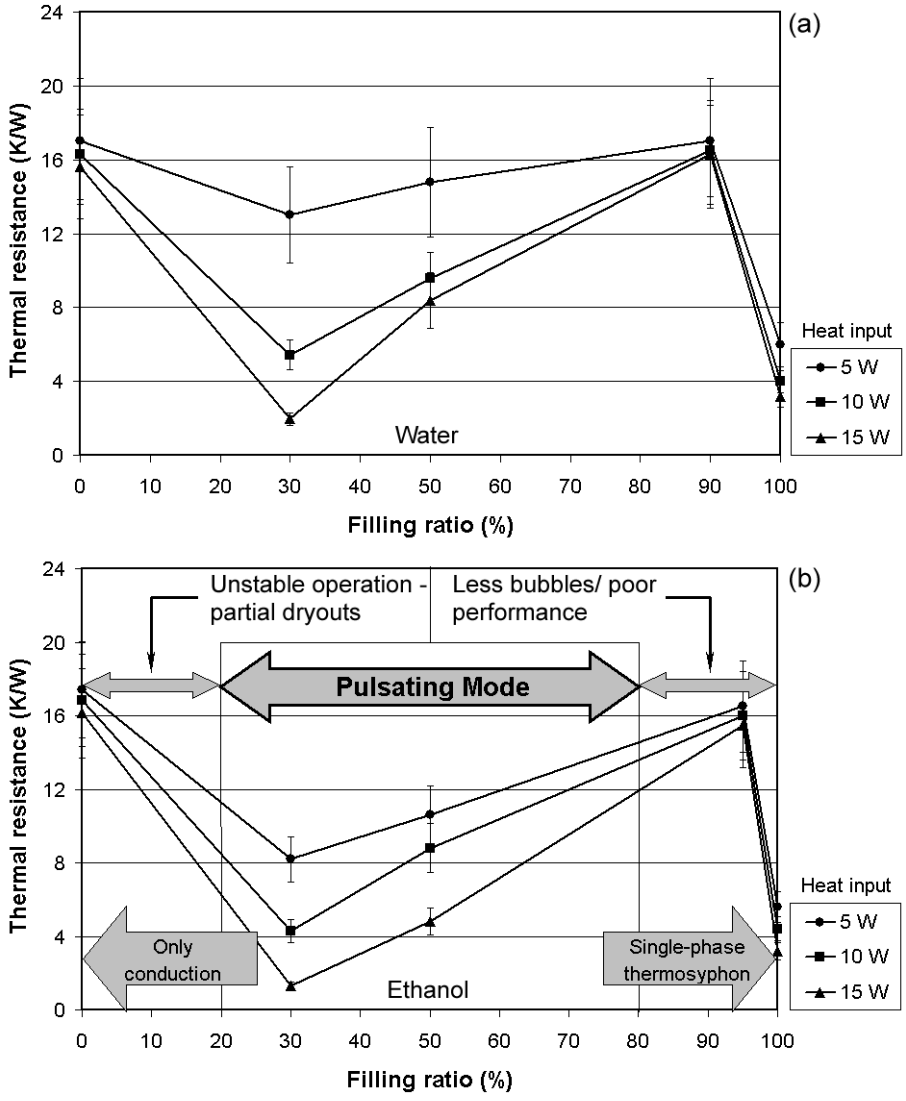

Figure 4-8: Effect of filling ratio for vertical heater down position (Experiment-I) for working fluids (a) water (b) ethanol

ethanol than for water. It is to be noted that for a given temperature gradient between the heater and cooler, ethanol has a higher saturation pressure slope than water. The results suggest that there is a critical input power below which the pulsating effect of the system provides no special advantage compared to the thermal performance of a 100% filled natural circulation device. In fact, at very low power levels, hardly any flow oscillations were seen.

In all the experiments with this set-up, it was observed that horizontal operation was not possible and resulted in a sharp increase in thermal resistance. All temperatures of the adiabatic section rapidly equalized and no macro movement of bubbles was seen. Bubbles only oscillated about a mean position with high frequency. All bulk movement ceased and the input power had to be stopped for safety. This behavior suggests that:

(a) Although surface tension predominates in the capillary dimension tubes used in the experiments, the very fact that the CLPHP stopped operating in horizontal position

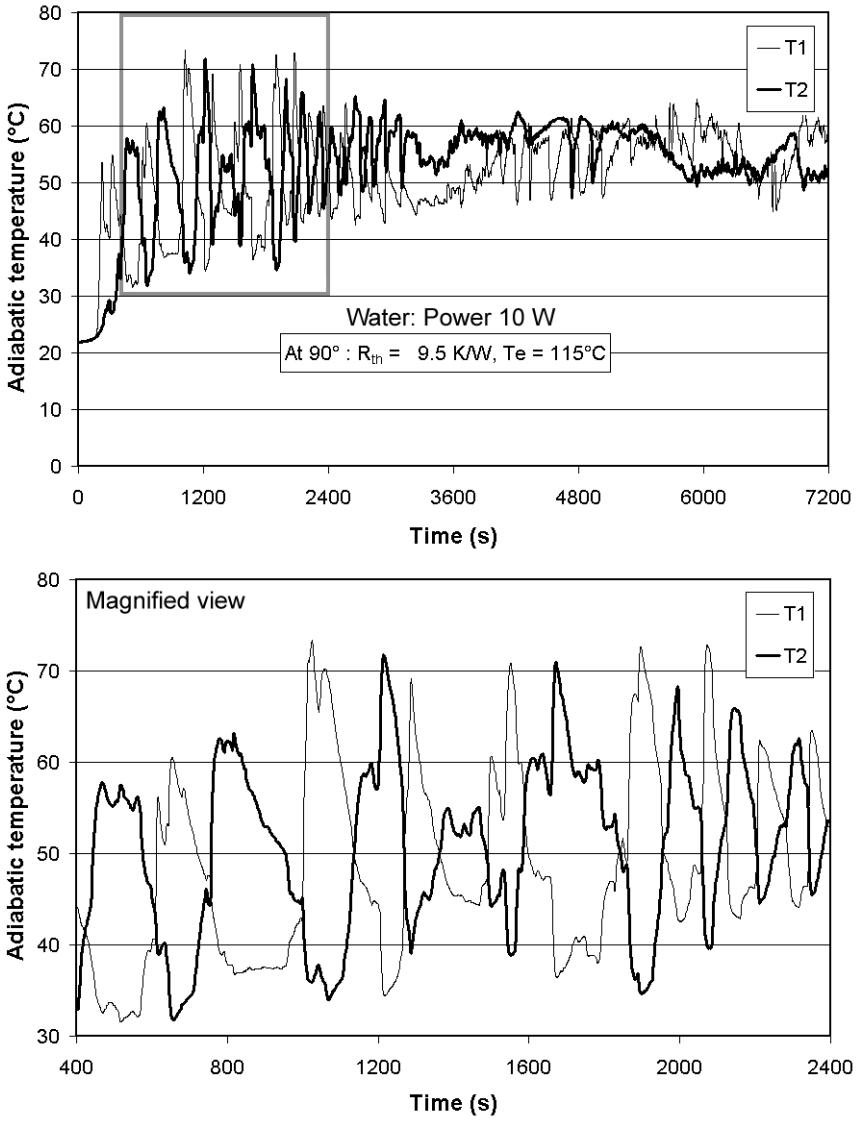

Figure 4-9: Temperature of adjacent tubes in the adiabatic section of CLPHP (Experiment-I) with filling ratio = 50% and water as the working fluid

confirms that the effect of gravity force is not insignificant. The effect of gravity will be later discussed separately.

(b) In the present experiments, the number of turns was likely to be too small for the CLPHP to operate satisfactorily in all the orientations with respect to the gravity vector. The dependence of CLPHP performance on increasing the number of turns is attributed to the fact that the overall degree of freedom is increased. This hypothesis will not only be discussed subsequently in detail but will also be confirmed.

(c) As suggested earlier, the input heat flux is also expected to be one of the parameters for generating internal perturbations. Due to the rather fragile nature of this set-up, it was not possible to achieve higher heat fluxes. This was done later in other experiments and its effect will be demonstrated in the coming sections.

A closer look at the temperature fluctuations, as depicted in Figures 4-9 and 4-10 (for

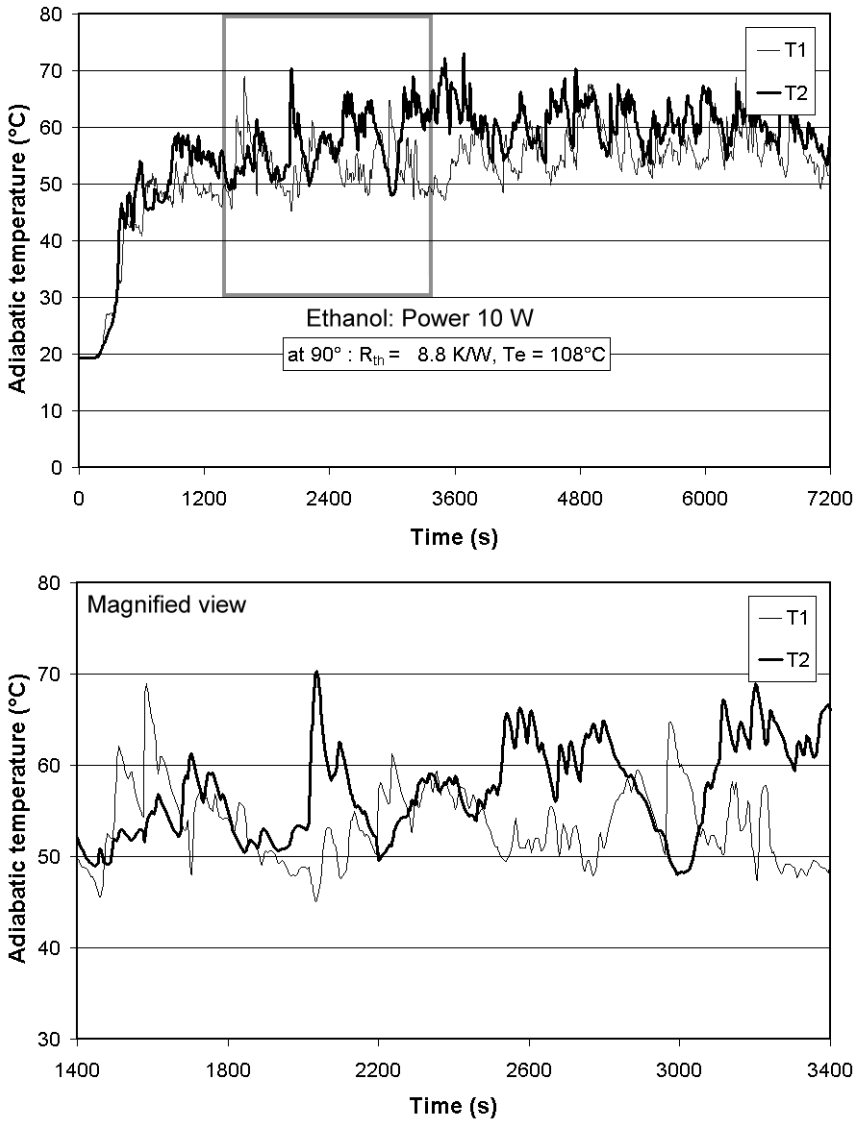

Figure 4-10: Temperature of adjacent tubes in the adiabatic section of CLPHP (Experiment-I) with filling ratio = 50% and ethanol as the working fluid

water and ethanol, respectively, both at an input power of 10 W) reveals that the CLPHP tubes in the adiabatic section remained alternatively hot and cold for extended periods of time. This suggests that there was a directed flow of the working fluid in the system. The direction of macro motion of these plugs frequently reversed and so did the tube temperatures in the adiabatic section, as shown. Adjacent inter-tube temperature difference in the adiabatic section increased up to a certain value after which it tended to equalize again due to a flow direction reversal. Flow visualization also indicated that there are alternating periods in which plugs/bubbles were moving rapidly ('activity' phase) and tending to stop for a while ('static' phase). In the static phase, only micro movement of bubbles with high frequency/low amplitude about a mean position was observed whereas in the activity phase they vigorously moved with higher amplitudes with various bubble patterns (refer Section 4.3.2.3). While the static phase was going on, there was a tendency of equalization of the adiabatic section tube temperatures. In the activity phase, when there was bulk fluid motion in one direction, the adjacent inter-tube temperature difference in the adiabatic section increased as hot fluid came from the evaporator in one tube and cold fluid flowed down from the condenser in the adjacent tube. This process continued and some degree of 'order' or pseudo periodicity was seen within the apparent 'disorder' of the PHP system. These processes, as described above, were only true for comparatively low power inputs (up to 15 W in this case). As the input power was increased, there was a drastic change in bubble-plug behavior. This will be described in Section 4.3.2.

4.2.3 Results of Experiment-II

Valuable preliminary phenomenological information was obtained from the results of Experiment-I. The results of Experiment-II, which are presented below, provided concrete quantitative data, confirming the various phenomenological observations of Experiment-I.

A typical time-temperature transient response of the average evaporator temperature for 100% ethanol filled CLPHP in vertical heater down position is shown in Figure 4-11 a. With increasing heat input to the device, the evaporator temperature rose resulting in a greater density gradient in the tubes. Simultaneously, the liquid viscosity also dropped diminishing the wall friction. For power input of 5 W, no fluid circulation was initiated. At 10 W, there was a sudden decrease of T_e as the liquid circulation started. This fluid circulation was observed by the fact that the respective adjacent tubes of the CLPHP became and remained alternatively hot and cold thereafter. The circulation direction that the liquid took was arbitrary; remaining fixed for a given experiment but changed with different experimental runs. There was a smooth decrease of the thermal resistance with increasing power input. The circulating liquid velocity must have been rising thereafter, resulting in a thermal response as depicted. When the filling ratio was reduced to 95%, there was a sudden increase in thermal resistance as depicted in the temperature-time variation of T_e in Figure 4-11 b. Only about 22 W of throughput was achieved to make average T_e = 100°C as compared to about 38 W in 100% filled thermosyphon mode of operation. Similar results and phenomenological trends were obtained in case of water and R-123 also.

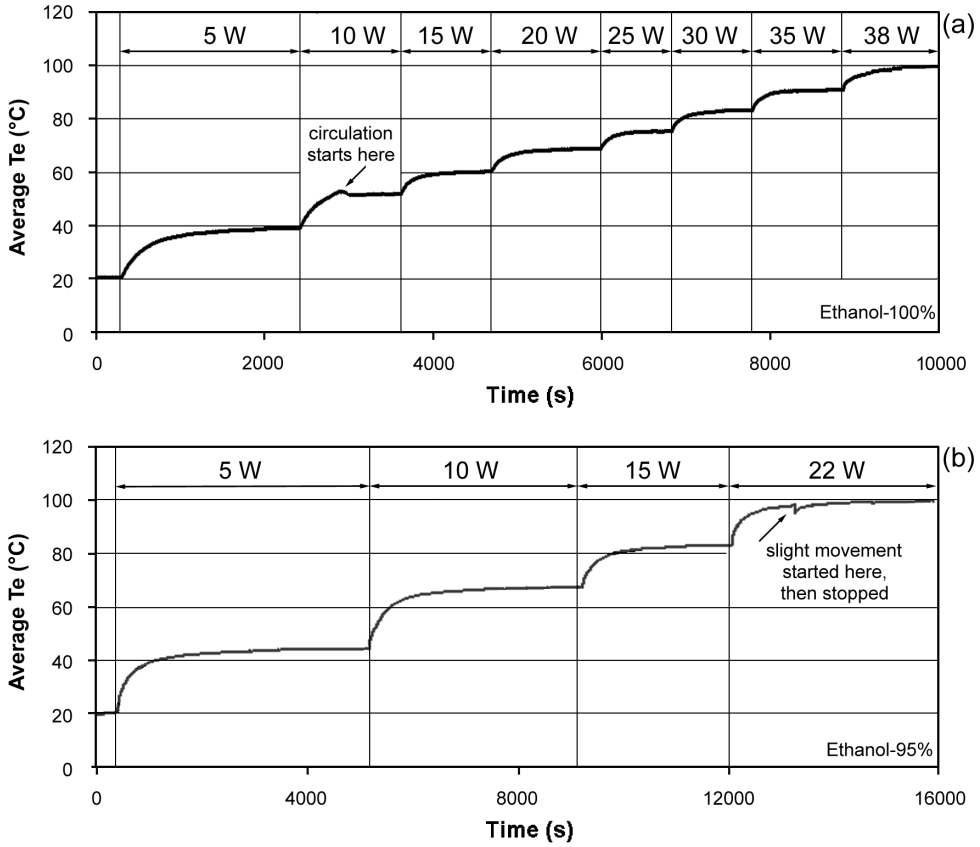

Figure 4-11: Transient variation of T_e with increasing heat input for vertically orientated ethanol filled CLPHP (Experiment-II) (a) filling ratio = 100% (b) filling ratio = 95%

Figure 4-12 shows the complete CLPHP profile of maximum heat throughput achievable with respect to the filling ratio for vertical heater down operation of the device. The maximum heat throughput values correspond to a specified maximum T_e (i.e. 100°C for water and ethanol and 60°C for R-123). This should not be mistaken with dry-out heat power. As can bee seen from the result, between about 20% and 80% filling ratio, depending on the working fluid, the device functioned in a true pulsating mode. The thermal performance improved, until a lower minimum-filling ratio, below which intermittent operation with partial or total dryout in the evaporator section commenced. For water, the maximum performance was observed at about 15% - 30% filling ratio. For ethanol and R-123, a range of filling ratios between 25% to 55% (ethanol) and 35% - 60% (R-123) gave practically the same maximum heat throughput. It may be concluded that there is a sizable plateau effect of maximum heat throughput with respect to the filling ratio.

Similar to the trend observed in Experiment-I, a partially filled CLPHP operated better than a 100% filled (single-phase thermosyphon mode) device only under certain operating conditions. For example, at FR = 85% ethanol, the maximum thermal power transported was about 42 W to attain an average evaporator temperature of 100°C. At this power, it was only a slight improvement over the 100% filled mode. For all the heating power range below 42 W, the performance of the 85% filled PHP was inferior to that of the 100% filled PHP (refer

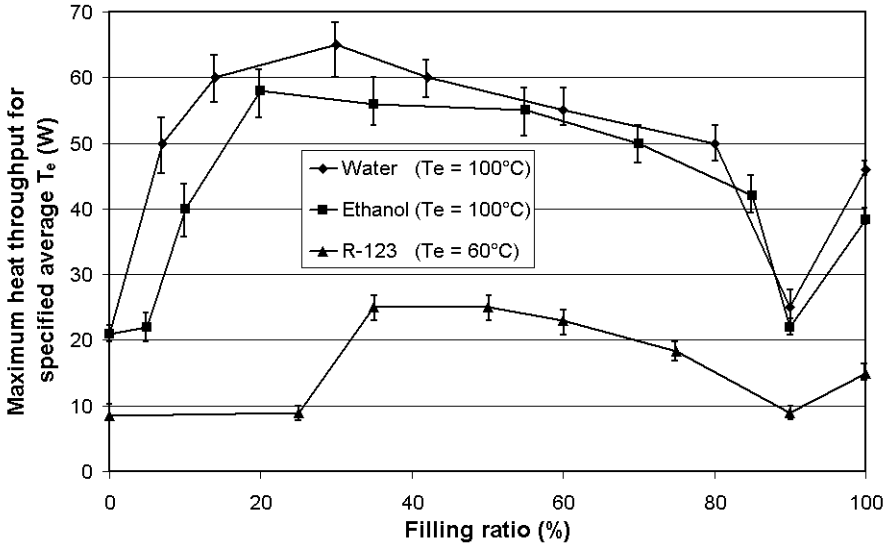

Figure 4-12: Effect of filling ratio on maximum performance of CLPHP (Experiment-II)

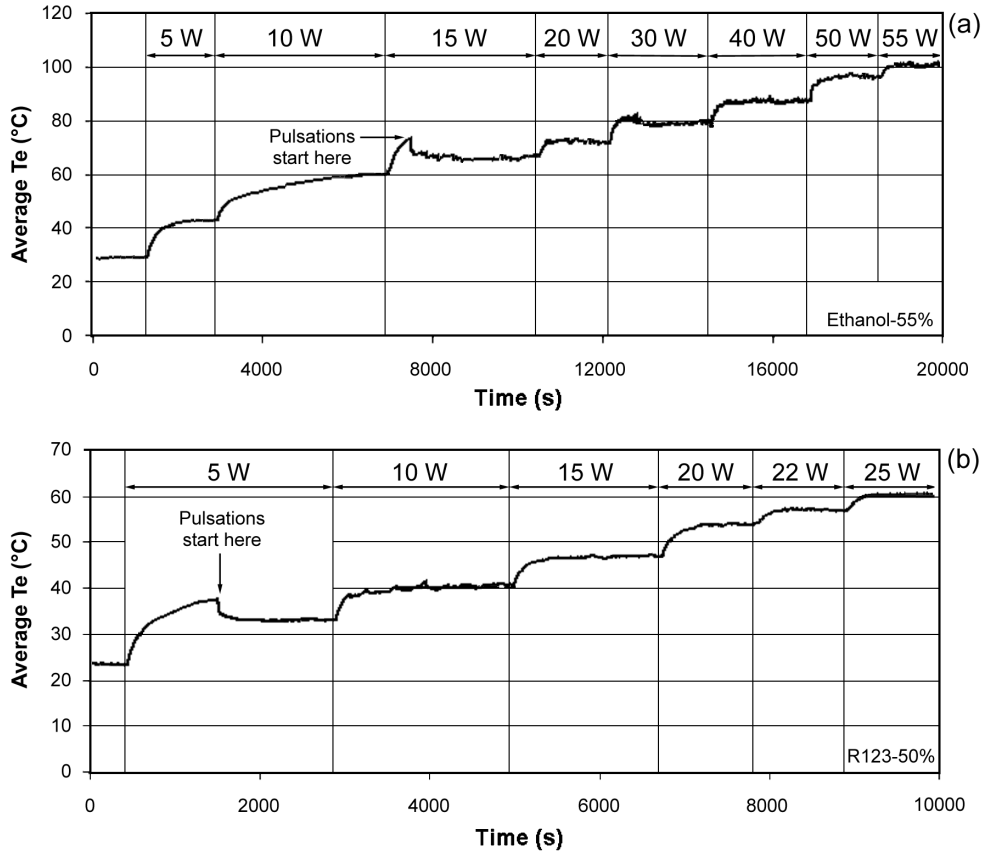

Figure 4-13: Transient variation of average T_e with increasing heat input for vertically orientated CLPHP (Experiment-II) (a) for ethanol with filling ratio = 55% (b) for R-123 with filling ratio = 50%

Figure 4-22). Up to about 15 W heat input, there was hardly any pulsating effect inside the tubes. Only after crossing this limit, macro level movements initiated resulting in improved performance. At low heating powers, T_e and corresponding P_{sat} was quite low. The overall degree of freedom of the device was also still small due to the presence of only a small number of bubbles. Simultaneously the presence of bubbles created additional frictional pressure drop and the advantage likely to be achieved due to their presence was not really observed under such working conditions. Below a -filling ratio of 55% and down to 20%, there was a clear advantage of a CLPHP as compared to a 100% filled mode of operation.

The typical transient response of an ethanol, 55% filled CLPHP in vertical heater down orientation is shown in Figure 4-13 a. Practically no pulsations were initiated till 15 W heat input. Thereafter the device functioned better than in the 100% filled mode of operation and self-sustained thermally driven oscillations were continuously maintained. Similar results for R-123 (50% filled, vertical heater down) are shown in Figure 4-13 b, where the pulsations were initiated at a low power input of 5 W only. At this filling ratio of R-123, the CLPHP was better than the 100% filled device at all power ranges as seen in Figure 4-22.

4.3 Effect of input heat flux

As indicated earlier, the input heat flux has emerged as a decisive parameter in defining the CLPHPs. In fact, as the results will demonstrate, the thermal performance strongly depends on the input heat flux. This is a direct consequence of (a) dependence of two-phase flow instabilities, and (b) dependence of internal flow patterns on the input heat flux.

4.3.1 Effect of heat flux on two-phase flow instabilities

The effect of input heat flux on various forms of two-phase flow instabilities is well documented. For example, experimental as well as analytical studies on density wave oscillations in single channel two-phase flow (open systems) by Ishii and Zuber [1970] and Saha et al. [1976] have indicated that these are strongly dependent on the input heat flux. The other factors include single and two-phase frictional pressure drop characteristics of the channel, inlet flow rate, level of inlet subcooling, system pressure and inlet/exit restrictions, if any. Their results are summarized in Figure 4-14 that shows the stability plane for density-wave oscillations developed from a linear stability analysis in which the disturbances are assumed to be small perturbations about steady state. The predicted stability conditions are plotted in terms of subcooling number and the dimensionless heat flux, defined as,

$$Su = N_{sub} = \frac{c_{P,liq}(T_{sat} - T_{in})}{h_{fg}}\left(\frac{\rho_{liq} - \rho_{vap}}{\rho_{vap}}\right) \tag{4-9}$$

$$Q^{*} = N_{pc}\big|_{eq} = \left(\frac{4 \cdot \dot{q} \cdot L}{D_{hyd} \cdot h_{fg} \cdot (G/\rho_{liq,in})}\right)\left(\frac{\rho_{liq} - \rho_{vap}}{\rho_{liq} \cdot \rho_{vap}}\right) \tag{4-10}$$

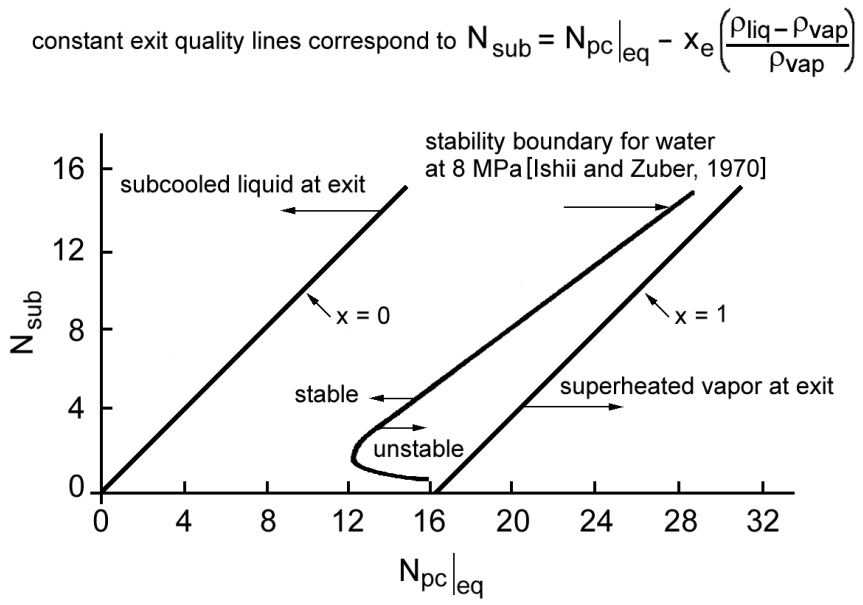

Figure 4-14: Stability boundary for water as predicted by Ishii and Zuber [1970]

The predictions of this analysis have agreed reasonably well with experimental determinations of the onset of density wave instability [Saha et al., 1976; Carey, 1992]. Looking at Figure 4-14, with respect to input heat flux, the results may be summarized by saying that for a specified flow rate with a non-zero level of inlet subcooling, increasing the flux above a certain limit induces flow instabilities. While the general phenomenological conclusions of this analysis fit well to CLPHPs, the inlet velocity of flow, which is explicitly known in the open system analysis, is unavailable in case of CLPHPs. The flow velocity inside CLPHPs is not well defined but is oscillating and completely dependent on the imposed thermo-mechanical boundary conditions. In addition, and in contrast, the inlet to the evaporator is typically always under two-phase flow conditions in a CLPHP and is different and temporally changing for each evaporator U-turn.

For a defined geometry of CLPHP, the input heat flux is directly responsible for the type of flow pattern that will exist in the channel, thus affecting the fundamental relaxation instabilities. Furthermore, the static Ledinegg type instabilities are also affected by input heat flux in case of CLPHPs since this directly affects the bubble pumping characteristics. Thus, one may hypothesize that the operating heat flux will directly affect the level of perturbations inside a CLPHP thereby affecting the thermal performance of the device. The experimental results of the present study coupled with visualization, have indeed strongly indicated towards this trend.

4.3.2 Effect of heat flux on flow patterns

The first and most obvious effect of input heat flux is on the internal flow patterns of the CLPHP. The results indicate that these flow patterns have far reaching influence on the performance of the device. The various observed flow patterns are described hereunder.

4.3.2.1 Fluid pattern after filling

Immediately after filling the CLPHP, the working fluid naturally distributes itself into various liquid-vapor plug-bubble systems in a random fashion. Distinct plugs are formed whose individuality is maintained since surface tension forces are dominant. This happens irrespective of the global orientation of the device during the filling process. (in Section 4.6 we will see how gravity affects the plugs even if the critical Bond number criterion, i.e., Eq. 4-6, is satisfied). After a short initial transient, following the closure of the main filling valve, the system rapidly comes to a steady pressure corresponding to the prevailing isothermal conditions. The contact angle of the menisci, of course, depends on the fluid-wall material combination. The maximum possible length of a liquid plug which can exist inside the tube depends on the thermo-physical properties of the fluid including contact angle and global orientation of the device while filling [Teng et al., 1999]; no attempt was made to record this aspect during the experiments with glass CLPHPs.

4.3.2.2 Overall flow pattern scenario with increasing heat flux

From visual observations for Experiment-I and Experiment-III an overall picture about the effect of heat input on the flow pattern of the CLPHPs can be developed (provided that the filling ratio is between about 20% to 80%, i.e. the true pulsating range of the device as described in Section 4.2.1).

- Since the driving force for the device comes directly from the input heat power, at very low heat inputs, practically nothing happens. The power is not sufficient to overcome the required driving pressure drop and the plugs/bubbles practically remain stagnant at their respective positions with an exception of occasional stray movements. It is interesting to note that in such a situation, although the evaporator temperature may reach sufficiently high values (e.g. over 100°C in case of water or ethanol), this does not initiate any oscillations. Such a condition normally leads to generation of very small bubbles in the evaporator region, a process phenomenologically similar to nucleate pool boiling. Thus, it seems that wall superheat is not the only criterion for the pulsating action to be initiated and to thrive thereafter. A minimum critical heat flux is needed to drive the system.
- As the input heat flux surpasses a critical value, oscillations are initiated. In the beginning, these oscillations are abrupt and there is no specified flow circulation direction in the tube loop. The flow pattern remains oscillating capillary slug flow. There are periods (of several seconds) in which macro motion of slugs stops for a while followed by an activity phase as described earlier in Section 4.2.2. The device performance in terms of overall thermal resistance remains quite poor.
- A further increase in heating power results in ‘stable’ oscillations whose amplitude increases with increase in input power. Eventually, the fluid oscillations in alternate tubes come in phase with each other thereby resulting in an overall fluid circulation in the device. The direction that the flow takes is arbitrary for a given experimental run. In this transition power zone, there is an occasional flow circulation direction reversal. Overall, capillary slug flow still prevails. Figure 4-15 depicts such a scenario for the glass CLPHP of

Experiment-I, filled with 50% ethanol and working in vertical orientation with a power input of 15 W. An imposed fluid circulation is clearly observable. On real time videos, secondary oscillations are seen superimposed on the circulating slug flow (refer Figure 4-16 a, b also). As soon as circulation begins, there is a noticeable decrease in the thermal resistance.

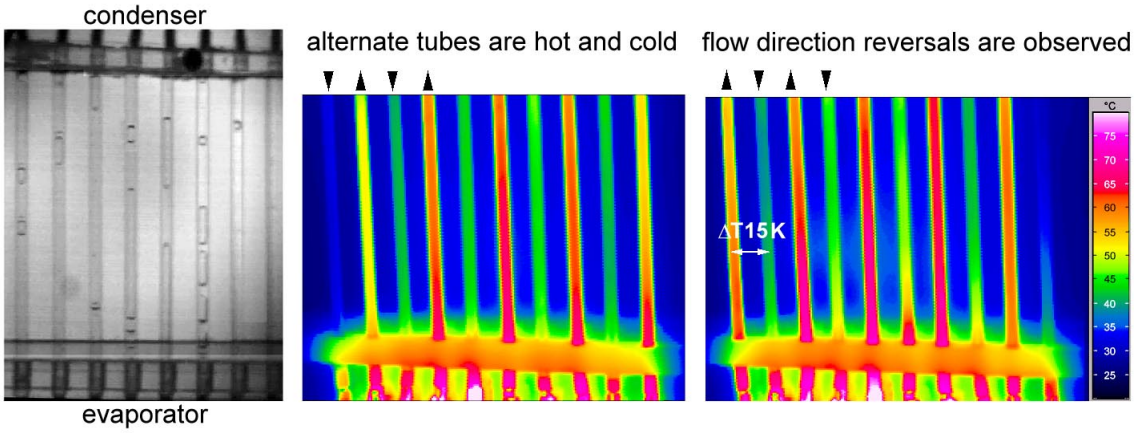

Figure 4-15: Snapshot and thermographs of the glass tube CLPHP (Experiment-I, vertical orientation, filling ratio = 50% ethanol, heat input = 15 W)

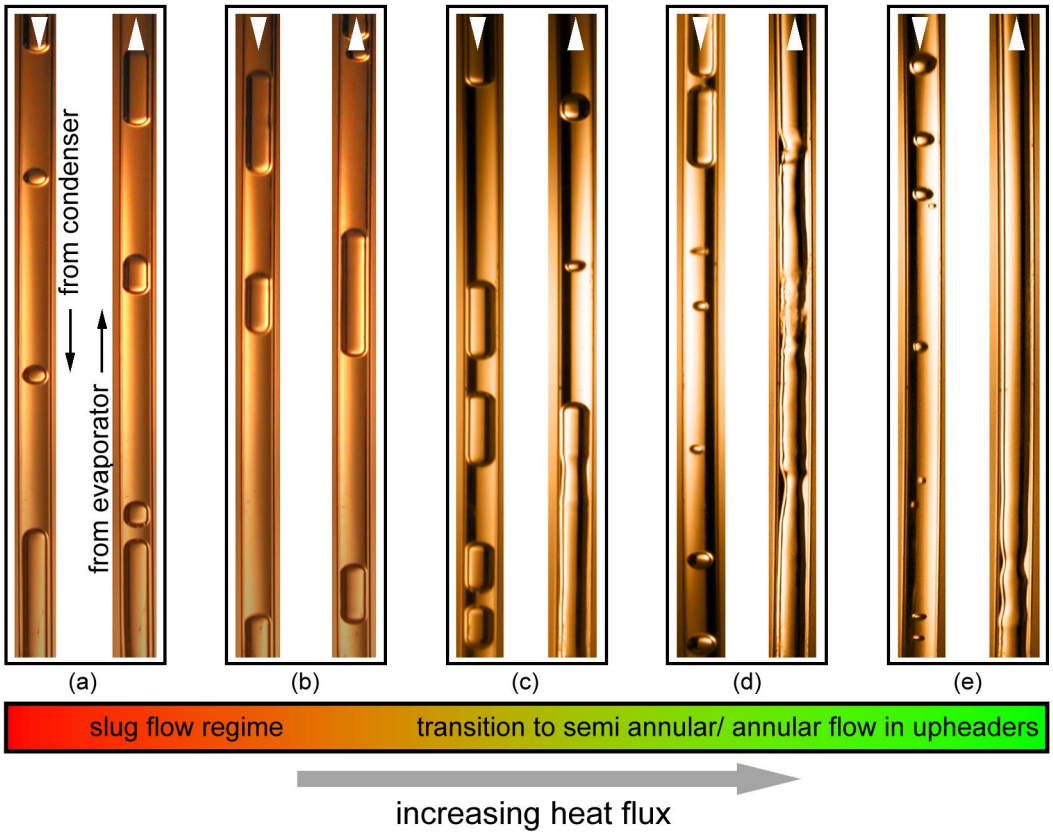

Figure 4-16: Effect of heat flux on the internal flow patterns inside the single loop device (Experiment-III)

- Increasing the heater power further increases the circulation velocity. The flow direction tends to remain more fixed as flow direction reversals become increasingly rare. This also marks the beginning of a flow transition from capillary slug flow in the entire device to a combination of capillary slug flow in the down-header tubes (from condenser to the evaporator) and semi-annular/annular flow in the up-header tubes (from evaporator to the condenser) as shown in Figure 4-16 c, d. These events correspond to a drastic decrease in the thermal resistance. The transition to annular flow is observed even at capillary tube dimensions of 2.0 mm. At this stage, a reduction in thermal input power results in a reverse transition scenario (from annular to slug flow) in the entire device, which corresponds to a higher thermal resistance. It should be noted that the slug-annular transition depends not only on the heat input but also on the geometrical constructional features. The length of tube sections in the condenser/evaporator will determine the flux at which heat is being rejected/fed in. The flow Weber number, entrainment due to Helmholtz type instabilities and subsequent 'bridging'/'flooding' phenomena and other forms of dynamic instabilities are the limiting factors of the slug-annular transition.
- The slugs in the cold down-headers keep shrinking in size with further increase in the input heat power as can be seen in Figure 4-16 e. The isochoric nature of the device forces this phenomenon. As the vapor volumetric fraction increases in the annular flow up-headers, since the net void fraction must remain effectively constant (provided respective phase densities are assumed not to be changing appreciably), the down-header bubbles must shrink in size. The results also indicate that the pulsating unstable slug flow behavior is again stabilized after a certain higher input heat flux. (In fact, this observation is in line with the classical experiments on two-phase flow instabilities in open systems as explained in Section 4.3.1 (refer Figure 4-14)). Therefore, ironically enough, the best performing closed loop pulsating heat pipe no more remains a true 'pulsating' device. Further increase in heat flux will lead to some sort of evaporator dry-out phenomenon. Unfortunately, dry-out powers could not be supplied in this study in view of the safety of experimental set-ups. The dry-out mechanism of CLPHPs thus remains unexplored. It is indeed worthwhile to concentrate efforts in this direction. Thus, we observe that the input heat flux governs the degree of pulsations in the device and essentially acts as a demarcation parameter. A generic description of the various features and transitional phenomena has been described above. The specific quantitative parametric values at which a particular phenomenon will occur depend on various factors such as the geometry, working fluid, exact filling ratio etc.

4.3.2.3 Special features of diabatic slug flow in CLPHPs

As noted above, at low heat fluxes in general, the flow pattern in the entire device can be categorized as oscillating capillary slug flow. Before proceeding further, it is not out of place here to first summarize the salient features of general capillary slug flow under adiabatic condition [Wallis, 1969]:

- The flow can exist in horizontal, inclined as well as vertical direction due to the strong dominance of surface tension. In other words, the general flow pattern in a capillary tube is not severely affected by the flow direction.

- If the wettability of the continuous phase is good, it has always been observed that the movement of the suspended phase takes place inside a thin film of the continuous phase.
- Separated flow is hardly seen. The flow pattern is nearly axisymmetric irrespective of the flow direction. As the pipe size decreases, the circumferential distribution of film thickness becomes uniform causing an axisymmetric flow pattern. The smaller the pipe size, the thinner the liquid film around a large bubble.
- For a general case, the velocity of bubbles in slug flow is affected simultaneously by viscous, inertia, interfacial tension and buoyancy forces (only in case of inclined/vertical flows).
- Small bubbles in a liquid plug or in a liquid film are scarcely observed.
- In horizontal slug flow, there is no drift flux due to buoyancy. Nevertheless, the bubbles still move faster than the average liquid velocity, as the available area for flow is less due to the presence of liquid thin film.

The net pressure drop in a typical slug flow is conveniently divided into three components:

(a) Pressure drop in the liquid plug,

(b) Pressure drop around the ends of the bubble and,

(c) Pressure drop along the body of the bubble, which is practically zero.

The last point is supported by the facts that, if the gas phase density and viscosity are much lower than those of the liquid phase, the gas in the bubble is practically at constant pressure. Further, if the bubble curvature is constant, pressure drop cannot exist in the bubble body. It has also been observed that the terminal velocity of cylindrical bubbles rising vertically upwards in stagnant liquid is generally unaffected by the length of the bubble, thus supporting the theory. Therefore, if we compare the pressure drop of two-phase capillary slug flow with that of single-phase flow, it is observed that an approximately triangular or saw-tooth alternating component of pressure drop is superimposed on the average pressure gradient as shown in Figure 4-17. This phenomenon on its own can excite oscillations and pressure perturbations in the flow.

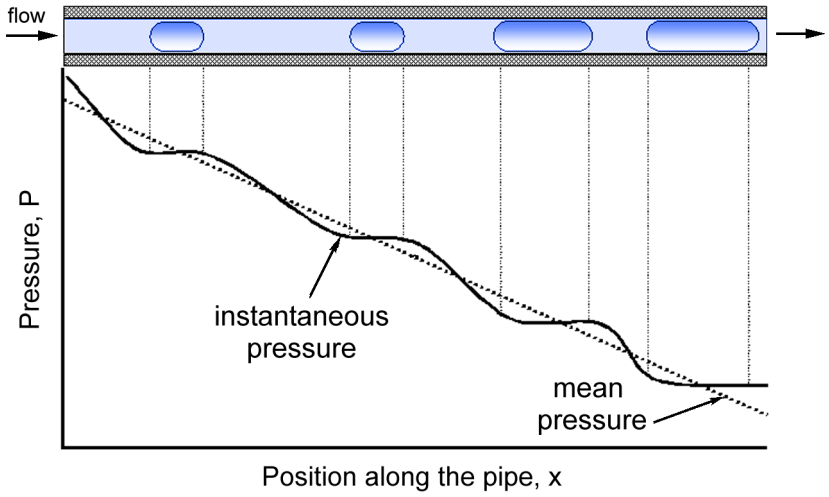

Figure 4-17: Pressure drop profile in typical slug flow conditions

In the background of this quick review of adiabatic capillary slug flows, attention is now focused on actual diabatic capillary slug flows at low heat fluxes in CLPHPs. While many of the flow characteristics are similar to those under adiabatic conditions, there are indeed some special characteristic features under diabatic and oscillating conditions encountered in CLPHPs. The observed features are summarized below:

Bubble size

- Frequently it is observed that, as the liquid plugs pass the evaporator U-bends, a small amount of liquid is always left behind in the bends. A boiling phenomenon qualitatively comparable to nucleate pool boiling within this small amount of entrapped liquid is observed. In this way, bubbles smaller than the tube diameter may be produced.
- Bubbles whose size is nearly equal to the tube diameter, the difference being attributed to the liquid thin film between the bubble and the tube, are more predominantly produced.
- Bubble length may or may not be comparable to the overall length of the PHP.

Bubble contact angle

- Depending on the physical properties of the working fluid and tube material, the leading and lagging dynamic contact angles of the vapor-liquid interface may be different as is predominantly seen in water compared to ethanol, as shown in Figure 4-18. This effect contributes towards the overall frictional flow resistance. This resistance is due to the capillary pressure difference between the plug front (in moving direction) and the plug end (against movement). The difference is caused by different curvatures, an effect of dynamic contact angle hysteresis [Carey, 1992]. The trailing slug curvature slips over a just wetted surface by the bulk liquid while the front meniscus has different conditions (refer Figure 4-19). Thus, applying the Laplace equation for capillary pressure gradient across a liquid-vapor interface in a tube of circular cross section:

$$F_{cap} = \pi \cdot D_i \cdot \sigma \cdot (\cos \alpha_{front} - \cos \alpha_{back})\big|_{dynamic} \qquad (4\text{-}11)$$

For water/glass, $\alpha_{front}\big|_{dynamic} \approx 80°$ and $\alpha_{back}\big|_{dynamic} \approx 42°$, were measured, i.e. a single water plug $(\sigma = 0.072\ N/m \text{ at } 25°C)$ in a glass tube (D_i = 2.0 mm) has to overcome an additional capillary resistance force equal to (-) $0.26 \cdot 10^{-3}$ N. For ethanol, the two dynamic contact angles were about the same and less than about 12°. Therefore, in this case the additional resistance is negligible. This additional resistance is additive and gets amplified if several plugs are simultaneously located in a channel. These cumulative pressure gradients damp oscillations and therefore fluid/solid combinations having large dynamic contact angle hysteresis should be avoided.

Bubble merging and breaking patterns

- Small bubbles, produced because of nucleate pool boiling in the evaporator section, rise in the adiabatic section of the tubes. Depending on the bubble rise velocity, relative movement of the bulk fluid, geometry of the device and local heat transfer characteristics, these bubbles may reach the condenser section with reduced sizes or may completely

collapse due to condensation while in transit. If a larger bubble is encountered on the way, these smaller bubbles usually merge with it as shown in Figure 4-20 a.

- A part of an expanding bubble breaks away from it and travels further to merge with another bubble encountered in the way as shown in Figure 4-20 b.
- A large bubble shrinks due to condensation and may sometimes become smaller than the tube diameter and immediately floats up due to buoyancy as shown in Figure 4-20 c.
- Two or more large expanding bubbles usually coalesce to form larger bubbles that in turn may be subdivided again into smaller components as shown in Figure 4-20 d.

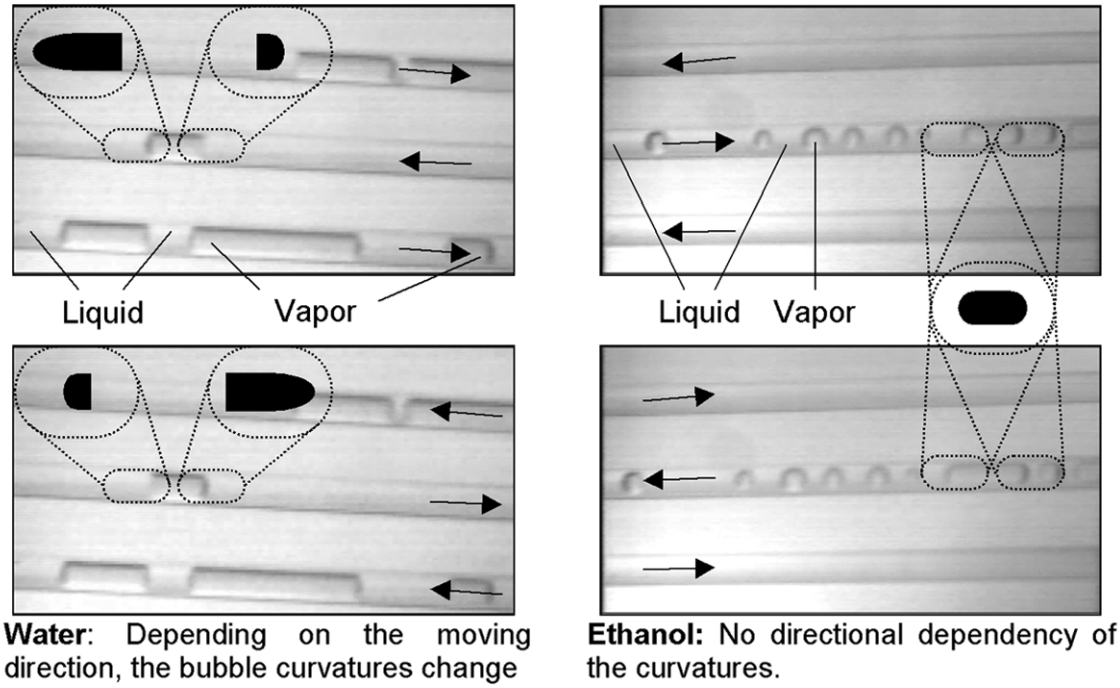

Figure 4-18: Effect on dynamic contact angle hysteresis on bubble shapes in CLPHPs (Experiment-1)

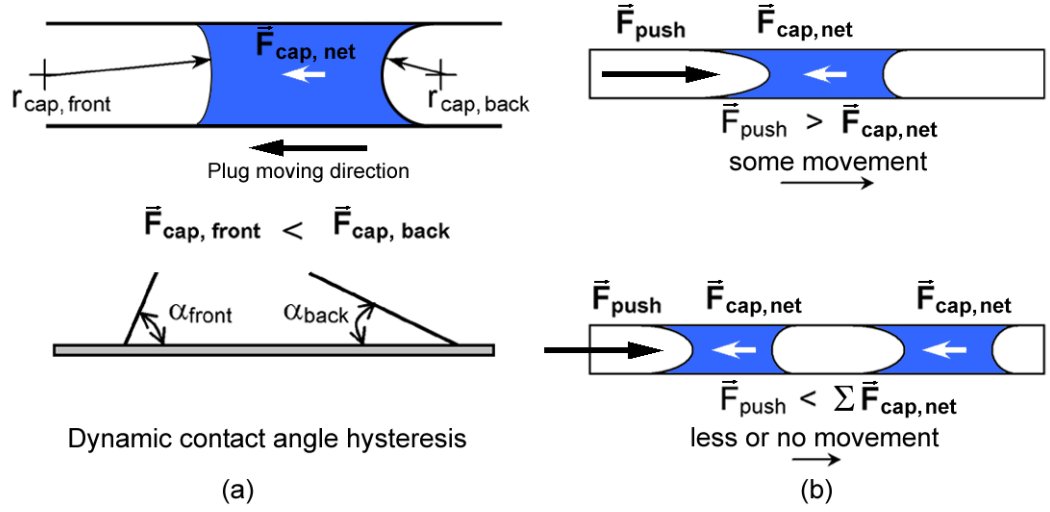

Figure 4-19: Dynamic contact angle hysteresis and its effect on capillary pressure

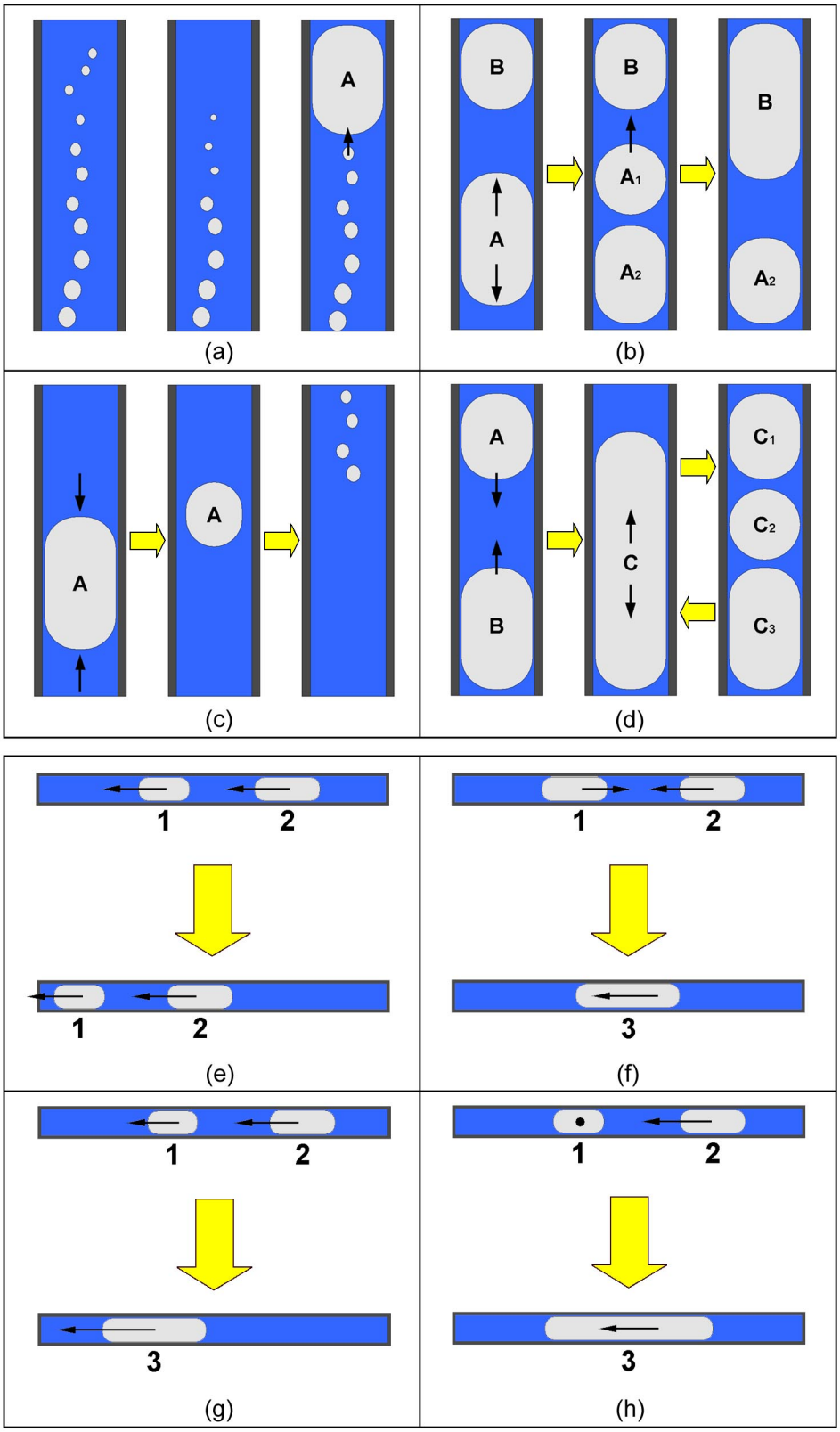

Figure 4-20: Classification of bubble patterns observed in CLPHPs

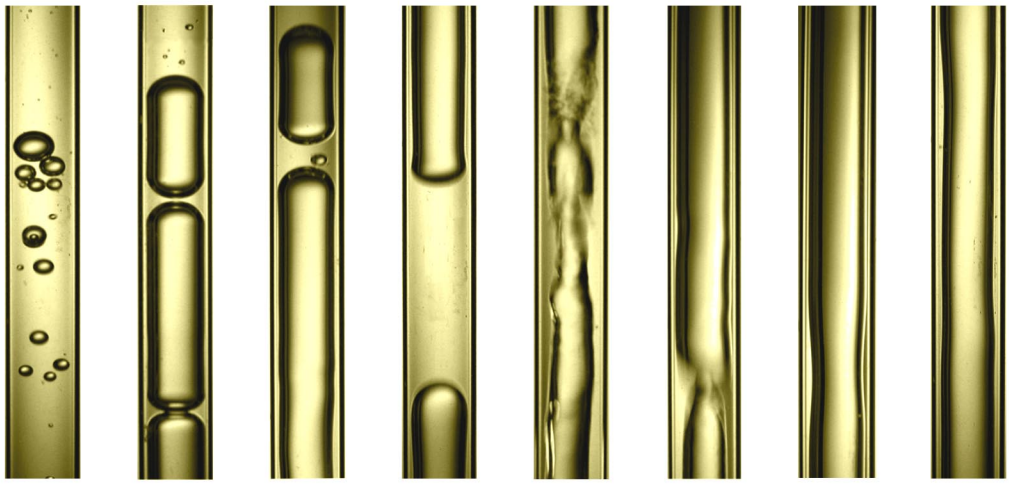

Figure 4-21: Snapshots of various types of internal flow patterns observed in CLPHPs (Experiments-I and III)

Bubble displacement patterns on micro and macro level

- Vapor bubbles may oscillate or vibrate with comparatively higher frequency about a mean position with small amplitude. These oscillations may or may not be superimposed by a macro displacement of the bubble along the length of the tube.
- As shown in Figure 4-20 e, two typical vapor bubbles 1 and 2 travel in the same direction with nearly comparable velocities taking along the liquid plug which is trapped between them. This is comparable to piston movement of the bubbles.
- Vapor bubbles 1 and 2 are both moving in the opposite direction, with simultaneous expansion, and finally merge together to form a larger vapor bubble 3 which continues to travel in the resultant direction as shown in Figure 4-20 f.
- Vapor bubbles 1 and 2 are both moving in the same direction, with simultaneous expansion, and finally merge together to form a larger vapor bubble 3 which continues to travel in the same direction as shown in Figure 4-20 g.
- Vapor bubble 1 is nearly stationary and vapor bubble 2 expands/travels and finally merges with bubble 1 to form a bigger bubble 3 that continues to travel. It is clearly observed that the vapor bubble 2, instead of acting as a 'piston' and pushing the liquid plug completely, travels through the liquid plug thereby displacing the in-between liquid which eventually passes through the thin layer around the inner wall as shown in Figure 4-20 h.

Figure 4-21 captures some examples of bubble/flow patterns observed in tested CLPHPs.

4.3.3 Results of Experiment-II

Figure 4-22 shows quantitative results for the effect of increasing heat flux on the thermal resistance of the copper CLPHP. The filling ratio is the third parameter to be varied and supplements the results of Section 4.2. These results provide the evidence for the discussions as stated in Sections 4.2.1 and 4.3.2.2.

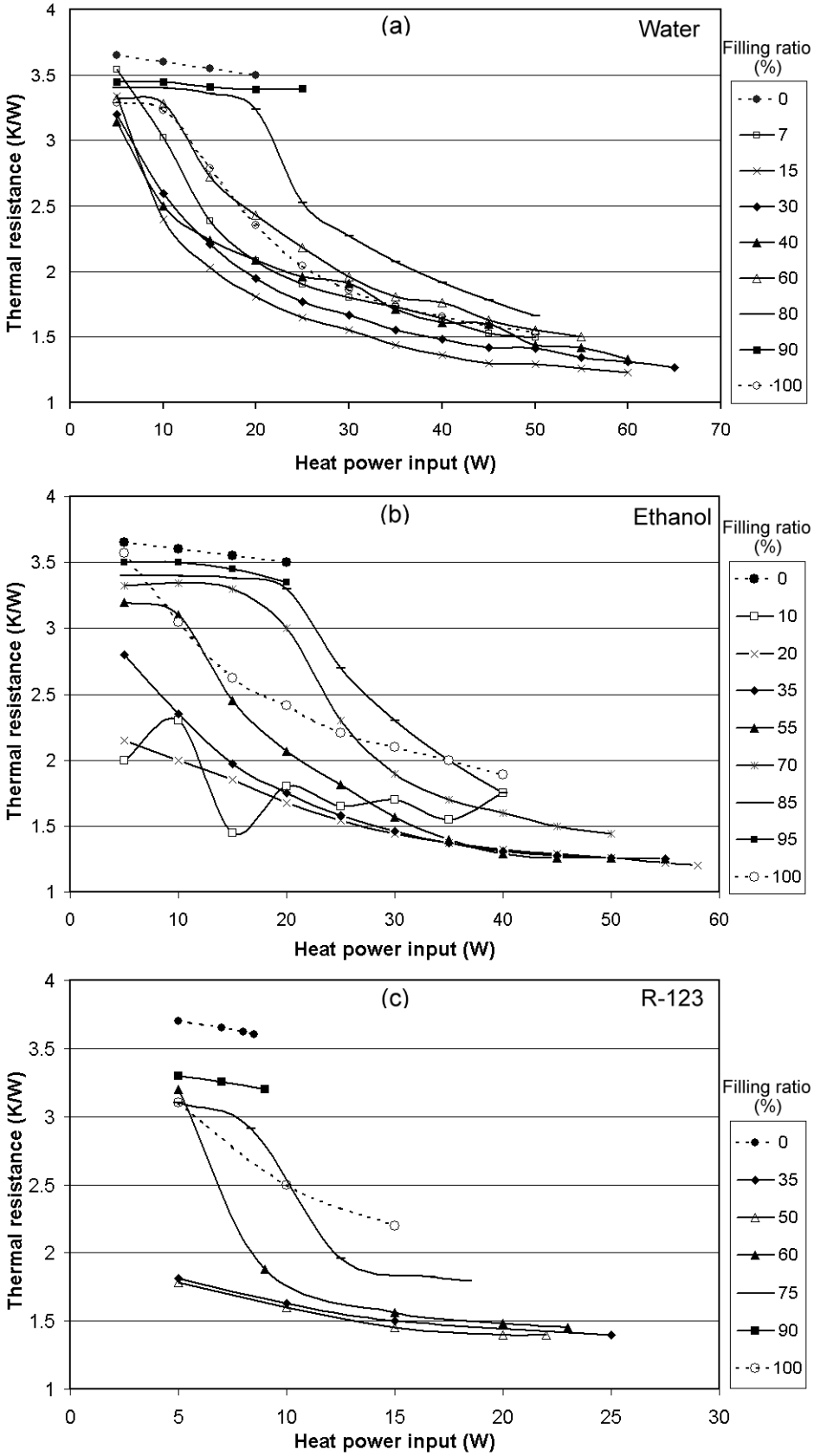

Figure 4-22: Effect of input heat flux on thermal performance of CLPHP (Experiment-II)

As can be seen, low input heat fluxes were not capable of generating enough perturbations and the resulting bubble pumping action was extremely restricted. Overall, this scenario resulted in a poor performance (i.e. very high thermal resistance). As the heat input was increased, it improved the heat transfer coefficient to a marked degree. Still higher input heat fluxes resulted in bulk flow taking a fixed direction that did not reverse with time. This circulation was manifested as adjacent tubes becoming alternately hot and cold. Interestingly, in such a case, lowest thermal resistance was observed. This is logical since the evaporator U-sections must have been experiencing convective boiling through the thin liquid film formed due to semi-annular/annular rather than nucleate type boiling in the earlier slug flow regime at low heating power. This was confirmed in Experiment-III.

4.3.4 Results of Experiment-III

Figure 4-23 depicts the observed phenomena in the loop operated in vertical heater down position, with FR = 60% ethanol and increasing input heat power. The corresponding

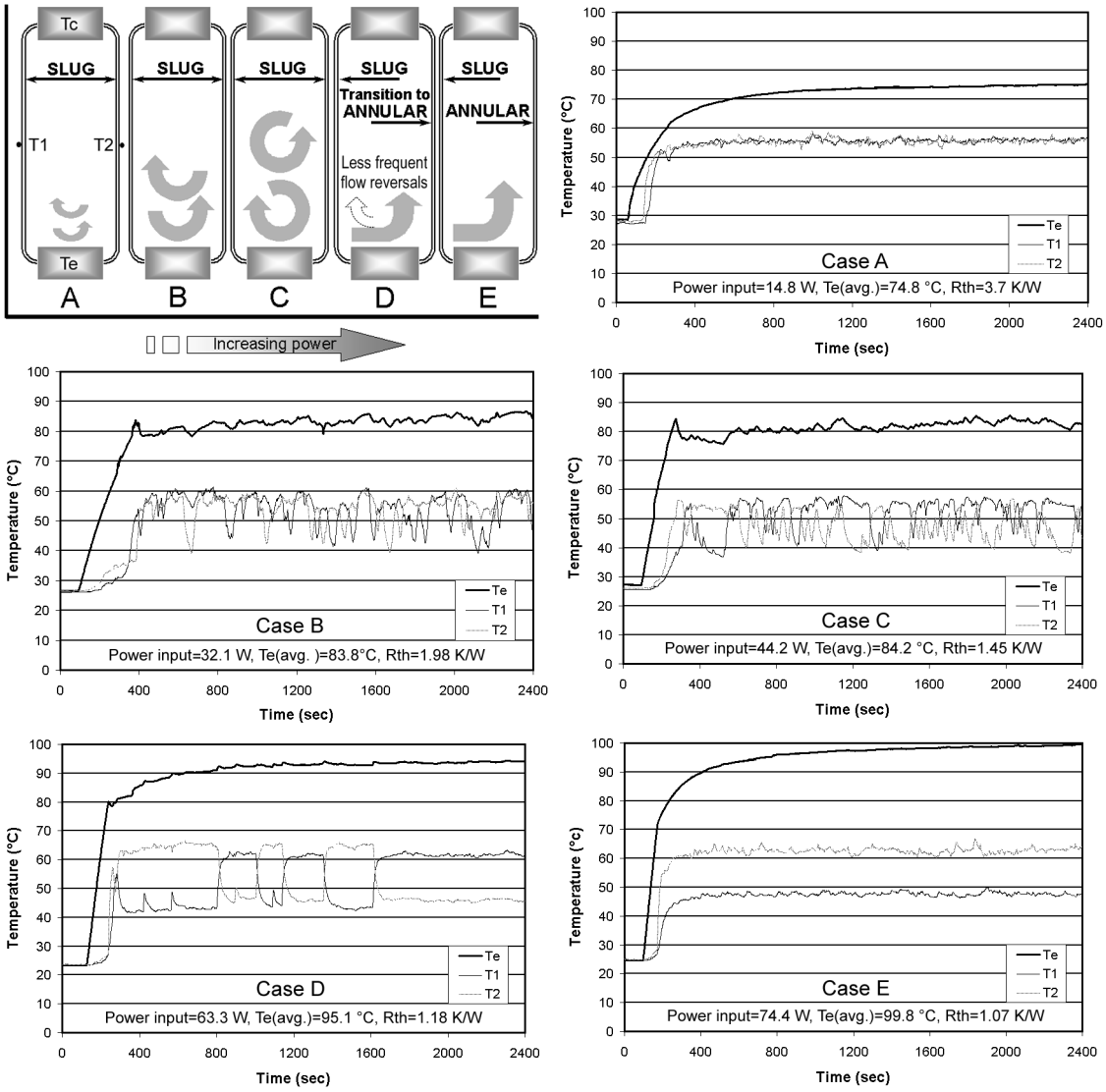

Figure 4-23: Effect of heat flux on the performance of single-loop device (Experiment-III)

recorded temperatures; T_e, T1 and T2, for each case along with the performance parameters are also shown. At low heating power, case A, low amplitude oscillations with slug flow in both tube sections were observed. Individual bubbles oscillated about a mean position and there was very little agglomeration or bulk movement. In fact, the bubbles in the adiabatic section acted as isolators, considerably thwarting the mixing of hot and cold fluid sections. The hot slugs remained oscillating in the evaporator zone resulting in considerably high thermal resistance. As the heat input was increased, case B and C, the oscillation amplitude increased. There was considerable improvement in the performance, with respect to the overall thermal resistance, as the amplitude became comparable to the overall length of the loop and more hot fluid was able to reach the condenser section. A complete turning of fluid started sometimes in the clockwise and sometimes anti-clockwise direction until the stage represented by case D was reached. Here, the flow turned in one direction for a considerable time before a direction reversal took place. This is also clearly represented by the changing pattern of the adiabatic tube temperatures, T1 and T2, for case D in Figure 4-23. During this time, the hotter tube section started to develop annular flow that changed back to slug flow by bridging/flooding action as the fluid traveled towards the cold end. When the input power was further increased, the flow direction reversal completely stopped. The fluid flow took an arbitrary direction, either clockwise or anti-clockwise, but then remained in the same fixed direction thereafter (Case E). In such a condition, fully developed annular flow was observed in one section (the up-header/hot fluid line) and bubbly/slug flow in the other section (down-header/cold feeder line). The device thermal resistance was observed to be the least in such a situation. As the heat power was further increased, the flow pattern remained similar and the size of the bubbles in the down-header/cold feeder line kept on shrinking as explained earlier. When the FR was increased (e.g. > 70%), it became increasingly difficult to sustain annular flow (since the overall system is isochoric) and tendency was towards slug flow in both the tube sections. This reduced the performance again as noted in Section 4.2.

4.3.5 Sensible vs. latent heat transfer

In a conventional wicked heat pipe or in a gravity thermosyphon, latent heat of vapor is the primary medium of heat transport. While prima facie, the two-phase flow characteristics of a PHP apparently suggest that latent heat may also play a sizable role; it is quite the contrary. This can be explained as follows:

A PHP is a constant volume device and if maintained throughout at a fixed temperature, liquid and vapor bubbles will be in thermodynamic equilibrium at saturated conditions. If a vapor bubble is now made to collapse by extracting heat from some area, thereby giving away its latent heat, there has to be a complimentary bubble generation elsewhere in the system, either by flashing or by receiving heat from the environment. This is necessary to sustain isochoric device boundary conditions. It follows that when a CLPHP is operating in a nearly steady state condition, the time averaged filling ratio remains practically constant (the only discrepancies, if any, will be essentially ephemeral due to non-equilibrium metastable conditions which may develop; heat and mass transfer having finite inertia). Operating the device at a slightly higher temperature necessarily maintains the same average filling ratio

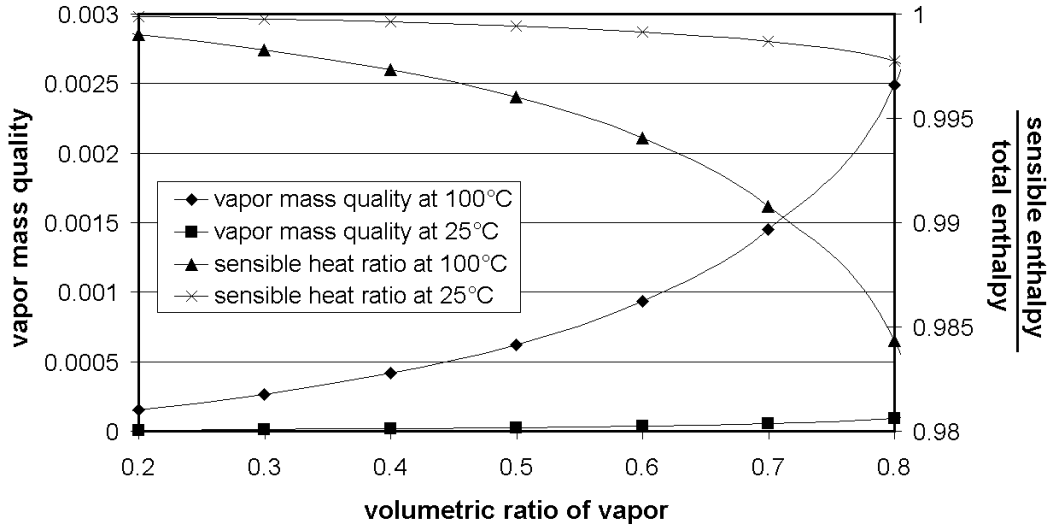

Figure 4-24: Operating range of vapor volumetric ratios in CLPHP and corresponding vapor mass quality highlighting the magnitude of sensible heat transfer

while the average vapor density in the bubbles increases. So, if the evaporator and condenser temperatures are fixed (thereby fixing the respective working pressures), an isochoric CLPHP system with a fixed volumetric filling ratio will have a fixed corresponding mass quality at the two respective temperatures. Figure 4-24 plots the volumetric ratio of vapor against the mass quality of vapor for ethanol at 25°C and 100°C. It is clearly seen that the overall mass quality of the vapor phase is extremely low for the range of applicable volumetric filling ratios of vapor (20% to 80%). Even if complete condensation and collapse of vapor bubbles is considered, the latent heat transported is significantly lower than the corresponding sensible heat transfer from liquid plugs during this time. For example, if saturated water and vapor mixture at 100°C leaves one of the evaporator U-tubes of a CLPHP and comes out of the condenser tube as saturated water at 25°C, assuming a FR = 50%, the ratio of sensible to latent heat transfer is about 1600. From a thermodynamic point of view, referring to the P-h diagram in Figure 4-25, the shaded gray area lying very near to the liquid saturation line can thus be marked. This zone essentially represents all the points on which the average mass quality, integrated over the whole device, at any given instant, must lie. Individual mass qualities, e.g. at evaporator/condenser U-turn exits will be different but the instantaneous average over the system must lie somewhere within this shaded zone.

Therefore, latent heat does not play a major role in the thermal performance of CLPHPs. Nevertheless, bubbles are certainly needed for self-sustained thermally driven oscillations. Indeed this is true only for the case when slug flow conditions exist throughout the device. As soon as there is a transition to semi-annular/annular flow, as explained earlier, the device operation tends towards a thermosyphon. This necessarily changes the latent heat impact in the overall scenario. Thus, it is extremely difficult to quantify the respective role of the sensible and latent portions as it depends on the internal flow patterns. It is logical to conclude that an annular flow regime is preferable since it improves the latent heat transfer bringing the device operation closer to an interconnected array of thermosyphons.

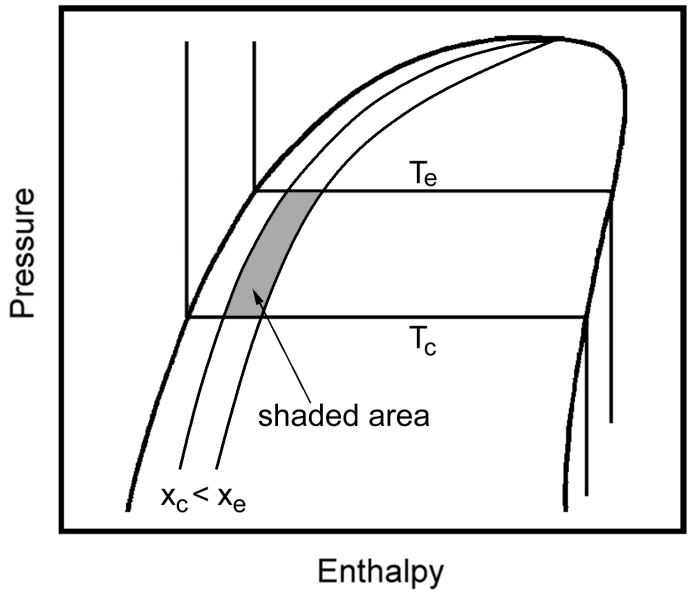

Figure 4-25: Zone depicting integral average mass quality in CLPHP operation (exaggerated for clarity)

4.4 Interim summary of results

Before proceeding further with more thermo-hydrodynamic subtleties of CLPHPs, it is worthwhile to summarize the evidences put forward until now and the ideas they support. Figure 4-26 highlights the main implications of hereto presented results. It highlights the operational definition of CLPHPs. There are at least three thermo-mechanical boundary conditions i.e. internal tube diameter, the filling ratio and the input heat flux, which are to be satisfied for the structure to behave as a true 'pulsating' device. The most interesting aspect is the fact that the best performing CLPHP, in terms of the overall thermal resistance, no longer behaves as a true 'pulsating' device. Alternating tube sections then have slug flow and annular flow respectively, the bulk flow tending to take a fixed direction. From a thermal performance point of view, CLPHPs are devices that lie in between extended surfaces metallic fins and conventional heat pipes/gravity assisted thermosyphons. The role of sensible and latent heat changes as per the prevailing internal flow patterns. With predominantly slug flow patterns in the entire device, latent heat plays a negligible role in the overall thermal performance. Further quantitative experimental data is certainly required to transform the loosely depicted phenomenological and qualitative definition of CLPHPs based on the boundary conditions, as shown in Figure 4-26, to more concrete foundations. In addition, near dry-out behavior, including the mechanism by which CLPHPs dry-out, itself requires further research.

With the individual effects of three major parameters having been discussed, we venture to explore the effects of two more decisive parameters viz. the number of turns and the operating orientation in the next sections.

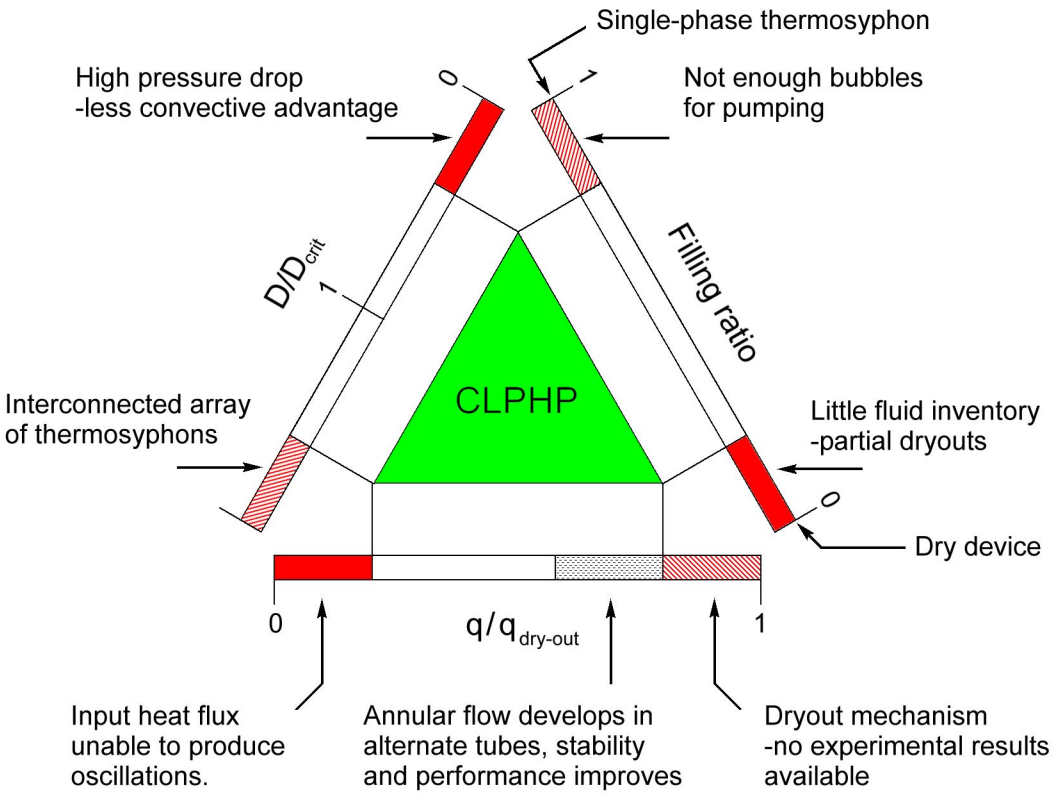

Figure 4-26: Thermo-mechanical boundary conditions for proper CLPHP operation

4.5 Effect of number of turns

4.5.1 Optimum number of turns

Consider that bare cooper rods of a given size are fitted to transport the heat and thereby cool the heater having a fixed input power. If only one copper rod is used, after the initial transient phase, the heater will come to some steady state temperature (T_e). As the number of copper rods is increased, since the net heater power ($\dot{Q}$) is fixed, the final steady state temperature of the heater will come down. Net heat handled per rod will decrease and so the overall system thermal resistance i.e. $R_{th} = (T_e - T_c) / \dot{Q}$, keeps decreasing as the number of copper rods increases. The limit is reached as per the available space in between the heater and the cooler so that, in the limit, all the copper rods together consume the entire available space. If the same system is cooled by a CLPHP, then, in this case, instead of bare copper rods there are copper pipes partially filled with a working fluid. Although a lot of conductive material is removed, the intention is to augment the heat transfer by internal self-sustained thermally driven convective two-phase flow. In a CLPHP, the heat transfer primarily takes place due to liquid convection (latent heat transfer through the vapor helps the bubble liquid pumping action, and thereby the sensible heat transfer), provided the CLPHP is optimally operating in the true pulsating regime.

If the number of turns of the CLPHP is small, then the heat handled by each turn will be quite high. It is obvious that since there is not enough fluid inventory and effective thermal cross sectional area available for heat transfer, the overall thermal resistance will be high. If the number of turns of the CLPHP is now increased (keeping the FR constant), as previously done with pure copper rods, what should be the effect on the overall thermal resistance of the device? Extrapolating the previous analogy, it is clearly seen that provided the heater power is fixed, as the number of turns of the CLPHP is increased, the net heat handled by each CLPHP turn reduces (the overall heat flux also simultaneously reduces). If we assume, for the time being, that the effective thermal conductivity (k_{CLPHP} as defined by $\dot{Q} = k_{CLPHP} \cdot A_{tot} \cdot (T_e - T_c)/L_{CLPHP}$) of the CLPHP is constant, then, as for the previous case of bare copper rods, the overall thermal resistance should come down. However, the effective CLPHP thermal conductivity, k_{CLPHP}, is not really a constant. In fact, it is dependent on the internal pressure fluctuations, flow patterns and on the existing temperature gradients.

Any decrease in the temperature of the evaporator actually reduces the local saturation pressure. If the condenser temperature is maintained constant, this primarily causes a reduction in overall pressure difference thereby reducing the driving potential. Thus, a monotonous increase in number of turns of a CLPHP will not have the same effects as in the case of bare solid copper rods. The effective thermal conductivity of a CLPHP is a strong function of the temperature differential existing between the evaporator and the condenser (apart from other factors already explained earlier). Therefore, for a given heat throughput requirement, an optimum number of turns must exist after which the pulsating effect of the fluid inside, and the heat transfer advantage thereof, will start to diminish.

4.5.2 Level of perturbations

A complete stop-over of all macro movements inside the loop, as shown in Figure 4-27, occurred many times in the single loop device tested in Experiment-III. This happened more frequently for FR < 50% (rarely for higher filling ratios) coupled with low input power. The 'self-sustained' oscillating character was then lost.

Such a behavior has never been reported for multi-turn CLPHPs, under comparable boundary conditions in the present study or in any other sources. Although, in a multi-turn CLPHP having a working fluid with low $(dP/dT)_{sat}$ like water, and at comparatively low heat input fluxes, flow visualization has indicated that there are alternating periods in which plugs/ bubbles are moving rapidly (activity phase) and tending to 'stop' for a while (static phase). As the input heat flux increases it becomes increasingly difficult to distinguish between the two phases since the period of the 'static' phase drastically reduces. This has already been discussed in Section 4.2.2.

Typical behavior of the loop under the conditions that lead to a complete stopover is as follows: the initial partial filling of the loop leads to a natural volumetric (mal-) distribution of phases in the two tube sections. As the heating power is switched on, the system starts to oscillate in the usual manner. If the combination of boundary conditions is favorable for a stopover, bubble agglomeration takes place leading to the formation of a single large bubble

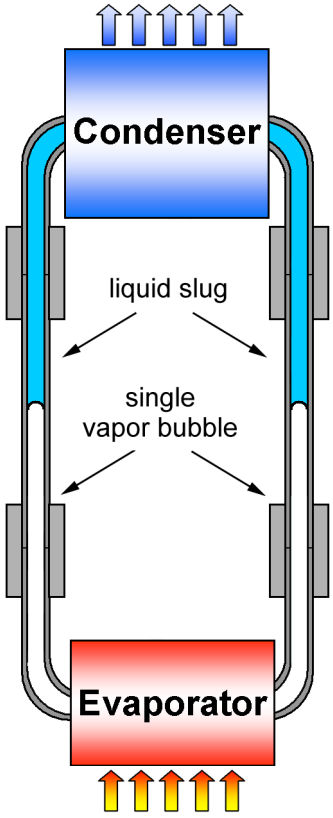

Figure 4-27: Stop-over phenomenon observed in the single loop device (Experiment-III)

which envelopes the entire evaporator section (refer Figure 4-27). Then oscillations die down completely and all macro motion of the fluid inside the tube stops leading to an increase of the evaporator temperature. As the number of turns keeps increasing, the probability of such a tendency towards complete stopover will essentially diminish, approaching practically zero as the number of turns exceeds a certain critical value.

4.6 Effect of operating orientation

One of the aims of good CLPHP design is to make the thermal performance, as far as possible, independent of the operating orientation i.e., the overall thermal resistance of the device should be independent of its global orientation. This is one of the major benefits claimed in favor of CLPHPs as compared to conventional heat pipes. The trend of the results of Experiment-I, II and III as regards to operating orientation, can be summarized as follows:

In all experiments, satisfactory operation was achieved in vertical heater down position, as has been demonstrated by the results presented in previous sections. By changing the orientation away from the vertical (towards horizontal, heater down in all cases), a change in the thermal resistance with respect to the reference vertical orientation was observed.

- Experiment-I: In this experiment, as has been mentioned before, the maximum heating power possible was only about 15 W resulting in a heat flux of the order of 1.0 W/cm^2. As will be recalled, all the experiments were conducted for 50% filling ratio. Under such conditions, only oscillating slug flow prevailed throughout the device. A small but

continuous increase of thermal resistance with respect to the reference vertical case was observed until nearly horizontal position. This increase was well within 15% of the reference value. Bringing the CLPHP to a horizontal position triggered a severe temperature excursion; the working fluids (water/ethanol) simply stopped oscillating resulting in very high thermal resistance. The input power to the device had to be stopped for safety. No attempt was made to run the device in top heat mode.

- Experiment-II: Here the flux level was about 3.5 W/cm^2 but still no operation in the horizontal mode was recorded. The thermal resistance remained practically constant from vertical to near horizontal operation (variation within 5% of the vertical value). These observations were recorded only for 50% filling ratio for all the three working fluids i.e. water, ethanol and R-123. Since the device was made of copper, no comments can be made about the internal flow patterns at various orientations. Top heat mode was not tested.
- Experiment-III: In this experiment although high heat fluxes were achieved, i.e. about 20.0 W/cm^2, there was only one fluid loop. While the general trend was the same as in the previous two experiments, in the inclination angle range of 45°-60° from vertical position, the thermal resistance always decreased slightly with respect to the vertical orientation. This happened whenever annular flow conditions existed in the up-header tube, as explained in Section 4.3.4. Near to horizontal, reverse transition to slug flow regime was frequently seen. No horizontal operation was achieved; the working fluid simply stopped oscillating. Top heat mode was not tested.

It can be seen that in all the three experiments proper horizontal operation was not achieved. Thus, gravity forces were indeed affecting the CLPHP performance. It remains to be seen whether this phenomenon is related to the imposed thermo-mechanical boundary conditions; in other words, whether or not there exist certain boundary conditions that will make the performance independent of gravity.

At a first glance, two physical phenomena affect the CLPHP performance with respect to orientation. The first is of course, the effect of gravity on the system, especially on slug flow characteristics and the second is the effect of total number of meandering turns on the level of internal temporal and spatial dynamic pressure perturbations.

As outlined in Section 4.1, classical experiments on the rise velocity of a single bubble in a cylindrical tube have shown that as the Bond number approaches a value approximately equal or less than 2, surface tension starts predominating over gravity forces. If it is assumed that surface tension indeed dominates in a particular experiment having $Bo \leq 2$, then what can we say about the shape of a typical slug-bubble element in vertical or horizontal orientation, especially regarding the symmetry of liquid film thickness around the bubble? Figure 4-28 shows the photograph of static ethanol vapor bubbles suspended in liquid ethanol inside D_i = 2.0 mm and 1.0 mm glass tubes respectively, taken at room temperature. Although the boundary conditions meet the critical Bond number criterion, the effect of gravity is clearly seen by the unsymmetrical shape of the bubble in the side view (View B). R-123 bubbles are more unsymmetrical as surface tension is still lower. These plug geometries do affect the pressure drop characteristics, interfacial waves, dynamic

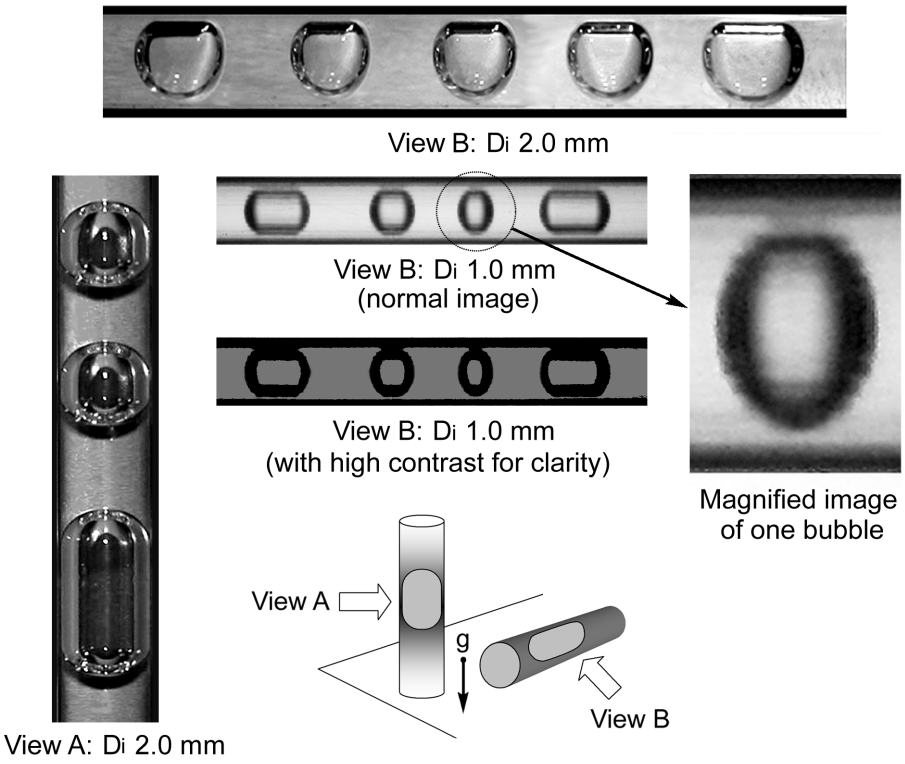

Figure 4-28: Effect of gravity on static ethanol bubbles suspended in liquid ethanol at room temperature

instabilities, bubble coalescence, bridging/flooding, etc. In addition, gravity will certainly play a role in determining the heat transfer characteristics of diabatic slug flow since there will exist unsymmetrical film thickness in the evaporator and condenser sections, depending on the global orientation of the device. Thus, we see that gravity does affect the slug flow dynamics in CLPHPs even though the boundary conditions satisfy the Bo_{crit} criterion.

In the discussion that follows, it will be clarified that in a non-operating, isothermal, partially filled CLPHP, the static pressure distribution traversing across the tube through the liquid plugs and vapor bubbles is drastically different in vertical and horizontal orientations. Although this explanation will be attempted in context to the single loop studied in Experiment-III, it can be easily extrapolated to a multi-turn CLPHP.

4.6.1 Static pressure distribution in CLPHP

4.6.1.1 Vertical operation

In the vertical orientation, gravitational body force acts on each plug and bubble (effect on a bubble is negligible). In a static condition, the probability that sections X-C-Y and section X-F-Y (refer Figure 4-29) have exactly the same volume fraction (or the mass fraction) of the respective phases is extremely rare. Moreover, the individual plug lengths will also vary in these sections. In addition, it is evident that the summation of static pressure by traversing once along the entire loop must be zero. The above facts necessarily suggest that the menisci geometry of individual bubbles must be different to satisfy both the above conditions.

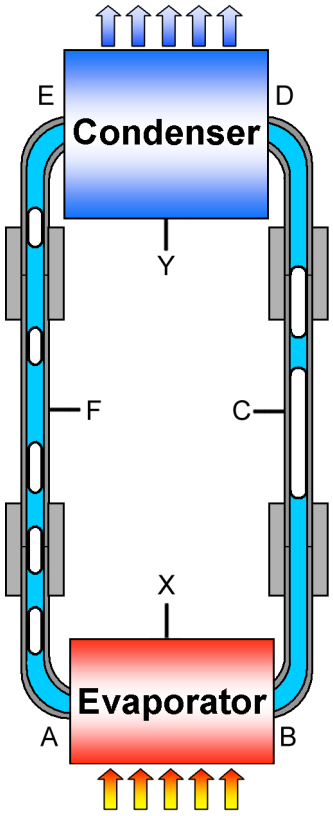

Figure 4-29: Schematic of the single loop device (Experiment-III)

Since the mass distribution (and lengths) of individual phases is different in sections X-C-Y and X-F-Y respectively, the dynamic pressure drop (or force) required to push the fluid by a small amount in anti-clockwise direction (X-C-Y-F-X) is different than in the reverse direction (X-F-Y-C-X). This is true even if the condition of no dynamic contact angle hysteresis is assumed and only the net effects of wall shear stress and gravity are considered. As a bubble forms in the evaporator and expands, a preferential direction of motion is automatically set depending on the path of least resistance (say X-F-Y-C-X). This explains the start-up direction of the two-phase loop. After the start-up, the section at the outlet of the evaporator (A-F-E) has a higher vapor volume fraction than the other loop section (D-C-B) because of evaporation and condensation processes. The process continues for at least some finite time before a combination of interfacial waves, perturbations, internal inhomogeneity of the heating/cooling process and continued non-equilibrium metastable conditions cause a flow direction reversal. The analysis of facts leading to flow reversal phenomenon needs further investigation. Also, in bottom heat mode there is a natural tendency for the liquid plugs to travel downwards, helped by gravity, towards the evaporator. Simultaneously the vapor bubbles have a natural tendency to travel towards the condenser due to their buoyancy.

4.6.1.2 Horizontal operation

In horizontal orientation, in the 'absence' of gravity, the static pressure distribution is quite different from that of the vertical case. In Figure 4-30 the static pressure distribution of three cases is compared (isothermal system of pure ethanol in two phases at 20°C, as shown).

Although the two sections X-C-Y and X-F-Y will have different mass distributions, as in the vertical case, this does not necessitate the contact angles of the various menisci to be different for maintaining the static pressure integral to be zero across the loop. If a bubble in the evaporator has to expand, apparently in the absence of any external/internal perturbations, dynamic contact angle hysteresis etc., there seems to be no preferred direction of least resistance. In this study, horizontal operation was not achieved in Experiment-I, II and III. Several results from other sources [Akachi and Polášek, 1997; Maezawa et al., 1995] for a multi-turn CLPHP suggest that horizontal operation is possible albeit not as good as the vertical operation. Some studies indicate near complete performance independence with respect to operating orientation [Akachi, 1996; Maezawa et al., 1997]. These apparently contradictory and uncomplimentary results seem to suggest that requirements for an orientation independent operation are:

(a) more number of CLPHP turns, which is responsible for higher degree of internal perturbations and inhomogeneity of the system,

(b) a high input heat flux leading to higher enhanced instabilities,

(c) these two aspects are not mutually exclusive and must simultaneously be satisfied.

The first hypothesis is strongly supported by the experimental results of Charoensawan et al. [2003] as already presented in Chapter 2 (refer Figure 2-10). The second hypothesis is supported by the fact that even for vertical bottom heat mode of operation, there is a critical minimum input heat flux requirement to initiate self exited oscillations, as explained earlier in Section 4.3.2.2. In the absence of gravity, this minimum critical heat flux is likely to be higher.

There can be yet another complimentary spatial construction/design feature to ensure nearly constant thermal performance with respect to global orientation. This can be explained as follows:

All the CLPHPs tested in the present work are inline designs in which the tube sections are in one plane. When such a design is made horizontal, the gravity vector is nonexistent on all sections of the tube simultaneously. Figure 4-31 suggests two design variations that, only by virtue of the construction and physical arrangement of tubes, should have a favorable effect on thermal performance variations with respect to operating devise orientation. Design variation-A has partially bent tube turns and so if this structure is operated horizontally, the gravity vector will still be partly functional. In variation-B the tubes are bent in a three dimensional manner and so the gravity will affect the flow irrespective of any global orientation of the heat pipe. These constructional variations are certainly believed to enhance the performance.

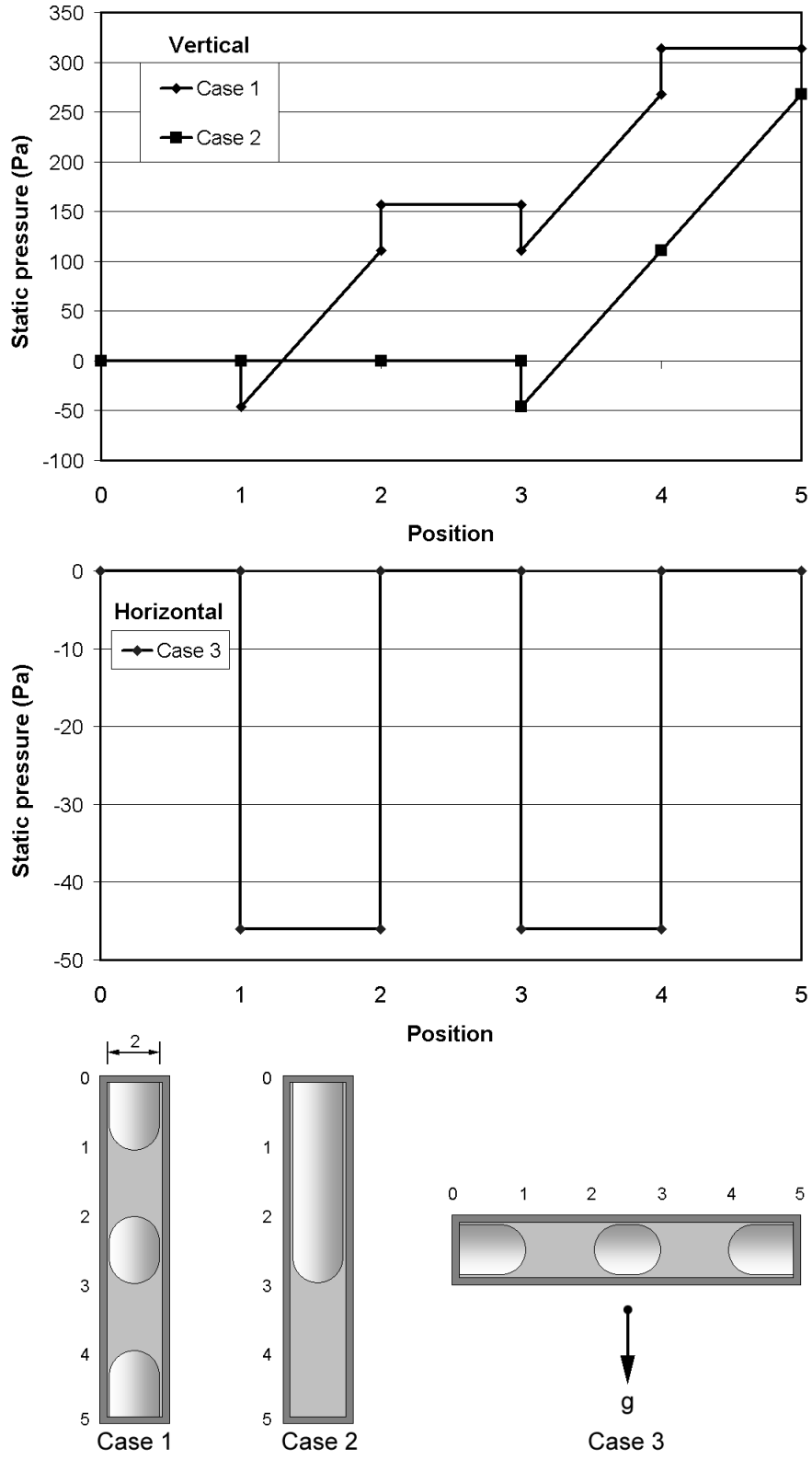

Figure 4-30: Static pressure distribution in the three cases (for an ethanol system)

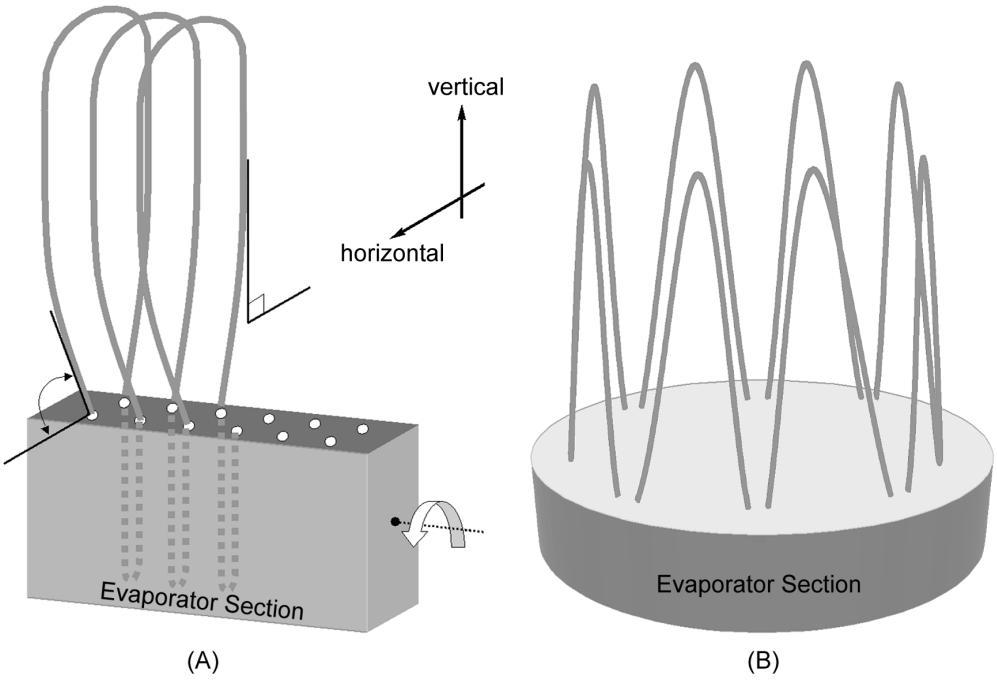

Figure 4-31: Proposed design variations for making the thermal performance of CLPHPs independent of operating orientation

4.6.2 Orientation independent operation

To prove the hypotheses put forward in the previous sub-section (4.6.1.2), regarding orientation independent CLPHP operation, Experiment-IV was planned. This set-up was distinctly different from all the previous set-ups with regards to the following:

(a) the number of turns was large enough; 20 turns each in evaporator and condenser,

(b) the possibility for incorporating fairly large heat fluxes (up to 12 W/cm^2, 400 W) and,

(c) the possibility to turn the CLPHP completely in any orientation.

During the course of this research, the experimental results from this set-up produced the first evidence that nearly orientation independent operation is indeed possible with CLPHPs. All the earlier hypotheses were also convincingly proven. The results are shown in Figures 4-32 to 4-35. All the results compliment the earlier trends as obtained in Experiment-I, II and III. While the results are self explanatory, the following are the main conclusions:

(a) A combination of large number of turns and high input heat flux ensures continuous CLPHP operation in any orientation. Both the requirements should be simultaneously satisfied to achieve this goal.

(b) In general, start-up by a step power level is only possible beyond a minimum heat flux. This minimum start-up power was much smaller in vertical bottom heat mode than in vertical anti-gravity mode. Beyond the critical heat flux, no 'stop-over' was ever detected and continuous operation was always achieved.

(c) The thermal resistance continuously decreases with increasing heat input until heat transfer gets limited by external air-side heat transfer coefficient.

(d) Although an optimum filling ratio exists, the sensitivity of the filling ratio parameter is not very high within the limits of 30% to 70%. This sensitivity further reduces with increasing heat input. At high enough heat input (with FR between 30% to 70%), the performance is nearly independent of the global orientation.

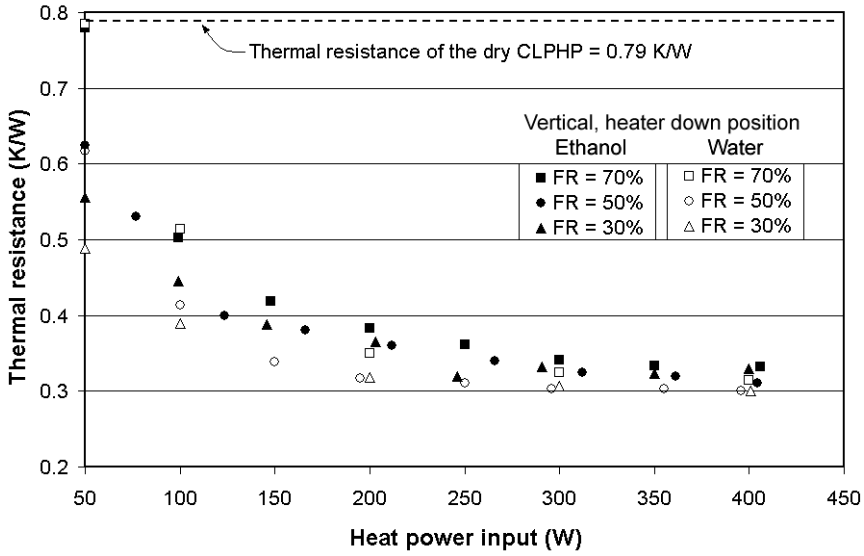

Figure 4-32: Effect of input heat flux on thermal performance of the CLPHP (Experiment-IV, vertical-heater down position). The performance becomes nearly independent of the flux (after 200 W corresponding to about 6 W/cm^2) and the filling ratio (between 30% and 70%) and becomes limited by the external air side heat transfer coefficient.

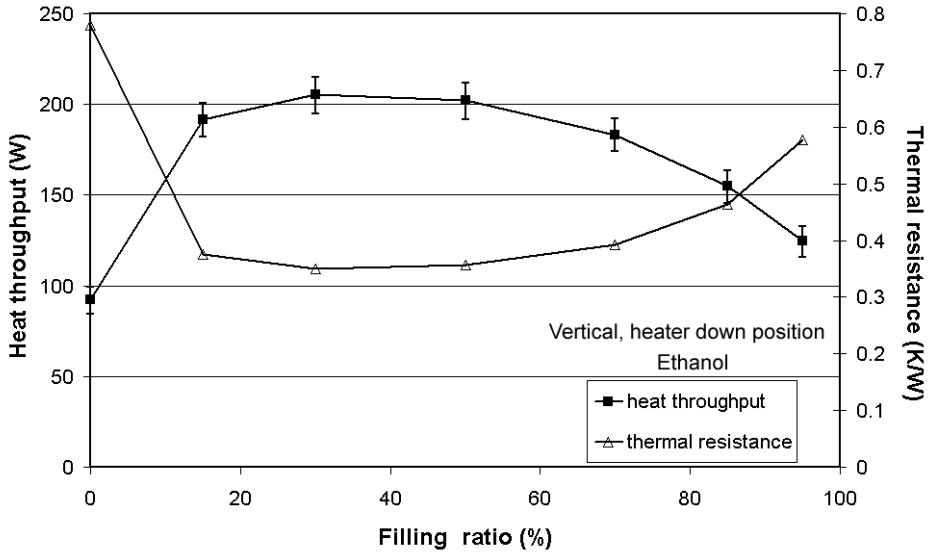

Figure 4-33: Effect of filling ratio on thermal performance of the CLPHP (Experiment-IV); heat throughput and thermal resistance correspond to an average T_e = 100°C.

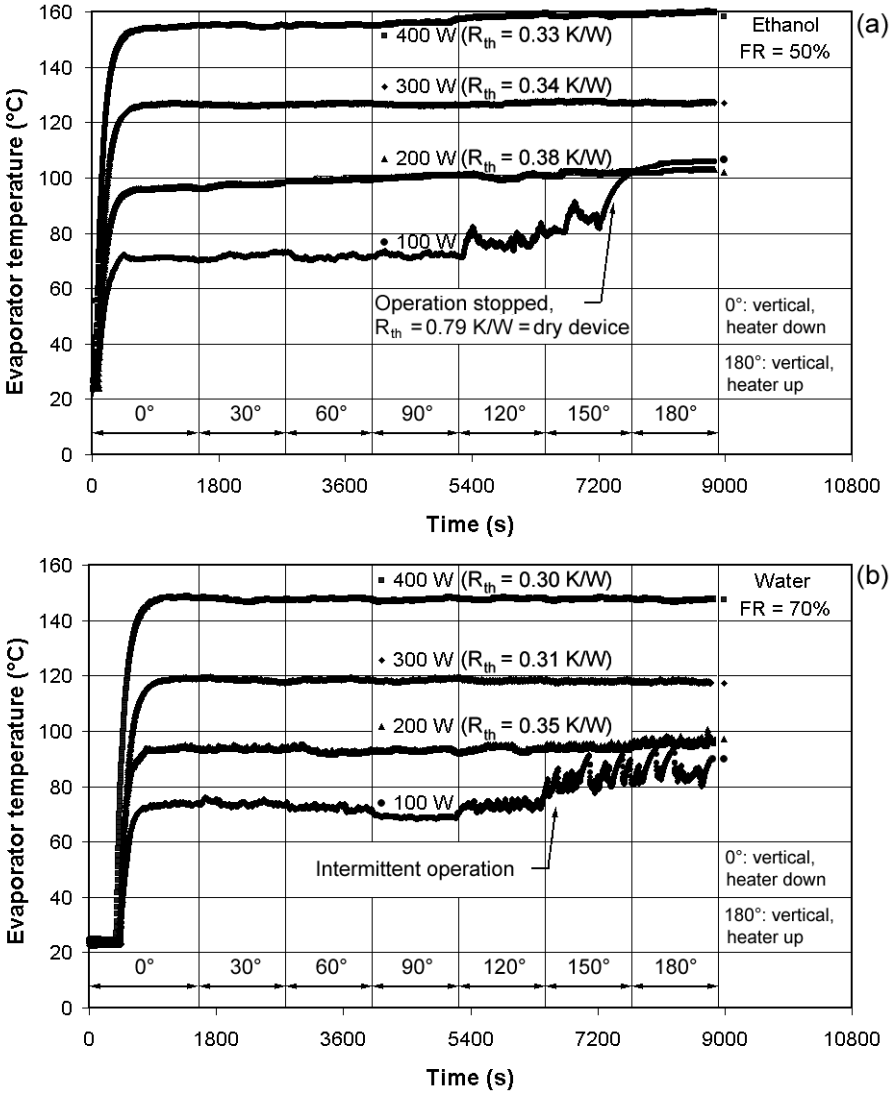

Figure 4-34: Effect of operating orientation on the average evaporator temperature of the CLPHP (Experiment-IV). (a) above 100 W, the performance is nearly independent of the orientation, (b) at 100 W, large scale temperature fluctuations are present and anti gravity operation is not ensured.

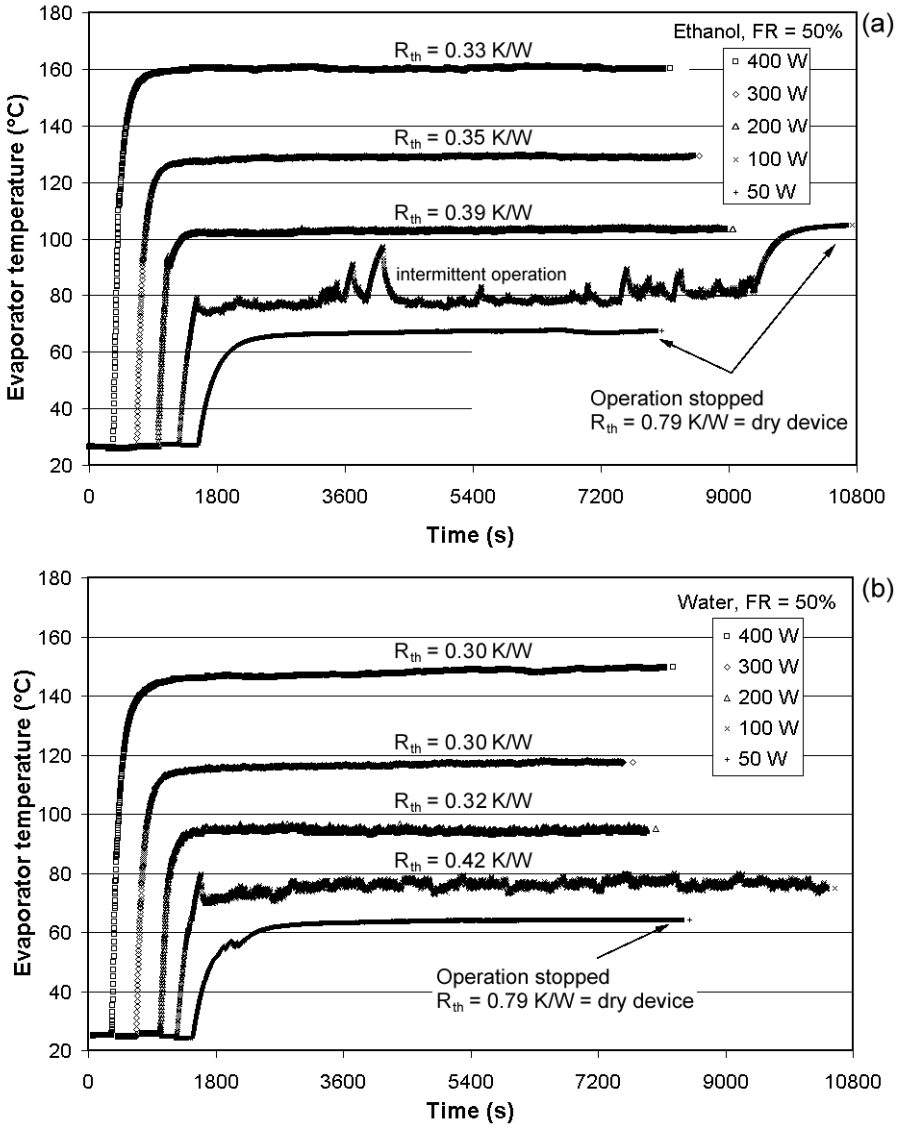

Figure 4-35: Anti-gravity (vertical, heater-up) start-up by step power input to the CLPHP (Experiment-IV). For very low input power (up to 50 W), no oscillations are initiated. For low heat input (up to 100 W), start-up is not ensured. Higher power levels ensure successful start-up and unhindered steady performance.

4.7 The 'Super-fin' analogy

One way of looking at CLPHP based systems is from an 'extended surfaces' point of view. This perspective was already introduced in Section 4.1. For example, the tubes of the CLPHP constructed in Experiment-IV may be seen as fins protruding out of the copper evaporator block. The Kenzan fins as depicted in Figure 2-7 earlier are also named accordingly. The thermal conductivity of the fin material has a strong effect on the longitudinal temperature distribution, which directly influences the degree to which the heat transfer rate is enhanced. Ideally, the fin material should have a large thermal conductivity to minimize the temperature difference from its base to the tip. In the limit of infinite thermal conductivity,

the entire fin would be at the temperature of the base surface, thereby providing the maximum possible heat transfer enhancement. An ideal heat pipe theoretically represents this case. In practice though, heat pipes also have a certain finite thermal resistance.

With this viewpoint, referring to Figure 4-36, three essential questions emerge:

(a) What is the comparison between CLPHPs, in terms of thermal resistance and weight, to an equivalent solid copper based fin system?

(b) What is the comparison between CLPHPs, in terms of thermal resistance and weight, to an equivalent conventional heat pipe fin system?

(c) What are the limitations of studying a CLPHP based system from a 'fin' point of view?

To partly answer these questions, performance testing of conventional mini-heat pipes, as detailed in Chapter 3 (refer Section 3.7) was undertaken. The operating adiabatic temperature was always maintained at a fixed value (by adjusting the condenser coolant temperature), as the heater power was increased in small steps. A sudden surge in evaporator temperature indicated a dryout. The input power just before the dryout gives the maximum performance corresponding to the fixed operating adiabatic temperature and is shown in Figure 4-37 a, b for vertical and horizontal configurations, for all the range of tested structures.

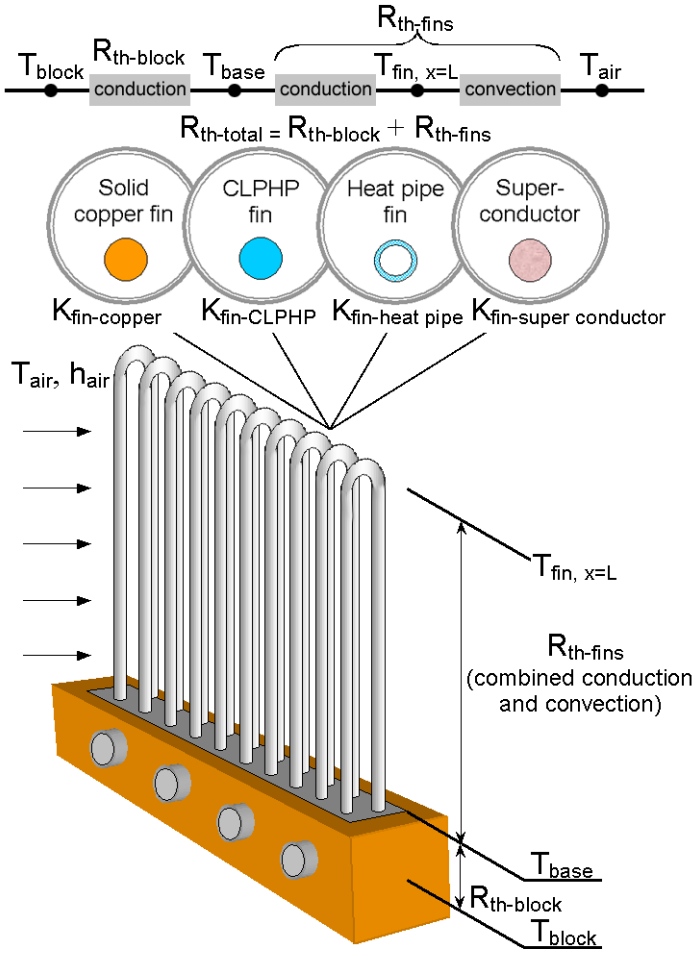

Figure 4-36: Extended surfaces 'fin' analogy for CLPHP systems

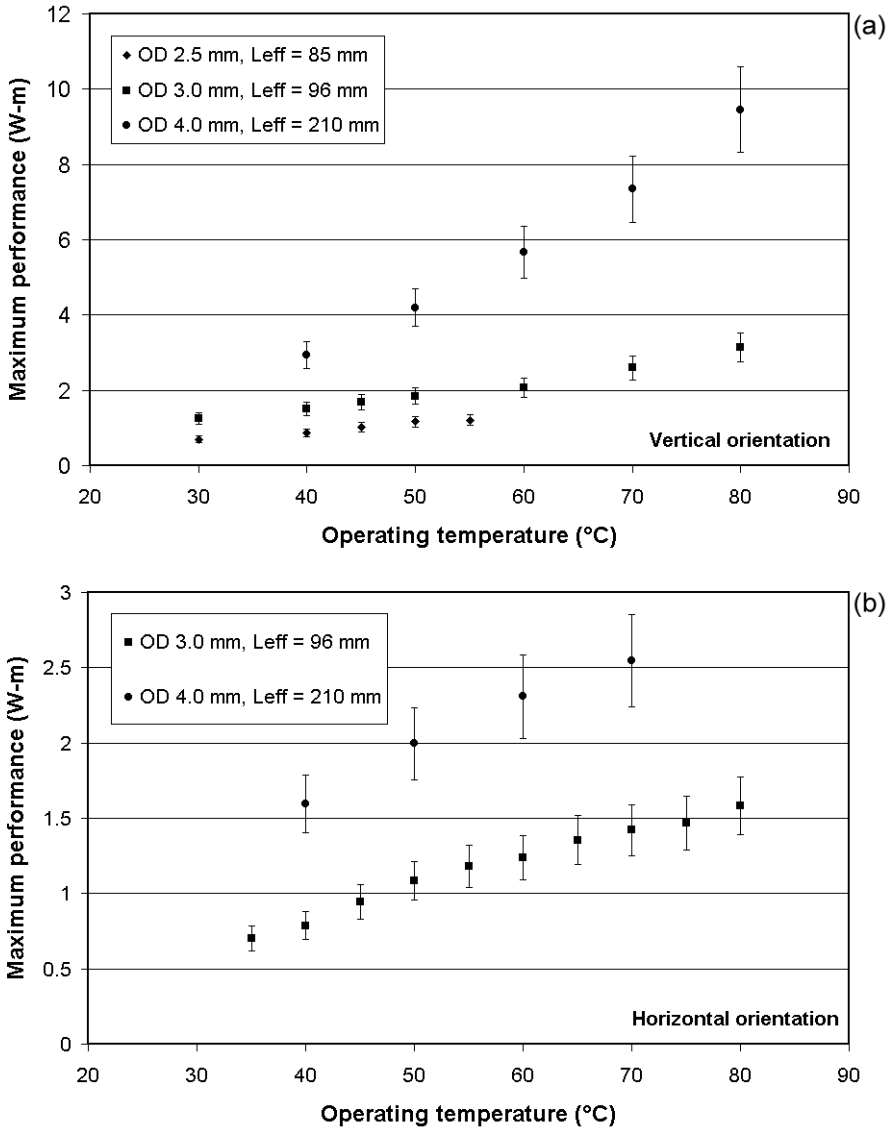

Figure 4-37: Maximum performance characteristics of mini-heat pipes (Experiment-V)

The maximum performance drastically reduces while the thermal resistance increases with decreasing heat pipe diameter. In addition, the manufacturing complexity of small diameter capillary heat pipes also increases with decreasing tube diameter. Based on the experimentally measured thermal resistance of the heat pipes, which remained nearly the same for the range of operating temperatures tested, the corresponding calculated effective conductivity (based on pipe OD) in vertical heater-down position is tabulated below:

Table 4-2: Effective thermal conductivity of mini heat pipes in vertical heater-down position

Pipe ID/OD (mm)	$\dot{Q}_{max}$ at T_a=60°C (W)	R_{th} (K/W)	L_{eff} (m)	A_c (m^2)	k_{eff} (W/mK)
3.0/4.0	27.0	0.3	210 x 10^{-3}	12.56 x 10^{-6}	55732
2.5/3.0	21.5	1.1	96 x 10^{-3}	7.07 x 10^{-6}	12344
2.0/2.5	16.0	3.25	85 x 10^{-3}	4.91 x 10^{-6}	5326

The above values of effective thermal conductivity provide an 'order of magnitude' indication to the designer of what is practically achievable by mini heat pipes. With an improved fabrication process it may be possible to somewhat enhance these figures but based on the fact that the tested mini heat pipes were supplied by competent and established manufacturers, the possible enhancement range is believed not to be significant.

In a similar manner, to find out the effective thermal conductivity of the CLPHP tested in Experiment-IV, T_{base} was always recorded along with T_e (= T_{block}) and T_{air} (refer Figure 4-36), to quantify $R_{th\text{-}block}$ and $R_{th\text{-}CLPHP}$. For calculating the latter, the air side heat transfer coefficient, i.e. h_{air} is needed. This was easily calculated from the results of the dry CLPHP test (no working fluid inside, i.e. FR = 0%), analyzing this case by standard equations dealing with one dimensional conduction in extended surfaces [Cengel, 2003], i.e.:

$$\dot{Q}_{fin} = M \cdot \left(\frac{\sinh(mL) + (h_{air}/mk_{fin})\cosh(mL)}{\cosh(mL) + (h_{air}/mk_{fin})\sinh(mL)} \right) (T_{base} - T_{air}) \text{ where,} \qquad (4\text{-}12)$$

$$M = \sqrt{h_{air} \cdot \hat{P} \cdot k_{fin} \cdot A_c} \text{ and } m = \sqrt{(h_{air} \cdot \hat{P})/(k_{fin} \cdot A_c)} \qquad (4\text{-}13)$$

From Eq. 4-12, knowing the copper CLPHP tube geometry and experimentally obtaining T_{block}, T_{base}, T_{air} and $\dot{Q}_{fin}$ (from a dry CLPHP), the air side heat transfer coefficient (h_{air}) applicable in Experiment-IV was measured to be 82 W/m²K. The respective resistances for the dry CLPHP were:

$\Rightarrow$ $R_{th\text{-}block}$ = 0.05 K/W, $R_{th\text{-}fins}$ = 0.74 K/W

$\Rightarrow$ $R_{th\text{-}total} = R_{th\text{-}block} + R_{th\text{-}fins}$ = 0.79 K/W

The air side heat transfer coefficient and the thermal resistance of the evaporator block, known from the dry-CLPHP test, are applicable in the entire range of CLPHP experiments. With this known h_{air}, Eq. 4-12 can again be used to determine the $(k_{fin})_{CLPHP}$ for all the cases of interest when the CLPHP is partially filled with the working fluid. For example, from Figure 4-32 we notice that the overall thermal resistance of the CLPHP is approximately in the range of 0.34 K/W for the filling ratio between 30% and 70% and heat input from 200 W to 400 W. Therefore we have,

$\Rightarrow$ h_{air} = 82 W/m²K and $R_{th\text{-}block}$ = 0.05 K/W, both obtained from the dry CLPHP test,

$\because$ $R_{th\text{-}total}$ = 0.34 K/W

$\therefore$ $R_{th\text{-}fins} = R_{th\text{-}total} - R_{th\text{-}block}$ = 0.29 K/W

T_{block} and T_{base} for each case were experimentally determined and the value of $R_{th\text{-}block}$ was rechecked and confirmed to be about 0.05 K/W. Thus, from Eq. 4-12, the average effective thermal conductivity (based on entire cross section area, i.e. tube OD = 3.0 mm) in the range FR = 30% to 70% and input power 200W to 400W was found to be, $(k_{fin})_{CLPHP}$ = 4500 W/mK.

The essence of this analysis is tabulated below and shown in Figure 4-38:

Table 4-3: Extended surface 'fin' analogy of Experiment-IV (vertical heater-down position)

N = 40 fins (i.e. 40 turn CLPHP), L = 125.0 mm, h_{air} = 82 W/m²K OD = 3.0 mm for copper fins, OD/ID = 3.0/2.0 mm for CLPHP, OD/ID = 3.0/2.5 mm for mini heat pipes						
T_{block} (°C)	T_{base} (°C)	T_{air} (°C)	**Heat throughput**			
			Solid copper fin (380 W/mK)	CLPHP fin (4500 W/mK)	Mini-heat pipe (12344 W/mK)	Superconductor (∞ W/mK)
160	140	24	206 W	400 W	431 W	451 W
126	111	24	154 W	300 W	323 W	338 W
92	82	24	103 W	200 W	215 W	225 W
			Mass per unit length			
			62.9 g/m	36.1 g/m (with 50% ethanol)	33.7 g/m	-----

It is clear from the Figure 4-38 that the nature of the mixed conduction-convection heat transfer represented by Eq. 4-12 is such that the heat throughput gets limited by the external heat transfer coefficient after a certain value of the fin thermal conductivity. The CLPHP tested in Experiment-IV, in general, operated quite close to the maximum heat throughput which was physically possible by the system boundary conditions. In fact, the device acted as a 'super fin' system. While in vertical heater-down position, the mini-heat pipes may give an advantage over the CLPHPs, the fact that CLPHPs operated with near equal performance level in all orientations makes a very strong case in their favor. In addition, as compared to solid copper fins there is a sizable weight advantage.

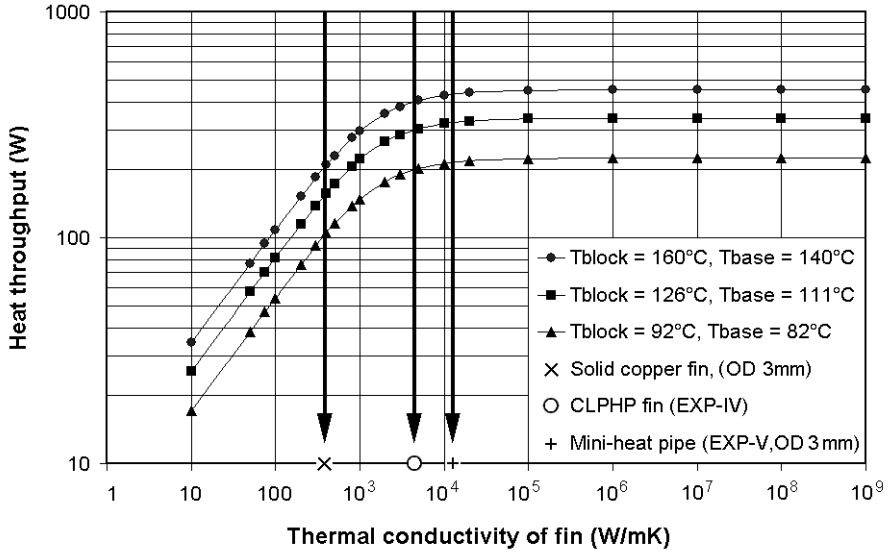

Figure 4-38: Heat throughput from fin system of Experiment-IV

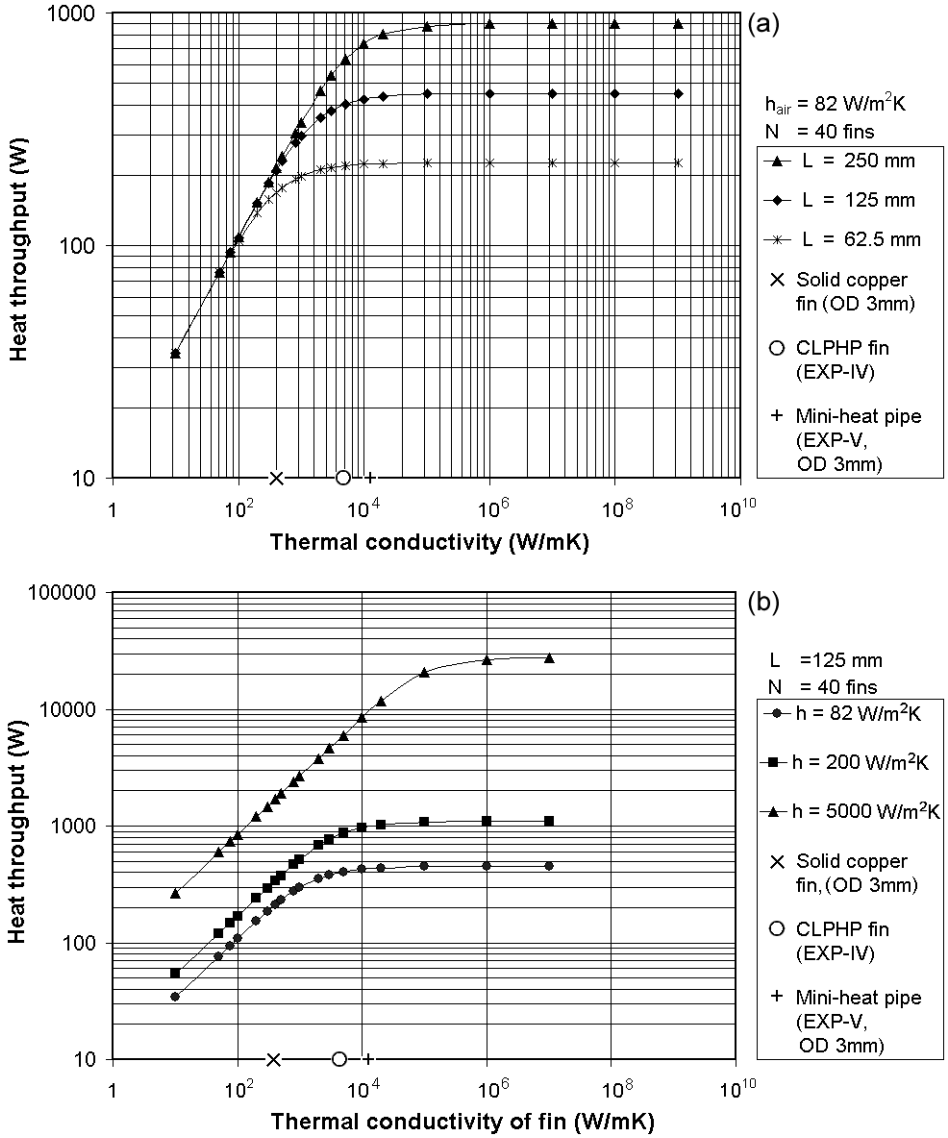

Figure 4-39: (a) Effect of length of the fin, (b) effect of external heat transfer coefficient on the total heat throughput (Simulated conditions are as per Experiment –IV).

The fin analogy, as presented above, indeed has some obvious limitations. From Eq. 4-12, it is quite easy to know the effect of fin length or the air side external heat transfer coefficient on the heat throughput for fin materials with constant thermal conductivity, as shown in Figure 4-39 a, b. These trends may not be extrapolated for the case of CLPHPs or for mini-heat pipes. In the former case, an increase in length will amount to greater dissipative losses affecting the effective thermal conductivity, while in the latter the maximum performance will decrease. Similarly, an increase in the external heat transfer coefficient may not always guarantee in increased performance of mini heat pipes. If a heat pipe is operating at a temperature T_1 with heat input of $\dot{Q}_1$, very close to the dryout power $\dot{Q}_{dry\text{-}1}$, under such operating conditions if the condenser capacity is increased, by either lowering the coolant temperature or increasing its flow rate, there is a risk of a dryout to occur. This will happen

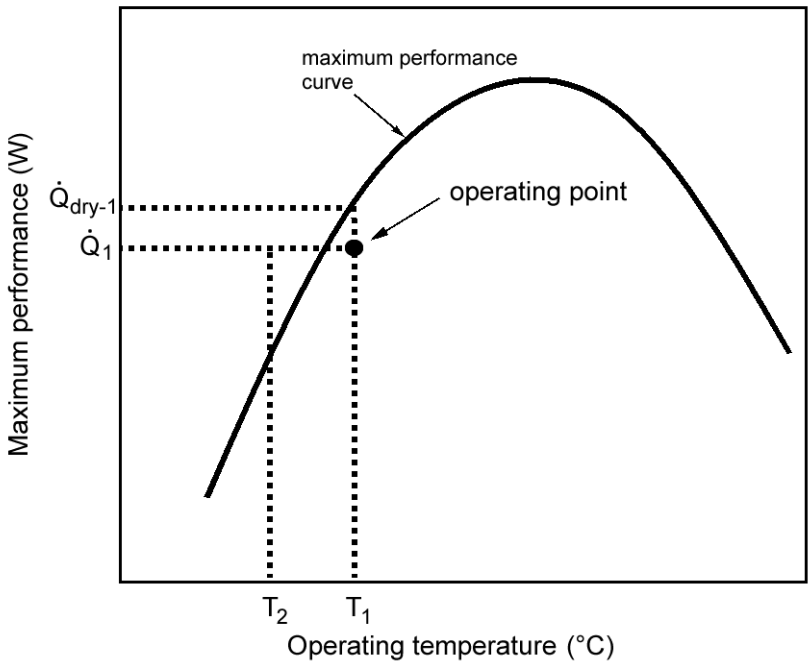

Figure 4-40: Dry-out in a conventional heat pipe due to increase in the condenser capacity

since the operating temperature drops to T_2 for which $\dot{Q}_1$ is too high (refer Figure 4-40). Although there is no well defined adiabatic operating temperature for CLPHPs, a similar trend regarding the effect of condenser capacity may occur since increasing the condenser capacity affects not only the thermophysical properties of the working fluid, but as a side effect, alters the slug-annular flow pattern transitions, thereby altering the final performance. This aspect has to be addressed while practical designing.

4.8 Closure

In this chapter, all the major results of the experiments on CLPHPs were compiled. The effect of five major influence parameters of CLPHPs have been studied in detail. It can be safely concluded that pulsating heat pipe technology is extremely interesting not only from the point of view of potential industrial applications but also from a scientific and engineering research point of view. It will be naive to state that phenomenal progress has been achieved as a result of the herein described experimental results. Nevertheless, it is believed that the results presented in this chapter will provide a concrete foundation for continuing work in search of an optimal solution. Mathematical modeling of these systems poses an even greater challenge. The next chapter attempts to tackle this problem offering some plausible engineering solutions.

CHAPTER 5

MATHEMATICAL MODELING

5.1 Genealogy of closed passive two-phase systems

The results of the experimental study have decisively proven that any attempt to mathematically analyze CLPHPs must address two strongly interdependent and vital aspects simultaneously, viz. the system 'thermo'-'hydrodynamics'. In Section 4.1, the hierarchical position of CLPHPs from a heat transfer or thermal point of view has been outlined. In this section, we look at the genealogy of closed passive two-phase systems with a broader outlook, combining the thermal and hydrodynamic implications; the aim being to categorically illustrate the problems associated with mathematical analysis of CLPHPs using conventional first principle strategies i.e. solving simultaneous equations of mass, momentum and energy.

Figure 5-1 shows the genealogy of closed passive two-phase heat transfer systems. While the 'family tree' is certainly not exhaustive, most relevant systems for the present discussion are included (in a wider sense, the systems represented by Figures 2-1 and 2-2 also belong to the same universal set). As will be evident shortly, although all the systems shown in Figure 5-1 have 'similar' working principles, there are decisive differences that significantly alter the fundamental heat transfer mechanism and thus the mathematical analyses.

Presence of a capillary wick for fluid transport is the fundamental characteristics of the first group (Group A) of the family, consisting of conventional and loop heat pipes. While the former has counter-current flow of the two phases, the latter design avoids it. For analysis of such systems, leading to the determination of maximum heat transport, based on capillary limit (neglecting pressure drops associated with phase change), we use [Faghri 1995],

$$(\Delta P)_{cap} \pm (\Delta P)_{gra} \geq (\Delta P)_{liq} + (\Delta P)_{vap} + (\Delta P)_{liq/vap} \quad \text{where,} \tag{5-1}$$

$$(\Delta P)_{gra} = (L_{eff}^{liq} \cdot \rho_{liq} \cdot g \cdot \sin\beta) - (L_{eff}^{vap} \cdot \rho_{vap} \cdot g \cdot \sin\beta) \tag{5-2}$$

The R.H.S. of Eq. 5-1 contains 'dissipative' terms that are always numerically positive while the L.H.S. contains the 'driving' terms that must be at least equal to the R.H.S. to keep the system running. Thus, all devices in this family can function in anti-gravity mode if the capillary pumping is greater than the gravitational head. The inter-phase shear interaction represented by $(\Delta P)_{liq/vap}$ is nullified in loop heat pipes by the geometrical construction of the device rendering it to be a better alternative to conventional designs.

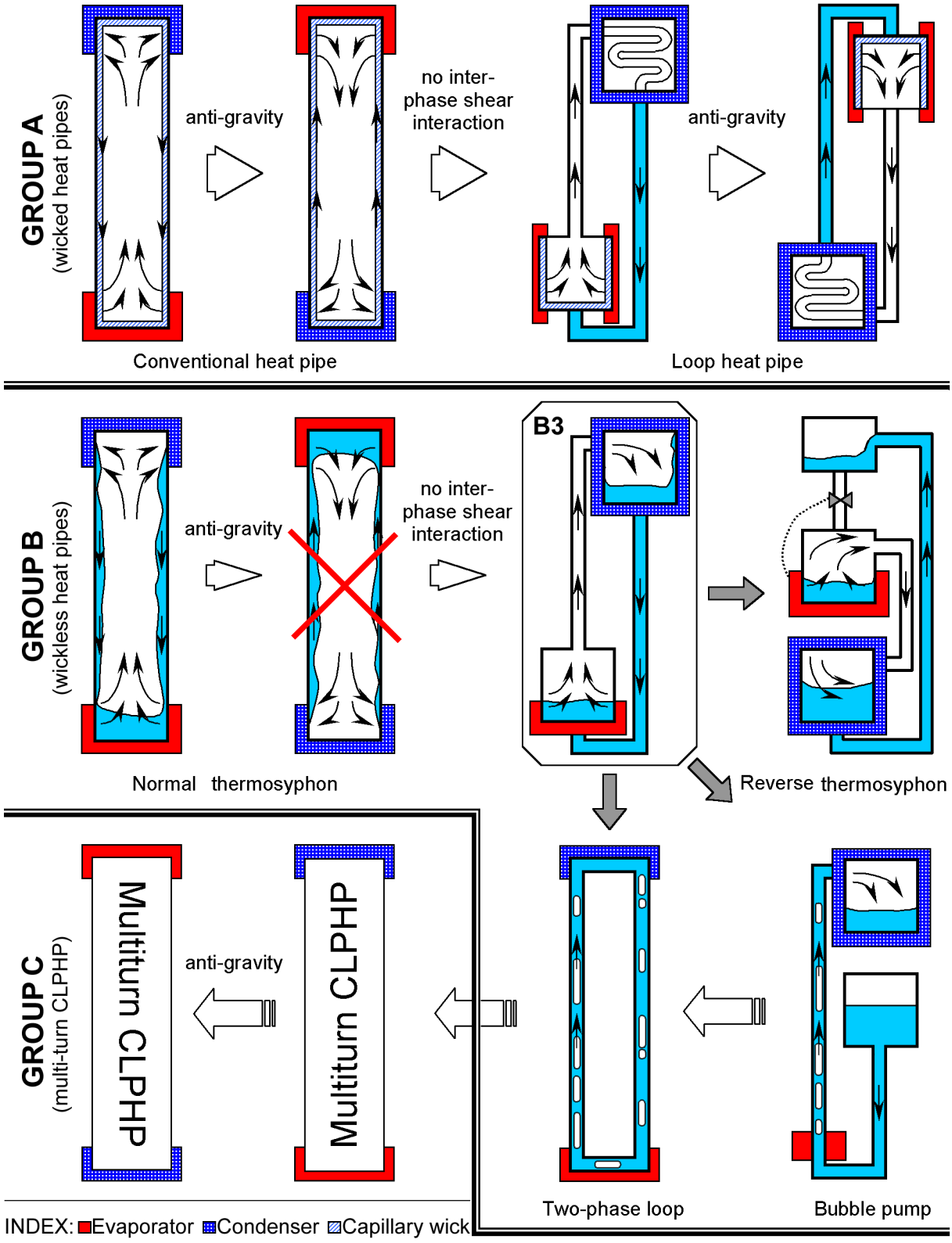

Figure 5-1: Genealogy of closed passive two-phase systems

If the capillary pumping of the first group of devices is made to vanish, we obtain the second group in the family (Group B). This is represented by the gravity-assisted thermosyphons. Here, the design equation reduces to,

$$(\Delta P)_{gra} \geq (\Delta P)_{liq} + (\Delta P)_{vap} + (\Delta P)_{liq/vap} \qquad (5\text{-}3)$$

Thus, in this group, only the gravity head provides the driving potential. Quite naturally, since the L.H.S. of Eq. 5-3 must always be positive for a viable system, anti-gravity (or zero gravity) operation is not feasible. Usually, $(\Delta P)_{liq/vap}$ limits the design, leading to counter-current flow limitation (CCFL) [Tien and Chung, 1978; Groll and Rösler, 1992]. Such failures can be avoided in design-B3, where the two phases flow in separate channels. This design represents a genealogical crossroad that will lead us to Group C devices including CLPHPs. It is to be noted that all the designs discussed so far were primarily based on latent heat transfer. Although sensible heating/cooling does take place, a near isothermal (or isobaric) assumption within the system necessarily nullifies its impact. This assumption generally is quite realistic for devices in Group A and B.

One variation of design-B3 can be done by reducing the size of fluid transport channels and the evaporator, to capillary dimensions. One common example of such a case is the standard bubble pump in which, instead of single-phase vapor flow from the evaporator to the condenser, flow of two-phase mixture results; a direct consequence of slug flow regime being established in the up-header. The two-phase loop studied in this research is also a 'genetic cousin' of the bubble pump. In both systems, the construction of the device forces a combination of sensible as well as latent heat transfer. This marks the first significant shift from the previously discussed cases. The second critical aspect is the fact that the gravity head and the dissipative terms are no more based on single-phase calculations but are governed by two-phase pressure drops (effective mixture density and viscosity for given boundary conditions including consideration for the flow regime). In addition, depending on the size of the capillary tubes being used, some capillary forces may have to be accounted for depending on their order of magnitude as compared to other applicable heads. What complicates the situation further is the inherent presence of two-phase flow instabilities in such systems.

Another variation of design B3 comes in the form of an anti-gravity reverse thermosyphon by incorporating a suitable remote operated valve [Sasin et al., 1995; Fantozzi et al. 2002]. Since there is neither capillary pumping nor positive gravity head, the driving potential must come from elsewhere. At the commencement of liquid heating in the evaporator chamber, the remote operated valve is kept closed. Boiling proceeds under nearly constant volume conditions (since there is always some liquid present in the condenser) thereby increasing the local vapor pressure and temperature. After a while, the evaporator pressure becomes high enough to push the liquid out of the condenser, against gravity, towards the accumulator. The evaporator gradually empties while the accumulator starts filling up. A stage comes when all

the evaporator liquid is boiled off. This stage is immediately followed by a rise in heater temperature and a drop in evaporator chamber pressure as the remaining vapor condenses. The remote valve can now be triggered to open by either of these signals creating pressure equalization in the accumulator and evaporator by gravity assisted liquid return. The cycle then repeats itself. Thus, we observe that a slight design variation necessitates a change in the driving potential; the applicable design criterion now becomes,

$$(\Delta P)_{sat}^{e-acc} - (\Delta P)_{gra} \geq (\Delta P)_{liq} + (\Delta P)_{vap} \quad \text{where,} \tag{5-4}$$

$$(\Delta P)_{sat}^{e-acc} = (\Delta P)_{sat}\big|_{e} - (\Delta P)_{sat}\big|_{a} \quad \text{and} \tag{5-5}$$

$$(\Delta P)_{gra} = (L_{eff}^{liq} \cdot \rho_{liq} \cdot g \cdot \sin\beta) - (L_{eff}^{vap} \cdot \rho_{vap} \cdot g \cdot \sin\beta) \tag{5-6}$$

With the preceding discussion we conclude that the 'driving' terms in this family of devices are $(\Delta P)_{gra}$, $(\Delta P)_{cap}$ or $(\Delta P)_{sat}$, acting individually or in a combination as per the case. The most complicated situation will arise if all the 'driving' terms are simultaneously present and two phases are not flowing separately but as a mixture; the design equation then takes the following form (again neglecting the pressure drops associated with phase change in the evaporator and the condenser):

$$\sum_{1}^{2}(\Delta P)_{cap} + \sum_{1}^{2}(\Delta P)_{sat} \pm \sum_{1}^{2}(\Delta P)_{gra}^{two-phase} \geq \sum_{1}^{2}(\Delta P)_{two-phase} \tag{5-7}$$

where 1 and 2 are specified locations in the system.

Multiturn CLPHP is a thermo-hydrodynamic genesis of a reverse thermosyphon (without control valve!), a bubble pump and a two-phase loop and hence represents the most complicated case; Eq. 5-7 becomes its effective design equation. Even if $(\Delta P)_{cap}$ is assumed to be negligible, given the fact that anti-gravity operation of CLPHPs is possible, some form of effective $(\Delta P)_{sat}$ must invariably operate so as to provide a positive driving potential. For all the cases in the family tree discussed so far, the respective applicable design equations become 'deterministic' by the construction of the devices and by imposing plausible assumptions. Contrary to this situation, Eq. 5-7 for CLPHPs seems to be both temporally and spatially 'dynamic'. Because of the multiturn inter-connected geometry, varying flow patterns coupled with instabilities, dynamic evaporator/condenser local heat transfer coefficients, unknown ratio of sensible to latent heat transfer, possible and indeed probable metastable conditions and multi-parameter system dependency, it was not possible to quantify and solve Eq. 5-7, in conjunction with the energy equation, during the course of this research program.

Therefore, two alternative modeling techniques have been developed and successfully implemented i.e.,

- Semi-empirical modeling with non-dimensional groups,
- Modeling by Artificial Neural Networks (ANNs).

Both methods have their own advantages and obviously some limitations. While the former is a time-tested technique, the latter is part of contemporary development, impetus being the availability of modern computational resources.

Semi-empirical modeling by non-dimensional numbers has been employed in a plethora of heat and mass transfer problems. These techniques are quite elegant and if adequately supported by experimental evidence, can be very efficient and accurate for engineering applications. In complex problems, efficacy may be limited by the complete identification of all the relevant non-dimensional groups affecting the system dynamics.

Artificial neural network based techniques are part of emerging modeling strategies. These techniques have been extensively studied and used in the last two decades in diverse fields ranging from image processing, flexible manufacturing to economic forecasts. Their application to thermal systems is in the burgeoning stages and still needs further research [Sen and Yang, 2000]. In view of the multi-parameter dependency and complex thermo-hydrodynamics of CLPHPs, ANNs seem to be a natural choice for modeling. On the other hand, it may be argued that ANN based models are in essence 'Black Boxes' and do not contribute to the physical understanding of the problem. While this fact cannot be totally denied, a properly trained ANN may be employed for parametric analysis, the results of which certainly enhance the basic understanding of a given problem. Further, ANN based tools are very convenient for operating engineers for analysis/prediction with only those limited parameters which are easily available or recordable.

5.2 Other issues in modeling heat transfer in CLPHPs

One critical issue in modeling CLPHPs is the existence of complex bubble dynamics (agglomeration/breaking/bridging/flooding etc.), including existence of various two-phase flow patterns with respect to the applied heat flux. This has already been highlighted in the previous chapters. This strong thermo-hydrodynamic coupling, in itself, makes mathematical analysis quite difficult. In addition, from the normal operation of the device, it is clear that flow boiling occurs in CLPHPs. The type and magnitude of internal 'flow' is a direct consequence of the applied heat flux, geometry and the inclination angle of operation. The input heat flux depends on N, L_e and Bo (which can be seen as a non-dimensional D_i). For example, as has been explained before, if Bo is larger than a specified Bo_{crit}, then all the working fluid will tend to settle down by gravity and the device will no longer be a pulsating heat pipe. Instead, it will function as an interconnected array of two-phase gravity assisted thermosyphons, with pool boiling dynamics primarily governing the performance. Thus, for a given geometry and filling ratio, the input heat flux and the 'flow' that results thereof leads not only to different two-phase flow patterns, as noted earlier, but also to different heat transfer governing mechanisms.

On one extreme, with very low input heat fluxes, 'nucleate pool boiling' or 'free convection nucleate boiling' may be the only dominant phenomena. There is practically no resulting 'flow'. A little increase in the heat flux gives rise to 'nucleate flow boiling'. On the other extreme, continuous increase of input heat flux will result in conditions where nucleate boiling is completely suppressed and 'convective flow boiling' becomes the dominant phenomenon (e.g. if annular flow quickly develops in the evaporator and heat transfer takes place through the liquid film-vapor interface). Thus, different input heat fluxes to the same device give rise to a range of heat transfer scenarios (because of different flow conditions).

In nucleate boiling, the heat transfer coefficient is chiefly dependent upon the heat flux and practically not at all upon the flow velocity. On the contrary, in convective boiling, the heat transfer coefficient is primarily influenced by the velocity of flow or by the mass flux $\dot{m}$, but on the other hand is scarcely influenced by the heat flux [Carey, 1992; Stephan, 1992]. Vapor mass quality is an additional independent variable for convective boiling. These facts give rise to the hypothesis that the time averaged effective heat transfer coefficient obtained in the evaporator U-turns of CLPHPs is a superposition of the respective heat transfers obtained by free nucleate boiling and convective flow boiling.

$$\left(h_{eff}\right)_{CLPHP} = S \cdot h_{NB} + F \cdot h_{CB} \tag{5-8}$$

The quantities S and F are essentially adjustment parameters (also referred to as 'suppression' or 'enhancement' factors [Chen, 1966]) to take into account the relative importance of nucleate pool boiling and convective flow boiling mechanisms. Such a hypothesis is also adopted frequently in modeling usual convective flow boiling in open systems. In open systems, the basic empirical correlations for modeling h_{NB} are of the form,

$$h_{NB} \propto C_1 \cdot \dot{q}^{n} \tag{5-9}$$

More detailed and well known models prescribed for h_{NB} by Rohsenow [1952] and Forster and Zuber [1955] are based on the assumption that the process of bubble growth and release induces motions of the surrounding liquid that facilitates convective transport of the heat from the adjacent surface. This hypothesis leads to the following generic form of models describing h_{NB},

$$(Nu)_{NB} = \left(\frac{h_{NB} \cdot L^{*}}{k_{liq}}\right) = C \cdot (Re^{*})^{n} \cdot (Pr_{liq})^{m} \tag{5-10}$$

In this equation, the characteristic length and velocity scales (L^{*} and Re^{*}) are appropriately selected as per the situation (e.g. bubble departure diameter and vapor superficial velocity). It is interesting to note that by such an appropriate substitution, these

Nusselt-Reynolds number correlations can be reduced to forms quite similar to Eq. 5-9 above. The relative success of these equations lies in the fact that it has been possible to explicitly deduce characteristic length and velocity scales from the thermo-mechanical boundary conditions of the problem.

For modeling h_{CB} in open systems, additional effects of the mass flux $\dot{m}$ and two-phase flow quality x^* must be included so that the equation takes the form,

$$h_{CB} \propto C_1 \cdot \dot{q}^n \cdot (\dot{m})^s \cdot \Phi(x^*) \qquad (5\text{-}11)$$

where the quantity C_1 is a strong function of the heated surface and the properties of the boiling liquid. In this case too, the characteristic liquid velocity scale is known a priori as the mass flux and geometry are specified in the open system.

Major hurdles in practical realization of Eq. 5-8 for design purposes in case of CLPHPs are as follows:

- The system is closed.
- The characteristic velocity scale is not explicitly known. It strongly depends on the input heat flux and other geometrical constructional features of the device. In addition, the 'average flow velocity' has a superimposed oscillating character.
- In general, there is not enough quantitative flow and heat transfer data available on two-phase open systems in mini-micro channels. More data and subsequent understanding is required on flow instabilities, pulsating and oscillating flows in mini-micro capillary tube systems and related issues. Data on CLPHPs is still scarcer.

Thus, it may be concluded that there are several complex inter-related issues distinguishing mathematical modeling of CLPHPs from conventional modeling of flow boiling in open systems. This further necessitates the application of alternative techniques for CLPHP modeling.

5.3 Modeling by non-dimensional groups

To determine correlations having broad applicability range, it is generally convenient to state the decisive thermo-physical properties for heat transfer as non-dimensional quantities. This proposal is a direct and natural consequence of foregoing discussion on the critical issues involved in modeling of CLPHPs. In addition, an exponential form of the correlation is preferable since such equations are well proven for heat transfer phenomena [Stephan, 1992]. To undertake this task, the thermal performance data as reported by Charoensawan [2003] was used, as already presented in Chapter 2. (refer Section 2.1, Figures 2-10 a, b). As will be recalled, this study involved systematic data generation for a range of metallic CLPHPs. In addition, flow patterns visualization studies were also separately done.

From these quantitative investigations and in conjunction with the internal flow patterns described therein, it can be concluded that the influence parameters consist of the inclination

angle (β), the thermophysical properties of working fluid, the tube inner diameter (D_i), the number of turns (N) and the evaporator length (L_e) as defined by the following equation,

$$\dot{q} = \frac{\dot{Q}}{\pi \cdot D_i \cdot N \cdot (2L_e)} = \Phi\left(\beta, \text{geometry, fluid thermophysical properties}\right) \quad (5\text{-}12)$$

Since the referred experiments were conducted at a fixed filling ratio of 50% of the working fluid, this parameter does not appear in the above equation. For a more generalized case, the effect of filling ratio also has to be included in Eq. 5-12. The identification of the important non-dimensional groups that affect the heat transfer characteristics of the device and the proper definition of the function Φ is needed for practical exploitation of Eq. 5-12.

Before proceeding further, it should be pointed out that in general, CLPHP experiments may be performed in two ways: (i) either by controlling the input heat flux and T_c, T_e being the dependent parameters (as has been done in the present work), or (ii) by controlling T_e and T_c (i.e. fixed ΔT_{sat}^{e-c}), the heat throughput then becomes the dependent variable. The experiments reported by Charoensawan [2003] were done with the latter strategy. In doing so, the maximum temperature difference occurring in the device was fixed (T_e = 80°C, T_c = 20°C) and this, in turn, gave the corresponding saturation pressure difference (ΔP_{sat}^{e-c}).

The equations stated in Section 5.2 already provide a broad hint of the important non-dimensional quantities of interest. It is obvious that some representative form of flow Reynolds number affects the heat transfer. As noted earlier, it is essential to find the characteristic velocity scale as per the specified boundary conditions. Since the reported experiments were done by maintaining the evaporator and condenser temperatures constant (i.e. ΔT_{sat}^{e-c} constant), the characteristic Reynolds number may be calculated as follows:

$$Re_{liq} = \frac{\rho_{liq} \cdot \upsilon^* \cdot D_i}{\mu_{liq}} \quad (5\text{-}13)$$

and since the frictional pressure drop in pipe flows is given by,

$$(\Delta P)_{liq} = \frac{f \cdot \rho_{liq} \cdot (\upsilon^*)^2}{(D_i / L_{eff})} \quad (5\text{-}14)$$

substituting Eq. 5-14 into Eq. 5-13 defines a non-dimensional group, sometimes referred to as Karman number in the context of pipe flows:

$$Ka_{liq} = f \cdot Re_{liq}^2 = \frac{\rho_{liq} \cdot (\Delta P)_{liq} \cdot D_i^3}{\mu_{liq}^2 \cdot L_{eff}} \quad \text{where} \quad L_{eff} = 0.5(L_e + L_c) + L_a \quad (5\text{-}15)$$

The fact that the Karman number is calculated for the liquid phase (and not for an equivalent homogeneous two-phase mixture) is based on the assumption that out of the total fluid losses, $(\Delta P)_{liq} >> (\Delta P)_{vap}$. Therefore, in Eq. 5-15 above, $(\Delta P)_{liq} \approx (\Delta P)_{sat}^{e-c} = f((\Delta T)_{sat}^{e-c})$. Thus, the Karman number gives an appropriate velocity scale for CLPHP modeling.

The next numbers of interest, which do not need explanation, are the liquid Prandtl number and the Jakob number, defined respectively as,

$$Pr_{liq} = \frac{c_{p,liq} \cdot \mu_{liq}}{k_{liq}} \tag{5-16}$$

$$Ja = \frac{h_{fg}}{c_{p,liq} \cdot (\Delta T)_{sat}^{e-c}} \tag{5-17}$$

the thermophysical properties being calculated at $(T_e + T_c)/2$. The liquid Prandtl number scales the single-phase convective effects on heat transfer while the Jakob number highlights the relative importance of sensible and latent portions of heat transfer. In addition, from the generic trends of the experimental data, an exponential function was found to be the best representation of the effect of inclination angle. Thus, Eq. 5-12 can be written as,

$$\dot{q} = \frac{\dot{Q}}{\pi \cdot D_i \cdot N \cdot (2L_e)} = C_1 \cdot (\exp(\beta))^p \cdot Ka_{liq}^q \cdot Pr_{liq}^r \cdot Ja^s \tag{5-18}$$

In the above equation, the constant C_1 has the dimension of W/m^2.

The Bond number (or alternatively the Eötvös number) is the ratio of surface tension and gravity forces and defined as follows,

$$Bo = D_i \sqrt{g \cdot (\rho_{liq} - \rho_{vap})/\sigma} = \sqrt{Eö} \tag{5-19}$$

If the Bond number exceeds a critical value ($Bo_{crit} \approx 2$) stable liquid plugs will not form and the device will not function as a pulsating heat pipe, as already explained previously. For $Bo > 2$ (for example in standard closed two-phase thermosyphons), the heat transfer limitations come from either nucleate pool boiling mechanism or counter-current flow limitations. Based on the facts it may be said, although without existence of evidence, in favor or otherwise, that Eq. 5-18 is only valid for situations where $Bo \leq Bo_{crit}$.

An attempt was made to correlate the entire data sets (a total of 248 data) of the experimental matrix reported by Charoensawan [2003]. This resulted in a correlation given by Eq. 5-20 below for which the fit is depicted graphically in Figure 5-2. Standard least

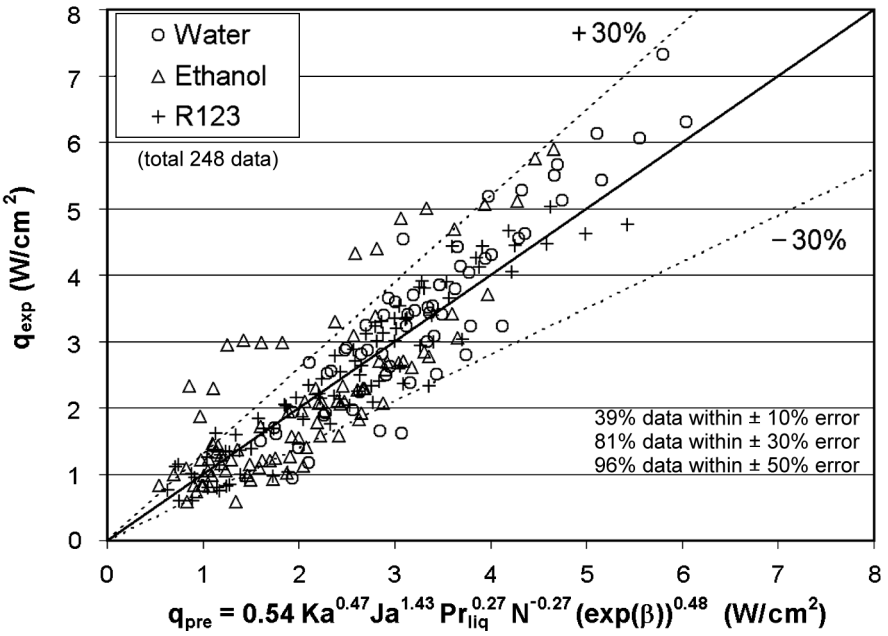

Figure 5-2: Comparison of the developed correlation (Eq. 5-20) with the entire experimental data reported by Charoensawan et al. [2003]

square curve fitting technique coupled with Gauss elimination method was adopted resulting in predictions within ±30%.

$$\dot{q} = \frac{\dot{Q}}{\pi \cdot D_i \cdot N \cdot (2L_e)} = 0.54(\exp(\beta))^{0.48} Ka^{0.47} Pr_{liq}^{0.27} Ja^{1.43} N^{-0.27} \qquad (5\text{-}20)$$

Eq. 5-20 essentially determines the maximum heat transfer achievable for a given CLPHP (with FR = 50%), which is imposed to a specified temperature difference ΔT_{sat}^{e-c} between the evaporator and the condenser. Alternatively, if heat flux and T_c is known, then an iterative solution by guessing T_e can be employed. (Note: $\dot{q}$ in W/m^2 and β in radians)

5.4 Modeling by artificial neural networks

An Artificial Neural Network (ANN) is a processing device, either an algorithm, or actual hardware, the design of which is motivated by the design and functioning of the human brain (biological neural cells, neurons) and components thereof [Aleksander and Morten, 1990]. This design motivation is what distinguishes artificial neural networks from other mathematical techniques. Although similar to linear regression analysis, neural networks are distinguished for utilizing non-linear mathematics and therefore can be used to model highly complex and non-linear functions unachievable by traditional means. ANNs try to mimic the biological network in order to learn the solution to a physical problem from a given set of training parameters.

The following steps briefly summarize any typical ANN modeling procedure:

Step 1 : Task identification and planning

1. Determination of the task to be performed by the network in the application.
2. Analysis of the available data for the application.
3. Choice of the inputs, including preprocessing of the input data to the neural network.
4. Choice of the desired outputs of the neural network, including post-processing of the outputs for use in the application.

Step II: Developing ANN architecture

5. Choice of the ANN learning method and algorithm to be used for training.
6. Setting of the parameters associated with the network chosen, including number of processing elements in each layer, type of processing elements and learning constants.

Step III: Training, verification and use

7. Training of the neural network on the data set aside for training.
8. Verification of the trained network on test data (previously unexposed to the ANN).
9. Analysis of the ANN results and possible retraining/modifications of network.
10. Final integration of the trained network into some application software, if necessary.

Before ANN is applied to model a particular problem, fundamental aspects of the problem itself are to be studied to judge the effectiveness of the technique. Whether CLPHPs are suitable for being modeled by ANN can be ascertained by the following:

- Networks accept a fixed number of inputs thus requiring a well defined input space.
- The performance of the network is directly proportional to the number of training examples to which it is exposed. Therefore, a reliable database should be large.
- A problem should be complex and non-linear enough such that no simple solution exists using the existing conventional technology.
- There should exist a well-defined quantifiable goal or performance measure.

A CLPHP, in general, satisfies the above-mentioned criteria. Although reliable data is not in abundance, the availability is enough to initiate modeling by ANN. To demonstrate the fact that CLPHPs can indeed be modeled by ANN techniques, the results of Experiment-II with ethanol as the working fluid were used. The experimental results have already been presented earlier in Chapter 4 (refer Figure 4-22 b). A total of 76 sets of data, for filling ratios from 0%~100% were recorded. Among these data, 52 sets of data for fill ratios between 20%~85% were in the typical range in which the device worked in the pulsating mode. Since the filling ratio and the heat input affect the thermal resistance simultaneously, these two parameters were chosen as inputs to the network. The overall thermal resistance, based on heater temperature and the cooling air temperature, was chosen to be the network output. 41 sets of data in the typical working range were set aside for training the network model, 11 sets of data were used for subsequent verification. The Stuttgart Neural Network Simulator Software was used for this study [SNNS, 1995].

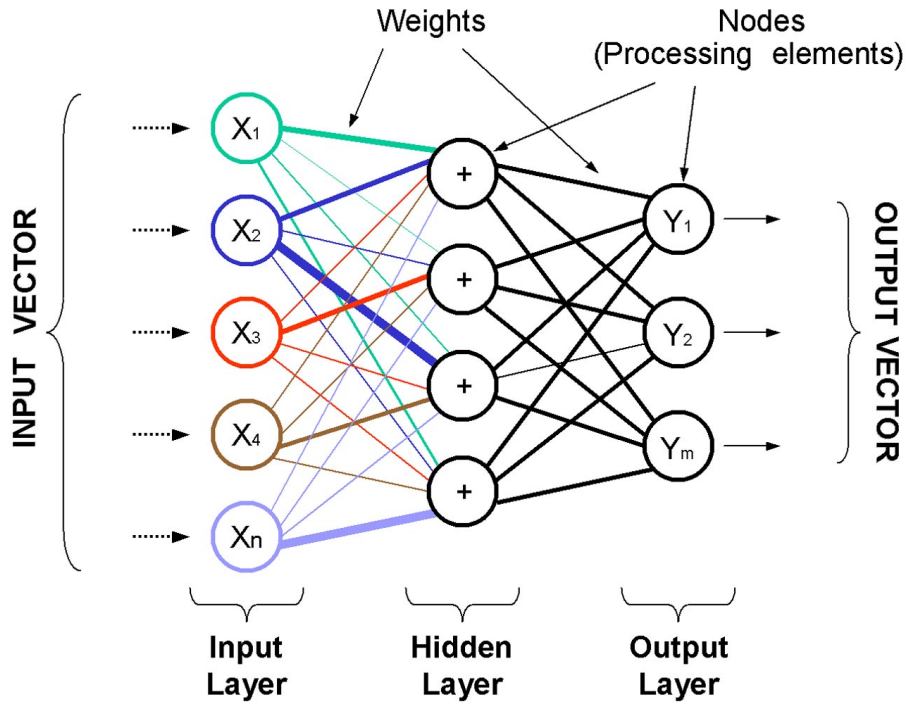

Figure 5-3: Typical ANN architecture

The ANN architecture selected for the study was a fully connected feed-forward multi-layer configuration using back-propagation momentum learning algorithm [SNNS, 1995]. This architecture has a strong ability to express complex non-linear mapping and has already found wide-ranging applications. The architecture of this type of ANN usually consists of an input layer, some hidden layers and an output layer. Each layer has some nodes representing artificial neurons. Each node is interconnected to the nodes of its preceding layer through adaptable weights and no lateral, self or back connection is allowed. Individual neurons have limited ability of calculation and expression but when they are connected with each other, the whole network achieves the ability to model complex functions. A network accepts an input vector and generates a response in the form of an output vector (refer Figure 5-3). Each neuron or node performs a very simple calculation. It sums all its inputs multiplied by their respective weights, then a squashing function is applied to this value. In this study, an identity function is used for output activation. For all other nodes, a sigmoid function is used as activation function. This mathematical function can perform non-linear input-output transformation actions and is therefore normally used in most applications [Aleksander and Morton, 1990].

Since available theory to choose network architecture is scarce, it is more a skillful art. In actual applications, a common method is to train various network architectures and then to choose the one that gives most accurate predictions for a given CPU time. Some suggested recommendations are [Sen and Yang, 2000; Kalogirou and Bojic, 2000]:

Kolmogorov equation (for one hidden layer)

$$N_h = 2J_i + 1 \qquad (5\text{-}21)$$

Rogers and Jenkins equation:

$$N_t = 1 + N_h(J_i + J_o + 1)/J_o \qquad (5\text{-}22)$$

Kalogirou equation:

$$N_h = 1/2(J_i + J_o) + \sqrt{N_t} \quad \text{where,} \qquad (5\text{-}23)$$

J_i : number of input neurons

J_o : number of output neurons

N_h : number of hidden neurons when there is only one hidden layer

N_t : number of training sets

According to the recommendatory equations, ten different configurations, as detailed in Table 5-1, were studied.

Table 5-1: Tested ANN configurations

Input nodes–Hidden Nodes (arranged in one or more layers)–**Output Nodes**

2-5-**1**	**2**-8-**1**
2-5-3-**1**	**2**-3-5-**1**
2-1-7-**1**	**2**-7-1-**1**
2-6-2-**1**	**2**-2-6-**1**
2-4-4-**1**	**2**-3-2-3-**1**

The best configuration having the least r.m.s.-error between the ANN trained output data and the experimental data after the same training cycles was found to be 2-6-2-1. This configuration has two input nodes corresponding to the heat load and the filling ratio; two hidden layers: the first layer has six nodes while the second layer has two nodes; and the output layer has one node representing the overall thermal resistance. Training of the network involves the iterative refinement of the associated 'weights' such that the pre-specified error condition is minimized. Training patterns are composed of a group of matching input and output vectors. The learning algorithm uses these sets of input and output vectors to train a network. It measures the difference between the desired output vector to the current actual output vector and the resulting error backpropagates to alter the connecting weights in the direction of reducing the error. This process runs many times until the error is within the specified tolerance. Then the network holds the weights constant and becomes a valid model for prediction.

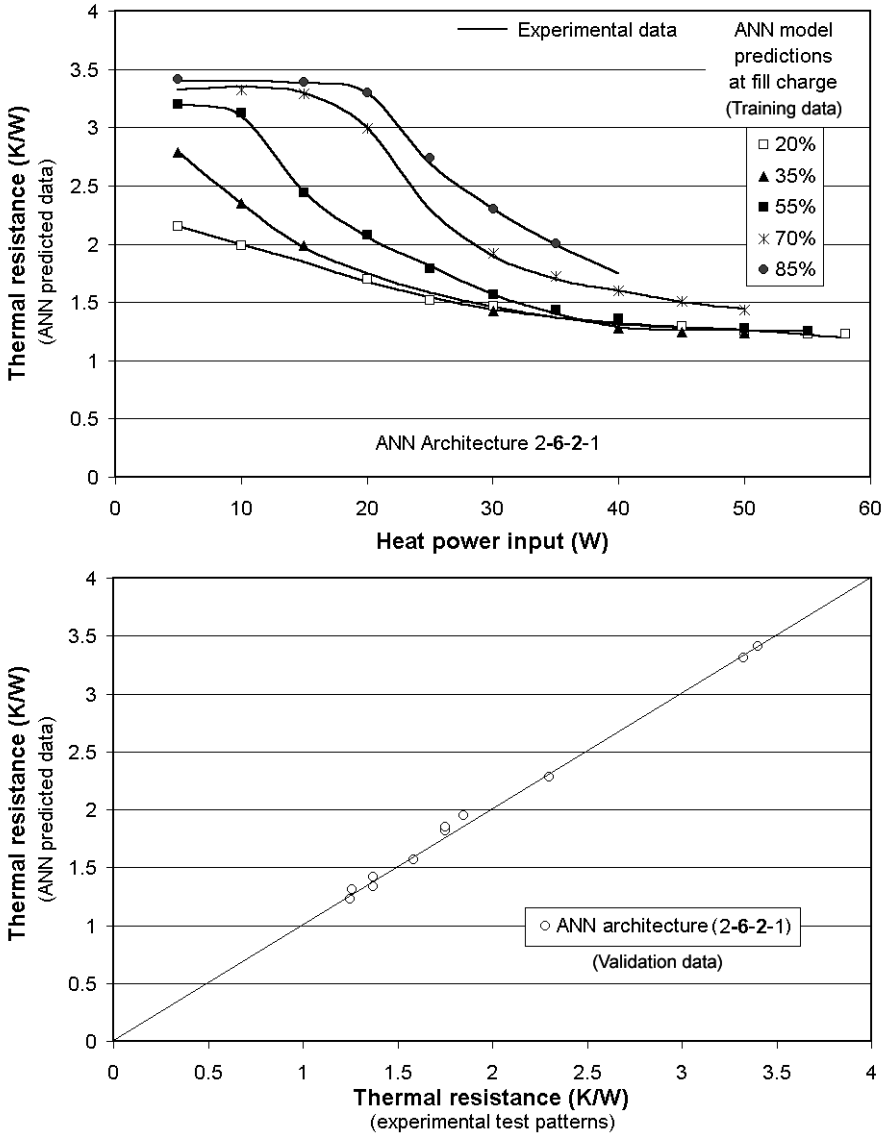

Figure 5-4: Comparison of ANN predictions with experimental data (typical pulsating range corresponding to FR between 20% and 85%)

The ANN was first trained with the data representing the typical pulsating working range (filling ratio between 20% and 85%) and the result is shown in Figure 5-4. Experimental curves are also indicated for comparison. The average scatter of the data is only within ±5.3% although the number of total data is not large enough.

Validation of the model is the next important step and this was done by testing the network with new sets of data that were not used for training. If the ANN generated output data are close to the test data, the network model is successful. Validation was done by the 11 data sets already kept aside for this purpose. A comparative graph of the ANN test data and the experimental data is shown in Figure 5-4 where it can be seen that the matching is satisfactory. The largest relative error between the predicted and experimental data is ±6.9%.

After having successfully trained the ANN with data sets representing the true pulsating range (i.e. FR between 20% to 85%), an attempt was made to investigate the effect of training

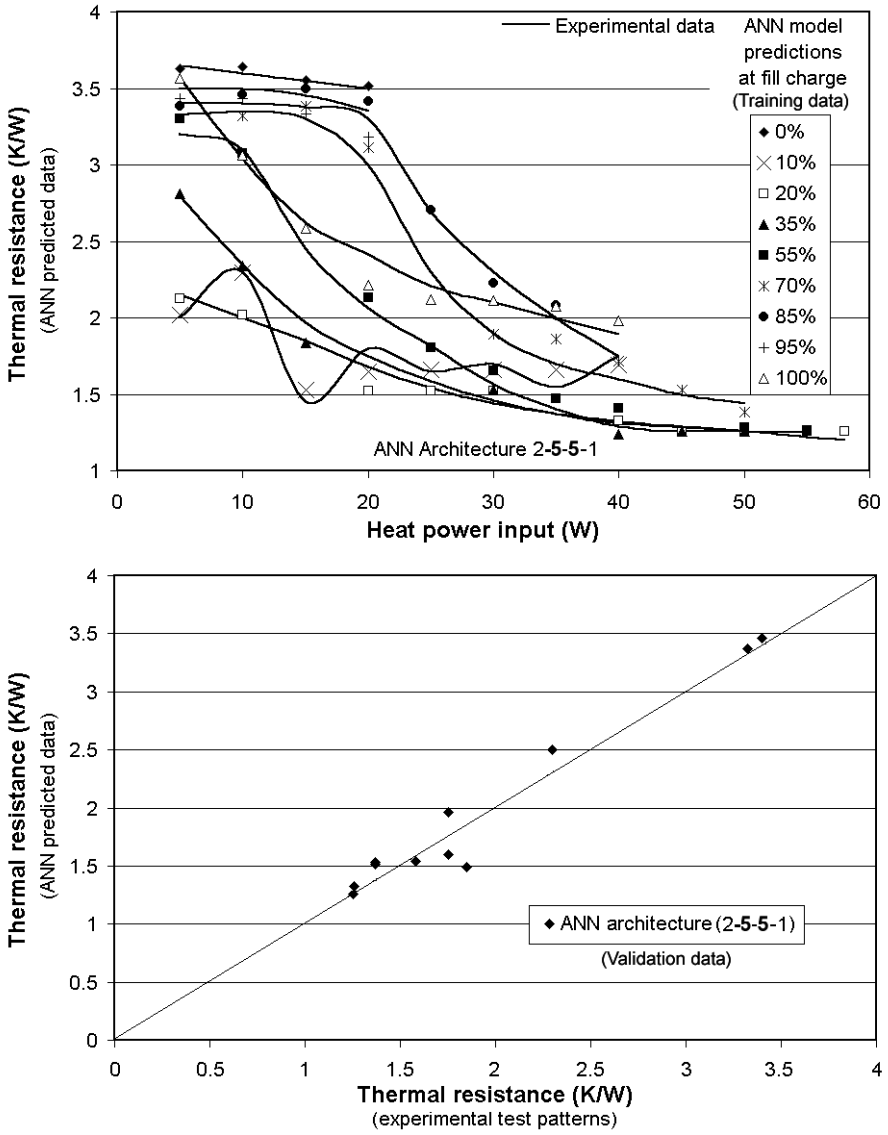

Figure 5-5: Comparison of ANN predictions with entire experimental data

the ANN with the entire range of 76 data sets covering the complete filling ratio range from 0% to 100%. It has been explained in Chapter 4 that the heat transfer mechanism is different for the different filling ratio ranges. The same 11 sets of data mentioned previously are used for model validation. The rest of the 65 data sets formed the training set of the network. Five different configurations, i.e. 2-5-5-1, 2-6-4-1, 2-4-6-1, 2-3-7-1, 2-7-3-1, as per the guidelines were studied. The configuration giving the best result was found to be 2-5-5-1 as shown in Figure 5-5.

Since ANN is a typical 'Black Box', unaware of the physical phenomena guiding the system dynamics, due to fully connected configuration, the results from the trained ANN model may tend to get adversely affected by those training data sets which represent different phenomenological regimes of the system. Thus, the ANN model trained with the data sets of the typical pulsating range of operation gives better results than the model trained with the

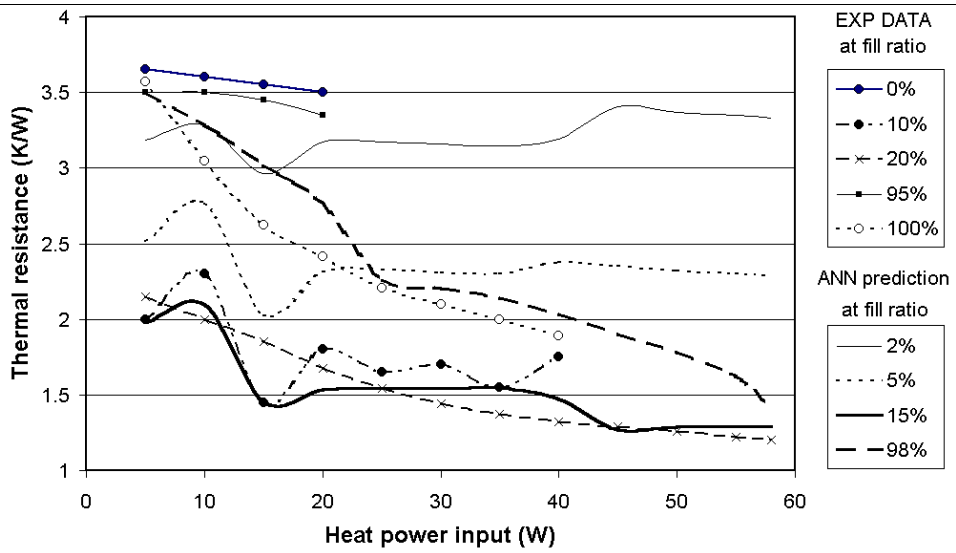

Figure 5-6: Unreasonable ANN predictions near critical filling ratios where thermo-hydrodynamics of the device drastically changes

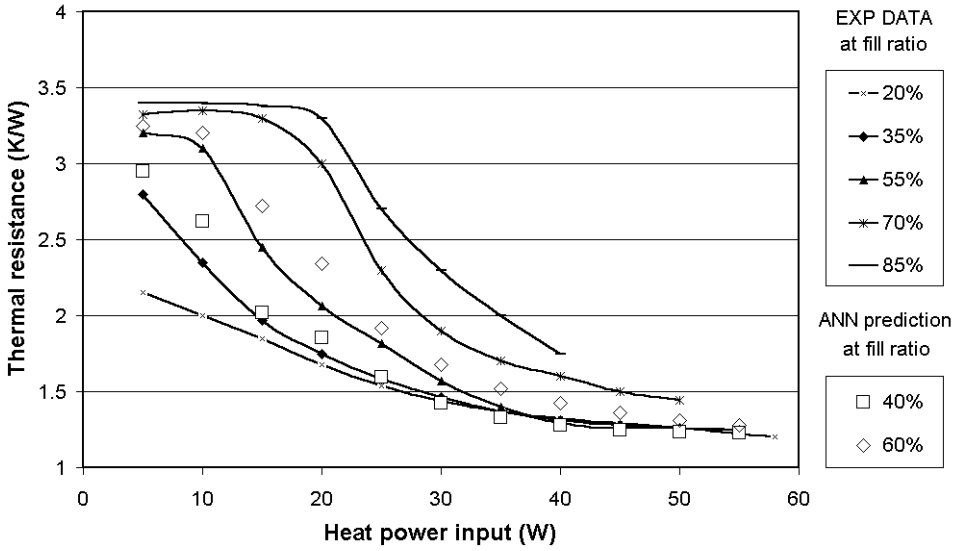

Figure 5-7: ANN predictions at filling ratio of 40% and 60% respectively

entire range of data. For example, in Figure 5-5 the ANN predictions of 20% filling ratio are affected by the unsteady, partial dryout conditions at 10% filling ratio (the oscillating curve). Also, predictions for points lying near phenomenological boundaries, e.g. 2%, 5%, 98% etc. were found to be quite unreasonable as depicted in Figure 5-6. However, the predictions for the filling ratio range of 20% to 80% were satisfactory. This is seen in Figure 5-7, where the ANN model is used to predict the behavior for a filling ratio of 40% and 60%. It is therefore very important that the ANN designer is well aware of the different physical processes of the system under study. Analysis of raw data is thus an essential prerequisite. The quantity of data representing the desired physical and phenomenological system dynamics should be sufficient to have a dominating effect on the model output.

5.5 Closure

In this chapter the problems associated with modeling CLPHPs by conventional techniques were highlighted. Based on the data generated in this study and that available in the open literature, two diverse modeling techniques were successfully employed. Although these techniques have major limitations, they do offer a solution to practical design engineers in their own unique ways.

CHAPTER 6

SUMMARY AND CONCLUSIONS

6.1 Summary

After their invention in the mid-nineties, the family of pulsating heat pipes emerged as a very promising candidate for heat transfer applications. These apparently simple looking devices are extremely intriguing for theoretical and experimental investigations alike. It is rare to find a combination of such events and mechanisms, like bubble nucleation and collapse, bubble agglomeration and pumping action, pressure/temperature perturbations, flow regime changes, dynamic instabilities, metastable non-equilibrium conditions, flooding or bridging etc., all together contributing towards the thermal performance of a device. The thermal performance objective function is multi-dimensional and embodies major multi-disciplinary two-phase flow physics.

The primary aim of this study was to study this complex thermo-hydrodynamics of closed loop pulsating heat pipes. To achieve this goal, five different experimental set-ups were envisioned, fabricated and tested. The set-ups were designed for flow visualization (including videography and infra-red thermography) coupled with standard thermometry. Only temperature measurement was employed for the system performance analyses; internal pressure measurements were not done. The different set-up designs allowed for studying various aspects of the complex thermo-hydrodynamic coupling guiding the device performance. Six major parameters emerged as the primary influence parameters affecting the system dynamics. These include:

- Internal diameter of the CLPHP tube,
- Volumetric filling ratio of the working fluid,
- Input heat flux,
- Total number of turns,
- Operational orientation and,
- Thermo-physical properties of the working fluid.

The study provides detailed discussion on the various design parameters. Apart from the multitude of geometrical, physical and operational variables, the performance is also strongly linked with the flow patterns existing inside the device. Subtle aspects of this two-phase flow dynamics and their interactions with the heat transfer characteristics have been highlighted leading to the formulation of primary design rules.

Mathematical modeling of the device operation has also been accomplished by applying

two approaches which are quite diverse in nature, viz. (a) Semi-empirical modeling with non-dimensional groups and (b) Modeling by artificial neural networks. The problems associated with conventional modeling by 'first principles' are also scrutinized.

At the end of this study program, although some nuances of the device operation still remain unexplored, it is believed that major advancement in the understanding of the thermo-hydrodynamics of CLPHPs has been accomplished. With the progress achieved so far, the prospects for this exemplary and unprecedented technology seems very promising.

6.2 Conclusions

The following are the major conclusions of the study:

1. A comprehensive literature search on pulsating heat pipes was carried out. Since the device is a rather recent invention, there is in general, a dearth of literature on the topic. The then state of the art indicated that although these devices were already finding market niches in electronics cooling, the physical understanding of the device was at a very primary stage. No authoritative mathematical models were in existence.
2. Closed loop pulsating heat pipes are complex heat transfer systems with a very strong thermo-hydrodynamic coupling governing the thermal performance. The cooling philosophy of these devices draws inspiration from conventional heat pipes on one hand and single-phase forced flow liquid cooling on the other. Thus, the net heat transfer is a combination of sensible heat of the liquid plugs and the latent heat of the vapor bubbles. If the internal flow pattern remains predominantly in the slug flow regime, then it has been demonstrated that latent heat will not play a dominant role in the overall heat transfer. If there is a transition to annular flow under the imposed thermo-mechanical boundary conditions, then the dominance of latent heat increases. The most interesting (disturbing!) aspect is the fact that the best performing closed loop pulsating heat pipe no longer behaves as a pulsating device. Alternating tubes then have slug flow and annular flow and the bulk flow takes a fixed direction. Strictly speaking, the term pulsating 'heat pipes' then becomes a misnomer. The construction of the device is such that on a macro level, the heat transfer mechanism can be compared to an extended surface 'fin' system. Although such an analogy provides important insight on the mechanism of heat transfer, extrapolations cannot be authoritatively done unless more experimental data base is available.
3. The internal tube diameter is one of the parameters which essentially defines a CLPHP. The physical behavior adheres to the 'pulsating' mode only under a certain range of diameters. The Eötvös number criterion i.e. Eö ≈ 4, for surface tension dominated adiabatic slug flow, only provides a tentative design rule for the internal diameter of a CLPHP. Although the Eötvös number of water and ethanol was much below the prescribed maximum limit of Eö ≈ 4, gravity forces were definitely seen to affect the performance (refer Appendix-I). Similarly, while the Eö number of R-123 is higher than the maximum suggested limit for the working temperature range, the CLPHP still worked quite effectively. This suggests that though at Eö > 4 the tendency of slug flow

diminishes as surface tension tends to reduce, a certain amount of liquid transport is still possible by the bubble pumping action in diabatic flows thereby providing substantial heat transfer. Beyond a certain maximum range of Eö, the device will function as an interconnected array of normal gravity assisted thermosyphons. Below a certain Eö, dissipative flow resistance will lead to a decrease in thermal performance.

4. The applied heat flux to the system is the most vital parameter for proper operation. Not only because of the fact that it provides the driving energy, it also catalyzes two important phenomena, i.e., (i) flow pattern transition in the device and, (ii) affecting the two-phase flow instabilities and thereby the level of internal perturbations. A certain minimum heat flux is required to overcome the dissipative flow losses. Thereafter, an increase in the input heat flux leads to a series of changes in the internal flow patterns (from slug to semi-annular and fully developed annular flow) which directly affects the heat transfer characteristics. The study strongly indicates that design of these devices should aim at thermo-mechanical boundary conditions which result in convective flow boiling conditions in the evaporator leading to higher local heat transfer coefficients. Also, in conjunction with a minimum number of turns, a minimum heat flux (in present experiments ≈ 5-6 W/cm^2, based on tube ID) is required additionally to make the thermal performance nearly independent of the orientation.

5. The volumetric filling ratio also affects the thermal performance. For a given heat throughput requirement, an operationally better performing and self-sustained thermally driven pulsating action of the device was only observed in the filling ratio range of about 20% to 80%, depending on the working fluid. Above this range, the overall degree of freedom and the pumping action of bubbles was insufficient for rendering good performance. Below a certain range of filling ratio, partial dryout of the evaporator was detected. The results also indicate that a 100% filled PHP (not working in the pulsating mode, instead as a single-phase buoyancy induced thermosyphon) is thermally better performing than a partially filled device under certain operating conditions. As the input heat flux increases this discrepancy essentially reduces.

6. It is obvious that the thermophysical properties of the working fluid, in conjunction with the geometry of the device, have profound implications on thermal performance. This affects the following:

   - The relative share of latent and sensible heat in the overall heat throughput,
   - The possibility of having different flow patterns in the device, e.g. slug-annular flow regime inter-transition,
   - The average flow velocity and overall pressure drop,
   - Bubble nucleation, collapse, shapes, agglomeration and breakage; pumping action; etc.

   Three working fluids with distinctly varying properties were tried in this research program (refer Appendix-I, II). Since the domain of activity was quite widespread, all the fluids could not be tested in the entire experimental parameter matrix. This was also partly because of the constructional limitations of experimental set-ups. Since the

thermal performance is a complex combination of the above listed phenomena, it is certainly difficult to prescribe or proscribe a certain fluid unless all the boundary conditions are exactly known and individual effects have been explicitly isolated and quantified. Different fluids are beneficial under different operating conditions. An optimum tradeoff of various thermophysical properties should be achieved depending on the imposed thermo-mechanical boundary conditions. In addition, explicit behavior with respect to the working fluid can only be stated if the maximum heat transfer is not limited by the external heat transfer conditions existing in the condenser.

7. A certain critical number of turns is required, in addition to the minimum heat flux requirement to make the performance of the CLPHP free of the operating orientation. This is attributed to the increase in level of internal perturbations.

8. The available models in the literature do not truly represent the thermo-hydrodynamics of the CLPHPs. In addition, models applicable for open systems are not directly applicable for closed CLPHPs. The fact that CLPHPs are closed systems in which the velocity scale is dependent on the imposed thermal boundary conditions (and is not known a priori) makes it all the more difficult for analysis. Therefore, a semi-empirical correlation has been developed to fit the available data based on non-dimensional numbers of interest. In the wake of the critical issues regarding modeling of CLPHPs, a semi-empirical approach seems to be quite satisfactory. For a more fundamental modeling approach, an additional reliable data base is needed in congruence to the wider research in mini/micro scale boiling heat transfer in open systems.

9. In addition, ANN based modeling has been successfully applied to predict the CLPHP performance with acceptable accuracy. Since modeling CLPHP behavior is rather difficult by traditional analysis, ANN based methods also appear to be good tools albeit with certain inherent limitations. In some aspects, subjectivity cannot be avoided e.g. the user has to face several uncertain choices which include the number of hidden layers, the number of nodes in each layer, the minimum number of training data sets, the initial assignment, the choice of test data, the data reduction and decomposition etc. Such choices are by no means trivial and are critical in achieving good ANN based models. In this study only two parameters i.e. the heat power input and the filling ratio, were used as the input parameters. In reality there exist various other parameters which affect CLPHP operation. To include all these parameters, reliable and ample experimental data are required. Here, there seems to be an inherent contradiction in the fact that while ANN can effectively model highly complex and non-linear systems, it is increasingly difficult to obtain reliable and abundant experimental data for such complex systems. Analysis of experimental data and understanding subtleties of the underlying phenomena can help network design, training and selection of learning algorithms. All of these are important for good quality ANN models.

10. CLPHP is a highly attractive heat transfer technology, which due to its simple design, cost effectiveness and excellent thermal performance is expected to find wide applications in electronics cooling and allied industry in the years to come.

6.3 Suggestions for future work

The study of Closed Loop Pulsating Heat Pipes presented in this thesis is one of the first systematic attempts to understand the thermo-hydrodynamics of the system. While many aspects of the complex operational characteristics have been covered, it will indeed be very naive to claim completeness in scope of the present research. The future aim should be directed towards making the technology of pulsating heat pipes to become a norm for the industry. Therefore, based on the experiences of the present study, the following suggestions may prove to be helpful in this direction:

1. The first and foremost aspect requiring immediate attention is the generation of more quantitative data for real time applications. This will throw more light on the suitability of this technology for various contemporary and futuristic potential applications in thermal management.
2. While there are a gamut of terrestrial application of the technology, simultaneous attention is also required for space and avionics applications. There are not enough studies so far which highlight the qualitative and quantitative trends of the pulsating flow in microgravity and varying gravity situations. Since the heat transfer characteristics are closely linked to the flow patterns, which in turn are affected by the body forces, any change in external body force field will have a profound effect on the thermo-hydrodynamics of the system. Such studies will certainly add another parameter in the thermo-mechanical boundary conditions governing the system performance, as depicted in Figure 4-26, i.e. the gravity force.
3. The PHPs tested so far, as is apparent in the literature, are all in the 'mini' diameter range. It will indeed be interesting to test a PHP in the sub-millimeter or even in the micrometer range. How small can a PHP be and still be thermally a useful device? In this connection, the importance of the fundamental understanding of two-phase heat transfer and fluid mechanics in mini/micro channels in the development of PHPs cannot be over-emphasized.
4. The dryout mechanism of the device certainly remains unexplored and is one of the most vital information which is needed at this stage for further acceptance of the technology.
5. There have been practically no reported studies on life testing of the device, effect of non-condensable gases, mixtures as working fluids, evaporator U-tube internal surface coated with porous material, PHPs as part of a satellite/space application radiator system, effect of vibrations, PHPs in avionics system etc. These and such related studies are essential for easy transfer of the conceptual technology from research labs to real-life situations.
6. Last, but certainly not the least, a comprehensive scheme for mathematical modeling of these intriguing devices from first principles still remains quite elusive and baffling.

References

1. Akachi H. and Miyazaki Y., ***Stereo-Type Heat Lane Heat Sink***, Preprints 10th Int. Heat Pipe Conf., Vol. 3/4, Session F, Stuttgart, Germany, 1997.
2. Akachi H. and Polášek F., ***Thermal Control of IGBT Modules in Traction Drives by Pulsating Heat Pipes***, Preprints 10th Int. Heat Pipe Conf., Vol. 3, pp. 8-12, Stuttgart, Germany, 1997.
3. Akachi H., Polášek F. and Štulc P., ***Pulsating Heat Pipes***, Proc. 5th Int. Heat Pipe Symp., pp. 208-217, Melbourne, Australia, 1996.
4. Akachi H., U. S. patent, ***Patent Number 4921041***, 1990.
5. Akachi H., U. S. patent, ***Patent Number 5219020***, 1993.
6. Akachi H., U. S. patent***, Patent Number 5490558***, 1996.
7. Aleksander I. and Morton H., ***An Introduction to Neural Computing***, ISBN 0-412-37780-2, Chapman Hall, 1990.
8. Azar K., ***The History of Power Dissipation***, Electronics Cooling, Vol. 6, No. 1, 2000.
   Available at http://electronics-cooling.com/html/articles.html.
9. Bar-Cohen, ***Trends in Packaging of Computer Systems***, in Cooling of Electronic Systems, edited by Kakac S., Yüncü H. and Hijikata K., Kulwar Academic Publishers, pp. 17-45, 1994.
10. Boure J., Bergles A. and Tong L., ***Review of Two-phase Flow Instability***, Nuclear Engg. Design, Vol. 25, pp. 165-192, 1973 (also ASME paper No 71-HAT-42).
11. Bowers M. B. and Mudawar I., ***High Flux Boiling in Low Flow Rate, Low Pressure drop Mini-channel and Micro-channel Heat Sinks***, Int. J. Heat Mass Transfer, Vol. 37, No. 2, pp. 321-332, 1994.
12. Bretherton F. P., ***The Motion of Long Bubbles in Tubes***, J. Fluid Mech., Vol. 10, pp. 167-188, 1961.
13. Brown W. D., ***Advanced Electronic Packaging***, IEEE Press, 1999.
14. Carey Van P., ***Liquid Vapor Phase Change Phenomena***, Hemisphere Publishing Corporation, pp. 76-83, 1992.
15. Cengel Y. A., ***Heat Transfer - A Practical Approach***, McGraw Hill, 1998.
16. Charoensawan P., ***Heat Transfer Characteristics of Closed Loop Oscillating Heat Pipes***, Ph.D. Thesis, Chiang Mai University, Chiang Mai, Thailand, 2003.
17. Chen J., ***Correlation for Boiling Heat Transfer to Saturated Liquids in Convective Flow***, Ind. Engg. Chem. Prog. Des. Dev., Vol. 5, pp. 322-329, 1966.
18. Chen H., Groll M. and Rösler S., ***Micro Heat Pipes: Experimental Investigation and Theoretical Modeling***, Proc. 8th Int. Heat Pipe Conf., pp. 396-400, Beijing, China, 1992.
19. Chi S. W., ***Heat Pipe Theory and Practice***, Series in Thermal and Fluids Engineering, ISBN 0-07-010718-1, Hemisphere Publishing Corporation, 1976.
20. Chisholm D., ***Two Phase Flow in Pipelines and Heat Exchangers***, George Goodwin, 1983.

21. Chrysler G. M., Chu R. C. and Simons R. E., ***Jet Impingement Boiling of a Dielectric Coolant in Narrow Gaps***, IEEE Trans. on Components, Packaging and Manufacturing Tech.-Part A, Vol. 18, No. 3, 1995.
22. Chu R. C., ***A Review of IBM Sponsored Research and Development Projects for Computer Cooling***, Proc. 15th IEEE Semi-Therm Symposium, pp. 151-165, 1999.
23. Chu R. C., Simons R. E. and Chrysler G. M., ***Experimental Investigation of an Enhanced Thermosyphon Heat Loop for Cooling of a High Performance Electronics Module***, Proc. 15th IEEE Semi-Therm Symposium, pp. 1-9, 1999.
24. Cotter T. P., ***Principles and Prospects for Micro Heat Pipes***, Proc. 5th Int. Heat Pipe. Conf., Tsukuba, Japan, pp. 328-335, 1984.
25. Delano A., ***Design Analysis of the Einstein Refrigeration Cycle***, Ph. D. Thesis, Georgia Institute of Technology, 1998.
Available at http://www.me.gatech.edu/energy/andy_phd/.
26. Duminy S., ***Experimental Investigation of Pulsating Heat Pipes***, Diplomarbeit, Institut für Kernenergetik und Energiesysteme, IKE-5D-313, Universität Stuttgart, Germany, 1998.
27. Dunn P. and Reay D. A., ***Heat Pipes***, ISBN 0-080-022127-0, Pergamon Press, 1982.
28. Faghri A., ***Heat Pipe Science and Technology***, Taylor and Francis, 1995.
29. Fantozzi F., Filippeschi S., Sasin V. J. and Savchenkova N. M., ***Heat Transport Device Based on Pulsating Thermosyphons with Forced Fluctuation of Pressure***, Proc. 12th Int. Heat Pipe Conf., pp.469-474, Moscow, Russia, 2002.
30. Forster H. and Zuber N., ***Dynamics of Vapor Bubbles and Boiling Heat Transfer***, A.I.Ch.E., Vol. 1, pp. 531-535, 1955.
31. Fukano T. and Kariyasaki A., ***Characteristics of Gas-Liquid Two Phase Flow in a Capillary Tube***, Nuclear Engg. Design, Vol. 141, pp. 59-68, 1993.
32. Gaugler R. S., U. S. patent, ***Patent Number 2350348-1944***, 1942.
33. Gi. K., Sato F. and Maezawa S., ***Flow Visualization Experiment on Oscillating Heat Pipe***, Proc. 11th Int. Heat Pipe Conf., pp. 149-153, Tokyo, Japan, 1999.
34. Grimley T. A., Mudawar I. and Incropera F. P***., Limits to Critical Heat Flux Enhancement in a Liquid Film Falling over a Structured Surface that Simulates a Microelectronic Chip***, Trans. ASME, J. Heat Trans., Vol. 110, pp. 535-538, 1988.
35. Groll M. and Khandekar S., ***Micro Heat Pipes***, Chapter 2.13.8, Heat Exchanger Design Handbook, Begell House, ISBN 1-56700-097-5, 2002.
36. Groll M. and Rösler S., ***Operation Principles and Performance of Heat Pipes and Closed Two-Phase Thermosyphons***, J. Non-Equilibrium Thermodynamics, Vol. 17, pp. 91-151, 1992.
37. Grover G. M., U. S. patent, ***Patent Number 3229759***, 1963.
38. Grover G. M., Cotter T. P. and Erickson G. F., ***Structures of Very High Thermal Conductivity***, J. Applied Physics, Vol. 35, pp. 1190-1192, 1964.
39. Harmathy T. Z., ***Velocity of Large Bubbles in Media of Infinite or Restricted***

Extent, A.I.Ch.E. Journal, Vol. 6, No. 2, pp. 281-288, 1960.

40. Hosoda M., Nishio S. and Shirakashi R., ***Study of Meandering Closed-Loop* Heat–*Transport Device (Vapor-plug Propagation Phenomena)***, JSME Int. Journal, Series B, Vol. 42, No. 4, pp. 737-743, 1999.
41. Incropera F. P., ***Liquid Cooling of Electronic Devices by Single-phase Convection***, ISBN 0-471-15986-7, John Wiley & Sons, New York 1999.
42. Incropera F. P. and Dewitt D., ***Fundamentals of Heat and Mass Transfer***, ISBN 0-471-30460-3, John Wiley & Sons, 1998.
43. Ishii M. and Zuber N., ***Thermally Induced Flow Instabilities in Two-Phase Mixtures***, Paper No. B5.11, Proc. 4th Int. Heat. Trans. Conf., Paris, France, 1970.
44. Itoh A. and Polášek F., ***Development and Application of Micro Heat Pipes***, Proc. 7th Int. Heat Pipe Conf., pp. 295-310, Minsk, Belarus, 1990.
45. Ivanovskii M. N., Sorokin V. P. and Yagadkin I. V., ***The Physical Principles of Heat Pipes***, Clarendon Press, 1982.
46. Kakac S., ***Introduction to ASI on Cooling of Electronic Systems***, in Cooling of Electronic Systems, edited by Kakac S., Yüncü H. and Hijikata K., Kulwar Academic Publishers, pp. 1-15, 1994.
47. Kalogirou S. A., Panteliou S. and Dentsoras A., ***Modeling of Solar Domestic Water Heating Systems Using Artificial Neural Networks***, pp. 335-341, Energy, Vol. 25, pp. 479-491, 2000.
48. Kawara Z., Takahashi O., Serizawa A. and Kohno M., ***Visualization of Flow in Heat Pipe by Proton Radiography***, Proc. 24th Visualization and Information Symp., pp. 27-23, Osaka, Japan, 1996.
49. Kurzweg U. and Zhao L., ***Heat Transfer by High Frequency Oscillations: A New Hydrodynamic Technique for Achieving Large Effective Thermal Conductivities***, Physics of Fluids, Vol. 27, pp. 2624-2627, 1984.
50. Lee W., Jung H., Kim J. and Kim J., ***Flow Visualization of Oscillating Capillary Tube Heat Pipe***, Proc. 11th IHPC, pp. 355-360, Tokyo, Japan, 1999.
51. Lin S., Sefiane K. and Christy J., ***Prospects of Confined Flow Boiling in Thermal Management of Microsystems***, Applied Thermal Engg. Vol. 22, pp. 825-837, 2002.
52. Maezawa S., Gi A., Minamisawa K. and Akachi H., ***Thermal Performance of Capillary Tube Thermosyphon***, Proc. 9th Int. Heat Pipe Conf., Vol. 2, pp. 791-795, Albuquerque, New Mexico, 1995.
53. Maezawa S., Nakajima R., Gi K. and Akachi H., ***Experimental Chaos in Oscillating Capillary Tube Heat Pipes***, Preprints 10th Int. Heat Pipe Conf., Vol. 3/4, Session F, Stuttgart, Germany, 1997.
54. Maezawa S. Nakajima S., Gi K. and Akachi H., ***Experimental Study on Chaotic Behavior of Thermohydraulic Oscillation in Oscillating Thermosyphon***, Heat Pipe Technology (Proc. 5th Int. Heat Pipe Symp.), Pergamon Elsevier, ISBN 0-08-042842-8, pp. 131-137, Melbourn, Australia, 1996.

55. Maezawa S., Sato F. and Gi K., ***Chaotic Dynamics of Looped Oscillating Heat Pipes* (Theoretical Analysis on Single Loop),** Proc. 6th Int. Heat Pipe Symp., pp. 273-280, Chiang Mai, Thailand, 2000.
56. Maidanik Y., Vershinin S., Kholodov V. and Dolggirev J., U. S. patent***, Patent Number 4515209***, 1985.
57. Moffat R. J., ***Air Cooling of Electronic Components***, in Advances in Thermal Modeling of Electronic Components and Systems, Vol. I, edited by Bar-Cohen A. and Kraus A. D., Hemisphere Publishing Corporation, New York, USA, 1988.
58. Moore G. E., ***Cramming More Components onto Integrated Circuits***, Electronics, Vol. 38, No. 8, 1965.
59. Moore G. E., ***Progress in Digital Integrated Electronics***, Proc. IEEE Int. Electron Devices Meeting, pp. 11-13, 1975.
60. Nakayama W., ***Thermal Management of Electronic Equipment: A Review of Technology and Research Topics***, Chapter 1 in Advances in Thermal Modeling of Electronic Components and Systems, Vol. I, edited by Bar-Cohen A. and Kraus A. D., Hemisphere Publishing Corporation, New York, USA, 1988.
61. Nishio S., Nagata S., Baba S. and Shirakashi R., ***Thermal Performance of SEMOS Heat Pipes***, Proc. 12th Int. Heat Trans. Conf., ISBN 2-84299-307-1, Vol. 4, pp. 477-482, Grenoble, France, 2002.
62. Peterson G. P., ***An Introduction to Heat Pipes: Modeling, Testing and Applications***, John Wiley & Sons, 1994.
63. Qu W. and Ma T., ***Experimental Investigation on Flow and Heat Transfer of a Pulsating Heat Pipe***, Proc. 12. Int. Heat Pipe Conf., pp. 226-231, Moscow, Russia, 2002.
64. Reid R. S., Merrigan M. A. and Sena J. T., ***Review of Liquid Metal Heat Pipe Work at Los Alamos***, Publication number LA-UR-90-3721, Los Alamos National Laboratory, New Mexico, USA, 1990.
Available at http://www.lanl.gov/orgs/esa/epe/Heat_Pipe_Site/Ht_Pipe_top.html.
65. Riffat S. B. and Ma X., ***Thermoelectrics: A Review of Present and Potential Applications***, Applied Thermal Engineering, Vol. 23, pp. 913-935, 2003.
66. Rohsenow W., ***A Method for Correlating Heat Transfer Data for Surface Boiling of Liquids***, Trans. ASME, J. of Heat Trans., Vol. 74, pp. 969-976, 1952.
67. Saha P., Ishii M. and Zuber N., ***An Experimental Investigation of the Thermally Induced Flow Oscillations in Two-phase Systems***, ASME J. Heat Transfer, Vol. 98, pp. 616-622. 1976.
68. Sasin V. J., Borodkin A. A. and Feodorov V. N., ***Experimental Investigation and Analytical Modeling of Auto-oscillation Two-Phase Loop***, Proc. 9th Int. Heat Pipe Conf., Los-Alamos, USA, 1995.
69. Sen M. and Yang K. T., ***Applications of Artificial Neural Networks and Genetic Algorithms in Thermal Engineering***, CRC Handbook of Thermal Engg., pp. 620-661, 2000.

70. Sert C. and Beskok A., ***Numerical Simulation of Reciprocating Flow Forced Convection in Two-Dimensional Channels***, ASME J. Heat Trans., Vol. 125, pp. 403-412, 2003.
71. Shafii M. B., Faghri A. and Zhang Y., ***Thermal Modeling of Unlooped and Looped Pulsating Heat Pipes***, ASME J. Heat Tran., Vol. 123, pp. 1159-1172, 2001.
72. Siegel R. and Perlmutter M., ***Heat Transfer for Pulsating Laminar Duct Flow***, ASME J. Heat Transfer, Vol. 84, pp. 111-123, 1962.
73. Simons R. E***., Application of Thermoelectric Coolers for Module Cooling Enhancement,*** Electronics Cooling, Vol. 6, No. 2, 2000.
Available at http://electronics-cooling.com/html/articles.html.
74. Smyrnov G. and Savchenkov G., USSR Patent, ***Patent Number 504065***, 1975.
75. Stephan K., ***Heat Transfer in Condensation and Boiling***, ISBN 0-387-52203-4, Springer Verlag, Germany, 1992.
76. Stuttgart Neural Network Simulator, ***SNNS User Manual V4.1***, developed at IPDHPS Universität Stuttgart and maintained by Universität Tübingen, Germany, 1995.
Available at www.ra.informatik.uni-tuebingen.de/SNNS/.
77. Suo M. and Griffith P., ***Two-Phase Flow in Capillary Tubes***, Trans. ASME, J. Basic Engg., pp. 576-582, 1964.
78. Swanepoel G., Taylor A. and Dobson R., ***Theoretical Modeling of Pulsating Heat Pipes***, Proc. Int. Heat Pipe Symp. (CD), pp. 227-234, Chiang Mai, Thailand, , 2000.
79. Teng H., Cheng P. and Zhao T. S., ***Instability of Condensate Film and Capillary Blocking in Small Diameter Thermosyphon Condensers***, Int. J. Heat Mass Trans., Vol. 42, pp. 3071-3083, 1999.
80. Tien C. L. and Chung K. S., ***Entrainment Limits in Heat Pipes***, Proc. 3rd Int. Heat Pipe Conf., pp. 36-40, Palo Alto, USA, 1978.
81. Tong L. S. and Tang Y. S., ***Boiling Heat Transfer and Two-Phase Flow***, Taylor and Francis, ISBN 1-56032-485-6, 1997.
82. Tong B. Y., Wong T. N. and Ooi K., ***Closed-Loop Pulsating Heat Pipe***, Applied Thermal Engineering, ISSN 1359-4311, Vol. 21/18, pp. 1845-1862, 2001.
83. Vader D. T., Chrysler G. M., Chu R. C. and Simons R. E., ***Experimental Investigation of Subcooled Liquid Nitrogen Impingement Cooling of a Silicon Chip***, IEEE Trans. on Components, Packaging and Manufacturing Technology-Part A, Vol. 18, No. 4, 1995.
84. Wallis G., ***One Dimensional Two Phase Flow***, McGraw Hill, 1969.
85. Wallis G. and Heasley J., ***Oscillations in Two-Phase Flow Systems***, J. Heat Transfer, Trans. ASME, pp. 363-369, 1961.
86. White E. and Beardmore R., ***The Velocity of Rise of Single Cylindrical Air Bubbles Through Liquids Contained in Vertical Tubes***, Chem. Engg. Science, Vol. 17, pp. 351-361, 1962.
87. Wong T., Tong B. Y., Lim S. M. and Ooi K. T., ***Theoretical Modeling of Pulsating***

Heat Pipe, Proc. 11th Int. Heat Pipe Conf., pp. 159-163, Tokyo, Japan, 1999.

88. Yadigaroglu G. and Bergles A., ***Fundamental and Higher-Mode Density-Wave Oscillations in Two-Phase Flow***, ASME J. of Heat Trans., pp. 189-195, 1972.
89. Zhang Y. and Faghri A., ***Heat Transfer in a Pulsating Heat Pipe with Open End***, Int. J. Heat Mass Transfer, Vol. 45, pp. 755-764, 2002.
90. Zhao T. and Cheng P., ***A Numerical Solution of Laminar Forced Convection in a Pipe Subjected to a Reciprocating Flow***, Int. J. Heat Mass Transfer, Vol. 38, pp. 3011-3022, 1995.
91. Zuo Z. J. and North M. T., ***Miniature High Heat Flux Heat Pipes for Cooling Electronics***, Proc. of SEE 2000, Hong Kong, pp. 573-579, 2000.

Publications from the present research

1. Charoensawan P., Khandekar S., Groll M. and Terdtoon P., ***Closed Loop Pulsating Heat Pipes-Part A: Parametric Experimental Investigations***, Applied Thermal Engineering, ISSN 1359-4311, Vol. 23/16, pp. 2009-2020 , 2003.
2. Khandekar S., Charoensawan P., Groll M. and Terdtoon P., ***Closed Loop Pulsating Heat Pipes-Part B: Visualization and Semi-Empirical Modeling***, Applied Thermal Engineering, ISSN 1359-4311, Vol. 23/16, pp. 2021-2033, 2003.
3. Khandekar S. and Groll M., ***An Insight into Thermo-Hydraulic Coupling in Pulsating Heat Pipes***, Int. J. of Thermal Sciences (Rev. Gén. Therm.), ISSN 1290-0729, Vol. 43/1, pp. 13-20, 2004.
4. Khandekar S., Dollinger N. and Groll M., ***Understanding Operational Regimes of Pulsating Heat Pipes: An Experimental Study***, Applied Thermal Engineering, ISSN 1359-4311, Vol. 23/6, pp. 707-719, 2003.
5. Groll M. and Khandekar S., ***Pulsating Heat Pipes: A Challenge and Still Unsolved Problem in Heat Pipe Science***, Archives of Thermodynamics, ISSN 1231-0956, Vol. 23/4, pp. 17-28, 2002. Also in Proc. Proc. 3rd Int. Conf. on Transport Phenomenon in Multiphase Systems (HEAT 2002), ISBN 83-88906-03-8, pp. 35-43, Baranów Sandomierski, Poland, 2002.
6. Khandekar S., Schneider M., Schäfer P., Kulenovic R. and Groll M., ***Thermofluiddynamic Study of Flat Plate Closed Loop Pulsating Heat Pipes***, Microscale Thermophysical Engineering, ISSN 1089-3954, pp. 303-318, Vol. 6/4, 2002.
7. Khandekar S. and Groll M., ***On the Definition of Pulsating Heat Pipes: An Overview***, Proc. 5th Minsk Int. Conf. (Heat Pipes, Heat Pumps and Refrigerators), Minsk, Belarus, 2003.
8. Groll M. and Khandekar S., ***Pulsating Heat Pipes: Progress and Prospects***, Proc. 3rd Int. Conf. on Energy and Environment, ISBN 7-5323-7335-5/TK-22, Vol. 1, pp. 723-730, Shanghai, China, 2003.
9. Khandekar S., Groll M. and Luckchoura V., ***An Introduction to Pulsating Heat Pipes***, Electronics Cooling Vol. 9/2, pp. 38-41, 2003.
   Available at http://electronics-cooling.com/html/articles.html.
10. Khandekar S., Groll M., Charoensawan P. and Terdtoon P., ***Pulsating Heat Pipes: Thermo-fluidic Characteristics and Comparative Study with Single Phase Thermosyphon***, Proc. 12th Int. Heat Trans. Conf., ISBN-2-84299-307-1, Vol. 4, pp. 459-464, Grenoble, France, 2002.
11. Khandekar S., Schneider M. and Groll M., ***Mathematical Modeling of Pulsating Heat Pipes: State of the Art and Future Challenges***, Proc. 5th ASME/ISHMT Int. Heat and Mass Transfer Conf., ISBN-0-07-047443-5, pp. 856-862, Kolkata, India, 2002.
12. Khandekar S., Cui X. and Groll M., ***Thermal Performance Modeling of Pulsating Heat Pipes by Artificial Neural Network***, Proc. 12th Int. Heat Pipe Conf., pp. 215-219, Moscow, Russia, 2002.

Appendix

(I) Variation of the critical inner diameter and Eötvös number with temperature

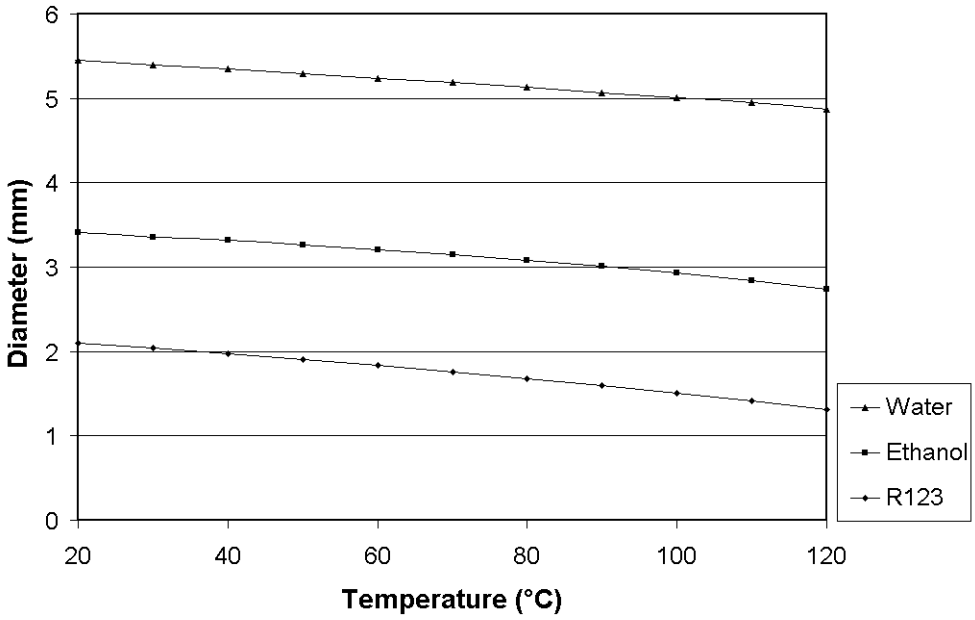

Figure Ax-1: Critical inner diameter of the CLPHP tube corresponding to the fixed criterion of Eö = 4

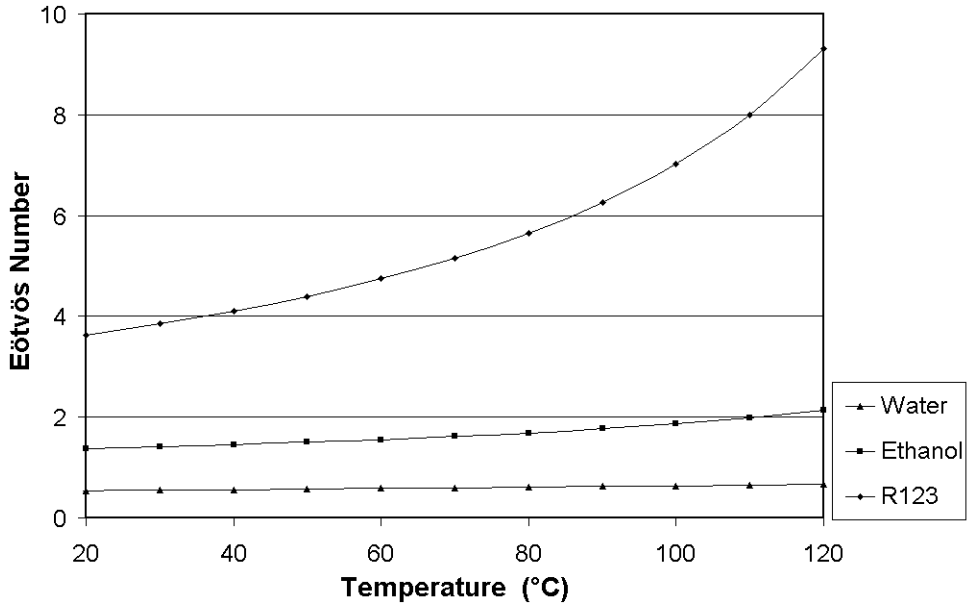

Figure Ax-2: Variation of Eötvös number with temperature if the inner diameter of the tube is fixed to be equal to 2 mm

(II) Thermophysical properties of the working fluids

The thermophysical properties have been taken from Heat Pipe Design Handbook [1979].

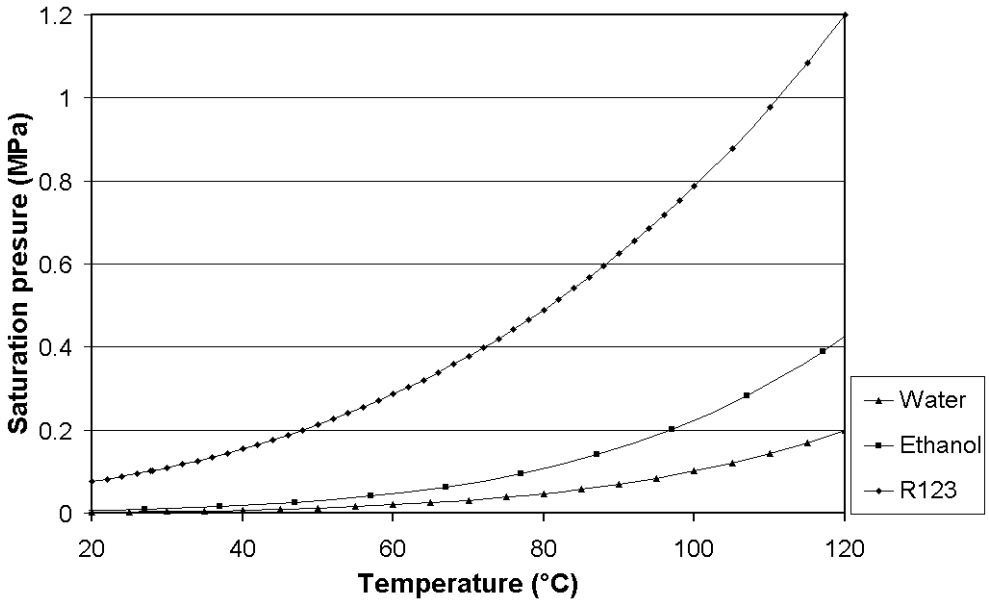

Figure Ax-3: Variation of saturation pressure of the working fluids with temperature

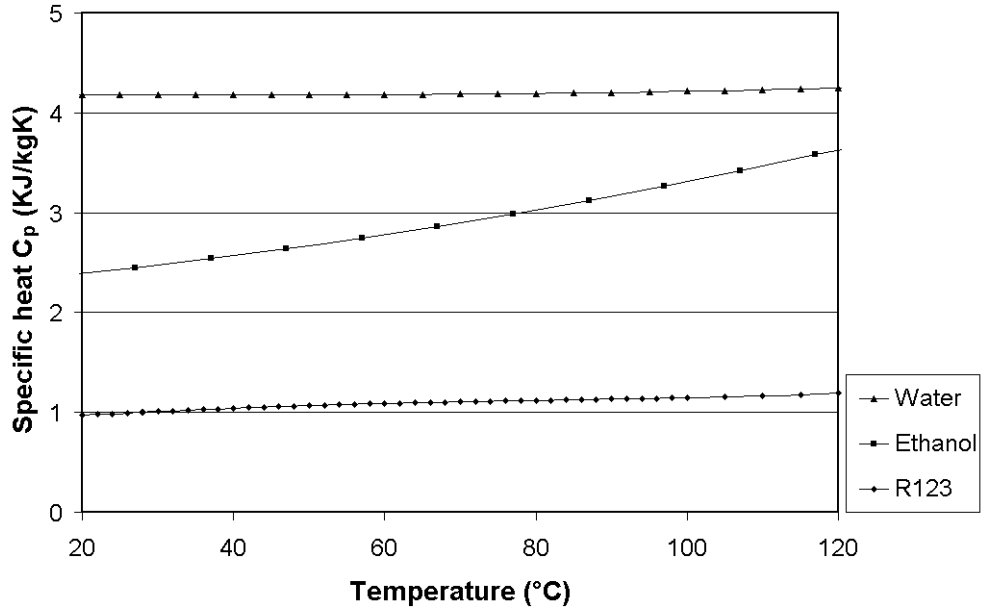

Figure Ax-4: Variation of specific heat of the working fluids with temperature

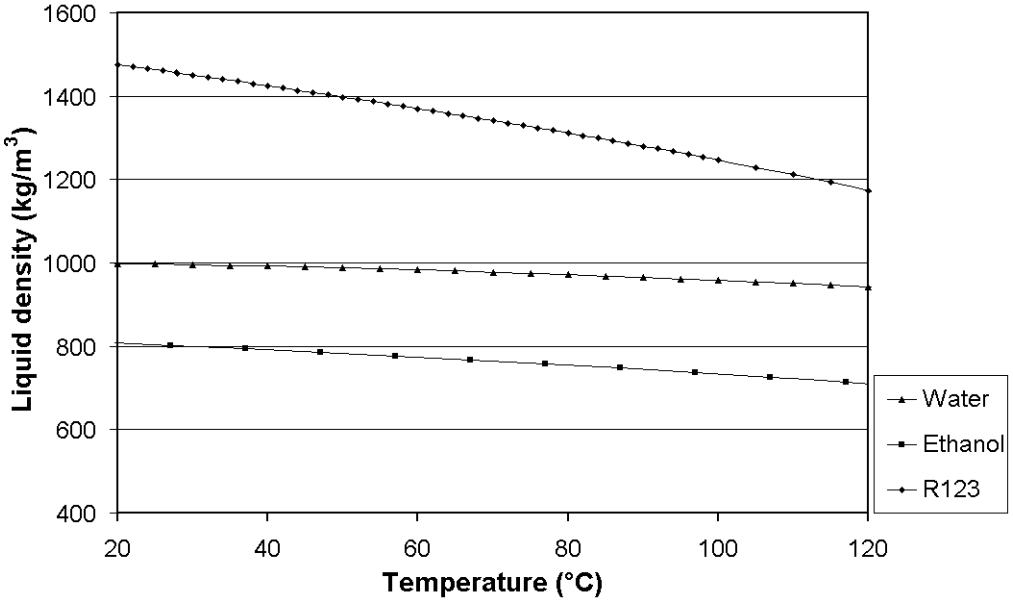

Figure Ax-5: Variation of liquid density of the working fluids with temperature

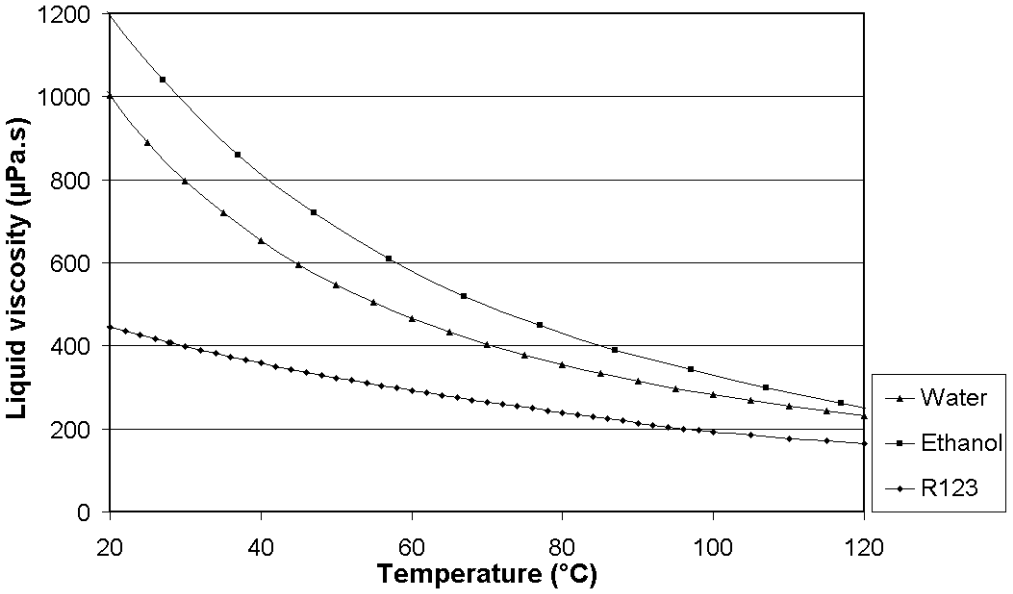

Figure Ax-6: Variation of liquid viscosity of the working fluids with temperature

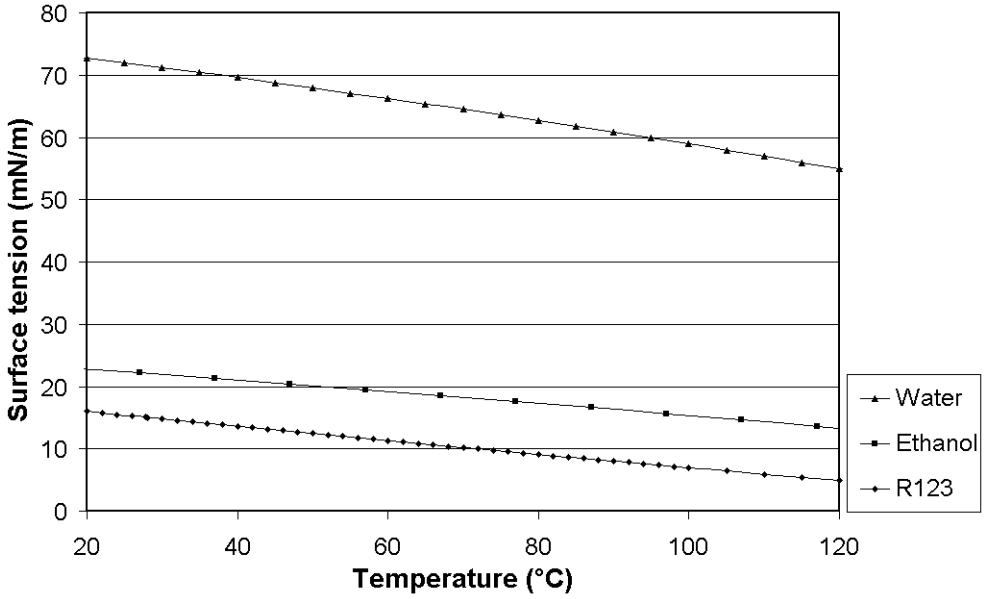

Figure Ax-7: Variation of surface tension of the working fluids with temperature

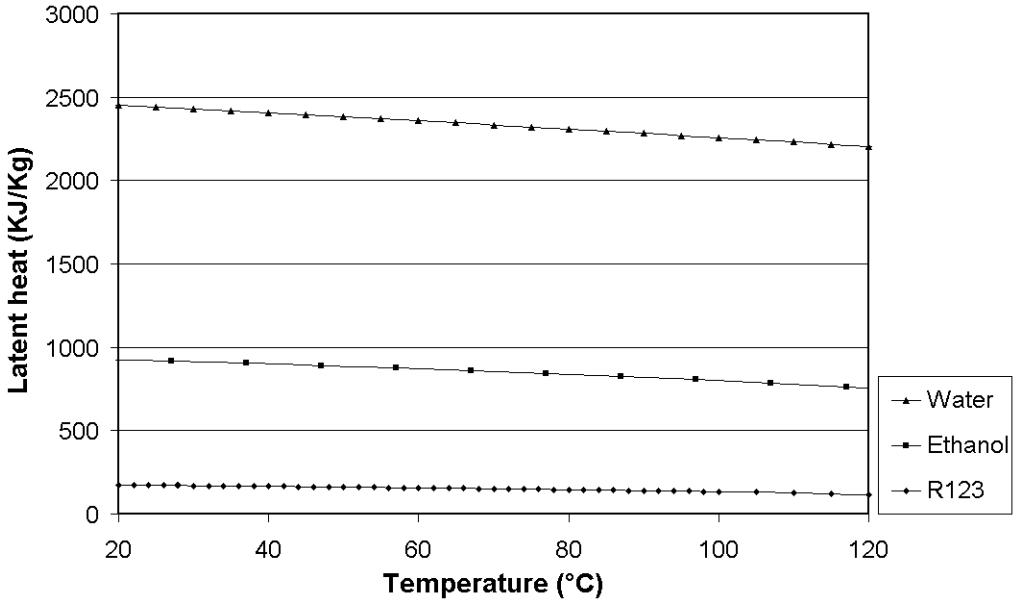

Figure Ax-8: Variation of latent heat of evaporation of the working fluids with temperature

(III) Uncertainty analysis

All scientific and engineering experiments are subject to a variety of errors. The consolidated effect of all the errors leads to a difference between the true value of a parameter as against the measured value by the observer. In most situations, we cannot talk very confidently about what the error in a measurement *is*, we can only talk about what it *might be* – about the limits that we feel, bound the possible error [Moffat, 1988].

From the point of view of reliability estimates of the error, experiments fall into two overlapping categories – single-sample and multi-sample experiments. Experiments in which uncertainties are evaluated by repeating all the measurements enough times, using enough observers and enough diverse instruments so that the reliability of the results could be assured by the use of statistics, are called as multi-sample experiments. Unfortunately, as most engineering experiments, the very nature of the experiments reported herein is 'single-sample'. Although, the experiments have been repeated as many number of times as was practically feasible from economic and time constraints, statistical methods can certainly not be applied. Therefore, single-sample uncertainty analysis, as has been proposed by Kline and McClintock [1953] and Moffat [1982], is applied for present analysis. In such an analysis, statements of reliability will be based in part on estimates since by definition, statistics cannot be applied to all of the errors. The basic strategy of analysis is as follows [Kline and McClintock, 1953]:

The desired result R of the experiment is calculated from a set of measurements represented by:

$$R = R(X_1, X_2, X_3, ..., X_N) \qquad \text{(A-1)}$$

where X_i represents the measured observation in the experiment. The objective of expressing the uncertainty δR in the calculated result can be estimated with good accuracy using a root-sum-square combination of the effects of each of the individual inputs. Thus, the basic equation for uncertainty analysis is given by:

$$\delta R = \left\{ \sum_{i=1}^{N} \left(\frac{\partial R}{\partial X_i} \delta X_i \right)^2 \right\}^{1/2} \qquad \text{(A-2)}$$

Each term represents the contribution made by the uncertainty in one variable, δX_i, to the overall uncertainty in the result, δR. This equation applies as long as:

- Each of the measurements was independent,
- Repeated observations of each measurement, if made, would display Gaussian distributions,
- The uncertainty in each measurement was initially expressed at the same odds.

The following table summarizes the quantities recorded during the course of this study and the associated estimates of the uncertainties associated with them based on instrument manufacturer's recommendations and calibration tests.

Table Ax-1: Uncertainty in measured quantities

Quantity	Range	Uncertainty
Temperature	-200 – 1200 °C	±0.5 °C
Voltage (DC)	0 – 50 V	±0.25 V
Current (DC)	0 – 3 A	±0.04 A
Voltage (AC)	0 – 400 V	±2.0 V
Current (AC)	0 – 10 A	± 0.1 A
Volume	0 – 10 ml	± 0.1 ml
Mass	0 – 200 gms	± 0.1 g
Length	0 – 150 mm	± 0.02 mm

The following quantities have been used for reporting the results of this study and for subsequent interpretations:

- Temperature at the location of interest
- Heat power input to the system
- Thermal resistance of the system
- Volumetric filling ratio of the working fluid
- Geometrical parameters like diameter, length and area of cross section

If there is only one thermocouple located at the area/location of interest then its value has been directed reported and the uncertainty value as pointed out in Table Ax-1 is applicable. When there are more than one thermocouples in a given specified area/section, the reported value of temperature is the arithmetical average of all the thermocouples at that location (this has been indicated in the text, wherever applicable.

In all the experiments, the heat power to the system has been calculated directly from the measured electrical power to the system.

$\dot{Q} = V \cdot A$, therefore from Eq. (A-2), (A-3)

$$\frac{\delta \dot{Q}}{\dot{Q}} = \left\{ \left(\frac{\delta V}{V} \right)^2 + \left(\frac{\delta I}{I} \right)^2 \right\}^{1/2} \quad \text{(A-4)}$$

In addition, calibration tests were performed to get a fair estimate of the losses to the environment through the insulation material. The heat loss estimation was based on: (i) simplified one-dimensional heat flow equations based on the thermal conductivity of the insulation material and convective heat transfer coefficient to the ambient (ii) measuring the temperature of the insulation material outside surface at steady state of a given experimental run. These losses have been subtracted from the reported heat input power in the results. The losses are in the range of 3%-7 %, depending on the experiment.

$$\dot{Q}_{in} = \dot{Q} - \dot{Q}_{loss} \quad \text{(A-5)}$$

Finally, the thermal resistance of the system is calculated as:

$$R_{th} = \frac{\Delta T}{Q_{in}} \text{ therefore from Eq. (A-2),} \qquad \text{(A-6)}$$

$$\frac{\delta R_{th}}{R_{th}} = \left\{ \left(\frac{\delta \Delta T}{\Delta T} \right)^2 + \left(\frac{\delta \dot{Q}_{in}}{\dot{Q}_{in}} \right)^2 \right\}^{1/2} \text{ where,} \qquad \text{(A-7)}$$

$\Delta T = T_e - T_c$ and from Eq. (A-2),

$$\delta(\Delta T) = \left\{ (\delta T_e)^2 + (\delta T_c)^2 \right\}^{1/2} \qquad \text{(A-8)}$$

The error estimation in the reported results has been done adopting the above calculation procedure; the errors being shown in the form of bars on the respective figures.

References

[1] Kline S. J. and McClintok F. A., ***Describing Uncertainties in Single Sample Experiments***, Mech. Engg., pp. 3-8, 1953.

[2] Moffat R. J., ***Contributions to the Theory of Single Sample Uncertainty Analysis***, Tran. ASME, J. of Fluids Engg., Vol. 104, pp. 250-260, 1982.

[3] Moffat R. J., ***Describing the Uncertainties in Experimental Results***, Experimental Thermal and Fluid Science, Vol. 1, pp. 3-17, 1988.

[4] ***Heat Pipe Design Handbook***, Prepared for NASA, USA, by B & K Engineering, 1979.